Magma injections and destabilization of basaltic volcanoes : A numerical study : Application to La Reunion (Indian ocean, France) and Stromboli (Tyrrhenian sea, Italy)

Thibault Catry

UNIVERSITÀ DI BOLOGNA

Dipartimento di Scienze della Terra e Geologico-Ambientali

DOTTORATO IN MODELLISTICA FISICA PER LA PROTEZIONE DELL'AMBIENTE
XXIII CICLO
Coordinatore: Prof. Rolando Rizzi

Settore scientifico-disciplinare di appartenenza
GEO/08 – GEO/10

Tesi di Dottorato

MAGMA INJECTIONS AND DESTABILIZATION OF BASALTIC VOLCANOES: A NUMERICAL STUDY

Application to La Reunion (Indian ocean, France) and
Stromboli (Tyrrhenian sea, Italy)

Presentata da:

Dott. Thibault Catry

Relatrice

Dott.ssa Claudia Romagnoli

Correlatore

Dott. Laurent Michon

Esame finale anno 2011

Foreword

This research thesis has been developed in the project « Analysis and modelling of the evolution of insular volcanoes : comparison between La Reunion Island (Indian océan, France) and the Aeolian Islands (southern Tyrrhenian sea, Italy). Our study has been carried out in a co-tutela between the University of Bologna (Dipartimento di Scienze della Terra e Geologico-ambientali, under the supervision of Dott.ssa Claudia Romagnoli) and the University of La Reunion (Laboratoire Géosciences Réunion, under the supervision of Dr. Laurent Michon), funded by a Vinci fellowship from the Università Italo-Francese (UIF).

A ma famille,

« L'enfance c'est des souvenirs de volcans, avec la certitude que c'est Haroun Tazieff qui a inventé la purée … »

Patrick Sébastien, Carnets de notes (2001)

Acknowledgements

Here it is, the final touch to this adventure!!!

My adventure with volcanoes started a long time ago when I first decided to become a paleontologist… ??? Indeed, I have to start the acknowledgements by thanking Steven Spielberg who, in 1993 with his movie Jurassic Park, revealed to me what I wanted to do in life: I wanted to have fun with dinausors on a tropical island, just like the professor Alan Grant (I have to say that's no sot far from my actual life, for the tropical part at least). I was 8 years old at this time and as you can see I had a very accurate idea of what research in Earth sciences was… I finally discovered what geology was when I arrived in high school. Quickly, one of my teachers told me to forget about paleontology and adviced me to go to a more open field of geology. I then decided to follow his advice and as lava flows seemed fun on TV, I decided to become a volcanologist. As you see, I was stubborn back then and some of my friends which will read these acknowledgements (I won't blame you if it's the only thing you read…) will probably tell themselves that I haven't changed that much. I cannot say they are wrong !!!!

My first contact with volcanoes occurred in July 2004, during my first holidays at La Reunion, where i had the chance to climb Piton de la Fournaise volcano with some of my best friends. Thank you very much to Mat, Bat, Lo, Dieu, Marie, Juju, Alex, Millou, Claire, Laura, and Ben. I spent great moments with all of you at Faidherbe and La Reunion (for most of you) and I always love the time we spend together one or twice a year…

This trip was a revelation, I was born to be a volcanologist and work on Piton de la Fournaise. I started my formation at Clermont-Ferrand where I met a lot of very nice people. Thanks to my friends from the Master 2005-2007 : Yann, Thomas, Emma, Celia, Marion, Joan, Jerome… A particular thanks to Pierre and Emilie for all the moments we spent together at Clermont and elsewhere. It was awesome to have you for holidays at La Reunion ; I look forward to our next adventure…

My love story with La Reunion continued in 2007 when Laurent Michon invited me for a 6 months reasearch experience on the Island. This year, Piton de la Fournaise gave me an incredible present with the eruption of April 2007… what an experience, fantastic memories. Thank you so much to Laurent and Nico for these amazing 6 months.

Few months later, my PhD began. Thank you so much to Claudia Romagnoli and Laurent Michon for giving me this opportunity and for your help and availability during these 3 years. Thanks a lot to Valérie Cayol for her precious help in the modelling approach and for her kindness and availability every time I came to Saint-Etienne, especially in last february when you greeted my at your home., with your nice family.

Working between France and Italy was not always fun (Italian administration is actually worse than the French one), but I discovered a nice country and met great people. Thanks to Fede, Claudio, Prof. Rossi, Daniele, Maria, Elisa, Giorgia, Gabriele, Francesco, Veronica. I really enjoyed the lab and Bologna thanks to you. Special thanks to my sweetest Francesca, my office-mate : you taught me the real Italian language, the one from Bologna, and most of all, you made me a great secretary. It was great sharing an office and the adventure of the PhD with you.

I can't finish the italian acknowledgements without thanking Arianna, my room-mate from Bologna. You really helped me when I arrived in Italy and then we spent good moments together.

Grazie mille a tutti, la mia esperienza a Bologna é stata molta bella grazie a voi. In bocca al Lupo per il futuro. Ci vediamo presto.

Now it's time to thank all the people from La Reunion. First of all, I want to thank Vincent Famin for his help during the PhD and for offering me a roof for 2 weeks when I was homeless (thanks also to Sandra). Vincent, I really enjoyed your Whiskies… Thanks to Andrea DiMuro for taking the time to share ideas about my PhD with me and to the staff of the OVPF. Thanks to Benoit Taisne for his help and the discussion we had the observatory during his missions. And Finally, my heartfelt

thanks to all my friends from La Reunion (those who offered me I place to sleep in particular, but to avoid jalousy, I will come to sleep in the beds I haven't tried yet in 2011) : Camille et Eric, Hélène et Guillaume, Dorian, Anne et Arnaud, Fadi, Benjamin, Ben, Marie, Flo, Julie. L, Marion, Khalid, Mag, Pierre, Julie M., Manu, Anthony, Jaco, Zarah, Fabrice, Geneviève, Francoise, Aurélie, Agnès, Johan, Mathilde.... Thanks a lot to the other members of the Laboratoire Géosciences for their kindness, it's been a pleasure working with you every day.

Merci à tous du fond du cœur, grace à vous, j'ai passé des moments merveilleux à La Réunion. Que de souvenirs magnifiques !!!!! J'espère qu'il y en aura encore beaucoup d'autres.

Je terminerai ces longs remerciements par une pensée toute particulière envers ma famille qui m'a toujours soutenu dans ma passion et cette idée un peu folle de travailler sur des volcans. Merci pour tout. Il n'y a rien de plus important que la famille. Ce travail vous est dédié.

Abstract

Most basaltic volcanoes are affected by recurrent lateral instabilities during their evolution. Numerous factors have been shown to be involved in the process of flank destabilization occurring over long periods of time or by instantaneous failures. However, the role of these factors on the mechanical behaviour and stability of volcanic edifices is poorly-constrained as lateral failure usually results from the combined effects of several parameters. Our study focuses on the morphological and structural comparison of two end-member basaltic systems, La Reunion (Indian ocean, France) and Stromboli (southern Tyrrhenian sea, Italy). We showed that despite major differences on their volumes and geodynamic settings, both systems present some similarities as they are characterized by an intense intrusive activity along well-developed rift zones and recurrent phenomena of flank collapse during their evolution. Among the factors of instability, the examples of la Reunion and Stromboli evidence the major contribution of intrusive complexes to volcano growth and destruction as attested by field observations and the monitoring of these active volcanoes. Classical models consider the relationship between vertical intrusions of magma and flank movements along a preexisting sliding surface. A set of published and new field data from Piton des Neiges volcano (La Reunion) allowed us to recognize the role of subhorizontal intrusions in the process of flank instability and to characterize the geometry of both subvertical and subhorizontal intrusions within basaltic edifices. This study compares the results of numerical modelling of the displacements associated with high-angle and low-angle intrusions within basaltic volcanoes. We use a Mixed Boundary Element Method to investigate the mechanical response of an edifice to the injection of magmatic intrusions in different stress fields. Our results indicate that the anisotropy of the stress field favours the slip along the intrusions due to cointrusive shear stress, generating flank-scale displacements of the edifice, especially in the case of subhorizontal intrusions, capable of triggering large-scale flank collapses on basaltic volcanoes. Applications of our theoretical results to real cases of flank displacements on basaltic volcanoes

(such as the 2007 eruptive crisis at La Reunion and Stromboli) revealed that the previous model of subvertical intrusions-related collapse is a likely mechanism affecting small-scale steeply-sloping basaltic volcanoes like Stromboli. Furthermore, our field study combined to modelling results confirms the importance of shallow-dipping intrusions in the morpho-structural evolution of large gently-sloping basaltic volcanoes like Piton de la Fournaise, Etna and Kilauea, with particular regards to flank instability, which can cause catastrophic tsunamis.

Riassunto

L'evoluzione della maggior parte dei vulcani basaltici é caratterizzata da fenomeni ricorrenti d'instabilità laterale. Diversi fattori, coinvolti nella destabilizzazione a lungo termine o in improvvisi collassi di fianchi vulcanici, sono stati identificati a partire dall'evento del Mount Saint-Helens del 1980. Tuttavia, l'influenza relativa dei vari parametri influenti sulla stabilità meccanica degli edifici vulcanici é difficilmente quantificabile, dato che gli scivolamenti di fianchi risultano generalmente da diverse cause interagenti. Questo studio si concentra su un confronto tra le caratteristiche morfologiche e strutturali di due sistemi basaltici, La Reunion (Oceano Indiano, Francia) e Stromboli (Mar Tirreno, Italia). Nonostante tali edifici vulcanici abbiano volumi e contesti geodinamici molto diversi, sono entrambi sottomessi ad un'attività intrusiva intensa lungo le rispettive *rift zones* e hanno subito destabilizzazioni laterali ricorrenti durante la loro evoluzione. Gli esempi della Reunion e Stromboli sottolineano il ruolo importante dei meccanismi di intrusione magmatica nella crescita e destabilizzazione dei vulcani, come testimoniato da dati di campagna e dal monitoraggio di tali vulcani attivi. I modelli "classici", infatti, considerano che il processo di collasso laterale in ambiente vulcanico può essere favorito dalla messa in posto d'una o più intrusioni verticali, causando movimenti dei fianchi vulcanici lungo una superficie di rottura preesistente. Nuovi dati di campagna acquisiti al vulcano Piton des Neiges (La Reunion), oltre a dati di letteratura su altri edifici vulcanici, hanno permesso di descrivere la geometria delle intrusioni sub-verticali e sub-orizzontali nei vulcani basaltici e, in particolare, di evidenziare l'importanza delle intrusioni sub-orizzontali nella destabilizzazione di fianchi vulcanici. Questo studio confronta i risultati della modellistica numerica sui campi di spostamenti superficiali indotti da intrusioni magmatiche sub-verticali e sub-orizzontali in edifici basaltici, tramite l'applicazione di un metodo di *Mixed Boundary Element,* con l'obiettivo di determinare il comportamento meccanico di un vulcano sottoposto ad un'iniezione magmatica sotto diversi campi di *stress*. I risultati dimostrano che un campo di stress anisotropico favorisce lo scivolamento laterale lungo le intrusioni, creato dallo *shear*

stress co-intrusivo, come origine di spostamenti alla scala del fianco vulcanico. Questi ampi spostamenti, preferibilmente legati ad intrusioni sub-orizzontali, possono probabilmente innescare dei collassi laterali a larga scala se la loro ampiezza compromette la stabilità dell'edificio. L'applicazione dei risultati teorici a casi reali di deformazione osservati sui vulcani basaltici (tra cui La Reunion e Stromboli durante le rispettive crisi eruttive del 2007) rivela che il modello di destabilizzazione legata ad intrusioni sub-verticali é un meccanismo in grado di causare collassi di fianchi su stratovulcani relativamente piccoli, ma con pendenze forti come Stromboli. I nostri dati di campagna e di modellistica numerica confermano, inoltre, il ruolo importante delle intrusioni sub-orizzontali nell'evoluzione morfo-strutturale di vulcani basaltici ampi e a basse pendenze (vulcani a scudo) come il Piton de la Fournaise (La Reunion), il Monte Etna o il Kilauea e, particolarmente, nel processo d'instabilità laterale, potenzialmente in grado di provocare catastrofici *tsunami*.

Résumé

L'évolution de la majorité des volcans basaltiques est marquée par des phénomènes récurrents d'instabilité latérale. De nombreux facteurs d'instabilité, impliqués dans des déstabilisations à long terme ou des effondrements de flancs instantanés, ont été recensés depuis l'événement majeur qui a frappé le Mont Saint-Helens en 1980. Cependant, le rôle de ces facteurs sur la stabilité mécanique des édifices est mal contraint dans la mesure où les glissements de flancs résultent en général de plusieurs causes simultanées. Notre étude se concentre sur une comparaison des caractéristiques morphologiques et structurales de deux systèmes basaltiques, La Réunion (Océan Indien, France) et Stromboli (Mer Tyrrhénienne, Italie). Nous avons montré que, bien qu'ayant des volumes et des contextes géodynamiques très différents, les systèmes sont tous deux caractérisés par une activité intrusive intense le long de *rift zones* et ont subi des déstabilisations latérales récurrentes durant leur évolution. Parmi les facteurs d'instabilité, les exemples de La Réunion et de Stromboli soulignent l'influence majeure des complexes intrusifs dans la croissance et le démantèlement des volcans, comme le prouvent les études de terrain et la surveillance des ces volcans actifs. Les modèles classiques considèrent que le processus d'instabilité latérale en domaine volcanique résulte de la mise en place d'une ou plusieurs intrusions verticales, entrainant des mouvements de flancs le long d'une surface de glissement pré-existante. De nouvelles données de terrain obtenues au Piton des Neiges (La Réunion), ainsi que des données de littérature sur d'autres édifices, ont permis de mettre en évidence le rôle des intrusions sub-horizontales dans les déstabilisations de flancs et de caractériser la géométrie des intrusions sub-verticales et sub-horizontales au sein des volcans basaltiques. Cette étude compare les résultats de la modélisation numérique des champs de déplacements de surface crées par la mise en place d'intrusions magmatiques à faible / fort pendage dans les édifices basaltiques, grâce à une méthode d'éléments frontières mixte (*Mixed Boundary Element Method),* dans le but de déterminer le comportement mécanique d'un édifice soumis à des injections magmatiques sous

différents champs de contraintes. Les résultats de cette étude montrent qu'un champ de contraintes anisotrope favorise le glissement le long des intrusions, généré par la contrainte cisaillante co-intrusive, à l'origine de déplacements à l'échelle du flanc de l'édifice. Ces déplacements de grande ampleur, préférentiellement liés à des intrusions subhorizontales, peuvent probablement déclencher des grands glissements latéraux si leur amplitude dépasse le seuil de stabilité de l'édifice. L'application des résultats théoriques à des exemples réels de déformation enregistrées sur des volcans basaltiques (dont La Reunion et Stromboli, au cours de leurs crises éruptives de 2007) révèle que le modèle de déstabilisation associée à des intrusions sub-verticales est un mécanisme pouvant générer des effondrements de flancs sur des petits édifices à fortes pentes comme Stromboli. De plus, nos données de terrain et les résultats de modélisation confirment l'importance des intrusions sub-horizontales dans l'évolution morpho-structurale des grands édifices basaltiques à faibles pentes comme le Piton de la Fournaise (La Réunion), l'Etna ou le Kilauea, et plus particulièrement dans les instabilités de flancs pouvant causer des tsunamis dévastateurs.

Contents

General Introduction

Basaltic volcanoes are complex systems whose behaviour and evolution involve various physical and chemical processes. More than half of the world's volcanoes are basaltic or include basalt among their products, and about one third of known eruptions, involving tens of volcanoes per year erupt basaltic magma (Walker, 1993). The nature (volume, shape…) and geological environment where basaltic edifices form strongly vary. Their evolution can occur over different time spans and is usually made of alternating phases of growth and destruction of the edifices. The recurrence of flank lanslides has been recognised as one of the most important dismantling processes on basaltic volcanoes, as testified by deposits related to flank collapses described on the flanks of basaltic systems like Hawaii (Moore, 1964 ; Moore et al., 1989 ; Mitchell et al., 2002), the Canary islands (Carracedo, 1999 ; Masson et al., 2002), La Reunion Island (Lénat et al., 1989 ; Labazuy, 1996 ; Oehler et al., 2008) or Stromboli Island (Kokelaar and Romagnoli, 1995 ; Romagnoli et al., 2009a and b). The various factors that cause volcano instability often occur concurrently and so their relative importance is difficult to evaluate. Lateral instability is thought to result mainly from repeated magmatic intrusions along rift zones coupled with movements along layers of weak material within the volcanic edifice. However, the diversity in the geometries of the edifices and their magmatic systems suggest that the evolution of basaltic volcanoes is controlled by other factors like the nature and behaviour of the basement, and the geodynamic context, whose role is poorly-understood.

This thesis focusses on the role of magmatic intrusions in the mechanism of flank destabilizations on basaltic volcanoes, through a comparative study of the volcanic edifices of La Reunion (Indian ocean, France) and Stromboli (southern Tyrrhenian sea, Italy), in order to understand how different basaltic systems can experiment similar evolution. The first chapter of the study is a review of the general evolution of basaltic volcanoes, in which :

1- Previous models of evolution of basaltic shield volcanoes and stratovolcanoes

are introduced.

2- We identify the main parameters involved in this evolution, with particular regard to their influence on flank instability.

The second chapter is dedicated to a comparison of the edifices of La Reunion and Stromboli, using recent bathymetrical data and DEMs obtained during oceanographic campaigns (2003-2006 for Stromboli, FOREVER and ERODER missions for La Reunion). In this part :

1- The nature and volumes of the edifices are compared.

2- The main morphological and structural features of the La Reunion and Stromboli are described and compared.

3- These features are correlated to the geodynamic contexts and regional tectonics of the areas of interest.

In the third chapter, we study the role of magmatic intrusions in the deformation of volcanic edifices through numerical models of surface displacements fields generated by different geometries of magmatic intrusions, emplaced under various stress conditions. This approach aims at using surface displacement patterns to:

1- Determine the characteristics of the intrusions.

2- Estimate the stress field conditions within basaltic volcanoes.

3- Determine mechanisms of flank-scale deformation and/or flank destabilization in relationship with the morphology and structure of basaltic volcanoes, through applications to real cases (Piton de la Fournaise, Stromboli and Mount Etna).

Keywords : Basaltic edifice, magmatic intrusions, rift-zones, destabilization, La Reunion, Stromboli, numerical models.

Chapter 1

Structure and evolution of basaltic volcanoes: a review.

More than 50 % of the volcanoes worldwide are basaltic or have a basaltic component in their emissions (Walker, 1993). Several types of basaltic volcanoes occur on land but the submarine mid-ocean ridges are probably the most extensive basaltic volcanic system on Earth.

The first chapter of our study starts with a review of the nature and structure of basaltic volcanoes in relationship with the environment in which they grew. Some general features on the evolution of basaltic volcanoes are then discussed. The role of the main factors involved in the evolution of basaltic volcanoes, with particular regards to lateral instability, is finally summarized.

1.1- Types of basaltic volcanoes

Basaltic volcanoes can be either polygenetic or monogenetic edifices. Walker (1993) distinguished five main types of basaltic volcanoes (Fig. 1.1): shield volcanoes, stratovolcanoes, flood basalts volcanoes, monogenetic volcanoes and central volcanoes.

Volcano type	Morphological features	Example(s)
SHIELD VOLCANO	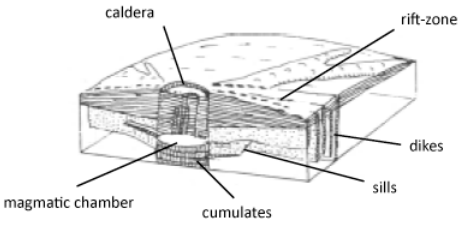	Hawaii, La Reunion
STRATOVOLCANO	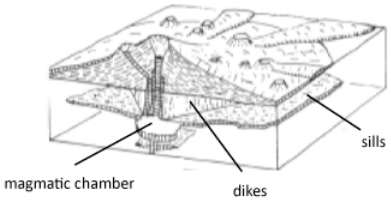	Fuji Stromboli Etna
FLOOD BASALTS VOLCANO	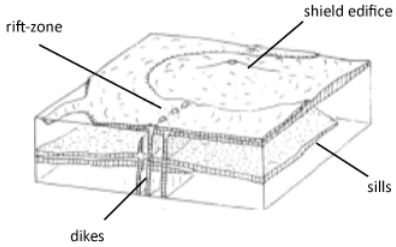	Deccan trapps
MONOGENETIC VOLCANO	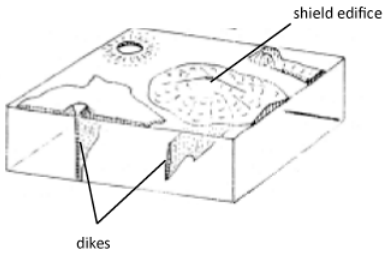	Honolulu monoge- netic field, Hawaii
CENTRAL VOLCANO	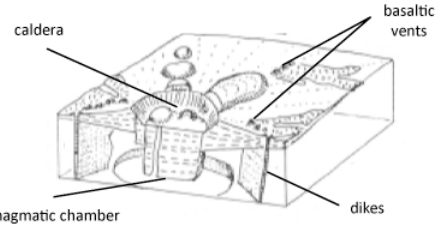	Vesuvius

Figure 1.1: The five different types of basaltic volcanoes (modified from Walker, 1993).

Basaltic volcanoes can develop on either continental or oceanic lithospheres. In oceanic setting, most of them are related to a long-lived mantle anomaly (La Reunion Island, Hawaii, Society Islands…). Volcanoes associated with hot spot magmatism are usually among the largest. Tenerife (Canary Islands) reaches an elevation of 8.5 km from the seabed to the top of the edifice. La Reunion edifice currently reaches more than 7 km while Mauna Loa volcano (Big Island, Hawaii) is the highest relief on the planet with more than 9 km of maximum elevation. In active geodynamic setting, the size of the edifice ranges from small-scale volcanoes, like Stromboli volcano in the Aeolian islands which reaches a maximum elevation of 3.5 km, to large volcanoes like Mount Etna (Sicily).

Shield volcanoes like Mauna Loa are made of piled thin lava flows and characterized by low sub-aerial slopes (less than 10°). The low-angle shield shape is related to high effusion rates and to the low viscosity of basaltic lava flows that travel on large distances from the emission point. Other shield volcanoes, like those of the Galapagos archipelago, also made of lava flows, show an alternation of concentric steep and gentle slopes that confers an overall overturned soup plate geometry to the edifice (Rowland and Garbeil, 2000). The steep slopes are interpreted as due to the superimposition of either pyroclastic cones (Rowland and Garbeil, 2000) or short lava flows (Naumann and Geist, 2000). It is worth noting that a well-developed intrusive system defining radial rift-zones develop on Mauna Loa-like shield volcanoes whereas the "overturned soup plate" volcanoes are generally associated with scattered concentric and radial intrusions (Chadwick and Dieterich, 1995). Summit calderas always cut both types of shield volcanoes.

Stratovolcanoes consist of steep edifices whose slopes are made of piled lava flows and pyroclastic deposits. The upper part of the edifice is characterized by the steepest slope values of about 35°. Stratovolcanoes are usually located on active plate boundaries, such as in arc settings. However, due to an alternation of explosive and effusive activity, basaltic stratovolcanoes like Nyiragongo may also develop in continental setting. Stromboli volcano and Mount Etna are good examples of basaltic stratovolcanoes, and well illustrate that the volumes of the edifices can widely range. In a way similar to shield volcanoes, stratovolcanoes are characterized by an intense intrusive activity, which is organized along rift zones. Stratovolcanoes located in active geodynamic setting are generally short-lived volcanoes compared to hot-spot related shield volcanoes.

Flood basalts like the Deccan Trapps (India) or the Columbia plateau (USA) are generally associated with the ascent of a mantle anomaly below the lithosphere, i.e. the first step of the hot-spot activity. They consist of voluminous lava flows (several km^3) covering large surfaces. For instance, the Deccan Trapps event that occurred 65 My ago, produced a volume of lava estimated at 1-2.10^6 km^3 and covered an area of 5.10^5 km^2 (Richards et al., 1989; White and McKenzie, 1995) over a period of activity that lasted approximately 1 My. Shield edifices can be created during flood basalt eruptions.

Basaltic volcanoes can be monogenetic volcanoes whose activity ceased after a single episode of eruptive activity. They usually occur as volcanic fields made of several small-scale cones that can be shield volcanoes, like at the Honolulu field (Hawaii). The formation of the volcanic field can span over several million years.

Central volcanoes like Vesuvius (Italy) present a bimodal composition made of basaltic and silicic products. Basaltic products are generally related to eccentric basaltic vents on the lower slopes of central volcanoes while the central part of the edifice is made of silicic material. Central volcanoes usually spread on large areas, their higher parts having steeper slopes than the lower parts due to the difference in the nature of the products. Summit calderas are common on central edifices.

Walker (1993) postulated that the type of basaltic volcano was dependent on 1- the magma input rate and 2- the frequency at which the magmatic system is replenished. These two criteria are partly determined by the geodynamic context in which the volcano is located, that controls the nature of the magma and the geometry of the plumbing system of an edifice. They will also partly depend on the evolution of the edifice. Nevertheless, the above examples well indicate that to a diversity of settings can be associated a diversity of structures and characteristics of basaltic volcanoes. In particular, the size and geometry of the edifices widely range, whatever the geodynamic context in which they were formed.

1.2- General insights into the evolution of basaltic volcanoes

Our study deals with the comparison between two basaltic island systems: La Reunion Island, a hotspot-related shield made of several basaltic edifices located in the Indian Ocean, and Stromboli Island, an island-arc volcano belonging to the Aeolian islands

system in the Tyrrhenian sea, southern Italy. As a consequence, this section of the study will refer to general features on the evolution of basaltic insular shields and stratovolcanoes.

1.2.1- Shield volcanoes related to hot-spot activity (Hawaiian-type volcanoes)

Based on extensive investigations on the volcanoes of Hawaii, Peterson and Moore (1987) proposed a multi-stage evolution for Hawaiian-type volcanoes, which can be divided in 4 main steps (Fig. 1.2):

1.2.1.1- Submarine pre-shield stage (stage 1 on Fig. 1.2)

This stage is characterized by rare eruptions of small volume. The submarine edifice has steep slopes, and the typical 2 or 3-armed rift zones may be already formed (Carracedo, 1996). In the case of Hawaiian volcanoes, this period can last about 200 000 years. The activity then slowly increases and the volcano enters the second phase of its construction.

1.2.1.2- Shield-building stage (stages 2 and 3 on Fig. 1.2)

Once the summit of the volcano reaches the surface, after an explosive phase due to the interaction between magma and water that can last several hundred thousands years, the volcano enters the subaerial stage of its evolution and the shield edifice starts to grow by accumulation of lava of tholeiitic composition on its slopes. During this stage, the volcano reaches the climax of its activity, forming 95 % of the total volume of the edifice. During this stage, basaltic shields can be affected by recurrent gravity destabilizations, partly due to overloading and oversteepening by accumulation of volcanic material on the slopes of the edifice.

1.2.1.3- Post-shield stage (stage 4 on Fig. 1.2)

The eruption rate starts decreasing together with the construction rate. The volume of the volcano barely changes in this period, during which it can be affected by explosive activity.

1.1.2.4- Erosional stage (stage 5 to 8 on Fig.1.2)

The post-shield stage is followed by an erosional stage that may last several million years. The volcanic activity ceases progressively. The volcano is incised by deep canyons and dismantled by major collapses events. This period can alternate with stages of

"rejuvenation" of volcanic activity but commonly erosion, combined with subsidence, remains strong enough to give place to submergence, so that the island becomes an atoll and finally a guyot.

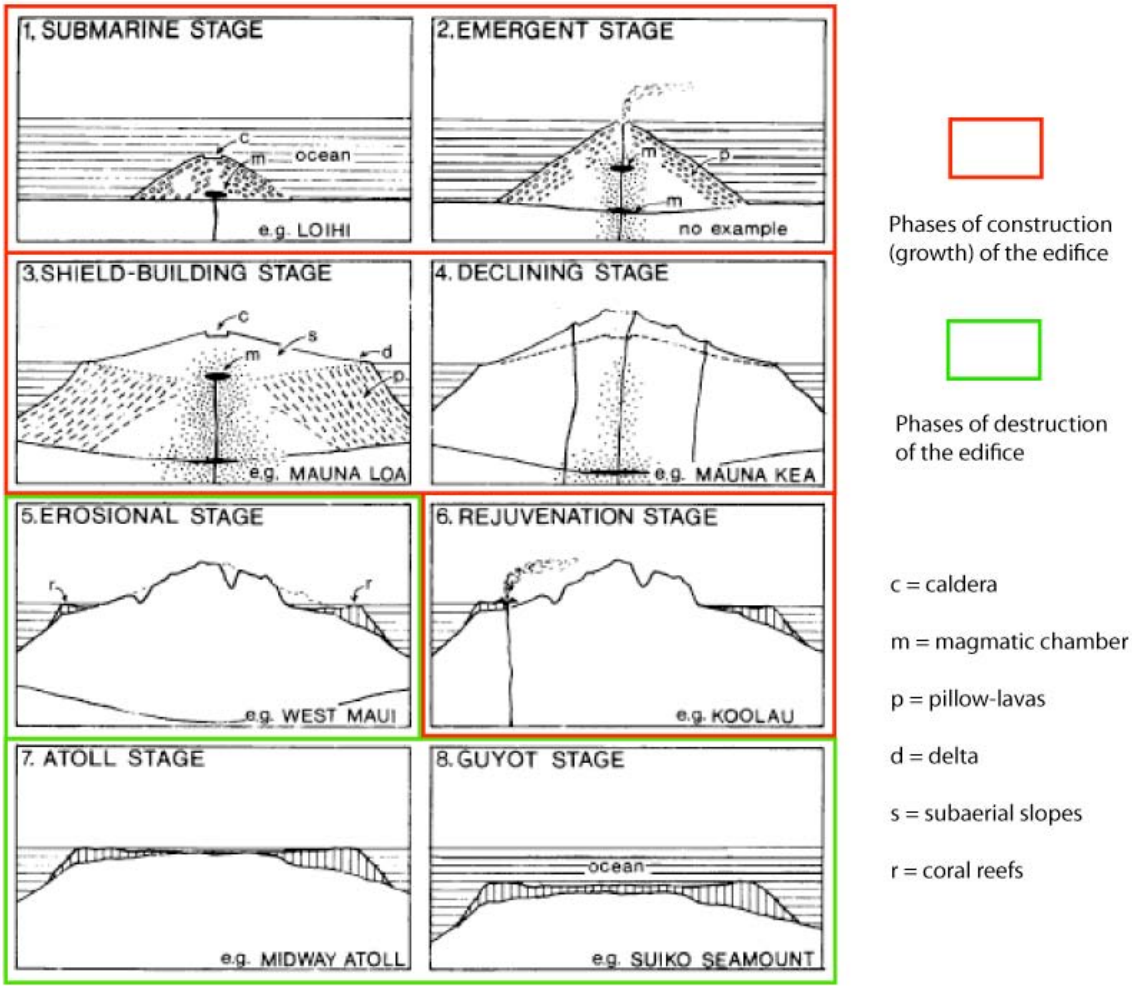

Figure 1.2: Main stages of the evolution of Hawaiian type volcanoes (modified from Peterson and Moore, 1987). See text for description.

The growth of shield volcanoes is favoured by repeated magmatic intrusions along rift-zones and lava flow accumulation on their slopes. However, they also experiment destruction phases, mainly due to caldera and flank collapses that are likely to occur at every step of the evolution of the shield volcano (Walker, 1993).

The example of Hawaii has to be considered just as a general model of evolution regarding all types of oceanic basaltic volcanoes. Indeed, other hot spot volcanoes like in La Reunion, in the Canary archipelago or in the Galapagos archipelago, although having a global similar evolution, can present specific evolutions related to different effusion rates,

geometry of deep magmatic and intrusive systems or local tectonic environments. Similarly, the relationships between rift-zones activity, lateral destabilization and erosion processes in the evolution of basaltic volcanoes are much more complex than evidenced by the model of Peterson and Moore (1987) as inter-connections exist between these phenomena on short-term and long-term periods in the life of a shield volcano.

Moreover, in hot spot settings, the activity of the plume combined with the plate movements generally creates trends of volcanic islands at different stages, like in the Canary Islands or Hawaii (Fig. 1.3).

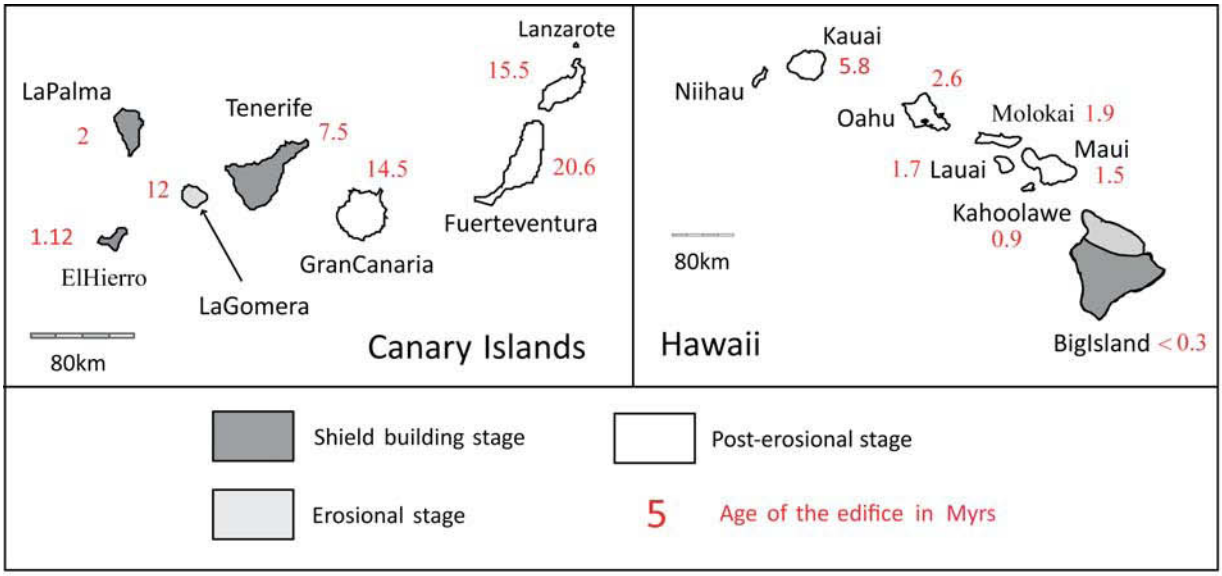

Figure 1.3: Examples of time-related evolution of volcanic edifices in some hotspot settings (modified from Carracedo, 1999).

Erosional processes are involved all along the evolution of shield volcanoes. Their importance is however variable considering the step of the evolution as when the magma supply rate is high and the activity reaches a climax (shield-building stage), the influence of the erosion in the morphological evolution of the volcanic edifice is strongly reduced. Conversely, when the activity decreases (post-shield and erosional stages), the effects of erosion on the edifice are not balanced by the accumulation of new volcanic material on the slopes, making erosion one of the principal factors of morphological changes of the edifice. Furthermore, erosional processes have a major role in the evolution of hot spot-related

shield volcanoes as most of them are located in tropical environments characterized by heavy rain falls (La Reunion island, Hawaii, Canary islands…).

1.2.2- Basaltic stratovolcanoes

Basaltic stratovolcanoes grow by accumulation of lava flows and pyroclastic material on their flanks. As their slopes are generally higher than the slopes of basaltic shields, reaching more than 30° in some cases, they are naturally more prone to experiment flank collapse during their evolution. Sector collapses were indeed identified for several edifices. At Stromboli volcano, the phases of growth of the subaerial edifice are regularly interrupted by large flank destabilizations both on the northwestern and southeastern flanks (Tibaldi, 2001; Romagnoli et al., 2009a and 2009b). Satake et al. (2001 and 2007) showed that the evolution of Oshima-Oshima volcano, a small-scale basaltic volcano located in the Japan Sea, was affected by a major sector collapse that generated a tsunami in 1741. Sector collapses characterize the evolution of Mount Etna volcano, a large-scale Sicilian basaltic stratovolcano (not insular, but located on the eastern coastal tract of Sicily), as testified by the Valle del Bove scar and by the occurrence of local Pleistocene and Holocene debris avalanche and debris flow deposits exposed on the eastern flanks of the volcano (Calvari et al., 2004; Del Negro and Napoli, 2002). Marine geophysical surveys revealed the presence of submarine landslide deposits on the lower flanks of Mount Etna (Pareschi et al., 2006; Chiocci et al., *in press*). The Monowai cone, a small and shallow submarine stratovolcano part of the Monowai volcanic center in the northern Kermadec arc, experimented two sector collapses since 1998 (Wright et al., 2008; Chadwick et al., 2008) while being in the early stages of its construction. Favoured by the steep slopes of the edifices, erosion participates to the dismantling processes of stratovolcanoes.

The evolution of hotspot related volcanoes (flood basalts included) occurs commonly on a time-span of several million years. Such long-term evolution is specific to this type of basaltic volcanoes as basaltic edifices located in active settings will be subducted or become inactive on shorter time intervals.

1.3- Gravitational instabilities affecting volcanic edifices

McGuire (1996) defines volcano instabilities as “the minimum level of destabilization where part or a whole edifice is prone to experiment a failure”. In the following sections, the occurrence of lateral instability on volcanoes (basaltic ones in particular) and the parameters involved in the control and trigger of the collapse mechanism will be discussed.

1.3.1 Occurrence of lateral destabilization in volcanic edifices

Before the lateral collapse of Mount Saint-Helens in 1980 (Voight et al., 1981; Lipman and Mullineaux, 1981), the occurrence of wide scars on volcanic edifices was explained as due to major erosion processes. The gravitational instabilities of Mount Saint-Helens provided a new interpretation on the origin of the large U-shaped structures affecting a large amount of volcanic edifices. Siebert (1984) proposed that the good correlation observed between the volume of scars and that of deposits on the flanks can be taken as an indicator that the main process involved in the formation of these features is a massive failure of a part of the volcanic cone. This is easily verified for recent landslide events while it is more difficult to establish this correlation for old events, mostly because of the erosion or filling of the scar and/or the reworking of the deposit. In this case, it is common to find a discrepancy between the volume of the deposit and the size of the scar.

In oceanic setting, the study of submarine parts of shield volcanoes and surrounding sea-floor by multi-beam and long-range side scan sonar techniques (Le Bas and Mason, 1996) underlined the major role of large-scale flank failure in the morphological evolution of volcanic oceanic islands. Flank collapse deposits started to be increasingly identified in most oceanic volcanoes, both on subaerial and submarine areas, such as in Hawaii (Moore et al., 1989 and 1994; Mitchell et al., 2002; Morgan et al., 2003; Figure 1.4), Stromboli (Kokelaar and Romagnoli, 1995; Tibaldi, 2001; Romagnoli et al., 2009a and 2009b), La Reunion Island (Duffield, 1982; Lénat and Bachèlery, 1990; Labazuy, 1996; Oehler, 2005; Oehler et al, 2008, Fig. 1.4), Canary Islands (Carracedo, 1994; Krastel et al., 2001; Masson et al., 2002; Mitchell et al., 2002; Hurlimann et al., 2004; Figure 1.4) and Lesser Antilles (Deplus et al., 2001; Le Friant et al., 2003) where these deposits were studied in terms of landslide processes and depositional mechanisms. In particular, about 70 huge landslide deposits are reported along

the submarine flanks of the Hawaiian chain (Moore et al., 1994, figure 1.4), being amongst the largest in terms of volume (table 1.1).

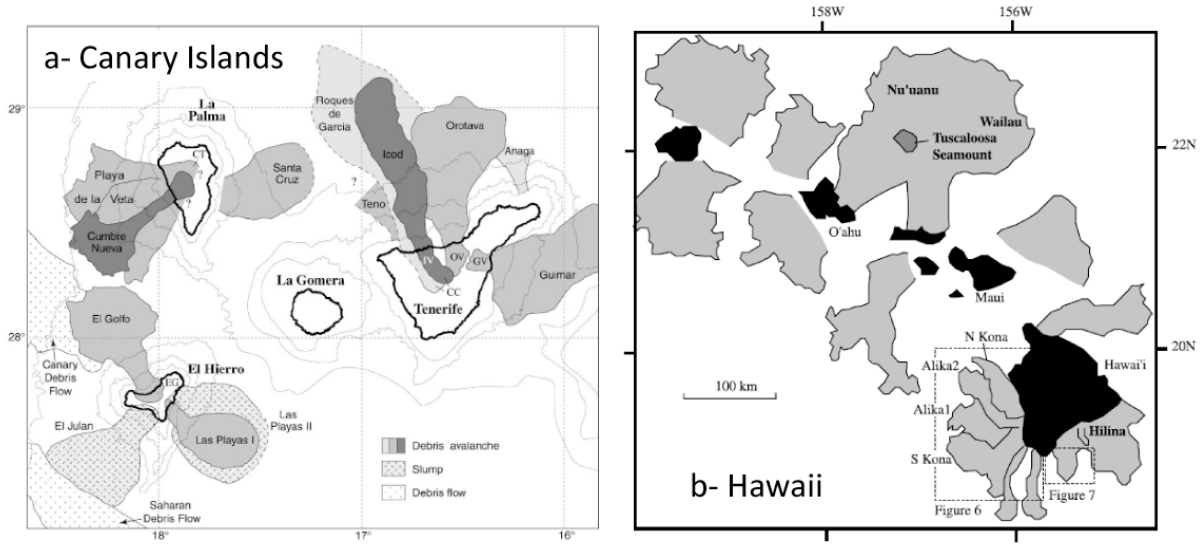

Figure 1.4: Major submarine landslide deposits identified offshore (a) Canary Islands (Masson et al., 2002), (b) Hawaii (Mitchell et al, 2002).

Moreover, the comparison of the volumes of the landslides between basaltic shields and basaltic stratovolcanoes (Table 1.1) reveals that for edifices of comparable size (large scale edifices like Etna and Piton de la Fournaise for instance), basaltic shield volcanoes are affected by more voluminous landslides than basaltic stratovolcanoes. In the submarine part of the Hawaiian chain, deposits with estimated volumes as high as 3000-5000 km^3 were identified, reaching areas located several hundreds of kilometres from their source (Fig. 1.4). Some major landslides also occurred in the Canary Islands (Fig. 1.4). However, the volume of the edifice is not the main factor responsible for the occurrence of lateral destabilizations on basaltic volcanoes as small edifices like Stromboli, Oshima-Oshima or Monowai also experiment recurrent collapses of their flanks (four major collapses occurred at Stromboli volcano in the last 13 kyrs, Monowai collapsed twice in the last 13 years…)

Volcano affected by the collapse	volume (km^3)	Volcano affected by the collapse	volume (km3)
Basaltic shield volcanoes		Basaltic stratovolcanoes	
Canary Islands		**Stromboli**	
El Golfo (El Hierro)	150-180	Paleostromboli	0.6 - 1
Las Playas 2 (El Hierro)	< 50	Vancori	2
Cumbre Nueva (La Palma)	95	Neostromboli	1
Orotava (Tenerife)	500	Pizzo sopra la Fossa	1
Hawaiian archipelago		Sciara del Fuoco	0.7
Alika 1 (Hawaii)	400	**Oshima-Oshima**	
Alika 2 (Hawaii)	200	1741 collapse	2.5
Wailau (Molokai)	1500	**Monowai cone**	
Nuuanu (Oahu)	3000-5000	1998-2004 collapse	0.09
North Kauai (Kauai)	1400	2004-2007 collapse	0.04
La Reunion Island		**Mount Etna**	
Piton de la Fournaise	500	Valle del Bove	16 - 21
		Fuji	1.8

Table 1.1: Volumes (in km3) of the main lateral collapse events that affected basaltic shield volcanoes and basaltic stratovolcanoes (from Moore et al., 1989; Holcomb et Searle, 1991 ; Hayashi and Self, 1992; Moore et al., 1994a; Mcguire, 1996; Clague and Moore, 2002; Masson et al., 2002; Tibaldi, 2001 ; Satake and Kato, 2001 ; Oehler, 2005; Pareschi et al., 2006 ; Chadwick et al., 2008 ; Romagnoli et al., 2009b).

These examples clearly indicate that the morphological evolution of all types of basaltic volcanoes is commonly made of alternating phases of growth and destruction of the edifices. In particular, an important role is played by lateral gravitational instability phenomena affecting volcanic edifices of variable sizes. These destabilizations are likely to occur at any step of the growth of basaltic volcanoes, either on hot spot volcanoes (Hawaii islands, Canary islands, La Reunion island, Capo Verde) or basaltic volcanoes located in active tectonic settings (Stromboli volcano, Monowai cone in the Kermadec or Mount Etna).

1.3.2 Controlling and triggering parameters of volcano flank collapse

1.3.2.1- Classification of the parameters

Volcanoes can be affected by repeated major flank collapses during their evolution. Flank failure occurs when the mechanical stability of an edifice is perturbed by an internal or external factor or when the edifice becomes unable to support its own load. Basically, a

sector collapse is a gravity-driven movement of a sector of the volcano, independently from its size, origin and type.

Several analogue and numerical studies have been carried out in the last years in order to better constrain the processes of collapse and the involved factors (Borgia, 1994; Russo et al., 1996; Van Wyk de Vries and Borgia, 1996; Lagmay et al., 2000; Tibaldi, 2001; Walter and Troll, 2003; Keating and McGuire, 2000; Apuani et al., 2005a and b; Acocella, 2005; Oehler et al., 2005; Tibaldi and Lagmay, 2006; Tibaldi et al., 2007).

Keating and Mc Guire (2000) proposed a first classification of the parameters involved in the control and/or trigger of lateral instability on volcanoes. They recognised internal parameters, referred to as "endogenetic", i.e. due to the structure of the volcano itself. For instance, the geometry of the edifice is a key factor: a volcano has to reach a critical load or a critical height before being possibly affected by sector collapses, On the other hand, these authors identified external parameters, referred to as "exogenetic", i.e. tectonic or environmental for example (Fig. 1.5 and Table 1.2). A more extensive discussion of the role of the parameters is carried out in section 1.3.2.2.

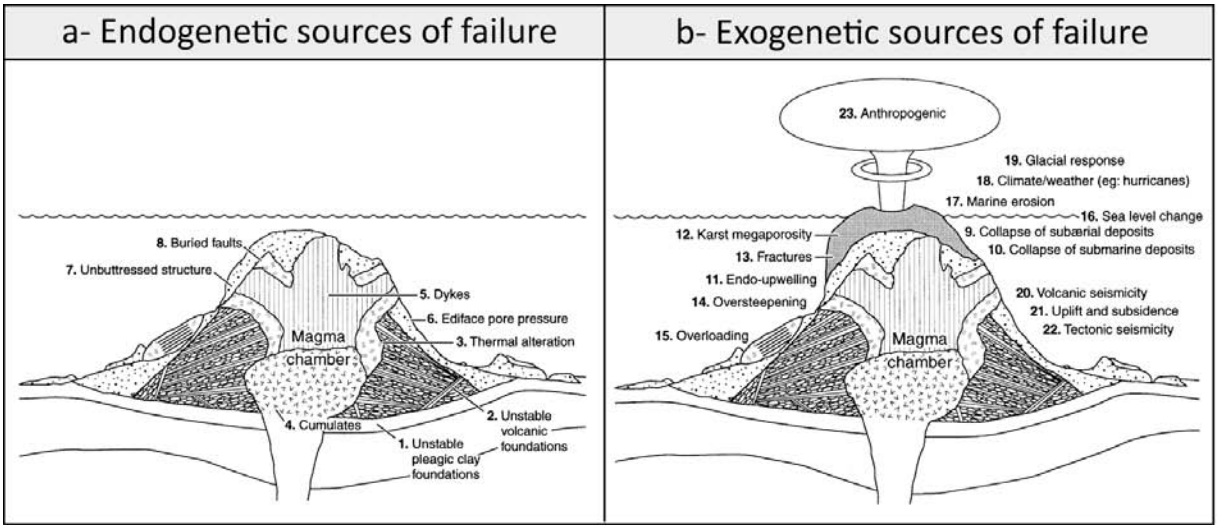

Figure 1.5: Endogenetic (a) and exogenetic (b) sources of failures on volcanic island edifices according to the classification of Keating and McGuire (2000).

Table 1.2 presents examples of lateral failure reported in different settings and the corresponding parameter of control/trigger involved in the failure mechanism.

a- Endogenetic sources of failure

Failure process	Mechanism	Examples
1. Unstable foundation—clays	Decoupling along low friction layer	Hawaii
2. Unstable foundations	Decoupling along low friction layer, with ball-bearing like character	Loihi, Savaii
3. Dykes	Physical displacement of flanks of volcano	Koolau Volcano (Oahu, Hawaii)
4. Cumulates	Physical displacement of flanks of volcano	Kilauea (Hawaii), Mt. Etna, Klyucherskoi volcano (Kamchatka)
5. Thermal alteration	Increase in pore pressure Reduction in strength	Hawaii
6. Edifice pore pressure	Liquidation of overpressured sediments	Mururoa, Ritter Volcano, Surtsey Volcano
7. Unbuttressed structure	Creep	Hawaiian Islands
8. Buried faults	Decoupling along pre-existing zone of low friction added overburden	Hilina System (Hawaii), Mururoa, Niue

b- Exogenetic sources of failure

Failure process	Mechanism	Examples
9. Collapse of subaerial deposits	Low cohesion material including ball-bearing like horizons, with low-friction surfaces, often dipping seaward	Hawaii, Ritter Island (PNG), Surtsey volcano (Iceland)
10. Collapse of submarine deposits	Low cohesion water-saturated material including ball-bearing like horizons, with low-friction surfaces	Savaii (Samoa)
11. Endo-upwelling	Excess pore pressure	Johnston Island, Mataiva, Niau lagoon (Mururoa), and Tikehau Atoll (Tuamotu chain)
12. Karst megaporosity	Void spaces and rocks of low mechanical strength	Johnston Island, Mid-Pacific Mountains, Mururoa Atoll
13. Fractures	Low mechanical strength	Johnston Island, Chapman Seamount, Mururoa Atoll, Horizon Guyot
14. Oversteepening	Low cohesion	Hawaii, Reunion Island, Canary Islands
15. Overloading	High pore pressure Low cohesion	Hawaii
16. Sea level change	Stress changes—foundation stress changes in magma chamber crustal loading/unloading	Hawaii, Pantelleria, Iceland
17. Marine erosion	Changes in pore pressures turbulence physically disrupting sediments and lavas	Hawaii
18. Climate Weather—hurricanes	Mass wasting high on volcano turbulence moving low cohesion rocks	Hawaii, Kahe Point, Oahu, Hawaii
19. Glacial response	Crustal loading	Pacific
20. Volcanic activity	Physical displacement of low cohesion material	Hawaii, Mt. St. Augustine, Ritter Volcano
21. Uplift and subsidence	Lithospheric flexure	Cross Seamount, Mehatia, Niue
22. Tectonic seismicity	Physical displacement of low cohesion material	Hawaii, Mururoa
23. Anthropogenic	Physical displacement of low cohesion material	Mururoa

Table 1.2: Examples of volcanic islands affected by endogenetic (a) and exogenetic-related (b) failures, with the corresponding main processes and mechanisms involved in the collapse event (from Keating and McGuire, 2000).

Endogenetic sources of failure are usually predominant in period of magmatic activity like during the shield-building stage of shield basaltic volcanoes for instance, while exogenetic sources can cause failure at any time of the evolution of the edifice. The nature of involved parameters seems to be partly time-related but the classification of Keating and McGuire (2000) does not take into account this information. Moreover, the fact that factors are endogenetic or exogenetic does not determine their role in the mechanism of lateral instability on basaltic volcanoes. As a consequence, we propose another classification of the factors of flank instability, based on time considerations in the evolution of the edifice. We

propose to distinguish the factors involved in long-term destabilisation processes from the ones involved in sudden destabilisation processes.

Long-term destabilizations	Sudden destabilizations
Basement of the edifice	Magmatic intrusions
Oversteepening	Seismic activity
Slopes overloading	Variation of edifice pore pressure
Low strength layers	Low strength layers
Uplift or subsidence	Neoformation of fractures
Environmental factors	

Table 1.3: Classification of the main factors involved in long-term destabilizations and sudden destabilizations (see 1.3.2b for description).

The classification presented in table 1.3 is not an exhaustive list of all the factors that might have a role in the mechanism of flank instability on basaltic volcanoes. Only the most important factors are introduced, some of them being involved both in long-term and sudden destabilization processes.

1.3.2.2- Role of the main factors of instability on basaltic volcanoes

In the following, the influence of some of the main factors involved in lateral instability affecting basaltic volcanoes is detailed (see table 1.2 for examples).

Factors of long-term destabilization processes

Role of the basement of the edifice

The role of the basement of volcanic edifices in the processes of lateral instability has been extensively studied in the past decades. Spreading of a volcanic edifice due to the deformation of a weak basement is a major process involved in the stability/unstability of volcanic flanks. Borgia (1994) showed that spreading occur at several scales, from

deformation of the substratum of a small scale edifice to the spreading of oceanic floor in the case of large shield volcanoes. According to Borgia (1994), the weight of the edifice onto its substratum and the long-term deformation of intrusive complexes are the main features involved in volcanic spreading. Experimental studies showed that spreading is controlled by the geometry and type of substratum and requires the presence of a low viscosity layer within the substratum (Merle and Borgia, 1996; Van Wyk de Vries and Matela, 1998). Spreading of a volcano is the consequence of the lateral flowing of the weak basement under the excess load of the edifice. When spreading is radial, inward-dipping structures (concentric ridges and thrust belts) are created at the bottom of the edifice, preventing lateral collapse of a volcanic flank (Merle and Borgia, 1996; Van Wyk de Vries and Borgia, 1996). However, when preferential spreading occurs in one direction (because of buttressing or the topography of the basement for instance), critical conditions of collapse can develop with the generation of outward dipping structures prone to favour sectorial instability (Van Wyk de Vries and Francis, 1997; Van Wyk de Vries et al., 2001). Lateral spreading was recognised at numerous volcanic edifices. Borgia (1994) established the major role of basal décollement in the basement spreading at Kilauea volcano. At Etna volcano, the southeastward movements of the flank of the edifice are partly correlated to the presence of weak sedimentary material within the basement (Borgia et al, 1992). Most oceanic shield volcanoes result from the development of a hot spot and lie on a seabed covered by weak oceanic sediments, easily deformable. Spreading of shield volcanoes associated to magmatic intrusions along rift-zones could generate lateral failures of the volcanoes as illustrated by the Hilina slump, which could result from the spreading of the southern flank of Kilauea volcano along pre-volcanism pelagic sediments (Moore et al., 1994; Morgan and McGovern, 2005a and b). On the basis of seismic investigations and numerical modelling of deformation, Got et al. (2008) showed that the oceanic crust underlying Big Island could control the growth of the Mauna Loa and Kilauea volcanoes. Indeed, the combined effects of the load of large Hawaiian shield volcanoes and the presence of weak material at the interface between the edifices and the oceanic crust are likely to control the morphology of hawaiian volcanoes and the occurrence of large destabilizations of their flanks.

At stratovolcanoes like Socompa volcano (Van Wyk de Vries et al., 2001), flank collapses and associated debris avalanches are interpreted as being the result of the spreading of the edifice along weak levels of ignimbrites. In some cases, like at Stromboli,

the direction of some collapses could be an effect of the dip of the substrate (continental slope) in this direction (Tibaldi et al., 2007). At some other edifices, the direction of failure is controlled by other factors, like the topography of the underlying surface (Siebert, 1984).

The reactivation of faults within the basement of a volcano is another factor that can contribute to trigger flank instability of the edifice. Collapse structures generally take place according to the tectonic framework of the region in a direction normal to the main volcanic and tectonic lineaments of the edifice (diking and fracturing trends, Tibaldi et al., 2007). Several authors underlined the influence of basements faults on the geometry of flank collapse (Merle et al., 2001; Tibaldi et al. 2005). Analogue models showed that the reactivation of a vertical fault below an edifice can generate a flank failure in the direction normal to the fault (Vidal and Merle, 2000; Merle et al., 2001).

Overloading of the flanks and oversteepening of the slopes

During the growth of basaltic edifices, extrusive activity is responsible for the accumulation of eruptive products (lava flows, fallout deposits…). Generally, volcanic flanks are in a state of stress at the equilibrium, the loading stresses due to topography and weight of the edifice being balanced by the stresses due to frictional forces (McGuire, 1996). The accumulation of material on the upper part a volcanic flank can increase the loading stresses and perturb this balance, generating local response (usually deformation) in order to re-establish the balance. If the amount of deformation created by the added load is sufficient to reach the failure threshold, part or the whole flank can be affected by lateral collapse.

The slopes of Hawaiian type shield volcanoes usually range from few degrees to 12° (Rowland and Garbeil, 2000). Some shield edifices, such as Piton de la Fournaise (La Reunion) and Canarian volcanoes, have peculiar slopes locally reaching 20 to 35°, especially on their submarine slopes. On stratovolcanoes, like Stromboli volcano, it is more common to find steep slopes reaching more than 35°. If the slopes of the volcano overcome the internal angle of friction of the material (of about 30°), the flank is likely to be affected by collapse. From this point of view, basaltic stratovolcanoes clearly have a greater potential for failure than shield volcanoes with more gentle slopes.

Volcano flanks submitted to lateral failure are commonly the less buttressed flanks of the edifices. The lack of lateral constraints favour the effects of slopes overloading and oversteepening on volcanic flanks free to glide, like the eastern flank of Etna facing the sea.

Neighbour volcanoes interact by buttressing each other flanks, as in the case of Mauna Loa and Kilauea in Hawaii, although the load added by the growth of the new edifice triggers spreading of the underlying flank (Morgan, 2006). At Piton de la Fournaise volcano (La Reunion Island), the unbuttressed eastern flank is unstable while the western flank remains stable as it is buttressed by the old Piton des Neiges volcano. Conversely, the presence of Les Alizés volcano on the southeastern flank of Piton des Neiges volcano likely prevented lateral destabilization of this latter in this direction. At Stromboli volcano, the northern flank is buttressed by the eroded Strombolicchio system, while the unbuttressed northwestern (Sciara del Fuoco) and southeastern (Rina Grande) flanks were recurrently affected by destabilizations (Romagnoli et al., 2009a and 2009b). The distribution of buttressed areas is thus one of the parameters that controls the location and geometry of areas prone to experiment lateral instabilities.

Low strength levels

- *Hydrothermal alteration*: long-term intense fluid circulations associated with hydrothermal activity within basaltic edifices, gradually weaken the core of the edifices favouring the alteration of volcanic material (Day, 1996). Famin and Michon (2010) proposed that hydrothermal alteration participated to a long-term slow mechanism of ductile deformation of the northeastern flank of Piton des Neiges volcano (La Reunion island).

- *Internal buried faults and mechanical heterogeneities*: long-term slipping of volcanic flanks can occur along buried detachment faults of internal mechanical heterogeneities within basaltic edifices like weak layers of pyroclastic material, hyaloclastites (Oehler et al., 2004) or volcaniclastic material (Masson et al., 2002). The superimposition of layers having different mechanical properties can create the heterogeneous conditions that favour preferential intrusions of magma along these discontinuities and cause flank deformation, enhancing collapse events if the threshold of mechanical disturbance of the flank is reached. Weak layers made of fallout deposits can also be low-strength layers acting as sliding planes along which large flank movements can occur (Oehler et al, 2005).

- *Presence of cumulates within the edifice:* Clague and Denlinger (1994) proposed that the ductile deformation affecting hot cumulates within Kilauea volcano would be a source of pressure on the southern flank of Kilauea, enhancing instability.

Vertical movements of the edifice

Uplift or subsidence of edifices under their own weight might perturb the stress equilibrium within the edifice. Subsidence of a volcanic edifice under its own weight is responsible for the sagging of the volcano, stabilizing the edifice (Van Wyk de Vries and Matela, 1998). The presence or absence of lithospheric flexure below hot spot shield volcanoes has an influence on the stability of the edifice. Conversely, a large landslide of volcanic flank can have isostatic consequences. Smith and Wessel (2000) estimated that the giant Nuuanu collapse (Hawaii) generated large lithospheric uplift, up to 100 m, in order to re-establish stress equilibrium.

Environmental causes of failure

Several basaltic oceanic volcanoes are located in areas submitted to tropical climates (Hawaii, La Reunion, Canary). A high precipitation rate may increase the chemical alteration of rocks to clays (as found in the breccia deposits associated to landslide events at Piton des Neiges volcano, La Reunion island, Famin and Michon, 2010), modify the pore pressure by water circulation trough rocks and the erosion rate (Iverson, 2000).

Sea level changes and marine erosion are other two factors involved in the stability of volcanic slopes: they participate to the construction and destruction of shore platforms surrounding the edifices and playing a role in the buttressing of volcanic flanks. A decrease of sea level fall can act on the state of stress of the edifice, the water pore pressure inside it and the erosion rates possibly enhancing flank instability (Menard, 1983; Iverson, 1995).

Factors of sudden destabilization processes

Influence of magmatic intrusions along rift-zones

Magmatic intrusions occur over long time-spans along preferential directions creating volcanic rift zones. The formation of the rift zones takes place in the early stages of the growth of the volcanic edifices (McDonald, 1972; Carracedo, 1996). Two types of rift zones can be distinguished:

- Deep rift zones whose direction is related to basement and crustal structures (Walker, 1999), where the magma path to the surface is controlled by the regional tectonic stress field.

- Intra-edifice rift zones that form at the periphery of collapse structures due to the weakening and fracturing of the area surrounding the collapse scar (extensional stress related to lateral movements facilitates magma intrusion to the surface, Tibaldi, 2004).

Several field studies carried out on Hawaiian islands (Walker, 1986 and 1987; Zbinden and Sinton, 1988) reveal the importance of magmatic intrusions in the structure of basaltic volcanoes as they allow the internal growth of a volcano. The relationship between dike intrusions and collapse on basaltic volcanoes has been broadly studied and there are numerous evidence that magma injection can trigger volcano collapse by "mechanical alteration" of its structure due to accumulation of incremental displacements associated to repeated intrusions along rift zones (Iverson, 1995; Elsworth and Voight, 1995). Displacements triggered by repeated intrusions of magma increase gradually the slopes of basaltic volcanoes. The intrusion of magma can be facilitated by lateral spreading of a volcanic edifice, causing extensional stress in the summit region and the formation of fractures at his surface as occurred at Kilauea and Etna volcanoes (Clague and Denlinger, 1994; Walter et al., 2005). Cryptodome intrusion is another trigger of lateral instability as testified by the 1980 collapse at Mount Saint-Helens (Lipman and Mullineaux, 1981; Donnadieu et al., 2001).

Eruptive activity, coupled with volcano-tectonic seismicity during crisis, is a common trigger of volcanic landslides. Walter et al. (2005) evidenced a clear interaction between magmatic events and flank failure during the 2002-03 crisis at Etna volcano. Flanks movements at Kilauea volcano have been correlated to magmatic activity (Delaney et al., 1993). At Piton de la Fournaise volcano (La Reunion island), the connection between magmatic activity and flank deformation during the April 2007 eruptive crisis is clear but has not been explained yet. Based on the example of the neighbour Piton des Neiges volcano, some authors suggested that the displacements observed on the eastern flank of the edifice could be generated by a sill intrusion but this hypothesis has not been tested yet (Famin and Michon, 2010).

Eruptive activity is also responsible for the overloading of the flanks of the edifice by volcanic material and the oversteepening of the volcano slopes.

Seismic activity

Seismic events (in subduction zones or in areas where regional crustal faults are active, for instance) are powerful triggers of volcano flank instability. Several examples were reported, where tectonic earthquakes triggered landslides, like in Ecuador (Tibaldi et al., 1995) or in Hawaii (1975 Kalapana event; Owen and Burgmann, 2006) that enhanced an incremental collapse of the southern flank of Kilauea volcano. It seems reasonable to assume that volcanic environments are also prone to experiment failure caused by regional seismic activity. Tectonic earthquake along a basement fault is prone to trigger lateral instability on basaltic volcanoes

Some studies showed that volcanic seismicity associated to caldera collapse on basaltic volcanoes could trigger flank instability: Marti et al. (1997) and Hurlimann et al. (1999) proposed that the seismic activity related to the formation of Las Canadas caldera on Tenerife island generated the flank destabilizations of Icod and La Orotava.

Low strength levels

- *Hydrothermal alteration*: hydrothermal alteration is not only involved in long-term mechanism of failure but also on sudden ones. In deed, together with slow alteration processes by hydrothermal fluids, rapid changes in temperature and pore fluid pressures can generate mechanical conditions under which a rapid failure of a volcanic flank can occur (Day, 1996). Reid et al. (2001) showed that heating from remote magma intrusion at depth can generate temporarily elevated pore fluid pressures in the edifice, capable of triggering flank destabilizations.
- *Internal buried faults and heterogeneities*: similarly to hydrothermal alteration, buried faults and internal heterogeneities participate to both processes. Failure are generally instantaneous phenomena that require rapid movements along pre-existing sliding planes to explain the extension of the deformation associated with flank movements and the large distances travelled by debris avalanche.

Edifice pore pressure

Magma pressure, creating a change in the pore pressure of the edifice, is an efficient mechanism of lateral collapse (Iverson, 1995; Elsworth and Day, 1999; Apuani et al, 2005).

Indeed, an increase in pore pressure reduces the frictional resistance along a sliding plane encouraging the effect of gravity on the unstable area. Another consequence of magma intrusion within volcanic edifices is the thermal effects resulting from the hot magmatic fluids responsible for alteration and weakening of the surrounding rocks, increasing their potential for failure (Elsworth and Day, 1999). The edifice pore pressure can also be modified under the effect of sea level changes (Iverson, 2000). Gressier (2010) showed that pore fluid pressure within a volcanic edifice plays a major role in determining the conditions and depth at which sills can be intruded.

The classification we present here is one possibility. Flank deformation and instability on basaltic volcanoes results of the combined effects of several of these factors, whose relative importance is difficult to evaluate (Mitchell et al., 2002). It explains in part why the mechanisms of flank failure on volcanic edifices remain only partially understood.

Chapter 2

Comparative study of two end-member basaltic systems: La Reunion Island and Stromboli Island.

Basaltic magmatism is found in all tectonic settings and the related volcanic edifices can have a wide range of morphologies and structures (see chapter 1), so that each type of volcano has its own characteristics. Here, the large-scale shield edifice of La Reunion is compared to the small-scale stratovolcano of Stromboli.

This chapter is divided into several sections : 1- Geological context of the studied areas, in order to characterize the main geodynamic and tectonic features of the two systems (part 2.1); 2- Evolution of La Reunion and Stromboli volcanoes (part 2.2); 3- Morpho-structural comparison of the two edifices is then carried out (part 2.3) in order to point out the main similarities and differences that may account in the understanding of the evolution of each area, and finally, 4- Summary giving a synthetic comparison of main features of both edifices and of factors involved in lateral instability for each of them (part 2.4).

This chapter aims at bringing preliminary answers to the following questions: 1- What is the influence of the morphology (nature, volume, slopes, structural features) and the geodynamic context of the volcanic edifices on the mechanisms that control their evolution ? 2- Which are the main processes (among those discussed in Chapter 1) involved in the evolution of La Reunion and Stromboli, with particular regards to flank destabilizations? 3-Do all basaltic volcanoes experiment a similar evolution, whatever their geometries and environments of formation?

2.1- Geological settings of the studied areas

This section introduces the main geodynamic and tectonic features of the areas of La Reunion and Stromboli, together with some insights on the crustal seismicity occuring in the areas.

2.1.1- Aeolian islands

The Aeolian Islands form a 150-km-long volcanic structure, the Aeolian Volcanic System (AVS), made of several active (Stromboli, Vulcano), recently active (Lipari, Panarea, Salina) or extinct (Alicudi, Filicudi) volcanoes (Fig. 2.1). The AVS lies on a 15-25-km-thick continental crust, between the southern Tyrrhenian Sea back-arc basin and the Calabrian arc, in a subduction context displaying an unusual tectonic complexity (Fig. 2.1) and encompassing active volcanism (Etna, Aeolian islands) and seismic activity (Goes et al., 2004). The Aeolian volcanism is the current manifestation of volcanic activity started during the Pliocene in the central sector of the Tyrrhenian Sea (de Astis et al., 2003). Many authors interpreted the existence of a volcanic arc as related to the active subduction of the Ionian lithosphere beneath the Calabrian Arc (Barberi et al., 1974; Ferrari and Manetti, 1993; Fig. 2.1). However, according to some others, the subduction process would have stopped about 1 Myrs ago and volcanism would be the consequence of post-subduction extension (Milano et al., 1994; Carminati et al., 1998).

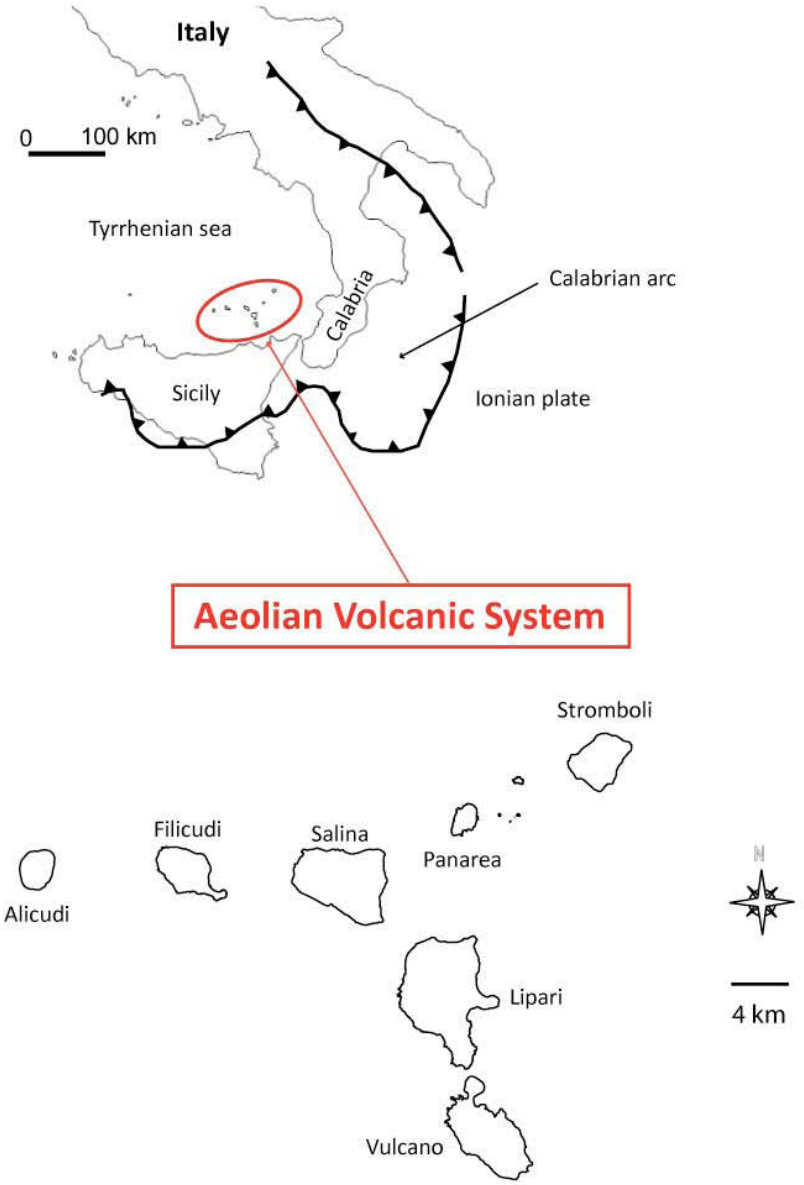

Figure 2.1: Geodynamic settings of the Aeolian Volcanic System located in the southern Tyrrhenian back-arc basin formed by the subduction of the Ionian microplate below the Calabrian arc (de Astis et al., 2003; Goes et al., 2004).

The regional structural setting of the AVS shows a complex stress field and a strong fragmentation (figure 2.2a). The Tindari-Letojanni lineament is a regional NNW-SSE trending lithospheric fault system displaying strike-slip movements (De Astis et al., 2003). The Aeolian archipelago can be divided into 3 parts: 1- a western part with extinct volcanism (Alicudi and Filicudi) controlled by the Sisifo-Alicudi fault system (Fig. 2.2a; Bortoluzzi et al., 2010), striking WNW-ESE (Manetti et al., 1989). 2- a central part characterized by historically active (Lipari and Vulcano) or recently active

(Salina) volcanic centers aligned along the Tindari-Letojanni fault system, and 3- an eastern branch with Panarea (where post-magmatic exhalative activity occurred also in 2002) and the persistently active Stromboli volcano likely controlled by a NE-SW oriented regional lineament, made of normal faults (Tibaldi, 2001; DeAstis et al., 2003).

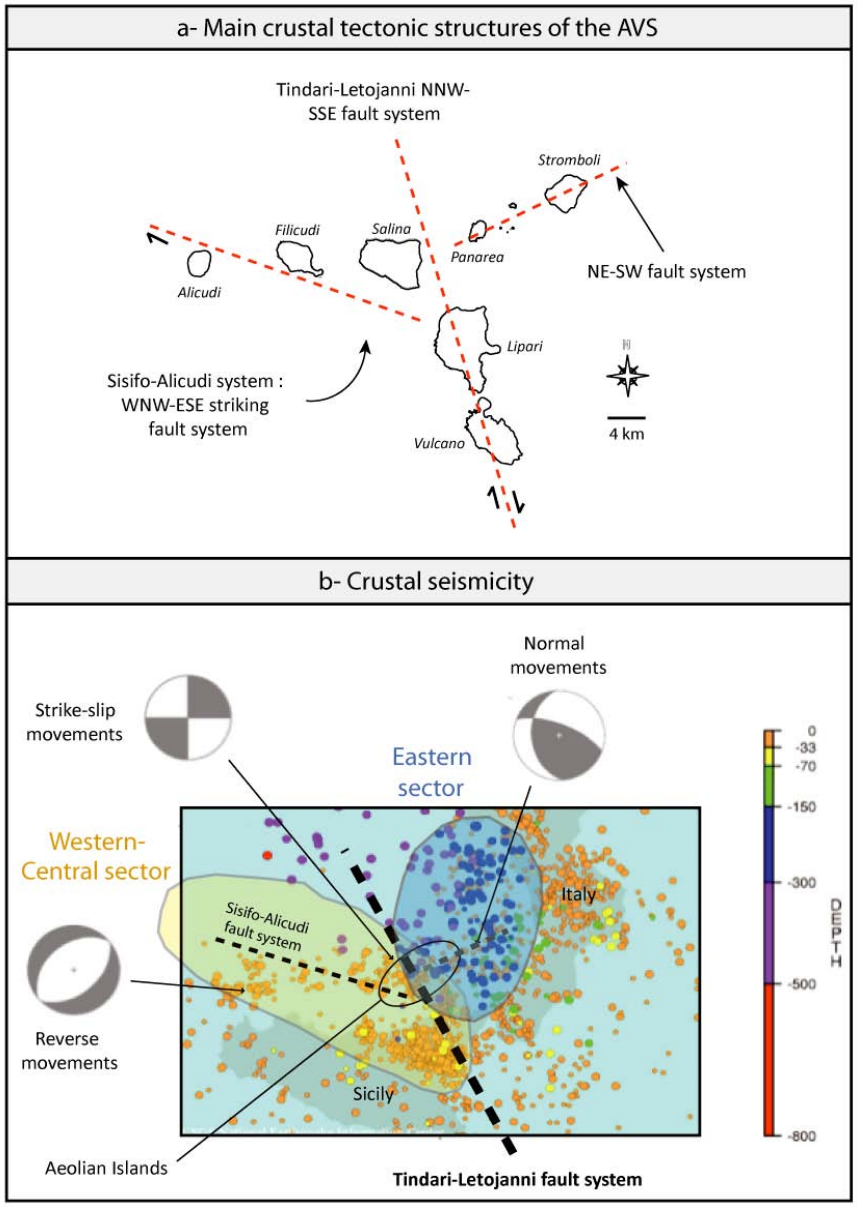

Figure 2.2: a- Sketch of the three main structural lineaments affecting the Aeolian Volcanic System; b- Distribution of crustal seismicity in the southern Tyrrhenian Sea for the period 1981-1996. The depth of the hypocenters of the earthquakes, main tectonic lineaments and the nature of the movements are indicated (modified from the USGS International Earthquake Information Center and De Astis et al., 2003, respectively).

The intense shallow crustal seismicity of the southeastern Tyrrhenian Sea proves that most faults are still active today (Jenny et al., 2006). Two different domains are identified from the distribution of the seismicity (Anderson and Jackson, 1987; DeAstis et al., 2003; Fig. 2.2b). The eastern domain is limited in the south and the east by the Calabrian arc and in the west by the Tindari-Letojanni fault. This area shows a low level of shallow crustal seismicity compared to the rest of the AVS (Falsaperla et al., 1999), probably due to the uprising of the isotherms located below, causing a mechanical strength weakening at crustal depth and preventing the storage of large stress in the crust (De Astis et al., 2003). In this sector, the earthquake focal mechanisms of the intermediate to deep events indicate an extensional regime which agrees with the development of normal faults in the crust (Fig. 2.2b). The focal mechanisms of low-magnitude tectonic earthquakes (Falsaperla et al., 1999) show in fact that both Panarea and Stromboli are affected by NW-SE extension, with major regional normal faults oriented NE-SW (de Astis et al., 2003; Fig. 2.2a). This extension is related to the rapidly extending Marsili oceanic basin at the north of the AVS and the southeastward migration of the Calabrian arc (DeAstis et al., 2003; Goes et al., 2004; Jenny et al., 2006). According to Gvirtzman and Nur (1999 and 2001) and Faccenna et al (2011), the whole area is likely affected by regional uplift, due to the rebound of the upper plate in the subduction zone causing mantle upwelling.

The western-central sector shows a shallow level of seismic activity, located in the upper 20 km of the crust. The earthquakes are mostly gathered along the Sisifo-Alicudi and Tindari-Letojanni fault systems, with prevalent reverse movements in the western sector and strike-slip movements in the central part. The western sector is not affected by intermediate and deep seismicity (Fig. 2.2b).

The Tindari-Letojanni fault system thus clearly separates two completely different tectonic domains, with distinct volcanic and seismogenic characteristics (Falsaperla et al., 1999): the eastern sector, characterised by active volcanism and intermediate and deep seismicity, can continue its expansion towards the SSE, while the western sector, with an extinct to recent volcanism, remains “blocked” (Falsaperla et al., 1999).

The complexity of the geodynamic and tectonic framework, the diversity of seismic activity and the magmatic characteristics described above make the Aeolian Volcanic System a complex subduction-related volcanic arc (De Astis et al., 2003). The different structural organization of various sectors of the archipelago have a major influence on the magmatic plumbing systems and is reflected by the different growth and evolution of the Aeolian volcanoes.

2.1.2- La Reunion Island

La Reunion is a 5 My-old shield volcano located east of Madagascar, in the eastern part of the Mascarene Basin, Indian Ocean (Gillot et al., 1994; Fig. 2.3b). Its formation could be the most recent manifestation of a hotspot activity initiated about 67 million years ago with the eruption of the Deccan Trapps (Courtillot et al., 1986; Duncan et al., 1989, Fig. 2.3a).

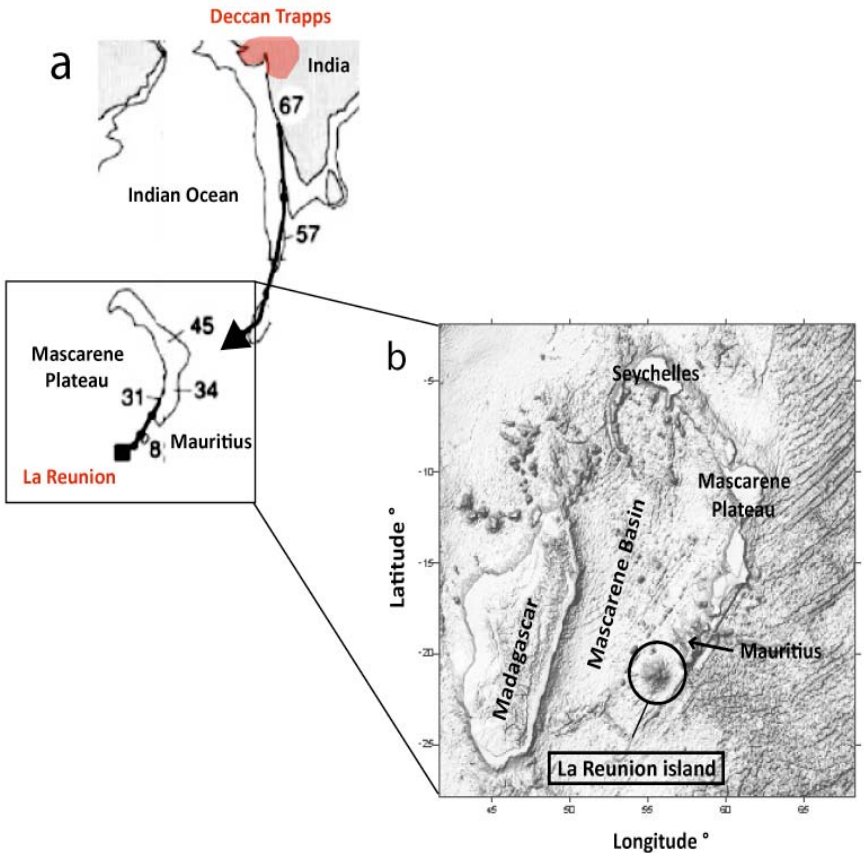

Figure 2.3: Geodynamic settings of La Reunion Island hotspot volcanic system (a, from Mahoney et al., 2002) inside the Mascarene basin (b).

La Reunion rises on a Paleocene oceanic crust, surrounded by an oceanic paleoridge oriented NW-SE in the south, and two transform faults at the NW and SE (the Mahanoro-Wilshaw and Mauritius faults, respectively, Fig. 2.4 and 2.5) and few isolated seamounts are present W-SW of the island.

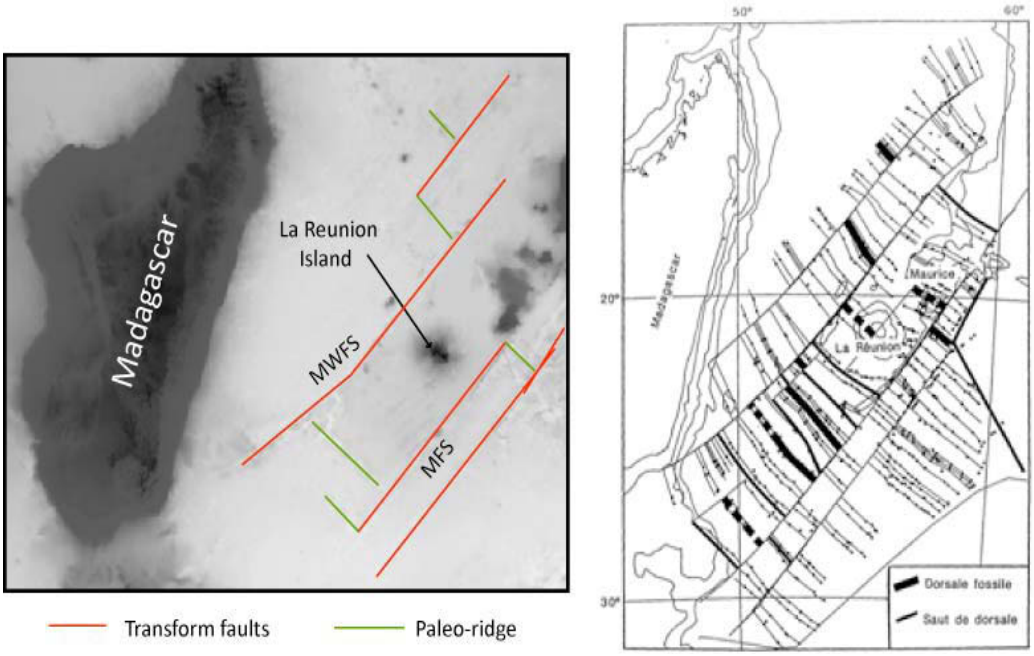

Figure 2.4: Main tectonic structures (transform faults) around La Reunion Island (from Schlich et al., 1990) and associated paleomagnetic patterns. MWFS = Mahanoro-Wilshaw fault system; MFS = Mauritius fault system.

In the vicinity of La Reunion, the transform faults form linear relieves oriented N 30-40°, parallel to the main structures of the Mascarene basin (Schlich et al., 1990; Oehler, 2005, Fig. 2.5). These faults systems are the natural boundaries of the volcanic system of La Reunion (Lénat et al., 2009; Fig. 2.4). The second main orientation is represented by the magnetic anomalies of the oceanic crust which trend in the N120-130° direction (Fig. 2.4). Secondary several minor faults are oriented N 55-60° and N 70-80°(Schlich et al., 1990; Fretzdorff et al., 1998; Lénat et al., 2001).

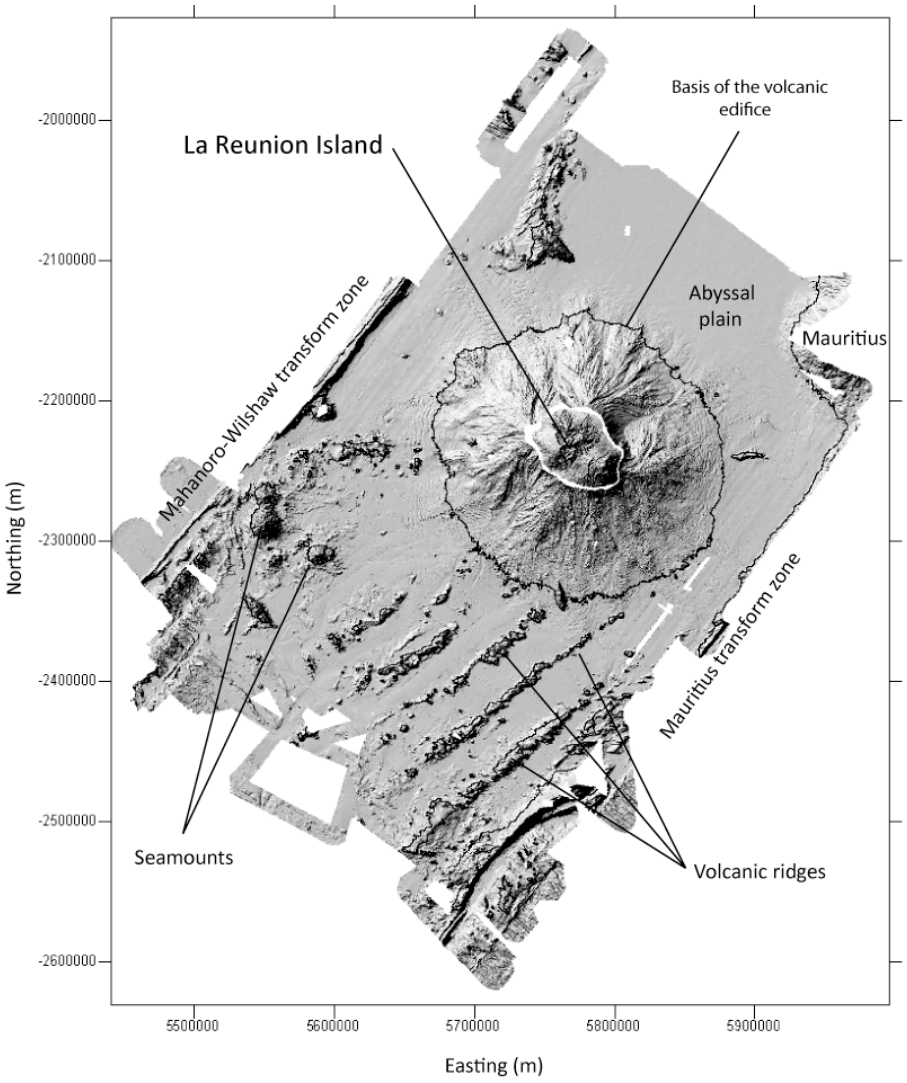

Figure 2.5: Bathymetry of the edifice of La Reunion and the surrounding oceanic floor (coordinates in UTM WGS 84). Data from the FOREVER and ERODER oceanographic campaigns.

Although a few earthquakes are recorded below the flanks of La Reunion and in the surrounding area (until about 100 km away from the island but they cannot be precisely located with the current seismic network of the Piton de la Fournaise volcano observatory), the level of crustal tectonic activity is considered very low in the vicinity of the island, meaning that the normal faults formed during oceanic accretion below the island and the main transform faults surrounding La Reunion are now probably inactive.

Data from seismic reflection revealed some interesting information about the crustal structure of La Reunion volcanic system: unlike Hawaii, Tenerife and Capo Verde, La Reunion island is not affected by crustal flexure due to the weight of the edifice (de Voogd et al., 1999; Gallart et al., 1999; Fig. 2.6). Michon et al. (2007a) proposed that the absence of flexure at La Reunion would be the consequence of the combined effects of 1- a thermal lithosperic erosion favoured by the small amount of displacement of the island relative to the hotspot (Charvis et al., 1999) and 2- magmatic underplating as testified by geophysical data (Charvis et al., 1999; Gallart et al., 1999; Fig. 2.6). Driad (1997) identified a layer of high seismic velocities that could correspond to magmatic under-plating below the edifice (Fig. 2.6). The existence of a low velocity zone evidences that the island lies on a sedimentary cover at the transition between the crust and the volcanic edifice.

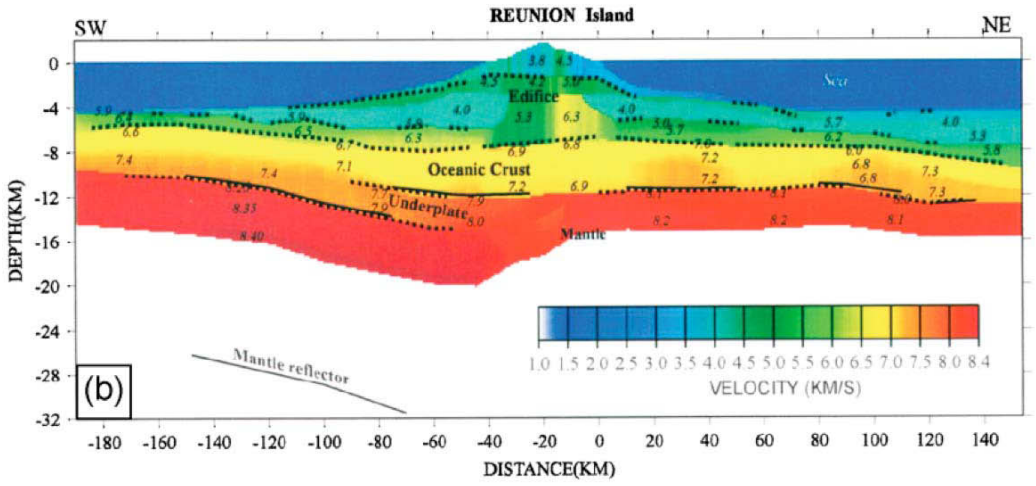

Figure 2.6: Seismic reflexion data showing the absence of crustal flexure below the edifice of La Reunion (Gallart et al, 1999).

2.1.3- Summary of main geologic characteristics of the studied volcanic systems

The settings of the two areas underline that La Reunion and Stromboli are end-member basaltic islands, located in very different geodynamic contexts (tectonically active or not). The major crustal structures controlled the growth of both volcanic edifices (Tibaldi et al., 2007; Michon et al., 2007a). They still play a role

in the evolution of Stromboli volcano but no longer have direct influence at La Reunion.

	Stromboli	La Reunion
Geodynamic context	subduction-related volcanism	hotspot volcanism
Nature of crust	15 to 25 km-thick continental crust	few km-thick oceanic crust
Regional tectonic setting	NW-SE extension	inactive Mascarene basin
Main fault trends	NE-SW fault system	N 30-40° and N 120-130° crustal faults
Secondary faults	NW-SE second-order structures	N 55-60° and N 70-80° crustal structures
Nature of faults	mostly normal NE-striking faults	normal faults below the island + transform zones in the vicinity
Crustal seismicity	mostly intermediate and deep earthquakes along main fault system	very low crustal seismicity
Age	110 kyrs (subaerial parts)	5 Myrs

Table 2.1: Summary of the main tectonic and geologic characteristics of Stromboli and La Reunion.

2.2- Evolution of Stromboli and La Reunion volcanoes (Piton des Neiges/Piton de la Fournaise).

This section aims at summarizing and comparing the main evolution stages of the volcanic systems of La Reunion and Stromboli, and tries to determine what is the influence of the geological framework and morpho-structural setting of these volcanic edifices on their evolution. Do similar structures and morphology lead to similar evolution? Do different geodynamics imply different evolution?

2.2.1- Evolution of Stromboli volcanic system

Together with the eroded Strombolicchio eruptive centre and some minor (eccentric) submerged vents, the composite volcano of Stromboli forms an 18 km long, a roughly NE-trending volcanic structure (Fig. 2.7). The lava neck of Strombolicchio is the remnant of a mostly eroded volcano, with an age of 204±25 ka

(Gillot and Keller, 1993) and a calc-alkaline basaltic-andesite composition. Rocks cropping out in the subaerial part of Stromboli have ages between 100 ka and the present days (Gillot and Keller, 1993) and were emplaced by effusive and explosive activity. Nowadays the volcano is in a persistent (Strombolian) explosive activity, with less frequent paroxysmal explosions and lava effusions (Rosi et al., 2000). Stromboli lies on a 15-to-25-km thick continental crust (De Astis, 2003) of the Sicilian-Calabrian slope, that forms the basement of the edifice (Boccaletti et al., 1984).

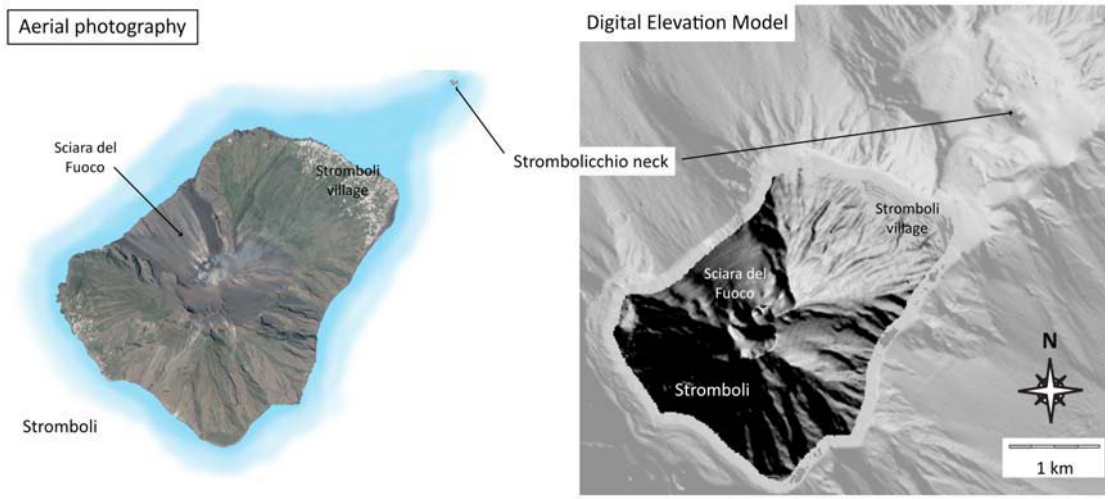

Figure 2.7 : a- Aerial view of the Island of Stromboli and the Strombolicchio neck ; b- Digital Elevation Model of the volcanic system of Stromboli (Stromboli + Strombolicchio).

A succession of collapse events has been reconstructed in the subaerial evolution of Stromboli (Tab. 2.2). The older (< 85 kyrs) history of the volcano is characterised by the occurrence of mainly vertical caldera collapses (Pasquarè et al., 1993; Tibaldi et al., 1994) whereas in the recent stages recurrent lateral collapses affected the northwestern flank of the island. Here, in particular, 4 major co-axial collapses were identifed for the last 13 kyrs, on the basis of field studies (Tibaldi, 2001, Fig. 2.8); the related deposits have been identified offshore (Romagnoli et al., 2009b; Fig. 2.9). The last lateral collapse formed the Sciara del Fuoco depression about 5000 years ago (Pasquarè et al., 1993; Kokelaar and Romagnoli, 1995; Tibaldi, 2001). Tibaldi et

al. (1994) estimated the collapse recurrence periods at 21 ky in the oldest stage and 4 ka in the youngest stage.

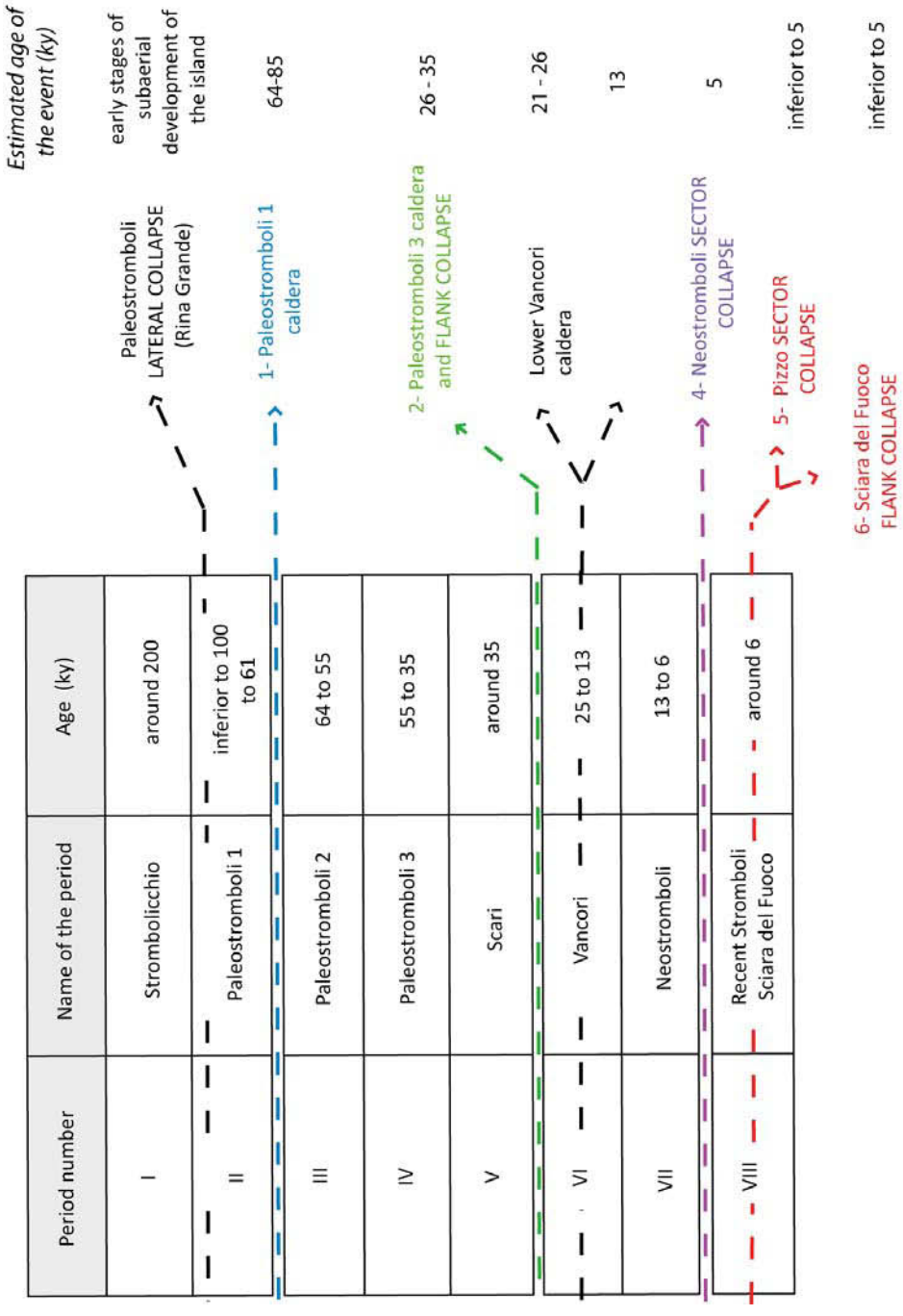

Table 2.2: Synthetic table summarising the volcanological evolution of Stromboli and related petrochemical characteristics. The succession of collapse events is also indicated (from Gillot and Keller, 1993; Pasquaré et al., 1993; Tibaldi et al., 1994; Tibaldi 2001 and 2003; Romagnoli et al., 2009a; see appendix 2 for the geological map of the island).

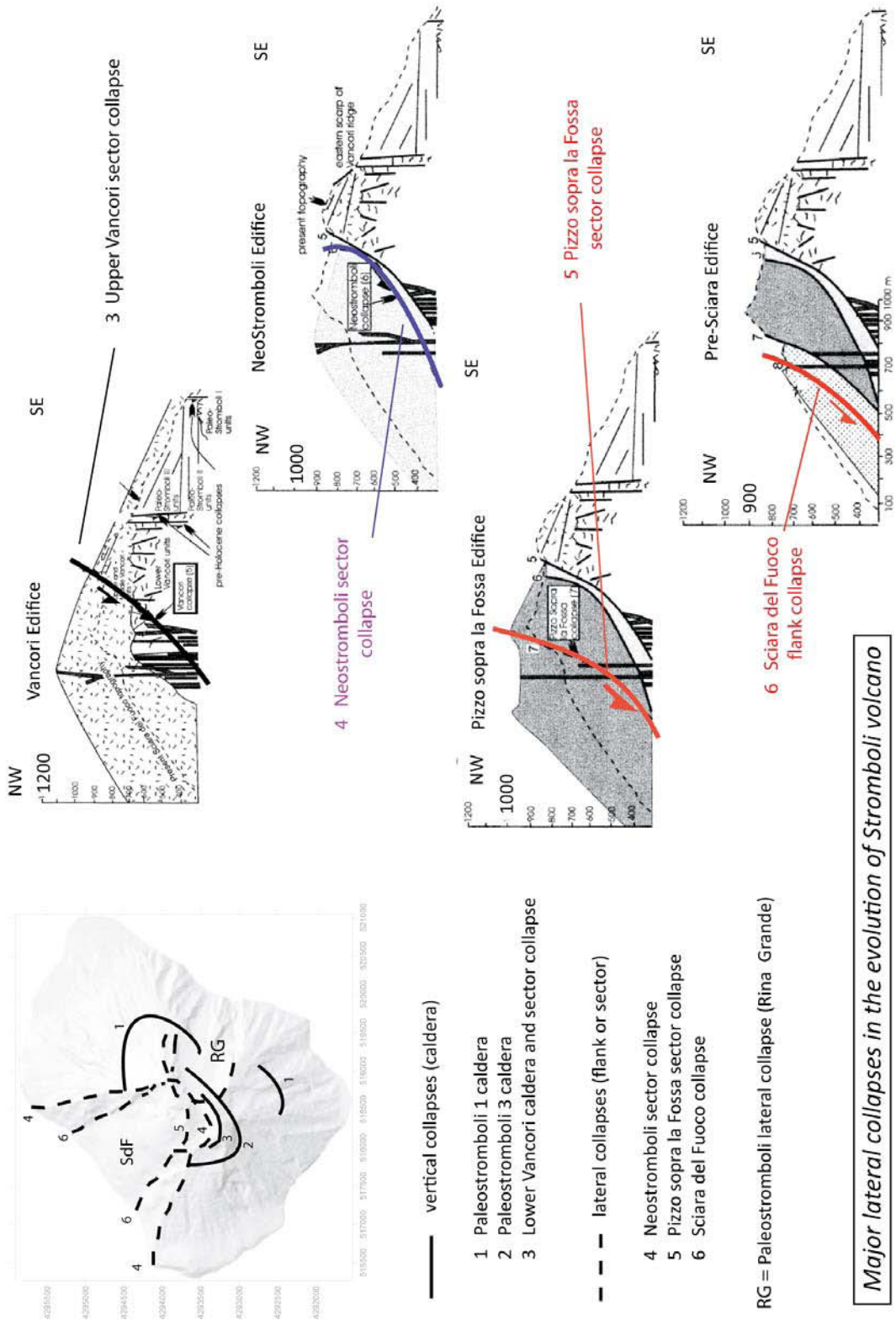

Figure 2.8: Morpho-structural evolution of Stromboli volcano in the last 13 ka, with the 4 major lateral collapses with affected its northwestern flank and created the Sciara del Fuoco feature (SdF). Numbers and colors of different events correspond to that of table 2.2.

Recently, the existence of major collapse scars in the Rina Grande area, on the eastern flank of the island, has been claimed from geophysical techniques and submarine data (Finizola et al., 2002 and 2003; Romagnoli et al., 2009a). The recognition of debris avalanche deposits on the eastern submarine flank of the island (Romagnoli et al., 2009a) suggested that repeated lateral collapses might have affected also this flank of the island (Fig. 2.9) and pointed out a structurally-controlled, bilateral flank instability of the volcanic edifice. The shifting of the main sliding direction from the eastern flank (where only shallower and smaller-scale landslides occurred in subsequent times) to the northwestern one, was accompanied by the migration of the eruptive activity on the island.

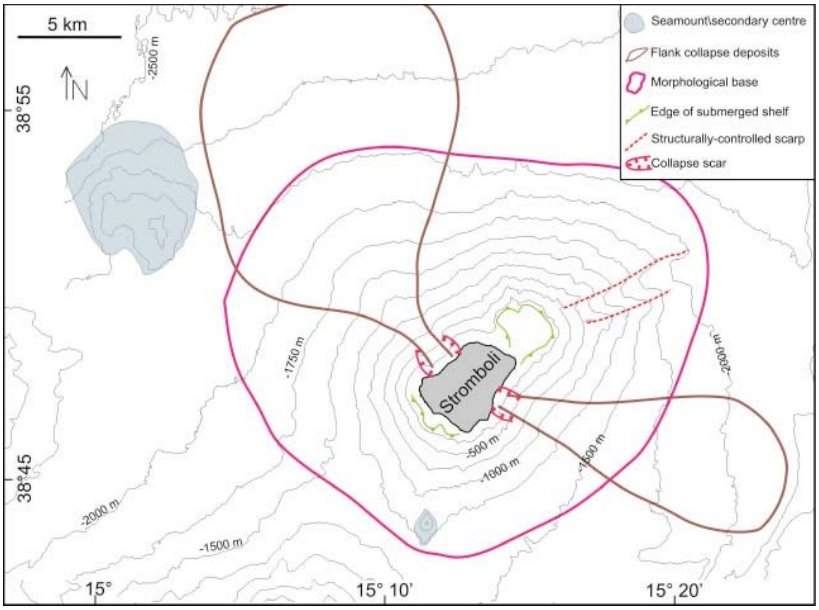

Figure 2.9: Submarine deposits associated to mass-wasting event affecting the northwestern and southeastern flanks of Stromboli volcano (from Romagnoli, in press, modified).

2.2.2- Evolution of La Reunion

La Reunion develops on a complex oceanic plate (Lénat et al., in press), whose structures play a major role in the volcano-tectonic evolution of the edifice (Michon et al., 2007a). It is a complex volcanic edifice made of 3 coalescent volcanic systems (see appendix 1 for the geological map). The subaerial part of the edifice is made of the Piton des Neiges and Piton de la Fournaise volcanoes, under which lies the hypovolcanic complex of Les Alizés volcano, nowadays totally dismantled (Fig. 2.10).

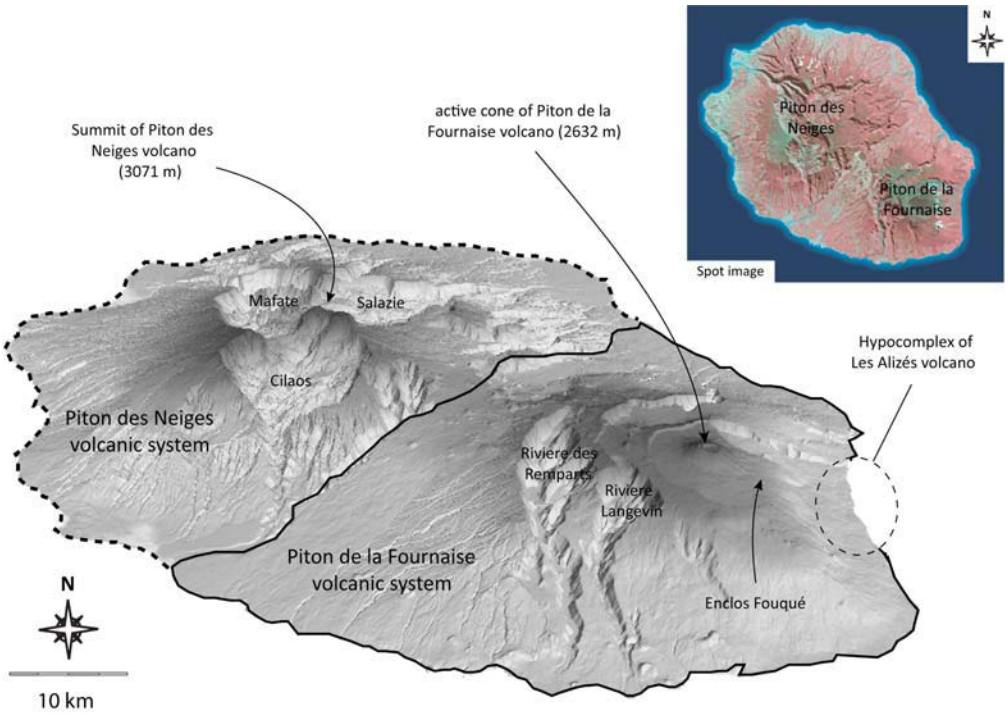

Figure 2.10 : The subaerial part of La Reunion volcanic edifice, with the three volcanic systems : the dormant Piton des Neiges volcano, the active Piton de la Fournaise volcano and the dismantled Les Alizés volcano.

The hypocomplexes of Piton des Neiges and Les Alizés are clearly identifiable on the Bouger anomaly map of La Reunion (Fig. 2.11), while no internal body seems to be associated with Piton de la Fournaise volcano.

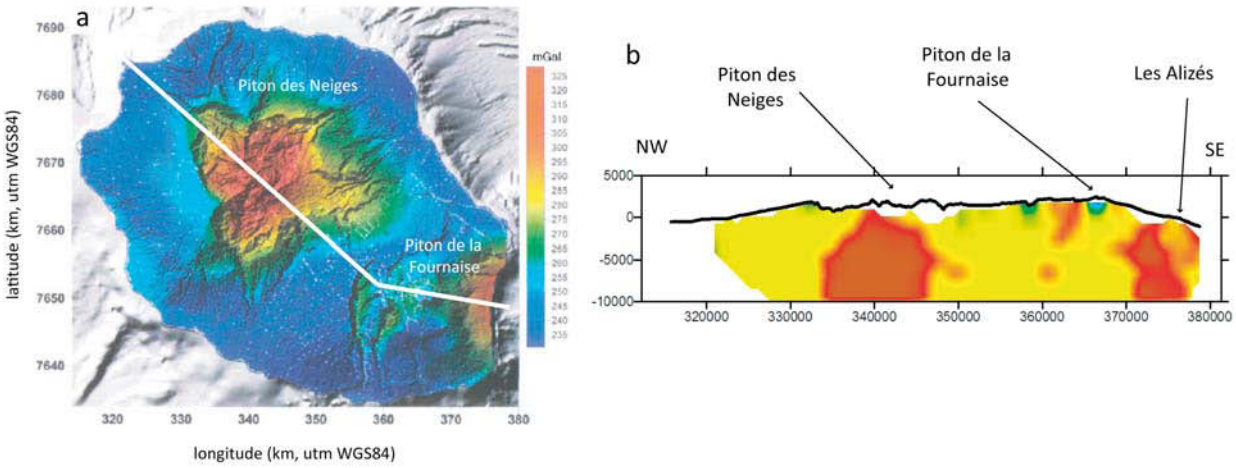

Figure 2.11: Map of gravity Bouger anomalies (a) and corresponding cross-section (b) (From Levieux, 2004; Malengreau et al., 1999).

The main growth and evolutionary stages of these three volcanoes are hereafter summarized:

Piton des Neiges volcano

The early formations of Piton des Neiges volcano were dated at 2.1 Ma (McDougall, 1971) and the last eruptive products at 12 ky (Deniel et al., 1992). Based on the lithologies and stratigraphical units, 4 phases are distinguished in its evolution (Upton and Wadsworth, 1965 and 1972; Billard and Vincent, 1974, Fig. 2.12):

- **Phase I** (pre 2.1 Myrs): submarine construction of the lava shield by superimposotion of picritic lava flows
- **Phase II** (2.1 - 0.43 Myrs) : intense growth of the volcano which emerges (Chevallier, 1979).
- **Phase III** (0.35 – 0.23 Myrs) : the activity restarts after a period of quiescence of 0.08 Myrs. Emissions of differenciated basalts represent 10 % of the volume of the massif (Gillot and Nativel, 1982).
- **Phase IV** (0.23 – 0.012 Myrs) : this is the last stage of the evolution of the volcano, made of several explosive phases whose products represent a low volume of the current edifice.

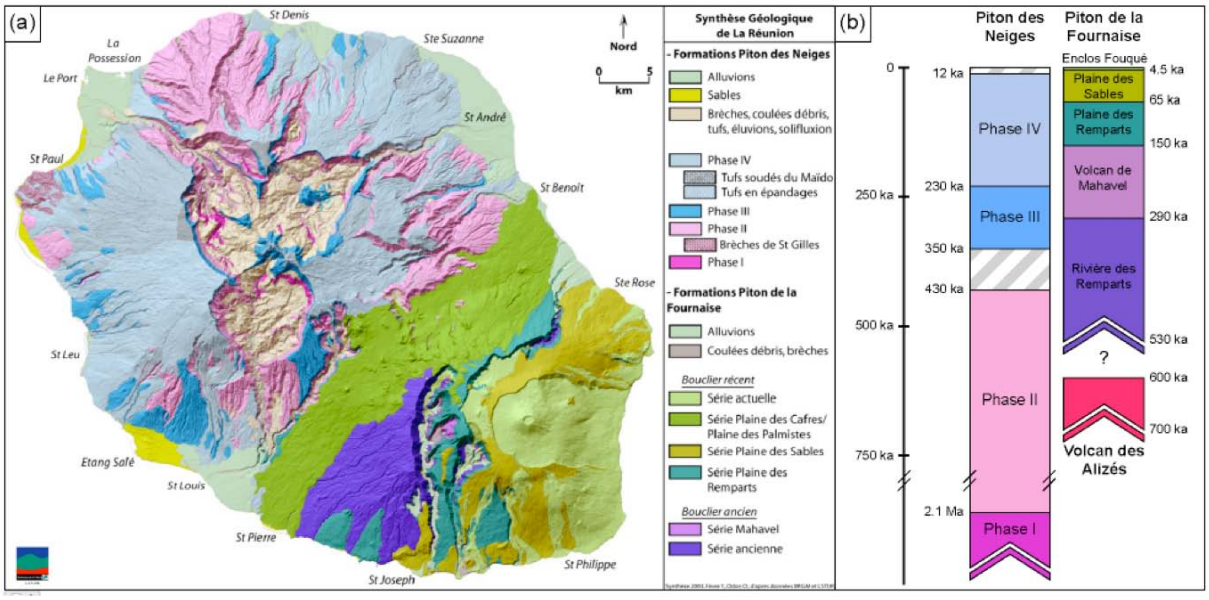

Figure 2.12: Synthetical geological map and geological history of Piton des Neiges and Piton de la Fournaise volcano (Kluska, 1997 and Welsch, 2010, see also appendix 1).

Piton des Neiges was affected by 3 major phases of destruction made of recurrent sectorial destabilizations of the northwestern, southern and northeastern flanks of the edifice, giving birth to the cirque of Mafate (> 1 Myrs), Cilaos (1 - 0.45 Myrs) and Salazie (0.6 – 0.43 Myrs) respectively (Kluska, 1997; Oehler, 2005; Fig. 2.10). Some debris-avalanche deposits were correlated to these events, both inland (Bret et al., 2003) and offshore, on the submarine flanks of the island (Oehler et al., 2008; see section 2.3.2.2).

Les Alizés volcano

The existence of Les Alizés volcano was recently discovered, thanks to magnetic and gravimetrical measurements and a drilling campaign carried out in 1986 in the Grand-Brulé (Rançon et al., 1989), which evidenced the presence of a dense magmatic body (made of gabbro and dunites) below the eastern flank of Piton de la Fournaise volcano. Recent datings at 3.3 Myrs by Smietana et al. (2010, appendix 6) on a submarine sample show that Les Alizés volcano emitted the oldest products identified on La Reunion. Its activity was partly contemporaneous with the activity of Piton des Neiges volcano until 0.5 Myrs, when the activity ceased because of the construction of Piton de la Fournaise west of Les Alizés volcano (Fig. 2.10). Products of its dismantling are found on the submarine slope of Piton de la Fournaise (Fig. 2.13).

Piton de la Fournaise volcano

The massif of Piton de la Fournaise lies on the eastern part of La Reunion Island (Fig. 2.10 and 2.13). It has been active since 530 ky ago (Gillot et al., 1990) and the construction of the edifice occurred in two stages, called the « old shield building phase » and the « recent shield building phase » (Fig. 2.14).

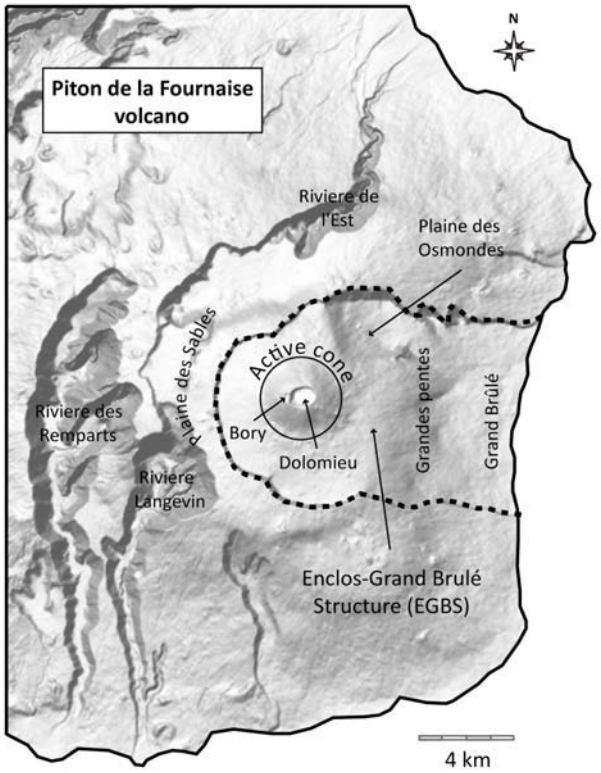

Figure 2.13: DEM and main features of the subaerial part of Piton de la Fournaise volcano (La Reunion).

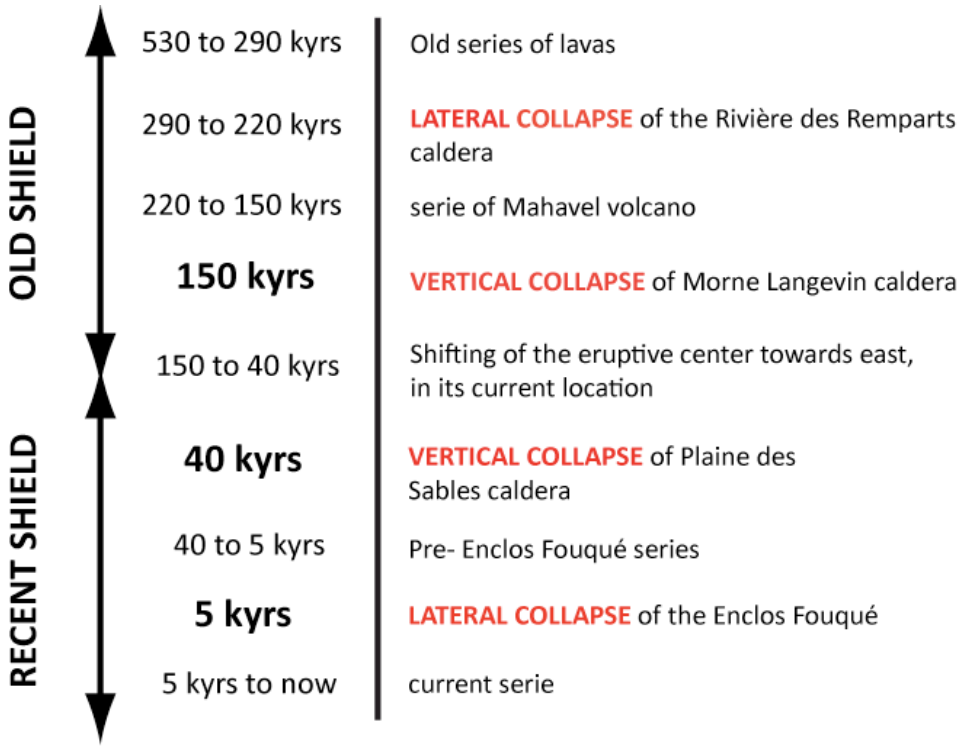

Figure 2.14: Synthetic geological history of Piton de la Fournaise volcano, with the main collapse events affecting the edifice.

The volcano experimented at least 4 main stages of collapse (Gillot et al., 1994; Merle et al., 2010, Figs. 2.14 and 2.15), which were responsible for the shifting of the eruptive center towards the east.

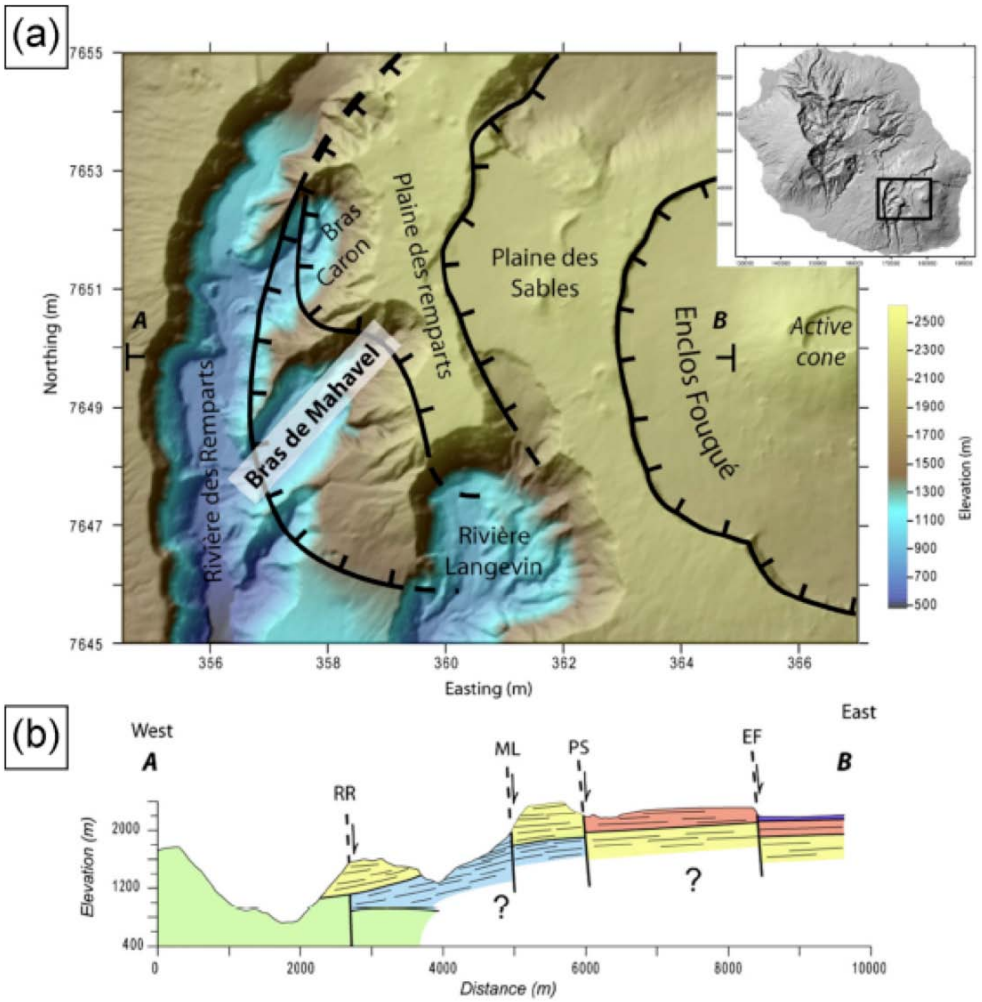

Figure 2.15: a- DEM of the southeastern part of La Reunion Island showing the 4 main collapse scars that crosscut the Piton de la Fournaise volcano; b- Simplified cross-section of the 4 collapse structures: RR = Rivière des Remparts, ML = Morne Langevin, PS = Plaine des Sables, EF = Enclos Fouqué (Merle et al., 2010).

The essential (96 %) of the current volcanic activity takes place within the Enclos Fouqué « caldera » (Villeneuve and Bachèlery, 2006, Fig. 2.16), whose origin is still a matter of debate (Michon and Saint-Ange, 2008). The eruptions of Piton de la Fournaise volcano are summital (as they occur within or at the periphery of summit craters Bory and Dolomieu, Fig. 2.13), lateral (if they occur on the flanks of the edifice) or distal (Peltier et al., 2007).

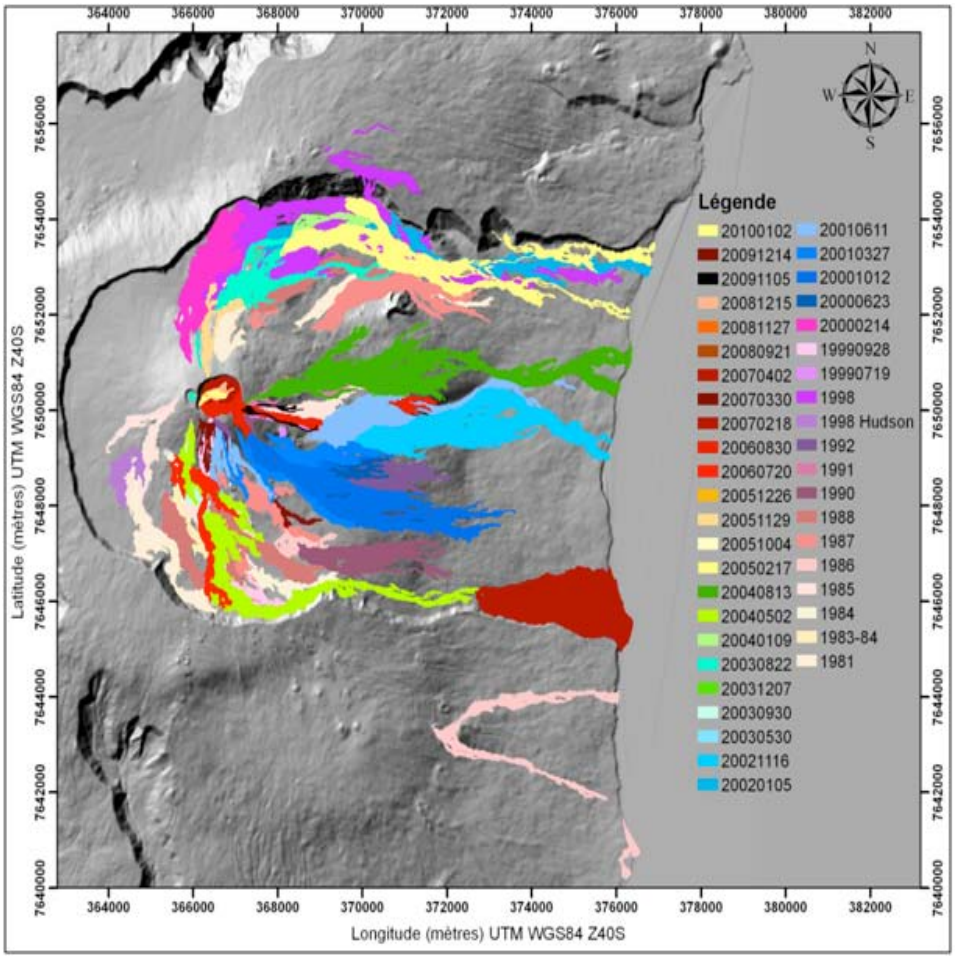

Figure 2.16: Post-1981 eruptions at Piton de la Fournaise volcano and associated lava flows (Servadio et al., 2008, appendix 8)

Together with lateral collapse, Piton de la Fournaise volcano is also affected by summit caldera collapses, like the one of April 2007; the study of this summit caldera collapse at Piton de la Fournaise is integrated to this study through an article to which the author of this thesis cooperated (Michon et al., 2009b, appendix 9).

2.3- Morpho-structural comparison

Differences in the geodynamics and tectonic activity of the studied areas commonly imply differences on the morphology and structure of the related volcanic edifices (Russo et al., 1996; Van Wyk de Vries et al., 1996; Merle et al., 2006; Michon et al., 2007a; Oehler et al., 2007) and on their evolution. In this section, a comparison of main morphological and

structural characteristics is made, in order to point out differences and similarities between La Reunion and Stromboli volcanoes. Before this, some indications are given on the nature and size of both volcanic edifices, enhancing the different scale of the two systems.

2.3.1- Nature and volumes of the volcanic edifices

As indicated in the previous section, both Stromboli and La Reunion are made of several coalesced eruptive centers (Fig. 2.7 and 2.10). The construction of both edifices is the result of interactions between the different volcanoes over time.

Stromboli Island is a polygenetic stratovolcano (the subaerial part is younger than 110 ky), rising up to 3 km above the seabed, with a maximum altitude of 924 m at the summit. The volcano is bounded by the Stromboli Canyon to the east and to the north. To the SW, a saddle connects Stromboli with nearby Panarea volcano. The submarine extension of the volcanic edifice can be described as symmetrical pattern with respect to a NE-SW axis. The most prominent feature of the NE flank is Strombolicchio Canyon, a major, flat-bottomed, N65°E oriented erosional feature (Fig. 2.17). Calculations made from the 10 m DEM of Stromboli, assuming that the basis of the edifice is located at a depth of -2200 m, give an approximate volume of the whole edifice of 334.8 km^3. Bosman et al. (2009) proposed that the subaerial portion of Stromboli edifice represented 2 % of the whole edifice. We re-estimated this volume at 1.13 % of the volume of the whole edifice. The volcanic edifice of La Reunion, is a flattened cone with a diameter of about 200 km and a height around 7000 m (Fig. 2.17b). Calculations on the new DEM of La Reunion edifice (obtained from oceanographic campaigns FOREVER and ERODER) give a total volume of about 51500 km^3. The subaerial part of the island estimated to 3% by de Voogd (1999) has been reappraised to 4.2% from the new bathymetry.

Nevertheless, the two edifices are absolutely not comparable in terms of volume. Calculations made on the basis of the DEMs of the two areas show that Stromboli represents approximately 0.7 % of the volume of La Reunion. This fact has to be taken into account when comparing the two systems.

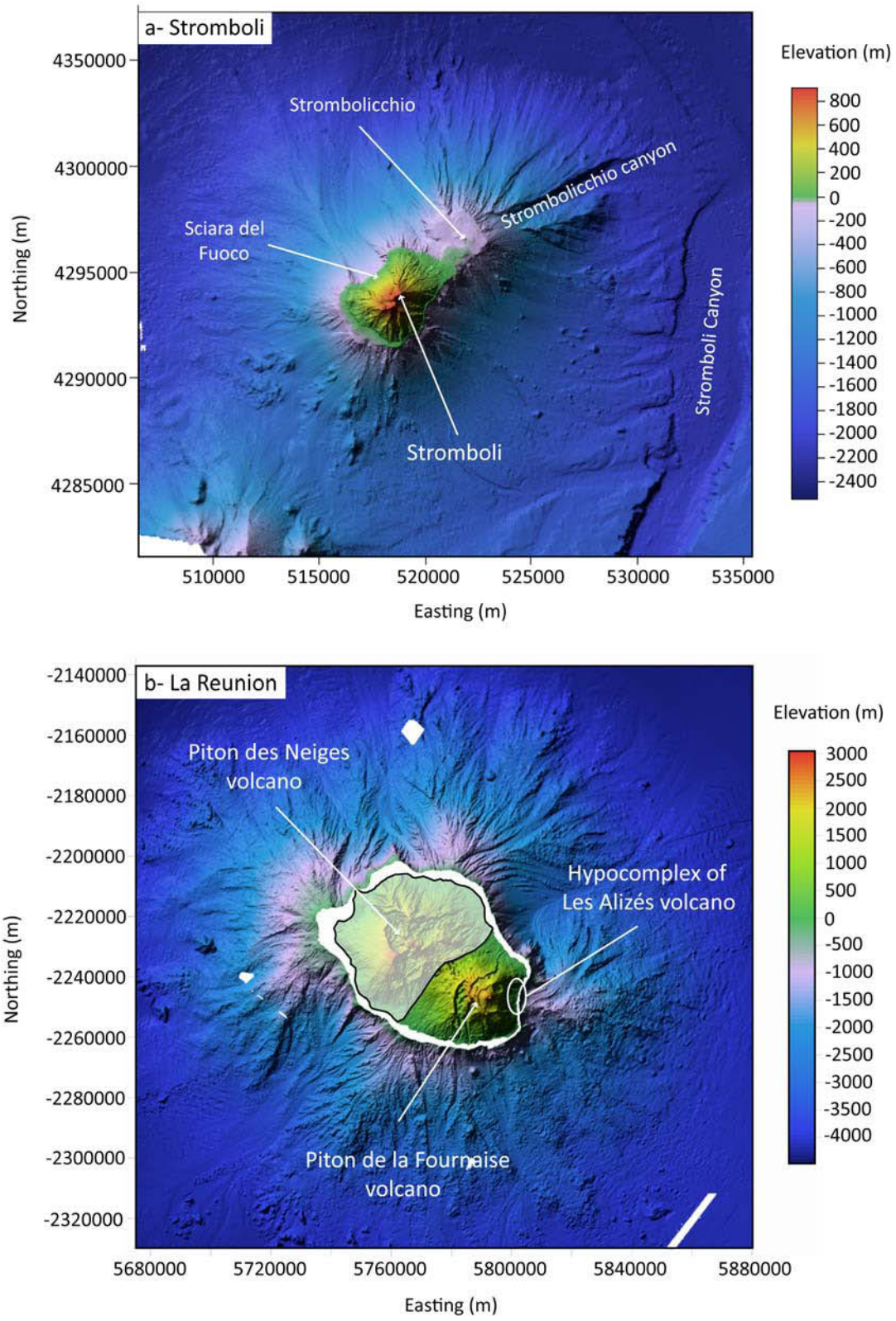

Figure 2.17: DEM of La Reunion (b) and Stromboli islands (a): both volcanic edifices are made of several coalesced eruptive centers. Data of the submarine and subaerial parts of Stromboli island from Bosman et al., 2009; Topography and bathymetry data of La Reunion island from the Institut Géographique National and from the FOREVER and ERODER missions; DEM of Stromboli from University of Roma and University of Bologna.

2.3.2- Morphological and structural features

The morphology of volcanic flanks is permanently modelled by volcanic constructional processes, landslides, erosional and sedimentary processes or tectonic movements. In volcanic edifices like La Reunion island (Lénat and Labazuy, 1990; Labazuy, 1996; Oehler 2005; Oehler et al., 2004 and 2007), Hawaii (Lonsdale, 1989) and most oceanic volcanoes, the growth of submarine portions is driven by the rate of intrusion within riftzones (see part 2.3.3) and the provision of sediments by lateral collapses. This latter phenomenon can affect the submarine flanks of a volcano contributing to its morphological evolution, as erosion processes do by creating canyons, gullies, etc.… The comparison of the submarine flanks of Hawaiian and Canary islands carried out by Mitchell et al. (2002) revealed that although both systems present similar characteristics, some major differences occur. These authors showed that the flanks of these islands are covered with debris avalanche deposits, associated with volcanic features and structures related to vertical movements of the islands. However, a detailled analysis reveals major differences in the nature of the deposits, the geometry of the volcanic features and the amplitude of vertical movements. Mitchell et al. (2002) suggested that these differences could be partly related to the age of the systems, their different geometries (slopes) and the different magma supply rate between Canary and Hawaiian islands, emphasizing the role of a range of factors on the morphology of basaltic edifices.

2.3.2.1- Morphology of the flanks of Stromboli and La Reunion edifices

Topographic profiles have been drawn across La Reunion and Stromboli (Fig. 2.18). Apart from the obvious discrepancy in the size of the edifice, the profiles also show that the slopes differ from an edifice to the other (Fig. 2.18, 2.19 and 2.20). La Reunion and Stromboli edifices are elliptical in shape. Slope profiles, as shown by Fig. 2.18 are not symmetrical. The NE-SW profile of La Reunion (red line on Fig. 2.18) is a section of the area located at the transition between the lower slopes of Piton des Neiges and Piton de la Fournaise volcanoes. Due to its position, this area is less affected by constructional and destructional processes that affect the other parts of the edifice, as the volcanic flanks themselves, and is gentler. The NW-SE profile of La Reunion (blue line on Fig. 2.18) is a central transverse section of the two edifices of Piton des Neiges and Piton de la Fournaise,

through areas submitted to volcanic construction and destruction by landslides and erosional processes. On the submarine part, the slopes of the submarine SE and NE flanks have very similar geometries, with a steep slope close to sea level that tends to decrease slowly with depth. On the contrary, the submarine NW and SW flanks exhibit different morphologies. The SW submarine flank has steeper slopes than the NW flank of La Reunion edifice. Similarly, the two profiles of Stromboli island show some similarities but also some major differences. The NW-SE profile exhibit general steeper slopes than the SW-NE profile, and no major slope break occur on the flanks of the edifice along a NW-SE oriented section. This orientation corresponds to the direction of main flank collapse events affecting Stromboli. On the contrary, the SW-NE section shows a slight slope break on the southwestern flank and an important slope break on the northeastern flank, not affected by collapse events.

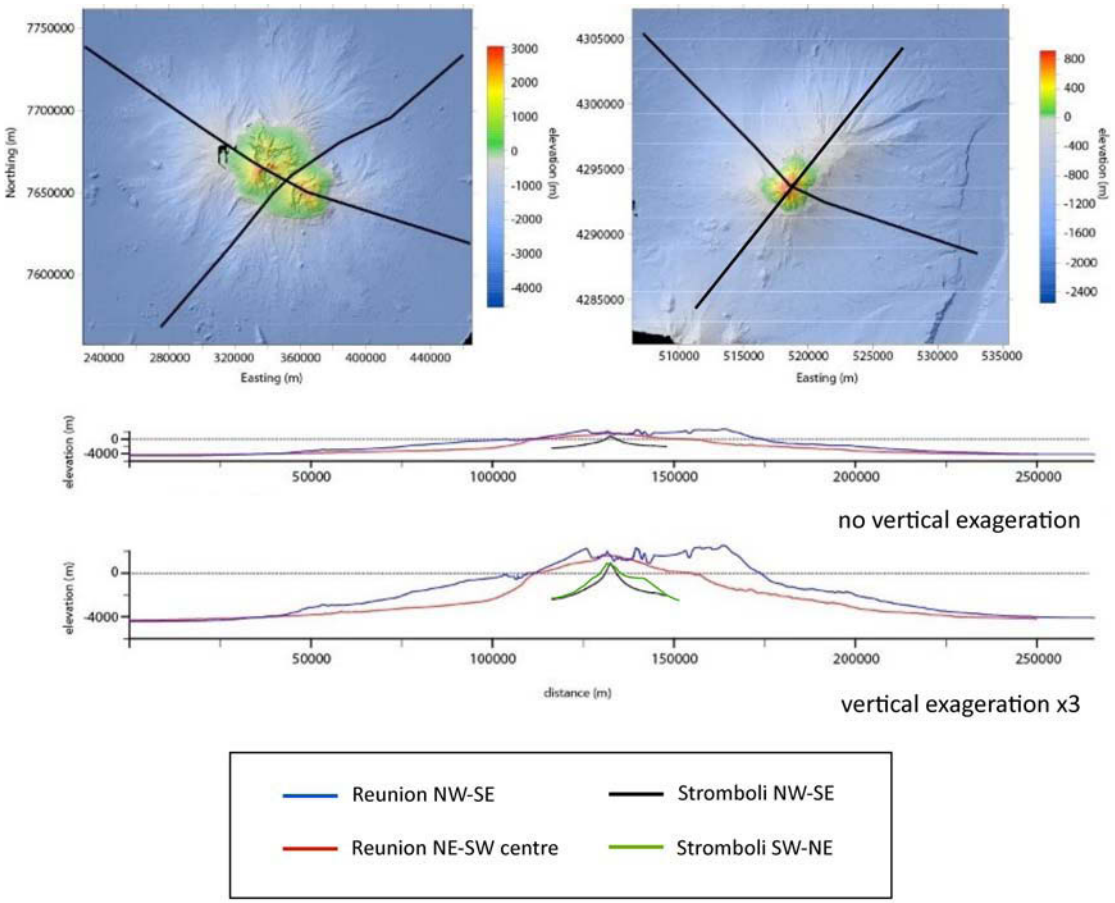

Figure 2.18: Topographic profiles across the edifices of La Reunion (NW-SE and NE-SW sections) and Stromboli (NW-SE section). No vertical exaggeration on the upper profiles and x3 vertical exaggeration on the lower profiles.

At Stromboli, the “buttressed” flanks are represented by the NE and SW flanks where earlier volcanic products (presently cutted by insular shelves down to about −120/−150 m) are present, particularly on the NE flank, due to the presence of Strombolicchio vent (Romagnoli et al., 2009a; Casalbore et al., 2010, Fig. 2.19a). These flanks show high gradients of their upper slopes (> 30°) and are marked by slope breaks. On the contrary, the unbuttressed NW and SE flanks show a continuous concave upwards profile, with a gradual (quasi exponential) lowering in the slope (Fig. 2.19a). Their remarkably-similar overall geometry is due to the similar structural, volcanic and depositional setting (Romagnoli et al., 2009a).

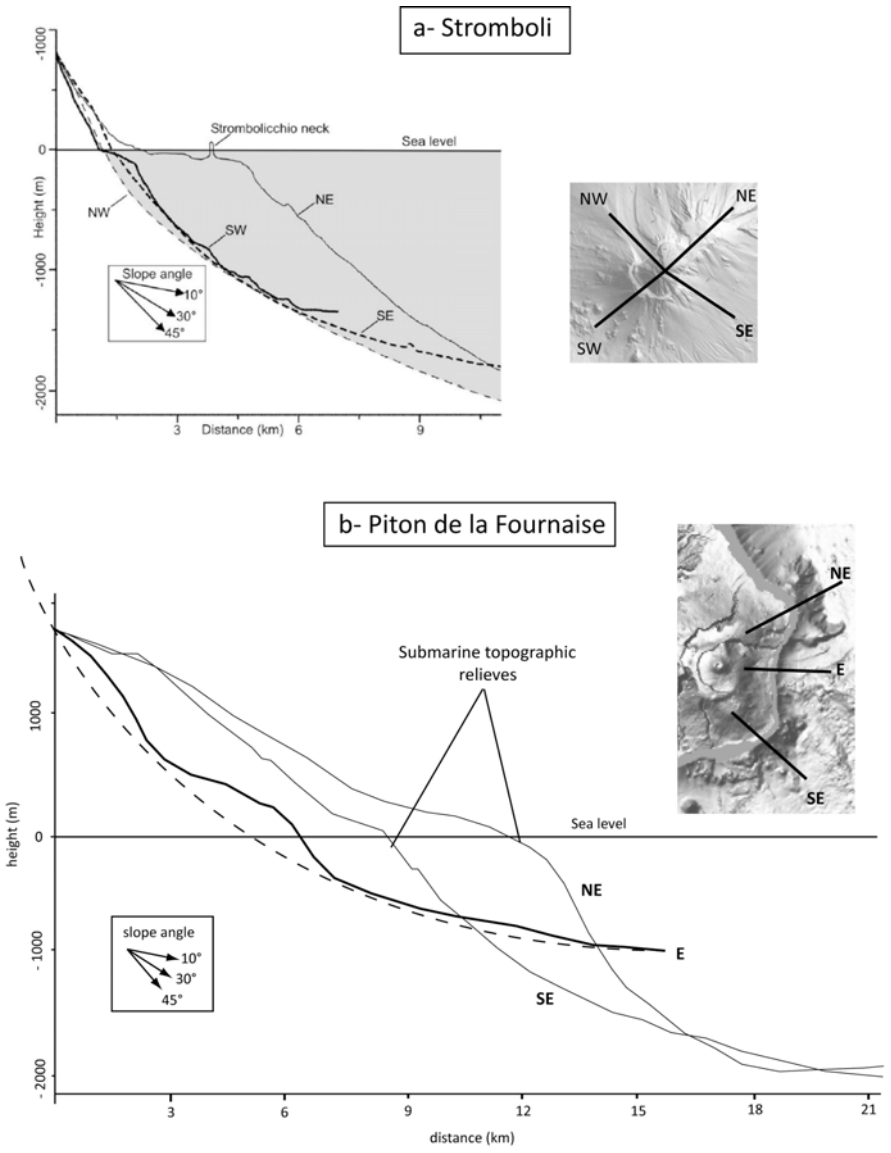

Figure 2.19: Topographic-bathymetric sections of submarine flanks of Stromboli (from Romagnoli et al., 2009a) and Piton de la Fournaise. Figures a and b are at the same scale.

At Piton de la Fournaise volcano, apart from the steep subaerial slopes, the unstable submarine flank (corresponding to the Enclos Grand Brulé structure) shows a gentler slope than the stable flanks (Fig. 2.19), probably due to the accumulation of mass wasting deposits (Oehler, 2005). However, the eastern profile shows that the unstable flank morphology is not as simple as in the case of Stromboli, as its shape does not follow a simple concave curve (dotted line in Fig. 2.19b), probably due to the occurrence of constructional processes. The stable flanks, corresponding to the submarine extension of the rift zones (see section 2.3.3), show very similar slope patterns as they likely experimented comparable growth rate and erosional processes.

The comparison of the profile of Stromboli Island (black line on Fig. 2.18) and the NW-SE profile of La Reunion indicate that the NW and SE flanks of Stromboli are steeper (both the subaerial and submarine parts) than the NW and SE flanks of La Reunion, even though the subaerial SE flanks have close morphologies. Stromboli volcano is marked by very steep slopes, reaching more than 35° on the major part of the island, both on subaerial and sumarine portions of the edifice. These are common slope values for a stratovolcano. On the contrary, La Reunion Island exhibits, on the whole, less steep slopes of about 10 to 15° (more typical of a basaltic shield volcano) with locally steeper slopes reaching around 25° (Fig. 2.20). On the submarine portion of La Reunion edifice, few structures, located close to the coast at the N and SW of Piton des Neiges volcano and at the NE and SE of Piton de la Fournaise volcano, show steeper slopes than the rest of the submarine edifice where slopes range between 5 and 15°. In both cases, extremely steeper slopes (> 45°) are reached in the areas where the volcanic edifices are cut by main collapse structures or erosive features. Lower slopes in shallow water sectors are due the presence of coastal shelves around the islands, reflecting the long-term competition between constructive and destructive processes during the growth and evolution of insular volcanoes (Menard, 1983).

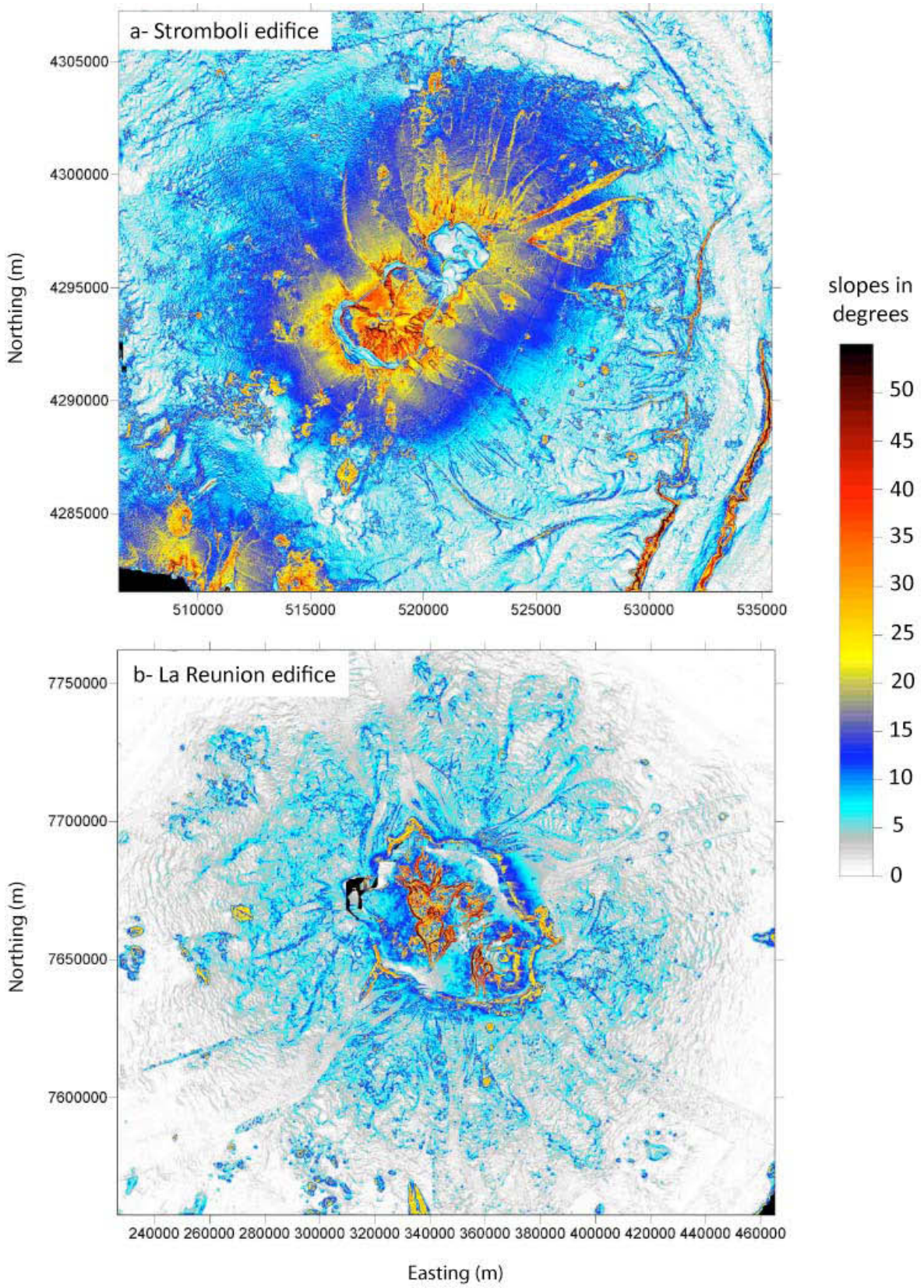

Figure 2.20: Slopes (in degrees) of the subaerial and submarine parts of the volcanic edifices of La Reunion and Stromboli.

2.3.2.2- Collapse scars and related deposits

In this section, peculiar features such as collapse scars and the characteristics of related deposits are described for both Stromboli and La Reunion. Stromboli and La Reunion are deeply marked by several collapse scars affecting the flanks of the edifices: the Sciara del Fuoco (northwestward) and Rina Grande (southeastward) scars for Stromboli and the Enclos-Grand-Brule collapse structure at Piton de la Fournaise volcano (Fig. 2.21).

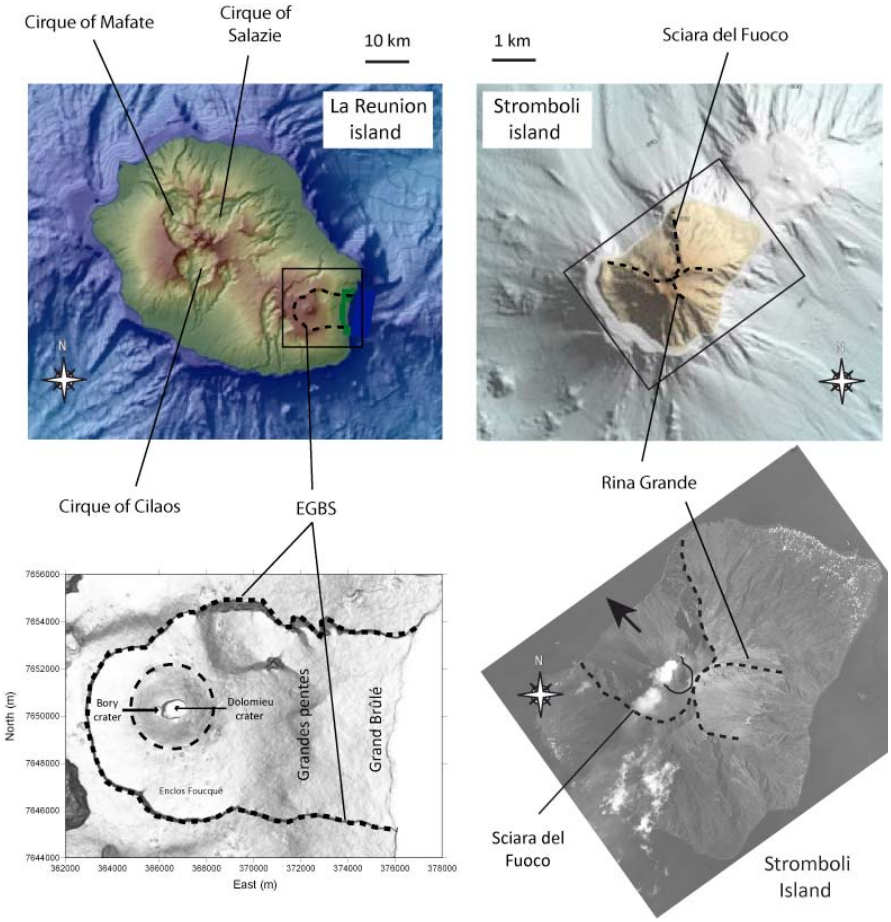

Figure 2.21: main collapse structures identified on the subaerial part of Stromboli and La Reunion. EGBS = Enclos Grand Brule Structure.

Although these structures look similar from a geometrical point of view, at La Reunion and Stromboli, they actually have a totally different origin. If it is clear that the Sciara del Fuoco and Rina Grande scars correspond to the upper limits of lateral flank collapses that occurred along the northwestern and southeastern flanks of Stromboli volcano, the origin of the

Enclos-Grand Brulé Structure at Piton de la Fournaise is still controversial. Several successive models have been proposed in order to explain the formation of this U-shaped structure at Piton de la fournaise volcano (Fig. 2.22).

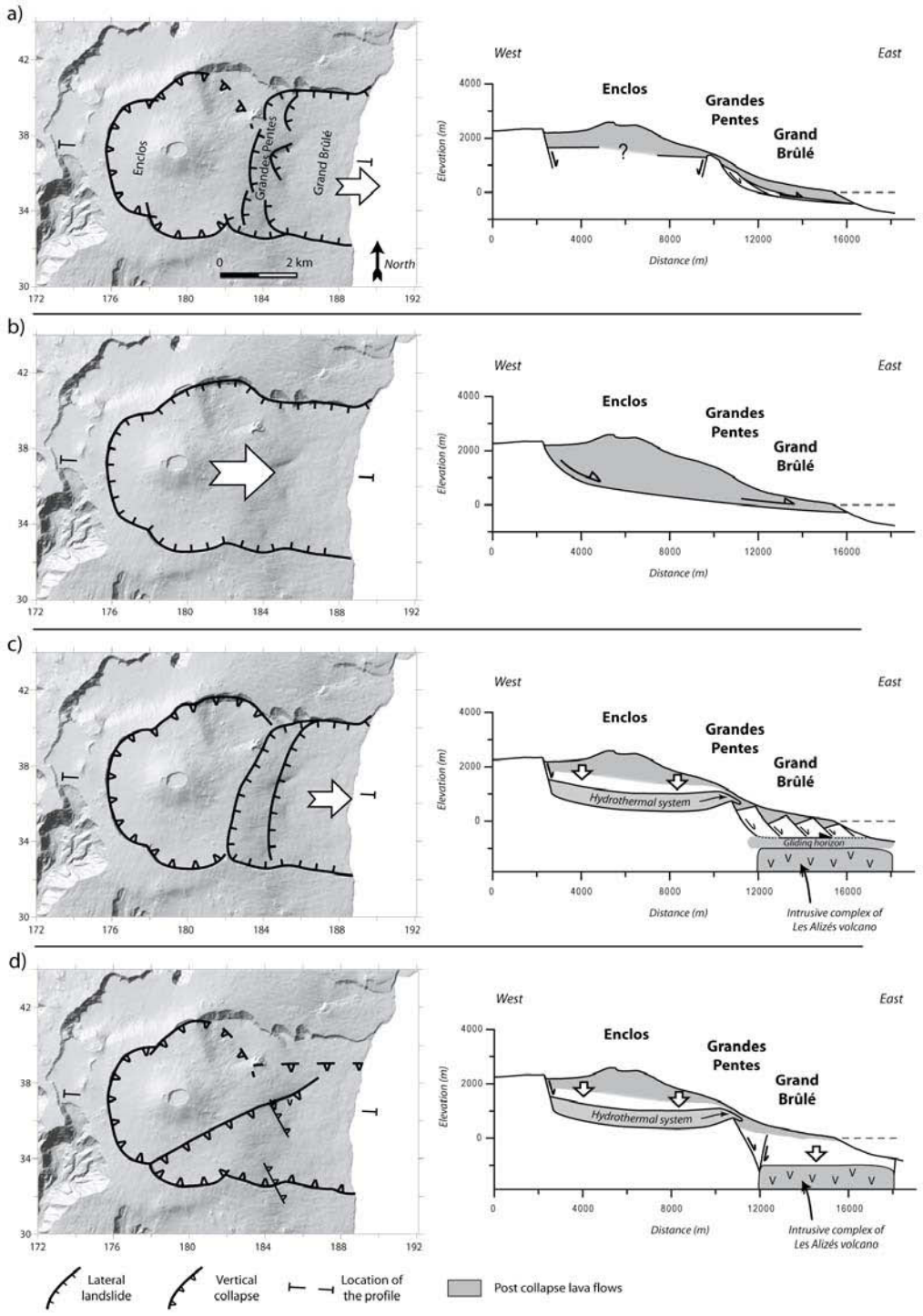

Figure 2.22 : Schematic views and cross sections of the successive models proposed for the formation of the Enclos-Grand Brulé Structure. See text for description (a from Bachelery, 1981 ; b from Labazuy, 1996 and Oehler et al., 2004 ; c from Merle and Lénat, 2003 ; d from Michon and Saint-Ange, 2008).

As shown by Figure 2.22, the formation of the Enclos-Grand Brulé structure (EGBS) is still a matter of debate. Some authors interpreted the Enclos depression as the result of repeated caldera collapses. In this case, the Grandes Pentes would be the head of a lateral landslide (Bachèlery, 1981, Fig. 2.22a). Another interpretation is that the entire EGBS results from a giant landslide that was also partly responsible for the debris avalanche deposits on the submarine flanks (Duffield et al., 1982; Gillot et al., 1994; Labazuy, 1996) (Fig. 2.22b). Merle and Lénat (2003) propose a third interpretation: the formation of the EGBS would be the combination of lateral movements of the Grand Brulé along a basal decollement plane (at the interface between the hypocomplex of Les Alizés volcano and the base of Piton de la Fournaise volcano) that triggered a vertical collapse of the upper part of the EGBS by spreading of the hydrothermal system (Fig. 2.22c).

Michon and Saint-Ange (2008) proposed a different model of formation of the EGBS (Fig. 2.22d). The continuity of the geological and morphological structures between the Enclos and the Grand Brulé escarpments suggests that this structure was not caused by one or several landslides as it is usually proposed (models a and b on Fig. 2.22) but is due to a mainly vertical collapse. The authors proposed that the collapse of the Grand Brulé, the lower half of the EGBS, was due to the downward drag related to the dense intrusive complex of the Alizés volcano, which is located 1 km below the Grand Brulé. In their model, the collapse of the Enclos is interpreted as the consequence of the deformation of the hydrothermal system of the pre-Enclos volcano (in this sense, this last model is close to the model c).

At Piton des Neiges volcano, the formation of the 3 sub-circular depressions («Cirques») of Mafate, Cilaos and Salazie is probably also related to large lateral collapse episodes (Fig. 2.23). Oehler (2005) on the basis of structural features and age constraints proposed that these depressions correspond to the remnants of headwalls of major lateral destabilizations that affected Piton des Neiges volcano. These scars were possibly reactivated later by caldera collapse events, gravitational spreading or subsidence of the hypovolcanic complex of Piton des Neiges volcano. They were also strongly affected by erosion that degraded their original geometry.

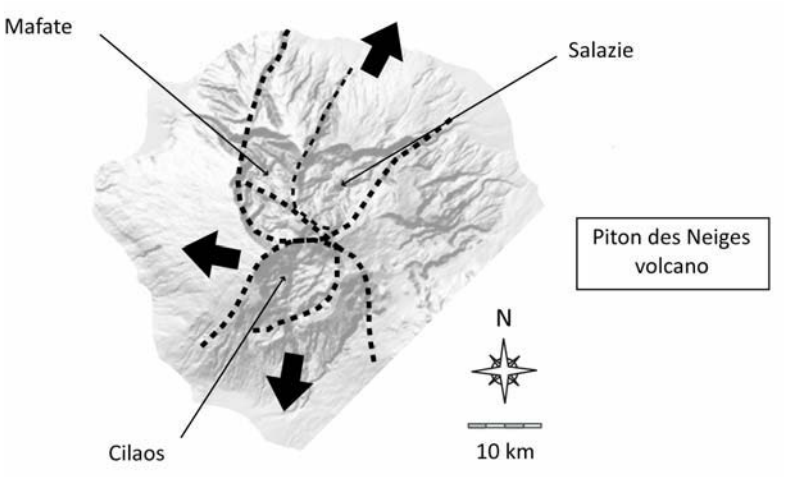

Figure 2.23: Relationship between headwalls of major flank destabilizations, walls of the « cirques » of Piton des Neiges volcano, La Reunion Island (modified from Oehler, 2005).

Collapse scars were identified both on the subaerial and submarine parts of Stromboli edifice (Fig. 2.24), while the submarine continuation of the Enclos-Grand Brulé Structure is not really clear on bathymetrical data (Lénat et al., 1989).

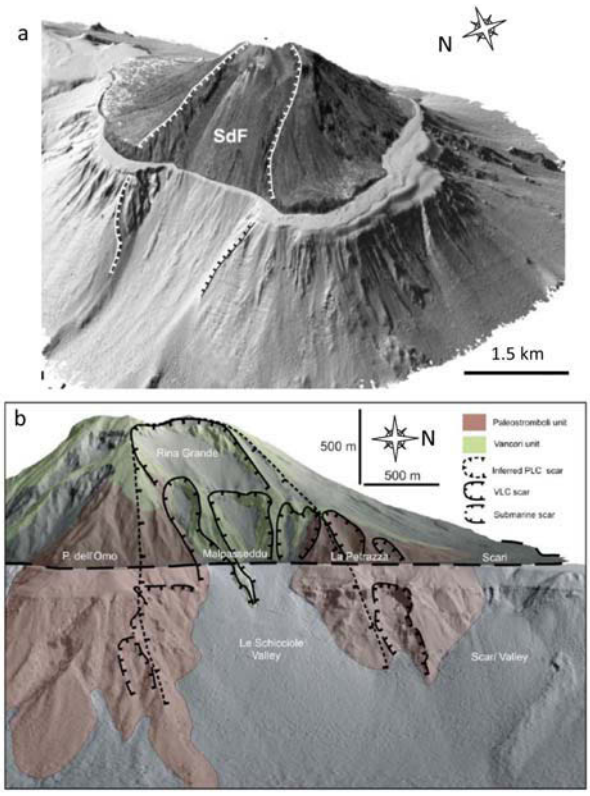

Figure 2.24: Submarine continuation of lateral collapse scars at Stromboli (a- SdF = Sciara del Fuoco, b- Rina Grande, Romagnoli et al., 2009 a and 2009b). White dotted lines show the lateral limits of the deposits associated with lateral collapse towards Northwest at Stromboli.

Debris-avalanche deposits are associated to lateral collapses. The lower submarine flanks of volcanic edifices are commonly covered by a volcaniclastic apron, the architecture of which is controlled by a number of factors. In particular, the common occurrence of flank instability along volcanic slopes gives rise to different types of mass-wasting deposits (from debris-avalanche deposits to volcaniclastic turbidites) on the nearby seabed, greatly contributing to the growth offshore of an insular volcaniclastic apron. The surface of the volcaniclastic apron surrounding Stromboli volcano, for instance, is covered by debris and volcaniclastic sediments for about 90% of its extension (Casalbore et al., 2010, Fig. 2.25). Both at Stromboli and La Reunion, widespread mass-wasting deposits have been recognized using geophysical techniques (Romagnoli et al., 2009a and 2009b; Oehler et al., 2008 ; Fig. 2.25).

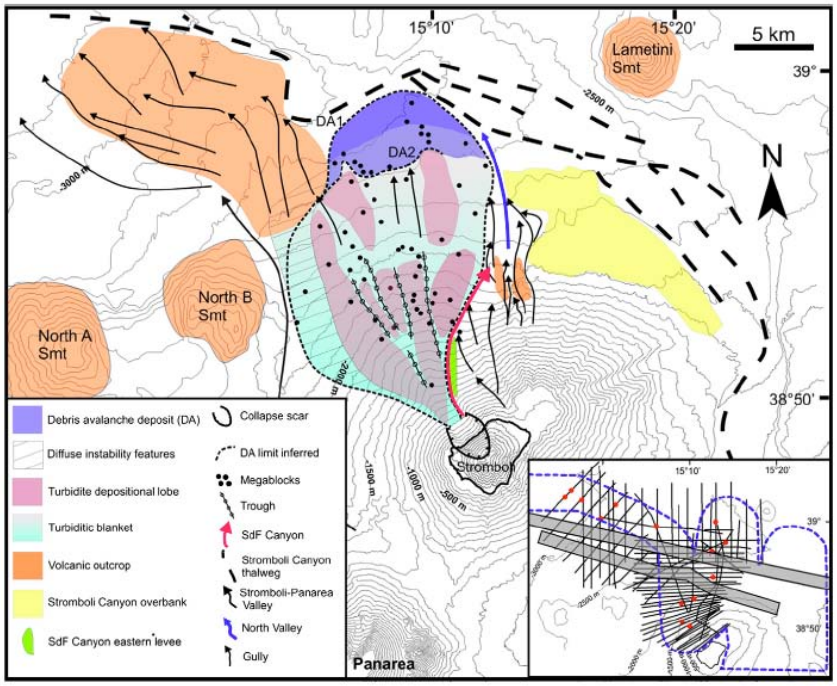

Figure 2.25: Main features of the northern submarine portion of Stromboli volcano, with the débris avalanche deposits associated to the recurrent collapses of the northwestern flank of the edifice (Romagnoli et al., 2009a).

At La Reunion, the volcaniclastic deposits form four main submarine bulges (Fig. 2.26a), whose geometry is described in table 2.3. These sedimentary bodies are mostly made of superimposed debris avalanche deposits presenting hummocky morphologies with variable amount of blocks of various size (Fig. 2.26b).

a- Submarine bulges arould La Reunion

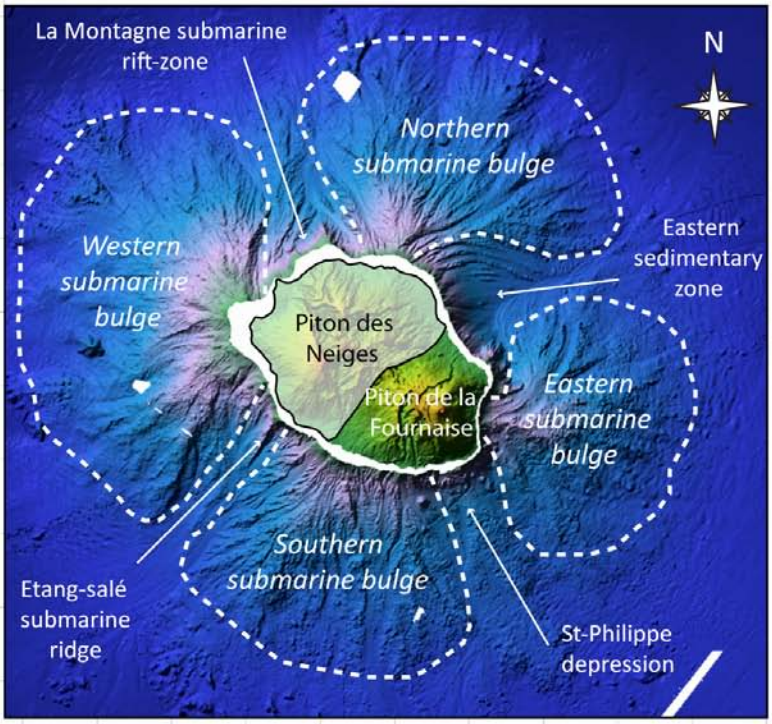

b- Debris avalanche deposits on the submarine flanks of La Reunion

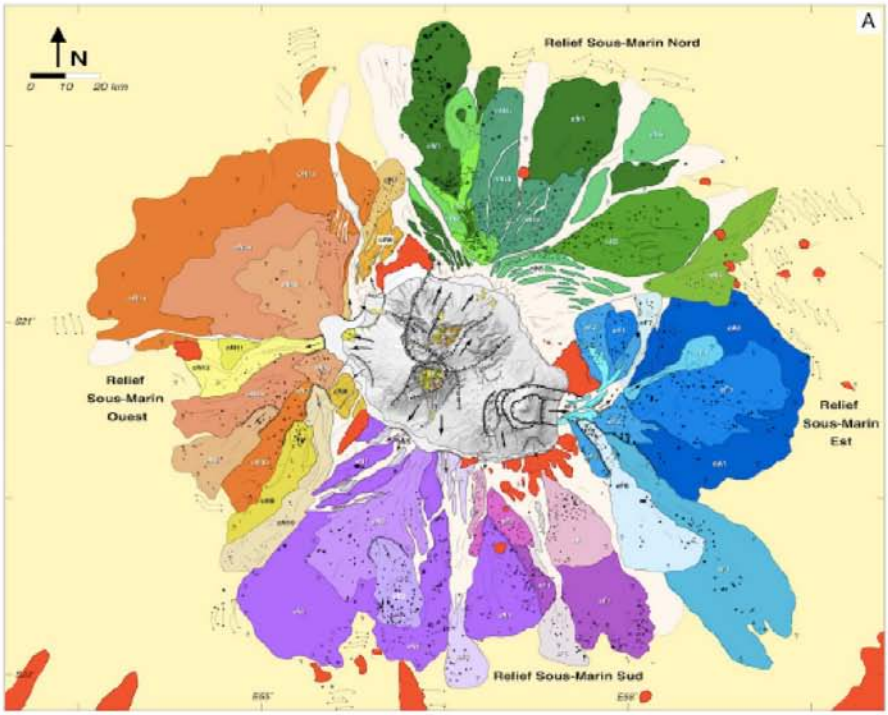

Figure 2.26: (a) The four main submarine bulges surrounding La Reunion Island (from Oehler, 2005) and (b) the corresponding débris avalanche deposits units identified by Oehler (2005). The limits of the bulges are just an indication to facilitate the understanding, they do not precisely refer to the limits defined by Oehler, 2005.

	Eastern submarine bulge	Northern submarine bulge	Western submarine bluge	Southern submarine bulge
location	Eastern slopes of PdF volcano	North/ northeastern flanks of PdN volcano	Northwestern/ western flanks of PdN volcano	Southwestern/ southern flanks of PdN volcano
longitudinal extension (km)	60	70	60	55-70
max depth (m)	-4000	-4000	-4000	-4000
covered area (km2)	4000	4000	4300	3600

Table 2.3: Geometrical characteristics of the four submarine bulges surrounding La Reunion Island (from Oehler, 2005).

The formation of these bulges would be the result of accumulation of volcaniclastic deposits associated to recurrent and multi-scale lateral destabilizations of the flanks of three volcanic edifices (Piton des Neiges, Les Alizés and Piton de la Fournaise) of La Reunion (Labazuy, 1996; Oehler et al., 2008; Fig. 2.27 and table 2.3).

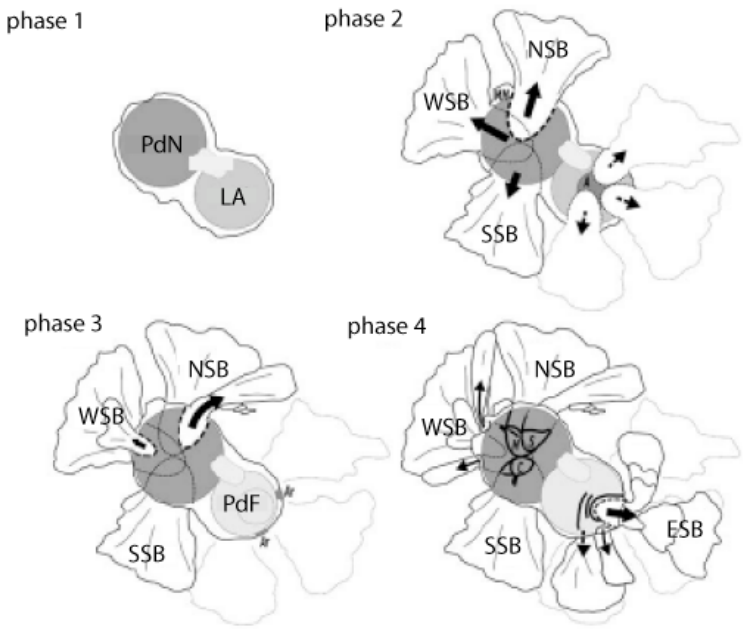

Figure 2.27: Recurrent phases of lateral instability affecting the volcanoes of La Reunion (modified from Oehler et al., 2004). PdN = Piton des Neiges volcano ; LA = Les Alizés volcano ; PdF = Piton de la Fournaise volcano ; NSB = northern submarine bulge ; SSB = southern submarine bulge ; ESB = eastern submarine bulge ; WSB = western submarine bulge.

2.3.3- Rift zones and other volcanic features

If a temporarily steady stress system dominates a volcanic edifice, dikes may group to form swarms and rift zones. These are principally vertical structures formed by hundreds or thousands of parallel-striking magma paths (Walker, 1999). In hotspot settings, the volcanic activity resulting from the ascent of a mantle plume is frequently radially distributed around a volcanic center and concentrated along volcanic rift zones, preferential path for magmatic intrusions (Walker, 1999). As documented for Hawaiian volcanoes (McDonald and Abbott, 1970), the orientation of the rift zones can be superimposed to main crustal orientations suggesting their control on the growth and volcano-tectonic evolution of basaltic shield volcanoes. On stratovolcanoes, some authors showed that the formation and structure of rift zones is partially controlled by regional structures and by topographical effects due to the morphology of the edifice, where intrusions are guided by gravitational stresses in steep edifices (Murray, 1988; McGuire and Pullen, 1989; Walker, 1999; Tibaldi, 2003). Annen et al. (2001) showed that intrusions along rift zones could contribute to more than 30% of the growth of basaltic volcanoes.

The edifices of La Reunion and Stromboli, as other basaltic volcanoes, exhibit well-developed rift zones, along which the large majority of magmatic intrusions are injected (Villeneuve and Bachèlery, 2006; Tibaldi et al., 2009). The existence of such active rift zones on the islands testifies, in fact, the intense intrusive activity that occurred within the edifices (both subjected to almost uninterrupted eruptive activity in the last centuries/thousand years). It is usually hard to discriminate whether the different orientation and geometries of structural features like rift zones are related to large-scale processes (regional stress field or crustal structures) or to local effects due to the intra-edifice stress field. Only the combination of several scales of observation may allow this distinction. Indeed, structures induced by local effects (such as the intra-edifice deformation or the landslide-induced stress field) or those due to magmatic overpressure are restricted to the edifice, whereas large-scale deformation may influence the development of multi-scale structures. Below, the distinction is made between the rift zones controlled by external processes or internal ones.

2.3.3.1- Rift zones controlled by external processes

Stromboli volcano is elongated in the NE-SW direction and shows a quasi-bilateral symmetry with respect to this axis. It is considered as the main magma-feeding zone of the island (oriented N 41°), along which dikes and eruptive centers are aligned (Fig. 2.28). The N41° intrusion zone at Stromboli is considered as structurally-controlled by regional tectonics (Tibaldi, 1996), as its orientation coincides with that of the main crustal fault affecting the northeastern sector of the Aeolian archipelago (Fig. 2.28). The submarine extension of the main N41° rift zone at Stromboli volcano is evidenced by the main alignment Stromboli-Strombolicchio (including the nearby Panarea island, Fig. 2.28). Apart from this, adventive cones and parasitic vents in the southern flank of Stromboli follow a radial pattern (Fig. 2.31).

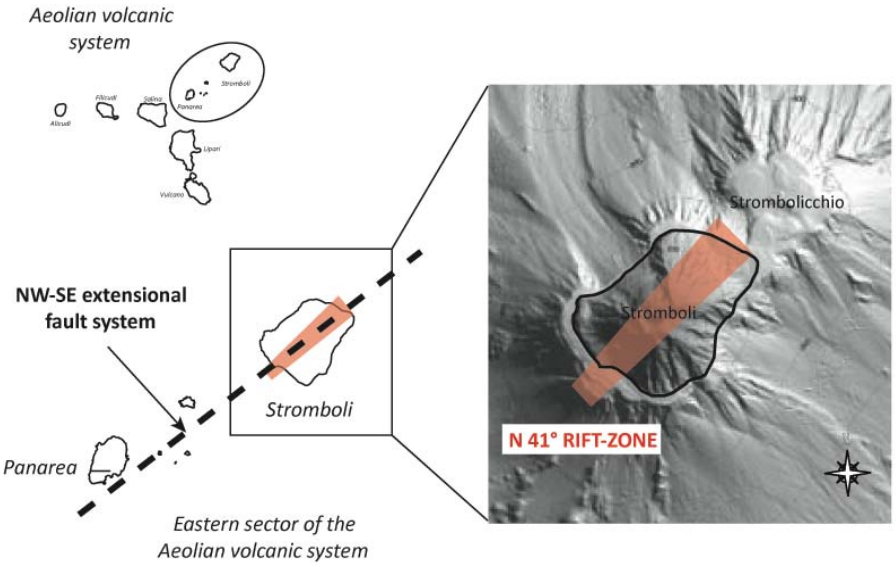

Figure 2.28: Orientations of the main crustally-controlled rift-zone at Stromboli volcano.

The edifice of La Reunion island is elongated in a N120-130° direction. Data for La Reunion show the recurrence of several structural trends (i.e., N30–40°, N70–80°, and N120–130°; Figure 2.29 and 2.30) from the crustal scale to the small-scale (magmatic system). The N30–40° and N120–130° trends correspond to (1) preferential directions of magmatic intrusion at both Piton de la Fournaise (recent intrusive activity) and Piton des Neiges, (2) the elongation of dense intrusive complexes in Piton des Neiges and between Piton de la Fournaise and Piton des Neiges (Malengreau et al., 1999), (3) two of the main fault trends of Piton des

Neiges (Chevallier, 1979), and (4) the regional orientations of the transform zone and spreading center (see 2.1.2). Even though N70° oriented faults are observed in Piton des Neiges (Chevallier, 1979), the N70–80° structural direction is mainly restricted to Piton de la Fournaise and between Piton de la Fournaise and the Mauritius transform zone. The orientation N 55-60° (Fig. 2.29) refers to the orientation of the volcanic ridges shown in Fig. 2.5.

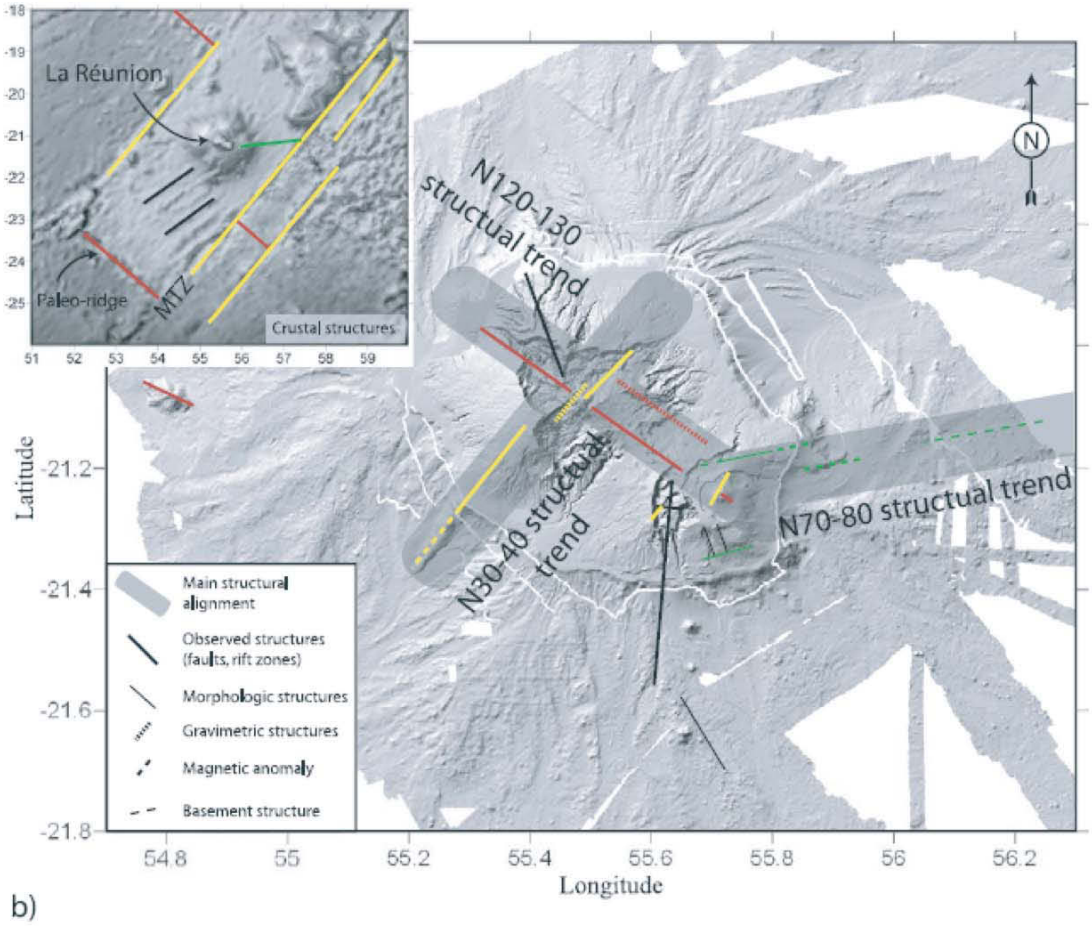

b)

	N30-40 trend	N55-60 trend	N70-80 trend	N120-130 trend
Piton de la Fournaise	N25-30 *(rift zone)*	N55-65 *(structural liniation)*	N75-80 *(structural liniation)*	N125-130 *(rift zone)*
Island structures	N30-40 *(faults, rift zones and intrusive complex at PdN)*		N70-80 *(faults at PdN, crustal highs, remnant of the Alizés volcano)*	N120-130 *(faults, rift zones and intrusive complex at PdN, seamount, island elongation)*
Crustal structures	N30-40 *(transform zones)*	N55-60 *(volcanic ridges)*	N80 *(crustal structure E of La Réunion)*	N120-130 *(regional crustal structure)*

Figure 2.29: a- Distribution of the main structures affecting the area of La Reunion Island at different scales; b- Summary of the main trends affecting Piton de la Fournaise volcano, Piton des Neiges volcano, the island and the surrounding crust (Michon et al., 2007a).

Michon et al. (2007a) interpreted the parallelism of these trends between the local (magmatic system) scale, the island scale, and the lithospheric scale as resulting from a structural control played by the oceanic crust in the past and present construction of La Reunion volcanic edifice.

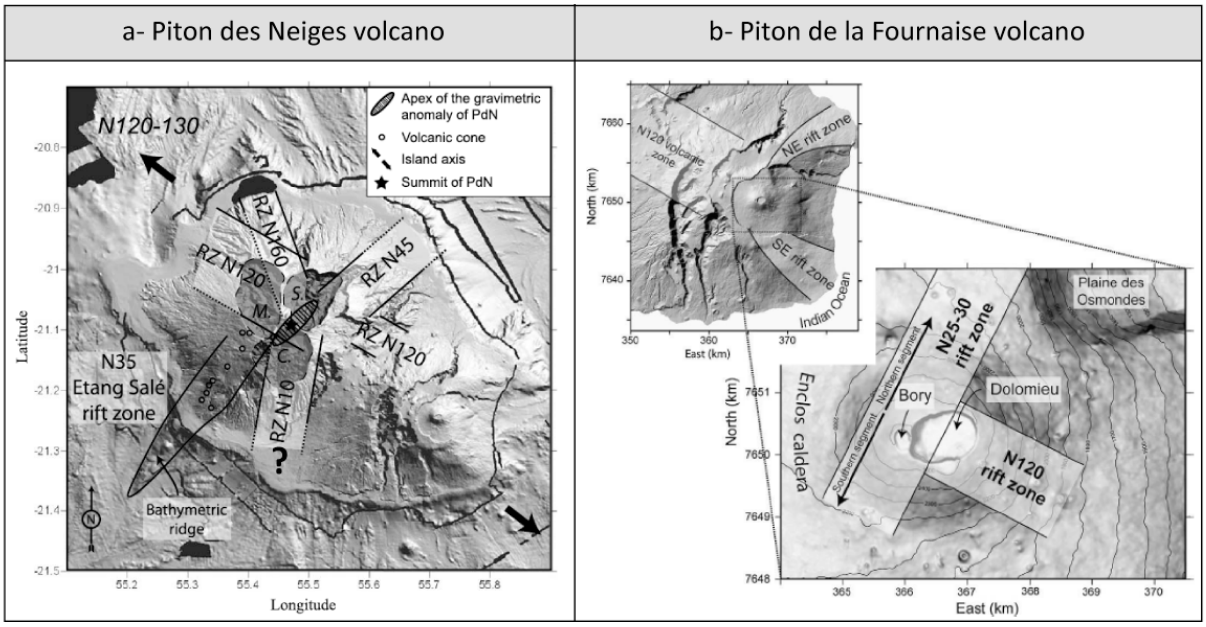

Figure 2.30: Orientations of the rift-zones at (a) Piton des Neiges volcano (the RZ N120, RZ N45 and N35 Etang-Salé RZ are rift-zones tectonically controlled by crustal structures (Fig. 2.28)) and (b) Piton de la Fournaise volcano (N25-30 and N120 rift-zones are controlled by crustal structures). From Chevallier, 1979; Michon et al., 2007a and 2009a.

Fig. 2.30 shows that Piton des Neiges volcano presents 3 main rift zones controlled by tectonic crustal lineaments: a N120 rift-zone on the NW and SE flanks of the edifice, a N45 rift-zone on the NE flank of the edifice and a N35 rift-zone on the SW flank of the edifice. Figs. 2.29 and 2.30 show that the NE rift zone and SE rift zone of Piton de la Fournaise volcano are oriented in a direction parallel to the N70-80 regional trend for the NE rift zone and to large scale faults for the SE rift zone (black lines on Fig. 2.29). Recent activity at Piton de la Fournaise volcano is concentrated along two main rift-zones oriented N 25-30° and N 120° (Michon et al., 2007a; Fig. 2.30b).

The submarine extensions of the rift zones at La Reunion form high-volume massive bodies, easily recognisable on bathymetric maps as morphological highs or ridges (Fig. 2.31). They

were described in detail by Oehler (2005). The submarine NE rift zone can be divided into two portions: 1- a upper portion until 800 m of depth made dismantled littoral formations and fragmented lava flows, 2- a lower portion from -800 m to -2200 m, with steeper slopes, that could correspond to anterior formations of Piton de la Fournaise volcano or remnants of the dismantled les Alizés volcano (Gailler et al., 2009; Smietana et al., in prep). The submarine SE rift zone is made of a massive part close to the coast, likely made of massive lava flows, that becomes less compact away from the island, where volcaniclastic sedimentary facies are predominant. The structure of the submarine part of La Montagne rift zone is similar to the structure of the submarine NE rift zone of Piton de la Fournaise volcano. It has steep slopes and is probably made of piled lava flows. The presence of erosional features testifies of its age and dismantling. McDougall (1971) estimated that the lava pile is approximately 1000 m thick and is cut by a dense network of dikes. The Etang-Salé submarine ridge, oriented N35°, is the continuation of a lineament of volcanic cones onland (Fig. 2.31), interpreted as an old rift-zone of Piton des Neiges volcano (Chevallier, 1979). Its elongated shape is similar to the submarine rift zones formed at Kilauea volcano (Hawaii).

Figure 2.31: Submarine extension of the rift-zones and related volcanic structures on the submarine flanks of La Reunion (a and b) and Stromboli (c) islands.

2.3.3.2- Rift zones related to internal processes

Apart from major tectonically-controlled rift-zones, basaltic volcanoes show a secondary type of rift-zones, whose formation is an effect of a local stress field related to collapse areas, fractured zones… (Walter and Troll, 2003; Walter et al., 2005). The volcano load and stress distribution are two important factors that control the formation of rift zones (Fiske and Jackson, 1972). Volcano spreading along weak failure plane is commonly considered to control diking and structural evolution of many large volcanoes (Borgia et al., 2000). Acocella and Tibaldi (2005) studied experimentally the consequences of a flank collapse on dike propagation within volcanoes, based on the example of Stromboli. Their models showed that dikes propagating close to the collapse scar or in an unstable edifice become subparallel to the walls of the collapse because of the local stress reorientation due to the unbuttressing of the flank. The experiments carried out by Walter and Troll (2003) indicated that in presence of an outward slipping flank along a basal décollement, intrusions tend to group to form tangential rifts along the unstable sector of the volcano (Fig. 2.32b and c), forming preferential areas of growth of the edifice. Second order rift zones are formed in a direction perpendicular to the collapse.

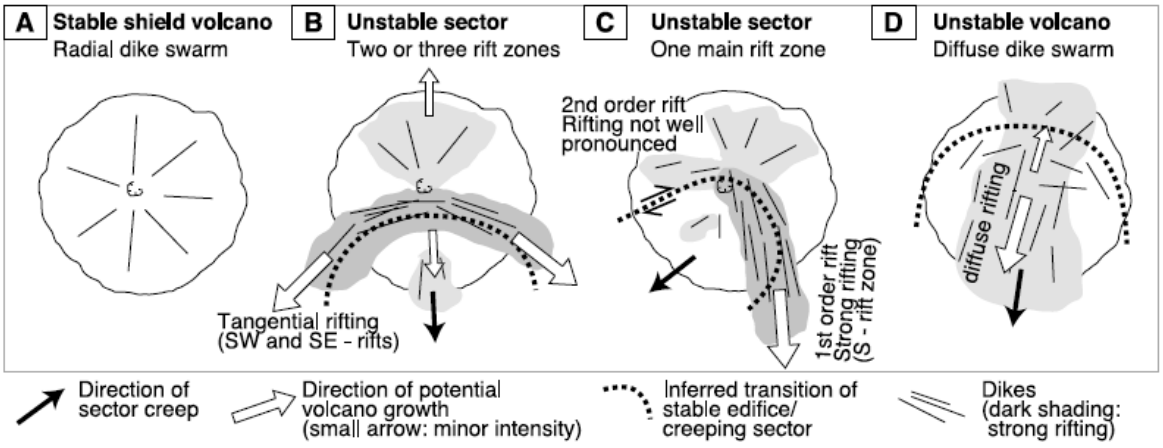

Figure 2.32: Geometry and direction of the rift zones on stable shield volcano (a) or under different conditions of flank instability (b, c and d). Intrusions gather tangentially to the collapse structures (b and c) when only a sector of the volcano is unstable. If the whole edifice is unstable, the orientation of intrusion within the edifice remains random (Walter and Troll, 2003).

At Stromboli volcano, the sidewalls of the Sciara del Fuoco collapse scar are also a preferential path for dike intrusions (Fig. 2.33) that developed in the last 13 kyrs. This geometry, in fact, has been attributed to the series of lateral collapses which affected this zone of the cone, and which locally influenced the orientation of the stresses due to the gravity force (i.e. distribution of rock masses) interacting with the stresses due to regional tectonics and a stationary magma level (Corazzato et al., 2008). In this view, it is considered that creeping of the northwestern volcano flank can favour the emplacement of NE-striking dikes in the summit crater zone (Tibaldi, 1996; Tibaldi, 2001; Tibaldi et al., 2003; Corazzato et al., 2008). A third, less developed N-trending intrusion zone corresponding to an intrusive activity that occurred onland between 85 and 55 kyrs, affects the south of the island, mostly recognizable in the offshore (Bosman et al., 2009; Fig. 2.31). Similarly to the Sciara del Fuoco rift-zone, based on the model proposed by Walter and Troll (2003), we propose that the N trending rift-zone could be associated to a stress reorientation caused by the southeastern unstable flank of Stromboli volcano (Rina Grande collapse). The submarine continuation of the N-trending secondary rift zone is clearly visible (N0° in Fig. 2.31c).

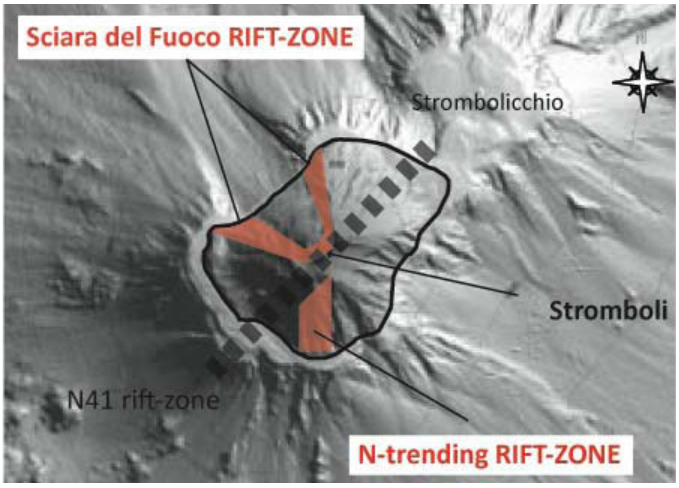

Figure 2.33: Rift-zones related to local stress field effects at Stromboli island. The formation of Sciara del Fuoco rift-zone is related to recurrent collapses of the NW flank of Stromboli while the N-trending rift-zone is associated with the 85-55 kyrs period of onland activity of the volcano.

At Piton des Neiges, the N160 rift-zone identified in La Montagne massif is not correlated to any gravimetric or magnetic anomaly, suggesting no structural control on its formation,

possibly due to a shallower position in the edifice (Michon et al., 2007a) and related to an independent geological process. The N10 rift zone described by Chevallier (1979) was not described by the next studies carried out in the Piton des Neiges volcano (Maillot, 1999; Chaput et al., 2010).

The study of rift zones orientations and structures within the edifices of La Reunion and Stromboli reveals that the evolution of these islands is controlled by the combined effects of 1- a regional stress field related to the geodynamic environment crustal structures of each area and 2- local stress fields related to the magmatic activity and morphological evolution of each edifice.

2.3.3.3- Geometry of the magmatic intrusions

Together with the direction of intrusion at depth defining the orientations of the rift-zones, the geometry of the magmatic intrusions provide useful data in the understanding of the nature of the stress field within the studied volcanic edifices at the time of the intrusion. On exctinct volcanoes, erosion gives access to the core of the edifice and brings to the surface a large amount of magmatic intrusions, while on active volcanoes erosion does not allow an access to the internal structures of the edifice.

Stromboli volcano (Fig. 2.34a)

Stromboli's evolution in the last 100 ka has been characterized by the persistent N 10–55° E intrusion direction, reflecting the influence on the magma feeding paths of a state of stress of Stromboli edifice, characterized by a NW-SE extension. After 13 ka ago, sheets mainly intruded along the sector collapse scarps in an amphitheatre geometry and along both sides of Sciara del Fuoco._Several authors studied the geometry (and petrology) of magmatic intrusions at Stromboli. From this data, Corazzato et al. (2008) and Tibaldi et al. (2009) characterized the sheet complex of Stromboli. They also studied the relationship between the structure of the sheet complex and the evolution of the edifice over time. Magmatic intrusions measured at Stromboli are mainly subvertical to vertical with dips ranging from 70 to 90° for 78 % of the intrusions. The thickness of the intrusions ranges between 0 and 5 m,

but a majority of intrusions (66 %) have a thickness lower than 2 m. Corazzato et al. (2008) observed that the steepest sheets (more than 45°) show a wider range of thickness.

Piton de la Fournaise volcano (Fig. 2.34b)

Letourneur et al. (2008) studied the dips of intrusions at Piton de la Fournaise volcano, measuring injections in the Bellecombe scarp (western wall of the Enclos caldera) and the Plaine des Osmondes (northern wall of the Enclos caldera). Their measurements reveal that 91 % of the intrusions are subvertical to vertical (dip ranging between 70 and 90°). Moreover, the majority of the intrusions are about 1 m thick (Letourneur et al., 2008).

Piton des Neiges volcano (Cirque of Cilaos, Fig. 2.34c)

Extensive field studies carried out by Marie Chaput et al. (2010, appendix 4; Catry et al., submitted, appendix 3; see also chapter 3) in the eroded Piton des Neiges volcano, where the intrusive complex outstandingly outcrops, reveal a wide range of dip for sheet intrusions. Unlike at Stromboli and Piton de la Fournaise where intrusions are quasi exclusively subvertical to vertical, all dips of intrusions are represented within Piton des Neiges volcano. 41 % of the intrusions are subhorizontal with dips lower than 30° while 17 % are subvertical with dip ranging from 70 to 90°. A major difference occur here between the active volcanoes of Stromboli and Piton de la Fournaise, and the extinct eroded Piton des Neiges volcano. However, in terms of thickness, 99 % of the intrusions have a thickness lower than 2 m, similarly to Stromboli and Piton de la Fournaise volcano.

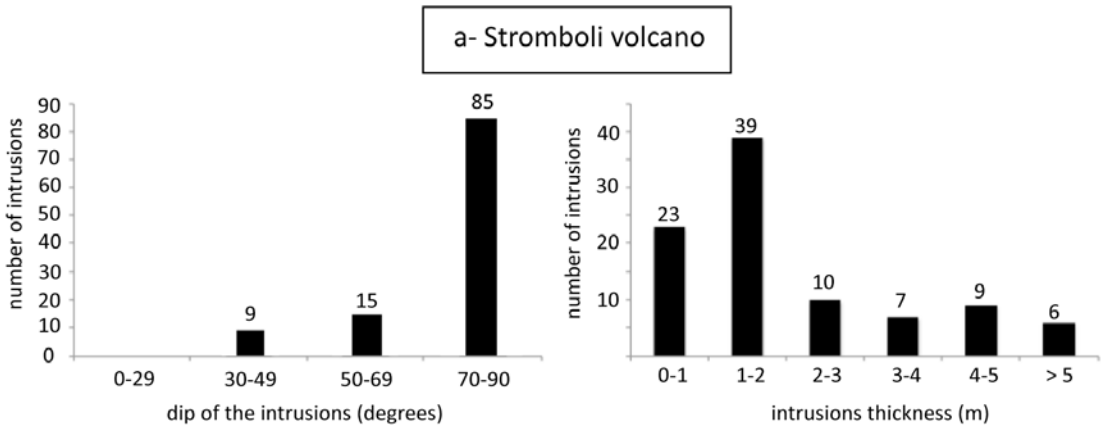

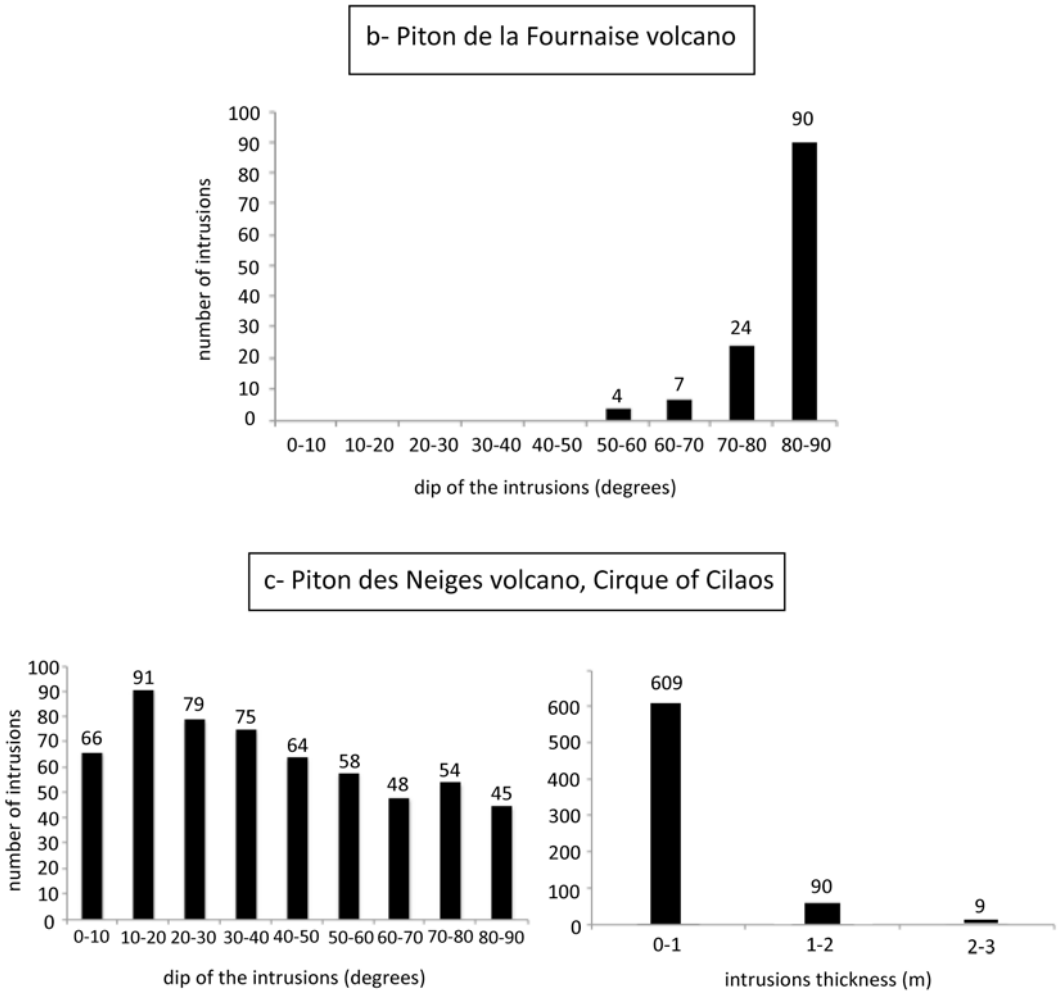

Figure 2.34: Histograms of the dip and thickness of the intrusions measured at (a) Stromboli volcano (from Corrazzato et al., 2008), (b) Piton de la Fournaise volcano (from Letourneur et al., 2008) and (c) Piton des Neiges volcano, Cirque of Cilaos (data from Marie Chaput et al., 2010).

The comparison of sheet complexes for these three edifices shows that deep intrusions (Piton des Neiges) generally have smaller dips than superficial intrusions (Stromboli and Piton de la Fournaise). The orientation and geometry (dip and thickness) of magmatic intrusions strongly depend on the driving internal magmatic pressure and the local stress pattern (Anderson, 1938 ; Walker, 1999 ; Gudmundsson 2005 and 2006). Therefore, variations in the depth of emplacement and geometry of magmatic intrusions within basaltic volcanoes imply variations of the local stress field under which intrusions are injected within a volcano. The relationship between nature of the stress field within volcanoes and geometry of magmatic intrusion will be broadly studied in chapter 3.

2.4- Summary

It has been showed that La Reunion and Stromboli are located in very different geodynamic contexts (sections 2.1.1 and 2.1.3): La Reunion is a 5 Myr-old hotspot-related basaltic shield located in the inactive Mascarene basin (Indian ocean) while Stromboli is a late-Quaternary subduction-related stratovolcano located in an active context of regional extension (southern Tyrrhenian sea). Apart from this major discrepancy of context, another major difference is the volume of the edifices. We calculated from recent DEMs that the volume of Stromboli edifice is less than 1 % of the volume of La Reunion edifice (section 2.3.1 ; Table 2.4). Finally, the study of subaerial and submarine flanks of the edifices shows that their morphologies are very different from an edifice to another, with variations of slope gradient, higher at Stromboli than at La Reunion (section 2.3.2; Fig. 2.17 to 2.19). At the same time, La Reunion and Stromboli present the same overall evolution, characterized by phases of growth through both effusive and intense intrusive activity along well-developed rift zones (section 2.3.3) and phases of destruction by recurrent major lateral destabilizations (section 2.2 ; Table 2.4).

	Stromboli	**La Reunion**
Nature of the edifice	basaltic stratovolcano	basaltic shield volcano
size of the edifice (km)	18 x 10	200 x 240
height from base to top (m)	about 3000	about 7000
volume of the edifice (km3)	350	51500
Flank morphology	typical stratovolcano steep flanks reaching 35°	typical shield volcano with mean slope of 10-15 °, reaching 25°
Rift-zones	well-developed: main N41 rift zone controlled by regional tectonics + 2nd order rift zones	well-developed: N30-40 and N120-130 rift-zones controlled by regional tectonics at PdN and PdF + 2nd order rift-zones
collapse scars	Sciara del Fuoco + Rina Grande	EGBS at PdF and limits of the cirques at PdN
Mass-wasting deposits	cover 90 % of surrounding area, 2 main fans`	all around the island formaing 4 bulges
occurrence of lateral instability	recurrent on the NW and SE flanks	recurrent at PdN and PdF

Table 2.4: Summary of the main morphological and structural features of the volcanic edifices of Stromboli and La Reunion. PdN = Piton des Neiges ; PdF = Piton de la Fournaise.

Table 2.5 quantifies the role of some key factors in flank destabilization of La Reunion and Stromboli that we discussed in the chapter 2, in reference to the parameters introduced in chapter 1. Some of these factors will be discussed with more detail in the next chapters.

factors of long-term destabilizations	**Stromboli**	**La Reunion**
Basement	✔	✔
Oversteepening	✔	
Slopes overloading		✔
Low strength layers	✔	✔
Vertical movements	✔	✔
Environmental factors	✔	✔
factors of sudden destabilizations	**Stromboli**	**La Reunion**
magmatic intrusions	✔	✔
variation of edifice pore pressure	✔	✔
neoformation of fractures	✔	✔
volcanic seismicity	✔	✔
tectonic seismicity	✔	
Low strength layers	✔	✔

Table 2.5: Main factors involved in long-term and sudden lateral destabilizations affecting the edifices of Stromboli and La Reunion (see chapter 1).

The occurrence of previous instabilities and the intrusive activity along rift-zones seem to be major parameters involved in the phenomenon of lateral instability both at Stromboli and la Reunion islands. Some other parameters like the morphology of the edifice (i.e. slope gradients for Stromboli) and the geodynamic context seems instead to have a secondary influence on the mechanism of collapse, as the two areas experimented a similar evolution

in very different environments, involving the same parameters but with different relative importance according to the area.

Chapter 3

Role of magmatic intrusions in the evolution of basaltic volcanoes: field data and numerical approach.

The contents of this chapter of the thesis partly refers to the submitted article introduced in appendix 3: Catry, T., V. Cayol, L. Michon, M. Chaput, V. Famin and C. Romagnoli, Cointrusive shear stress triggers flank collapse on basaltic volcanoes, *Journal of Volcanological and Geothermal Research*, **submitted** (November 2010).

Magmatic intrusions along volcanic rift zones are an important mechanism involved in the evolution of volcanoes. It allows their internal growth by repeated injections in preferential areas, forming the core of the edifices, as it has been observed within eroded volcanoes (Walker, 1986 and 1987; Annen et al., 2001). Some volcanoes, like Stromboli Island, release large amounts of gas while emitting small volumes of magma, suggesting that the major part of the magma remains stored within the edifice (Allard et al., 1994; Allard, 1997; Aiuppa, 2008). Dieterich (1988) studied the formation of Hawaiian rift zones and indicated that rift intrusion and lateral spreading could be major contributions to volcano growth. The extrusion of magma also contributes to the surface growth of the volcano by accumulation of lava-flows on its flanks (Annen et al., 2001). Intrusions along rift zones not only participate to the construction of a volcano but they can also induce destruction processes, triggering flank deformation that may lead to lateral destabilization.

3.1- Previous studies

The relationship between magmatic injections and flank stability has been broadly studied since the catastrophic event of May 1980 at Mount Saint-Helens (Voight et al., 1981). As soon as 1964, Moore recognized the importance of large flank failures on oceanic shield volcanoes like Hawaii. Failure on gently sloping basaltic volcanoes is mechanically problematic as failure on slopes of 10 to 15° generally occur on weak, altered materials (Denlinger and Iverson, 1990). It thus seems reasonable to assume that additional forces are required on volcano flanks to generate lateral failure.

Vertical injections of magma, called *dikes*, provide the excess pressure able to trigger the mechanism of flank failure and large-scale lateral instability on oceanic shield volcanoes. The calculations of Iverson (1995) show that realistic magma injection forces are unlikely to trigger large sectorial flank movements unless frictional resistance to sliding is very low. Moreover, this model requires an unrealistic amount of intrusions of reasonable dimensions to account for the observed surface deformation of volcanoes. Other authors (Elsworth and Voight, 1995; Elsworth and Day, 1999) emphasized the clear potential of vertical intrusion of magma for the development of voluminous flank failures of active volcanoes (Canary Islands and Capo Verde for instance). Results show the mechanical influence of excess pore pressure induced around the intrusion by combined effects of mechanical and thermal strains, likely to trigger large flank collapses on oceanic volcanoes at different timescales. However, their models require the pre-existence of a basal shear plane dipping outward (i.e. *detachment*) or landward (i.e. *décollement*) along which the unstable flank may slide, pushed by recurrent vertical injections of magma into the rift zones (Swanson et al., 1976; Dieterich, 1988, Fig. 3.1). Borgia et al. (1996, 2000) showed that at many volcanoes lateral spreading of the edifice can be facilitated by basal *décollements*. Theses models not only imply mechanical problems but also arise the question of the nature and structure of the pre-existing basal sliding plane, as they are usually to deep to be directly observed.

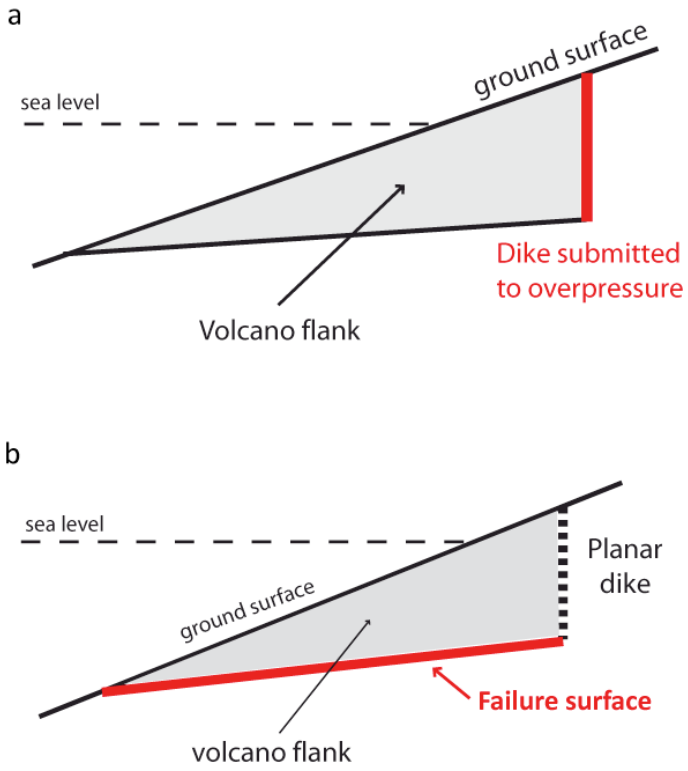

Figure 3.1 : (a) Model of the geometrical relationship between vertical intrusions of dikes and flank collapse on oceanic shield volcanoes, (b) Existence of a failure surface below the unstable volcanic flank (from Dieterich, 1988 ; Iverson, 1995 ; Elsworth and Voight, 1995 ; Elsworth and Day, 1999).

The extent of regional deformation at Etna and Kilauea, for instance, is larger than can be explained by shallow dikes injected from a shallow reservoir, suggesting the existence of deep-seated flank instability (Borgia, 1994; Denlinger and Okubo, 1995; Borgia et al., 2000; Tibaldi and Groppelli, 2002; Acocella et al, 2003; Morgan et al., 2003; Neri et al., 2005). A basal subhorizontal decollement plane has been reconstructed beneath the east flank of Etna volcano at a depth of about 5 km below sea level. This surface has been inferred from different sets of data such as field evidence, the distribution of seismicity and surface deformation, and the deformation pattern observed during east flank movement (Borgia et al., 2000; Acocella et al., 2003; Neri et al., 2004; Lundgren et al., 2004), suggesting a thrust-type fault plane with a slight (5-10°) westward dip (Fig. 3.2a). An additional detachment plane may be located at shallower depths (2-3 km bsl), with a slight eastward dip (Tibaldi and Groppelli, 2002; Bonforte and Puglisi, 2003; Lundgren et

al., 2003). At Kilauea volcano, permanent movements of the Hilina slump favour seaward displacement of the southern flank, which is accommodated by slip along a basal *decollement* horizon modelled near the base of the volcano (Owen et al., 2000; Fig. 3.2b), probably facilitated by sediments on the oceanic plate (Iverson, 1995) or viscous dunite beneath the edifice (Clague and Denlinger, 1994).

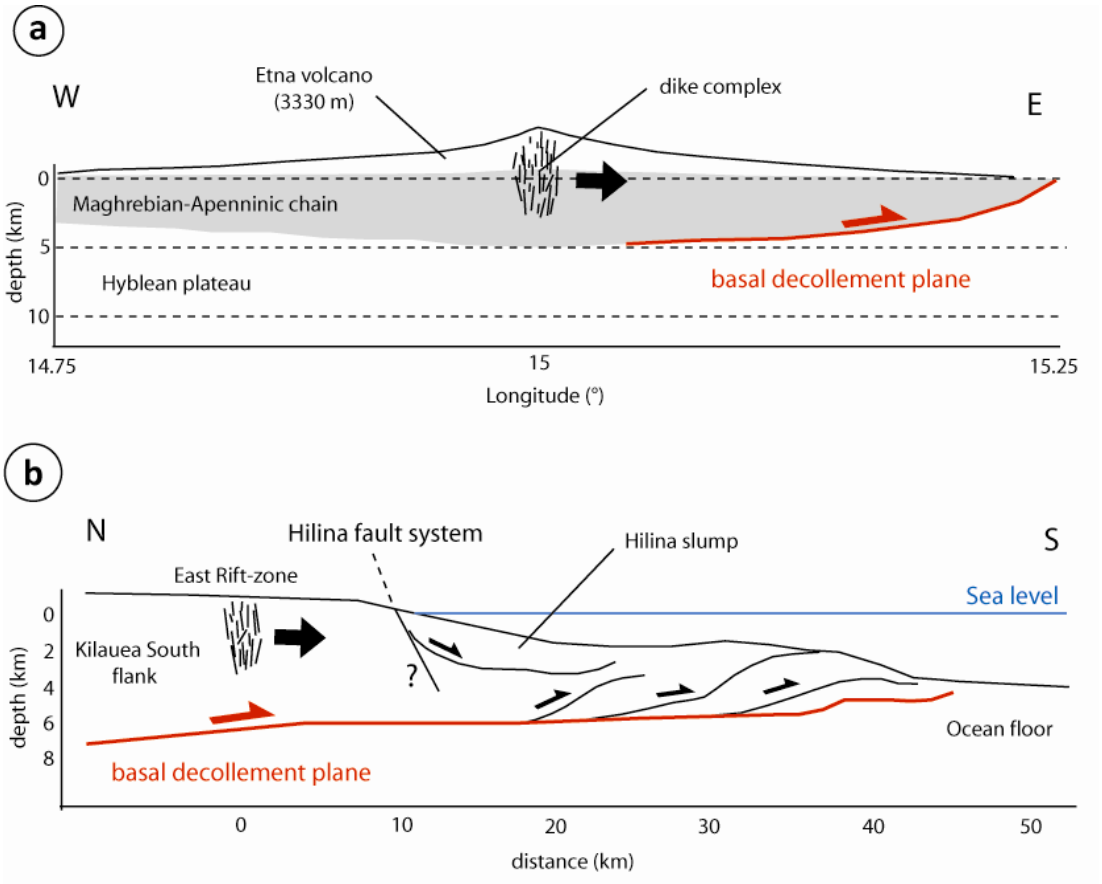

Figure 3.2: Internal structure of the mobile flanks at Etna and Kilauea volcanoes. Movements occur along deep basal subhorizontal décollement planes (from Borgia et al., 1992; Moore et al., 1994; Rust and Neri, 1996; Morgan et al., 2003; Neri et al., 2005; Lipman et al., 2006). Black horizontal arrows indicate magma-related slip movements.

Morgan et al. (2003) provided some insights on the structure of the sliding plane, on the basis of seismic reflection profiles showing the main structural features of the Hilina slump affecting the mobile southern flank of Hawaii (Denlinger and Okubo, 1995; Okubo, 2004, Fig. 3.3). However, a natural example of the structure, exhibiting

the relationship between intrusions and failure surface, is still missing to successfully understand the mechanisms of failure triggering.

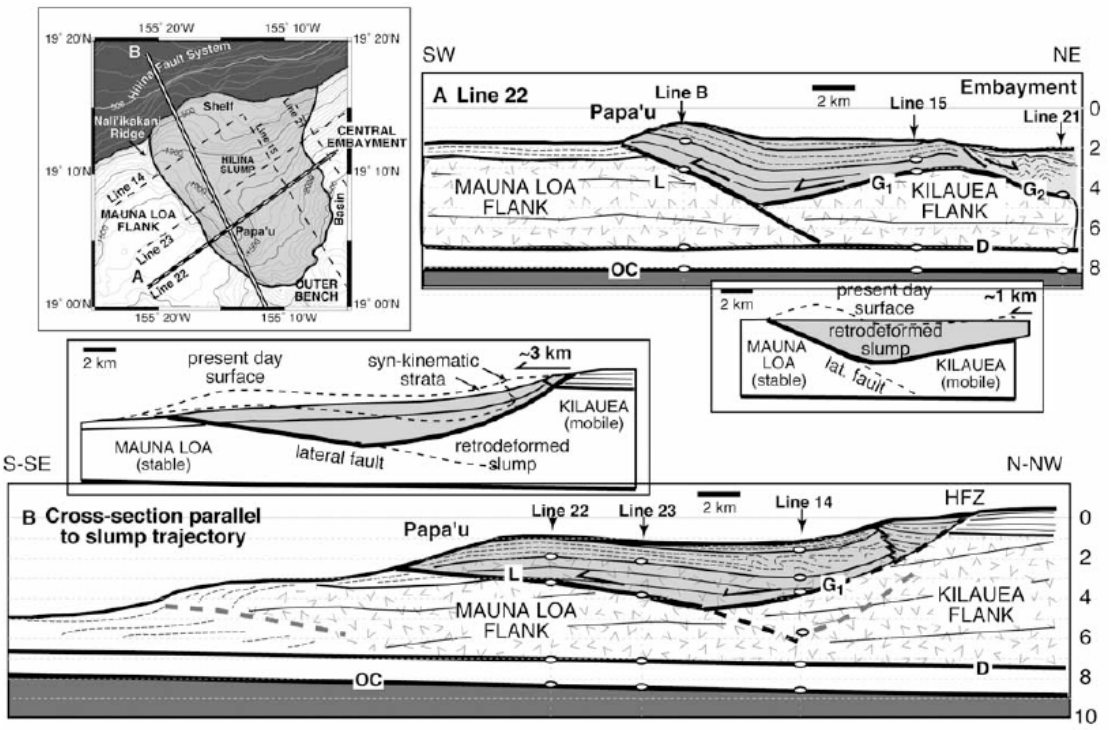

Figure 3.3: Reconstructed cross sections of the Hilina slump affecting the southern flank of Hawaii, with failure surface at the base of the slump (Morgan et al., 2003).

An alternative end-member model has been recently proposed, in which the injection of subhorizontal intrusions (i.e. *sills*) along planes of weakness activates flank sliding by the sole action of gravity (Famin and Michon, 2010). These authors report the unique association of a pile of sheared subhorizontal intrusions at the contact between a debris avalanche deposit and a frozen magmatic chamber, in the inner Piton des Neiges volcano (Cirque of Salazie, La Reunion island, Fig. 3.4). The intrusions injected in a detachment fault that concentrated both ductile and brittle deformation, and were responsible for a combined mechanism of failure along the detachment: slow slip movements triggered by hydrothermal alteration due to hot fluids from intruding sills and rapid co-intrusive slip of the volcano flank triggered by sill injections themselves.

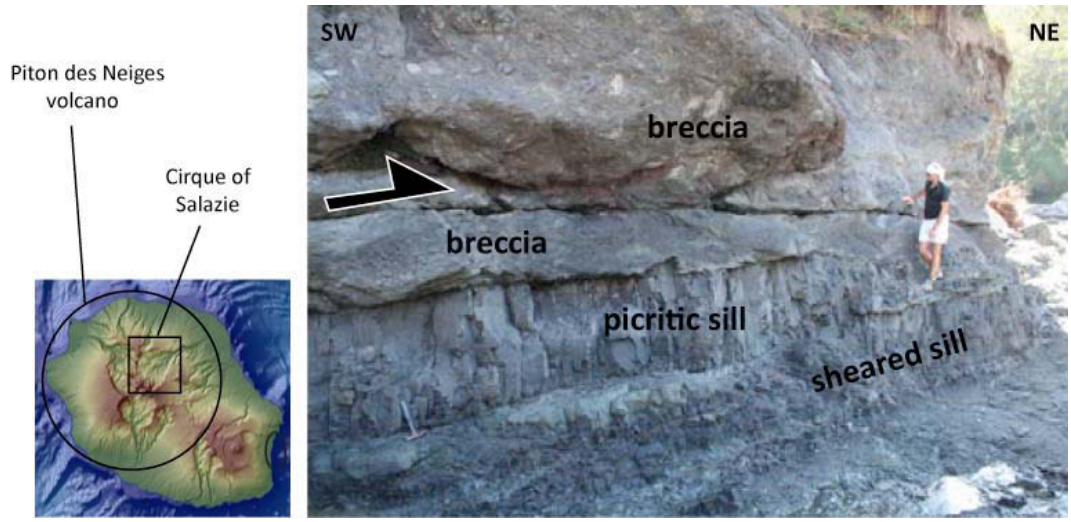

Figure 3.4: Injection of a pile of sheared sills within a detachment at the contact with an overlying debris avalanche deposit in the rivière du Mât, Cirque of Salazie, Piton des Neiges volcano (La Reunion Island, from Famin and Michon, 2010).

Although recent field data from Piton des Neiges volcano tend to prove the role of subhorizontal intrusions in the mechanism of flank collapse on oceanic shield volcanoes, the mechanical ability of such low-dipping intrusions to destabilise a volcanic edifice remains to be tested. However, it is clear from previous studies that there is a close relationship between magmatism and flank instability in the evolution of basaltic volcanoes.

In this section of the study, we investigate how planar intrusions can induce or enhance flank collapse in a volcano, depending on their geometry. To do so, we first provide a review of the most commonly observed intrusion geometries in basaltic volcanic edifices undergoing recurrent collapses. In volcanic nomenclature, sheet intrusions are commonly divided into *dikes* and *sills*, according to their geometric relationship with the host rocks. *Dikes* are high-angle sheet-like intrusions at crosscutting the host rock bedding while *sills* are low-angle intrusions subparallel to the host rock layering. However, the distinction between the two types of intrusions is commonly unclear in the literature: the inclination of the intrusion is often the only criteria taken into account in defining its nature. In order to avoid confusions, as our study deals with the influence of intrusions geometry in the deformation fields

of basaltic volcanoes, we prefer to refer to dikes as subvertical (or high-angle) intrusions and to sills as subhorizontal (or low-angle) intrusions.

3.2 Geometries of magmatic intrusions within basaltic volcanoes

In basaltic setting, magma is injected in the edifice as sheet intrusions rooted in a magma reservoir. Field analyses carried out on active and extinct basaltic volcanoes in Hawaii, American Samoa, Fogo, Tenerife, Stromboli and La Réunion have revealed that steeply-dipping intrusions (Fig. 3.5c) are dominant in the upper part of the edifices (< 1 km depth; Walker, 1986; Zbinden and Sinton, 1988; Walker and Eyre, 1995; Day et al., 1999; Marinoni and Gudmundsson, 2000; Tibaldi, 2003; Letourneur et al., 2008). These intrusions are concentrated along preferential pathways (i.e. rift zones).

A strikingly different geometry has been described for the intrusive complex injected in the lowermost units of the volcanic edifice of La Gomera (Canary archipelago), where most of the sheet intrusions present outward shallow dips ranging 0° to 30° (Cendrero, 1970; Ancochea et al., 2008). These intrusions are related to the development of a shield volcano that underwent successive flank collapses (Ancochea et al., 2006); then the volcano was cut by sub-vertical dikes related to the younger edifice (Ancochea et al. 2006). Abundant shallow dipping intrusions also developed in the submarine sequence of La Palma (Canary archipelago), above the plutonic complex (Staudigel and Schmincke, 1984; Fernandez et al., 2002). In a way similar to La Gomera, shallow-dipping intrusions are cut by subvertical dikes related to the younger edifice (Staudigel and Schminke, 1984). In the southern part of Piton des Neiges volcano, the deeply incised extinct volcano of La Reunion (section 2.2.2), about 45 % of sheet intrusions have a dip lower than 30° (Fig. 3.5d and 2.34c) and on the northern flank of Piton des Neiges, the majority of sheet intrusions also dip outward at low angle (≤ 30°, Fig. 3.6). These intrusions, which display radial outward dip directions, are either scattered in the lava pile or concentrated in narrow deformation zones.

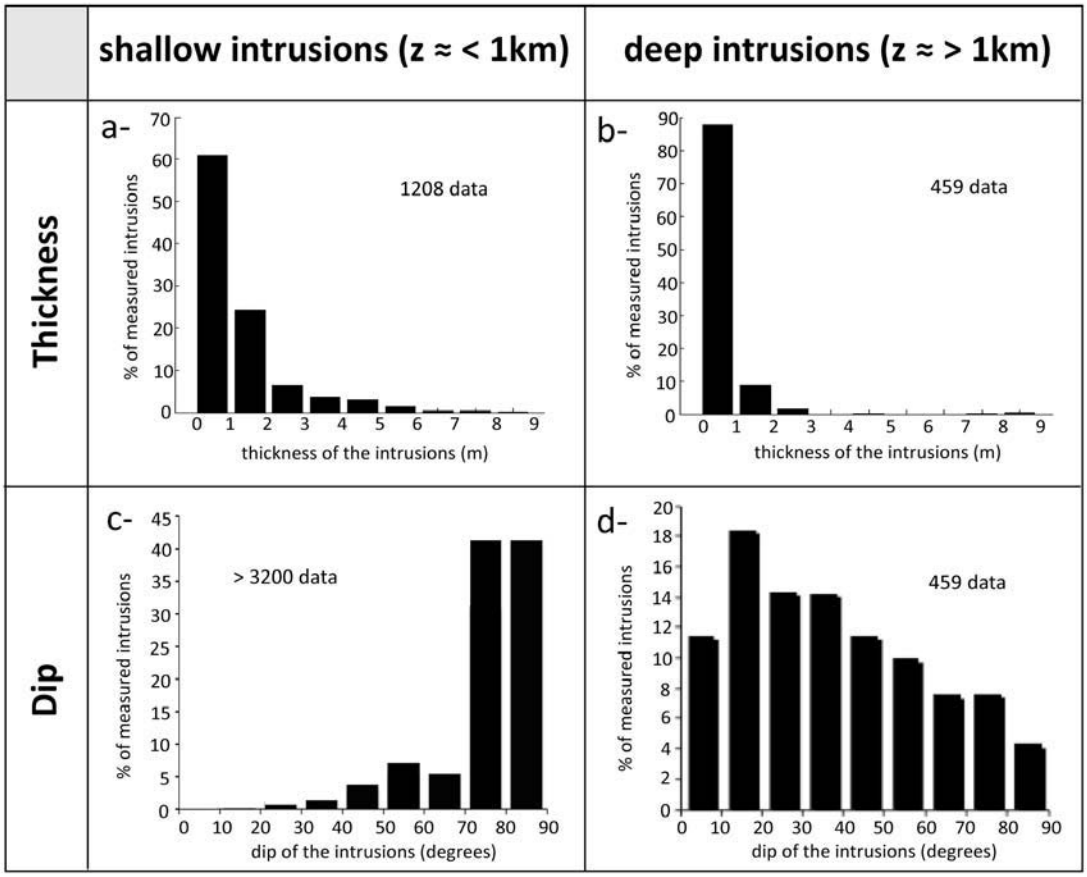

Figure 3.5: a and c- Histogram representing the opening and dip of 1208 and more than 3200 sheet intrusions from previous studies of shallow intrusions (depth < 1km) measured in poorly eroded basaltic volcanoes; b and d- Histogram representing the opening and dip of 459 deep sheet intrusions (depth > 1 km) from the highly eroded Piton des Neiges volcano (measurements were made in the Cirque of Cilaos, La Reunion Island, Chaput et al., 2010). Datasets (a and c) are based on field studies by: Walker, 1986; Zbinden and Sinton, 1988; Walker and Eyre, 1995; Day et al., 1999; Marinoni and Gudmundsson, 2000; Tibaldi, 2003; Letourneur et al., 2008.

Figure 3.5 a and b show that in basaltic volcanoes the majority (60 % at poorly-eroded volcanoes and 90 % on highly eroded volcanoes) of sheet intrusions are less than 1 m thick. This data gives an interesting insight on the relevance of the modelled opening of intrusions (see section 3.3) and on how to define overpressure within the fracture.

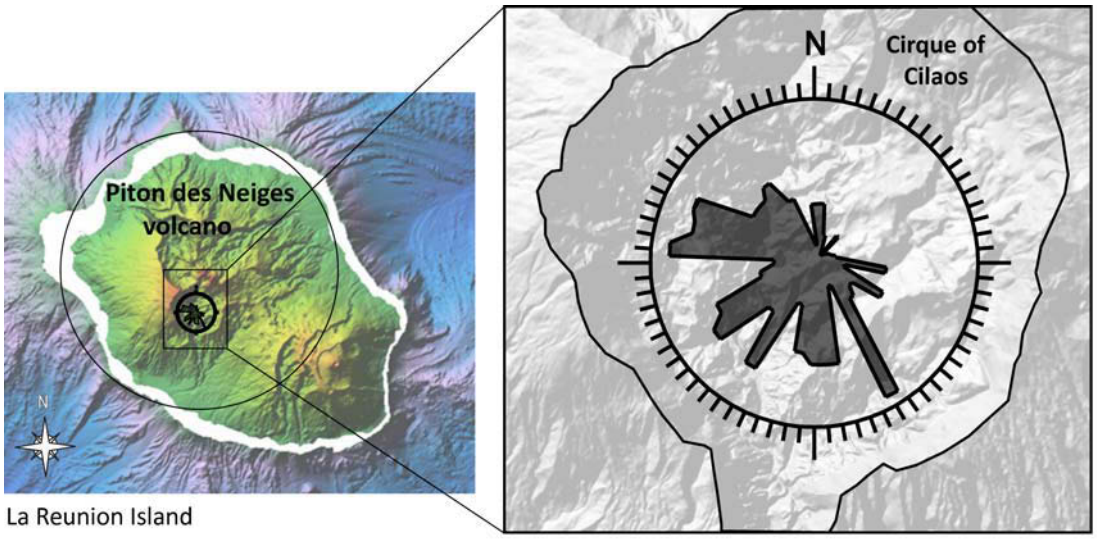

Figure 3.6: Rose diagram showing the dip directions of subhorizontal intrusions in the Cirque of Cilaos (Piton des Neiges volcano, data from Chaput et al., 2010).

Thus, besides subvertical intrusions, subhorizontal magma injections may occur in basaltic volcanoes. The difference in the structural level cut by each intrusion geometry, i.e. in subsurface for subvertical intrusions and at depth for subhorizontal ones, suggests that magma is mostly injected subhorizontally at depth and subvertically in the upper part of the edifice. In the following sections, we aim at understanding with a numerical Boundary Element Method the role of subvertical or subhorizontal magma injections in the volcano stability.

3.3- Numerical modelling of sheet intrusions: methodology

Theoretical studies indicate that magma should intrude perpendicular to the least principal stress (Anderson, 1938). If magma intrudes in a preexisting fracture or fault (Currie and Ferguson, 1970; Gudmundsson, 1983), or is guided by a rheological contrast (Kavanagh et al., 2006; Menand, 2009; Maccaferri et al., 2010), it might be emplaced in a direction oblique to the minimum principal stress. As a result, both normal and shear displacements may occur. Furthermore, Watanabe et al. (2002) showed that intrusions are not always emplaced perpendicular to $\sigma 3$ due to the competition existing between the external stress and the internal pressure of magma within the fracture. Because of this effect, it might take time for an intrusion

to re-orientate according to the local stress field. Thus, we developed numerical models with different stress conditions, in which we test the influence of shear on a volcanic edifice during intrusions of planar fractures of various geometries.

3.3.1 Model description

In order to study the response of a volcano to such fractures, we use a Mixed Boundary Elements numerical Method (MBEM; Cayol and Cornet, 1997) for linear elastic, homogeneous and isotropic media. The MBEM is a fully three-dimensional method which considers realistic topographies as well as any number and geometry of sources, such as magma reservoir, intrusions or faults. This method is based on the combination of two boundary element methods: the Direct method (Rizzo, 1967) and the Displacements Discontinuities method (DD, Crouch, 1976). The MBEM was developed by Cayol and Cornet (1997) from the pre-existing *COMPUTE3D* code (Curran et al., 1994) only based on the Direct method. The Direct method is well adapted to massive structures (reservoirs) while the DD method is more efficient for discontinuities like fractures. The combination of the two methods was made integrating the boundary conditions of the DD method to the equations of the Direct method (Cayol and Cornet, 1997). The MBEM method permits to discretize a 3D space by its surfaces (topography and surfaces submitted to stress like the intrusions), decreasing the calculation time. The precision and applicability of the MBEM for modelling volcanic deformation processes have already been tested and applied in several studies (Cayol and Cornet, 1997; Beauducel and Cornet, 1999; Cayol et al., 2000; Dieterich et al., 2000; Froger et al., 2004; Fukushima et al., 2005 and 2010).

In the model, boundary conditions are not displacements but stresses, the stress at the surface is considered null. In this work, perturbations (driving stresses) of the initial state of stress are calculated and applied to the fractures in order to investigate the resulting displacement field. Our model is static, as we are interested in the final deformation produced by the intrusion. The topography and the fractures (sheet intrusions) are meshed by triangular elements. Mesh density

increases in areas where deformation gradients are expected to be the largest and decreases farther (Fig. 3.7a).

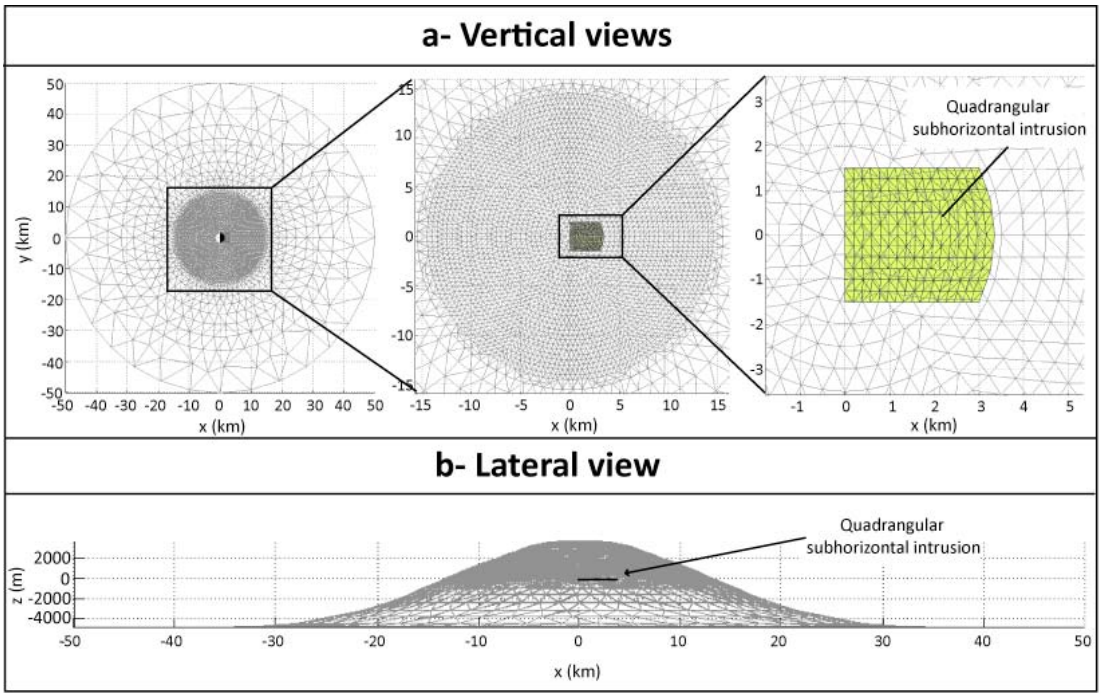

Figure 3.7: Geometry and mesh of the topography in vertical (a) and lateral (b) views. The mesh is denser in the summit part, above the area where fractures (in green) are located.

Slopes of basaltic volcanoes usually range from few degrees to 12° (Rowland and Garbeil, 2000) although some volcanic edifices, such as Piton de la Fournaise and Stromboli, have unusual slopes locally reaching 20 to 35°. An axial-symmetrical cone-shaped topography with 20° slopes is thus used (Fig. 3.7b). This assumption seems reasonable as the slope of the edifice has little influence on displacements if it is not steeper than 20° (Cayol and Cornet, 1998). The role of a steeper slope will be discussed in section 3.4.

3.3.2 Fractures geometry

Since the geometry of subhorizontal fractures is poorly-constrained by field data, we assumed both kind of fractures (subvertical and subhorizontal) are planar

and have a simple quadrangular shape (Fukushima, 2005; Fig.3.8a), with 3 km-long sides. Here, the size of the intrusions is such that both subhorizontal and subvertical fractures have the same area. Following field studies, we assume that subvertical fractures have dips ranging from 60 to 90° and that subhorizontal ones have dips ranging from 0 to 30° (Fig. 3.8b).

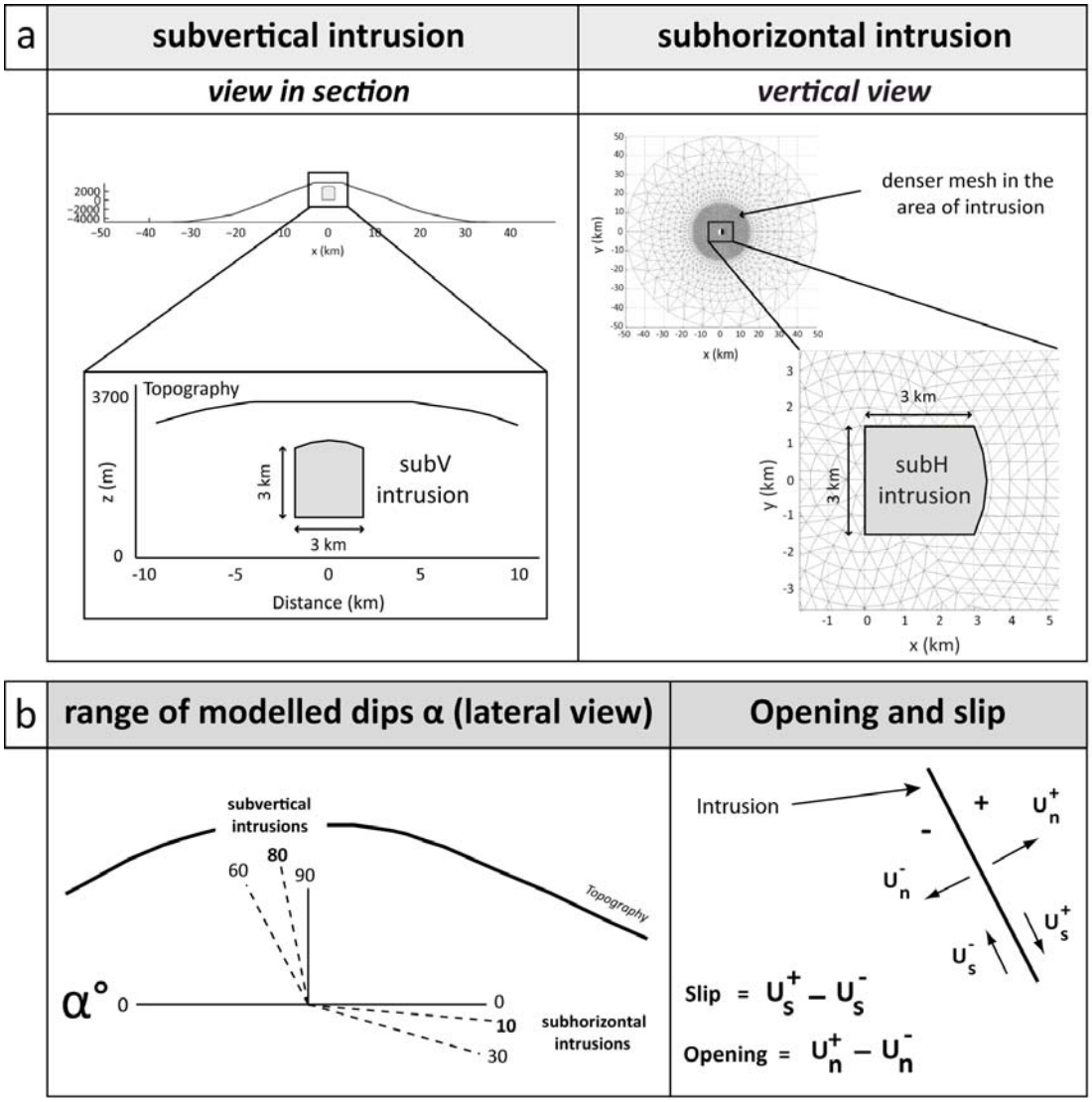

Figure 3.8: a- Geometries of subVertical (subV) and subHorizontal (subH) fractures considered in the model and b- the range of assumed dips and definition if the opening and slip of the fractures. These representations are not at scale. Both type of fractures have the same area in the model.

The fractures are assumed to be emplaced from a reservoir located at 2.5-3 km below the summit of the edifice, corresponding to the level of neutral buoyancy in basaltic edifices (Tilling and Dvorak, 1993). Neutral buoyancy is the level where magma density equals the density of the surrounding rocks. This is broadly the depth of the top of summit reservoir determined at Kilauea, Mauna Loa, Krafla (Tryggvason, 1984) and Piton de la Fournaise (Peltier et al., 2007 and 2008; Nercessian et al., 1996; Battaglia et al., 2005). In our models, the top of the subhorizontal fractures and the bottom of the subvertical ones are located at z = 0, beneath the axis of symmetry of the topography.

The opening and slip calculated for every types of fractures are displacement discontinuities, as defined by Fig. 3.8b. The slip is the difference between displacements occurring along the fracture, on each side of the fracture, while the opening is the difference between normal displacements on each side of the fracture.

3.3.3 Principal stresses in the edifice

Initial principal stresses in the elastic medium are assumed to be parallel to the geographic axis at the location of the intrusions. The x axis is oriented in the East-West direction and the y axis in the North-South direction. Indeed, maximum principal stress directions resulting from gravity-loaded models were shown to be subvertical except for the shallowest part of the edifice where they become parallel to the ground surface (Cayol and Cornet, 1998; Letourneur et al., 2008). These principal stresses will be refered to as σ_v and σ_h for the vertical and horizontal principal stresses, respectively.

We define the stress ratio *k* as

$$k = \sigma_h / \sigma_v \qquad (1)$$

In this study, displacements associated to injections in edifices loaded by two different initial state of stress are compared: (i) the initial stress is assumed to be

isotropic with terms equal to the weight of rocks such that the ratio *k* is 1; (ii) the initial stress is assumed to be anisotropic, such that the maximum principal stress is vertical and the ratio *k* is <1.

A crude estimate of the crust stress ratio *k* is given by considering a half-space deforming uniaxially under its own weight (no horizontal extension). For this special case, the stress ratio is determined to be (Jaeger and Cook, 1979):

$$k = \frac{\sigma_h}{\sigma_v} = \frac{\upsilon}{(1-\upsilon)} = 1/3 \text{ for } \upsilon = 0.25 \qquad (2)$$

This loading neglects both pore fluids and the fact that the state of stress in a edifice results from the successive episodes of tectonic loading and faulting. In volcanic islands as well as on continental crust, stress changes created by fluids movement, whether magmatic (Dieterich et al., 2000), acqueous or gasous (Roeloffs, 1996; Segall et al., 1994) or resulting from fault motions (Stein et al., 1992; Segall et al., 2006), may trigger seismicity. In situ stress measurements in deep wells and boreholes worldwide (Townsend and Zoback, 2000) show that the Coulomb failure theory, using friction coefficients, μ, in the range of 0.6-1, gives predictions that are consistent with the measurements. These studies also indicate that pore pressures are close to hydrostatic. Assuming the crust is in a state of failure equilibrium, we can compute the stress ratio *k* of a fluid saturated crust as:

$$\frac{\sigma_h}{\sigma_v} = \frac{\sqrt{1+\mu^2}-\mu}{\sqrt{1+\mu^2}+\mu} + 2\frac{\rho_w}{\rho_r}\frac{\mu}{\sqrt{1+\mu^2}+\mu} \qquad (3)$$

where, ρ_w and ρ_r are the density of water and the bulk density of volcanic rock, respectively. Taking ρ_r= 2700 kg/m^3 and considering friction coefficients corresponding to extreme values of laboratory experiments, we get ratios of σ_h / σ_v ranging from σ_h / σ_v = 0.5 for μ= 1 to σ_h / σ_v = 0.9 for μ= 0.6.

Here, we have chosen to investigate the displacements induced by stress anisotropy such that: $0{,}6 < k < 1$ (4)

3.3.4 Applied traction perturbation

Along the fracture surface, the stress perturbations tensor corresponding to the intrusion of magma in the elastic rock matrix is defined as :

$$\Delta\sigma(z) = \begin{bmatrix} P_m(z) - k\sigma_v(z) & 0 & 0 \\ 0 & P_m(z) - k\sigma_v(z) & 0 \\ 0 & 0 & P_m(z) - \sigma_v(z) \end{bmatrix} \qquad (5)$$

where $P_m(z)$, the magma pressure is created by the magma density, ρ_m, in the inclined fracture with its top at z_0, and an constant overpressure ΔP_0, inherited from the magmatic source:

$$P_m(z) = \rho_m g(z_0 - z) + \Delta P_0 \qquad (6)$$

We assume that, in the edifice, the maximum principal stress σ_v is lithostatic. It is given by

$$\sigma_v(z) = \rho_r g(z_{surf} - z) \qquad (7)$$

Here, z_{surf} is the elevation of the surface above each fracture element.

Figure 3.9 presents a description of the model parameters, in the cases of subvertical and subhorizontal fractures.

a- Model parameters in the case of a subvertical intrusion

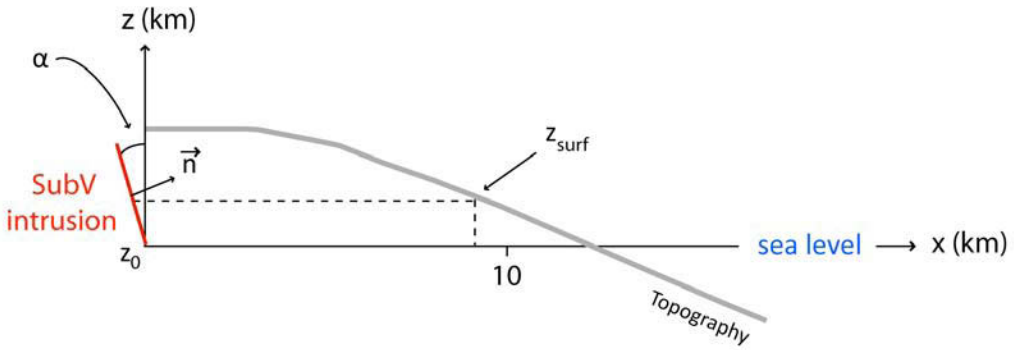

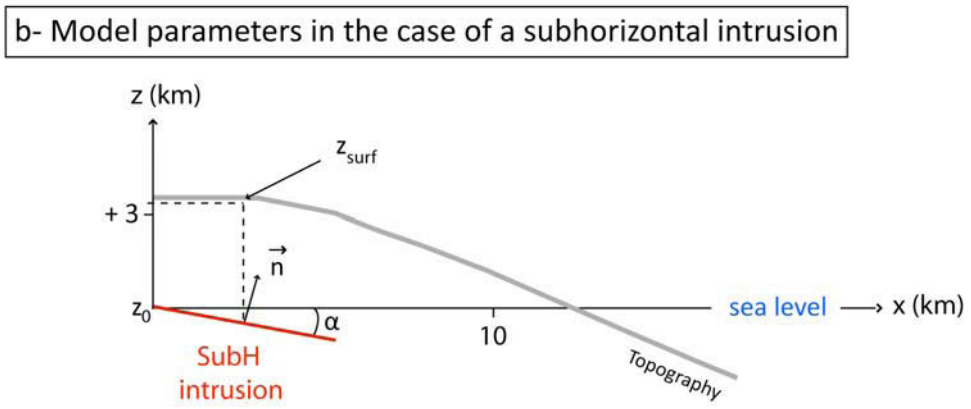

Figure 3.9: Main parameters involved in the calculation of the displacements associated to a subvertical (a) or subhorizontal (b) fracture. α is the dip of the fracture (cf Fig. 3.8b), $\vec{n}$ is the vector normal to the fracture and z_{surf} is the elevation of the surface above each element of the fracture. SubV = Subvertical; SubH = Subhorizontal.

Normal stress change, $\Delta\sigma_n(z)$, and shear stress change, $\Delta\tau(z)$, resolved on the fracture, dipping at an angle α, can be computed from equation (5) and are given as:

$$\Delta\sigma_n(z) = P_m(z) - \sigma_v(z)(k\sin\alpha^2 + \cos\alpha^2) \qquad (8)$$

and

$$\Delta\tau(z) = \sigma_v(k-1)\cos\alpha\sin\alpha \qquad (9)$$

Practically, in our boundary element code we apply tractions vectors, T, to each triangular element of the fractures corresponding to:

$$\mathrm{T} = \Delta\sigma(z)n, \qquad (10)$$

where $\Delta\sigma(z)$ is given by (5) and $n = (\sin\alpha, 0, \cos\alpha)^{\mathrm{T}}$ is the unit normal vector to the fracture.

In the calculations, we the take the same bulk density of rocks as used for defining ranges of stress ration ρ_r= 2700 kg/m^3. The picritic magma density is taken as ρ_m= 3200 kg.m^{-3}. We also compute the value of ΔP_0 so that the mean value of the normal stress change $\Delta\sigma_n(z)$ corresponds to normal stress change generally inferred for intrusions. From the inversion of GPS and InSAR displacements associated to recent eruptions of Piton de la Fournaise volcano (Peltier et al, 2007;

2008; Fukushima et al., 2010), values of overpressure were determined to range from 0.3 to 6 MPa. At Stromboli volcano, using ground-based InSAR displacements and forward numerical modelling, Casagli et al. (2009) estimated overpressures of 0 to 1 MPa for the pre-effusive displacements of the 2007 eruption. At Sierra Negra volcano (Galapagos Island), a sill overpressure of 4.5 MPa was estimated at a depth of 2 km from the inversion of InSAR data. In our models, we assume a mean value of normal stress change of $\overline{\Delta\sigma_n(z)}$ = 1 MPa.

3.3.5 Normalization of the results

Pollard et al. (1983) studied analytically the surface displacements in volcanic rift zones associated with the emplacement of a magma-filled crack in a homogeneous and elastic medium using a Boundary Element Method. In 2D, they showed that the walls of the crack undergo displacements depending on the normal stress applied to the crack, its length and the elastic parameters of the medium in which the fracture intrudes, i.e. the Young's modulus E and the Poisson's ratio υ. In this study, we extend these normalizations to our 3D case with shear and normal stresses applied to the fractures and take into account the surface and the total stress applied to the fracture. We normalize the opening and slips of the modelled fractures, the internal and surface displacements due to the fractures under different states of stress (normal, shear or mixed) dividing the modelled values by a parameter *dnorm* defined as:

$$dnorm = \frac{\sqrt{[\Delta\sigma_n(z)]^2 + [\Delta\tau(z)]^2}}{E} \cdot S \cdot 2(1-\upsilon^2)$$

dnorm is a function of the total stress variation $\sqrt{[\Delta\sigma_n(z)]^2 + [\Delta\tau(z)]^2}$, the surface of the fracture S and the elastic parameters (E, υ) of the medium where intrusions are emplaced. Normalized values of displacements are expressed in m^{-1}.

When modelling results are not normalized, calculated values of displacements along the fracture (opening and slip) and of the edifice (internal and surface displacements) are specific to one geometry of fracture, submitted to a specific

stress field and emplaced within a specific medium characterised by its elastic parameters, and can not be compared to results obtained in other conditions. The purpose of normalization of the displacements is to generalise our study to fractures having variable geometries, emplaced under various stress conditions (different values of normal and shear stresses) within medium characterized by different elastic parameters. Trough the study of normalized results, we aim at:

1- facilitating the comparison of surface displacement fields generated under various conditions,

2- giving simple keys to the determination of the nature of the fractures (subhorizontal or subvertical),

3- estimating the value of the fracture dip,

4- estimating the depth of the fracture,

5- giving insights on the nature of the initial state of stress within the edifice, from the study of the recorded surface displacements of volcanic edifices.

3.4- Numerical modelling of sheet intrusions: Results

In order to understand the role of the loading conditions and of the fracture dip in the edifice deformation, we compare internal and surface displacements fields induced by:

1- intrusions submitted to purely normal stress changes (pressure changes) as induced by subvertical or subhorizontal intrusions perpendicular to $\sigma 3$,

2- purely shear stress changes as induced along faults and

3- normal stress changes combined with shear stress changes as created on intrusions emplaced at an angle from $\sigma 3$,

for (i) a subvertical plane with a 80° dip (α = 80°), as described in the upper parts of basaltic volcanoes (Fig. 3.5c), and (ii) a subhorizontal plane with a 10° dip (α = 10°),

as in the deeper parts of volcanoes (Fig. 3.5d). Then, modelling results for several dip angles of fractures are presented, and finally we compare the maximum opening and slip at the fracture surface and the internal and surface displacements of the edifice as a function of the dip α and stress anisotropy k, in order to extract criterion of determination of the nature (dip and depth) of the fractures and the stress field within the edifice. In the section 3.5, all modeled displacements are normalized by *dnorm* and expressed in m^{-1}.

3.4.1- Edifice displacements associated with subhorizontal or subvertical fractures.

We model the amplitudes and directions of internal and surface displacements caused by the subhorizontal and subvertical fractures within the edifice. Surface displacements can either be vertical displacements (uplift movements being counted positively) or horizontal movements (outward movements being counted positively). In order to compare surface displacements patterns between subvertical and subhorizontal fractures, and to propose keys of determination of the fracture geometry from surface displacements, we define surface displacement ratios, using maximum amplitudes of displacements of "blocks" in motion: the hangingwall and footwall of subvertical fractures (Fig. 3.10a1) and the head and toe of subhorizontal fractures (Fig. 3.10b1).

For a subvertical fracture, we define :

- the maximum horizontal displacement of the fracture hangingwall as Mb (Fig. 3.10a2)

- the maximum horizontal displacement of the fracture footwall as Ma (Fig. 3.10a2)

and the surface horizontal displacement ratio is defined as: $\boxed{R(X) = \frac{Mb}{Ma}}$

- the maximum vertical displacement of the fracture hangingwall as Mb' (Fig. 3.10a3)

- the maximum vertical displacement of the fracture footwall as Ma' (Fig. 3.10a3)

and the surface vertical displacement ratio is defined as: $\boxed{R(Z) = \frac{Mb'}{Ma'}}$

Moreover, we study the variations of the ratios of maximum horizontal by vertical displacements, defined as:

$\boxed{R(X/Z)_{hw} = \frac{Mb}{Mb'}}$ for the fracture hangingwall

$\boxed{R(X/Z)_{fw} = \frac{Ma}{Ma'}}$ for the facture footwall

On the other hand, For a subvertical fracture, we define :

- the maximum horizontal displacement of the fracture toe as Md (Fig. 3.10b2)

- the maximum horizontal displacement of the fracture head as Mc (Fig. 3.10b2)

and the surface horizontal displacement ratio is defined as: $\boxed{R(X) = \frac{Md}{Mc}}$

- the maximum vertical displacement of the fracture toe as Md' (Fig. 3.10b3)

- the maximum vertical displacement of the fracture head as Mc' (Fig. 3.10b3)

and the surface vertical displacement ratio is defined as: $\boxed{R(Z) = \frac{Md'}{Mc'}}$

We also define $\boxed{R(X/Z)_{hd} = \frac{Md}{Md'}}$ for the fracture head and $\boxed{R(X/Z)_{toe} = \frac{Mc}{Mc'}}$ for the fracture toe.

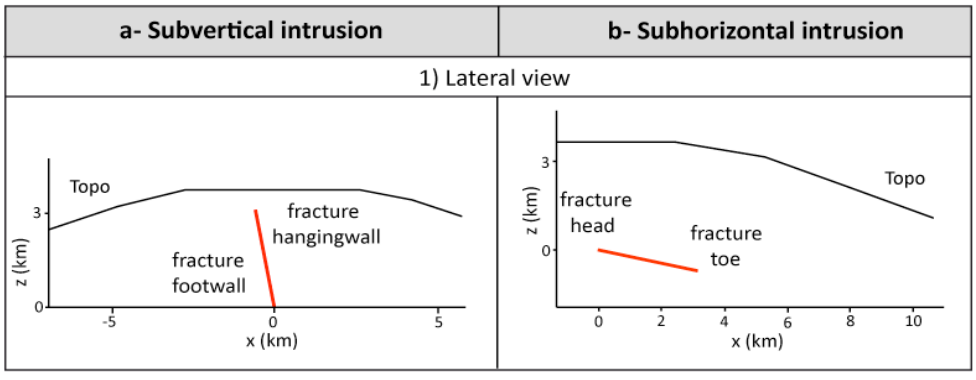

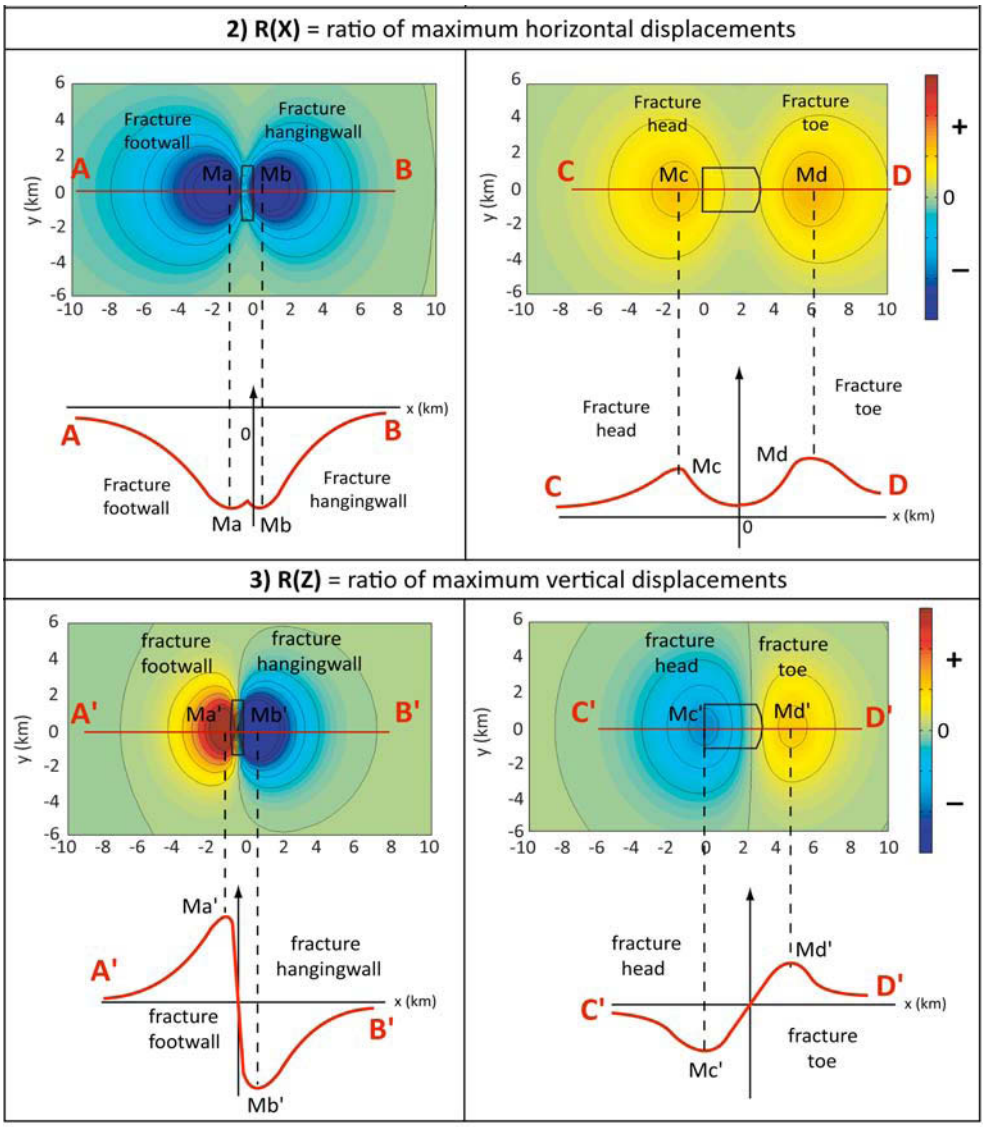

Figure 3.10: Nomenclature of the surface displacement ratios used in the comparative study of displacement fields caused by subvertical (a) and (b) subhorizontal fractures. 1- Definition of the hangingwall and footwall of a subvertical fracture, and of the head and toe of a subhorizontal fracture. 2- Definition of the horizontal displacement ratios R(X) for both types of intrusions and 3- Definition of the vertical displacement ratios R(Z) for both types of intrusions.

3.4.1.1- Subvertical fracture (α = 80°)

Figure 3.11 presents the normalized opening and slip affecting a subvertical fracture under various stress modes: a- normal stress only, b- shear stress only and c- a mixed mode of stress where normal and shear stresses occur. When submitted to normal stress only (assumed to be constant and equal to 1 MPa, Fig. 3.11a), a 80° subvertical intrusion with 1 MPa internal overpressure is opened in a direction

normal to the fracture, with a maximum opening at the center of the intrusion. Slip along the fracture is negligible as no shear stress occurs at the surface of the intrusion. If only shear stress occurs at the surface of the fault, this latter is affected by small values of opening while the slip along the fault reaches high values spread on a large part of the surface of the fault, with a maximum at the center (Fig. 3.11b). Finally, under a stress mode combining normal and shear stresses, the intrusion is affected by opening and slip. Maximum values are located at the center of the fracture. However, the maximum amplitude of slip under a mixed mode of stress is smaller than the maximum slip under shear stress only. Similarly, the maximum opening in a mixed mode is smaller than the maximum opening under normal stress only (Fig. 3.11c).

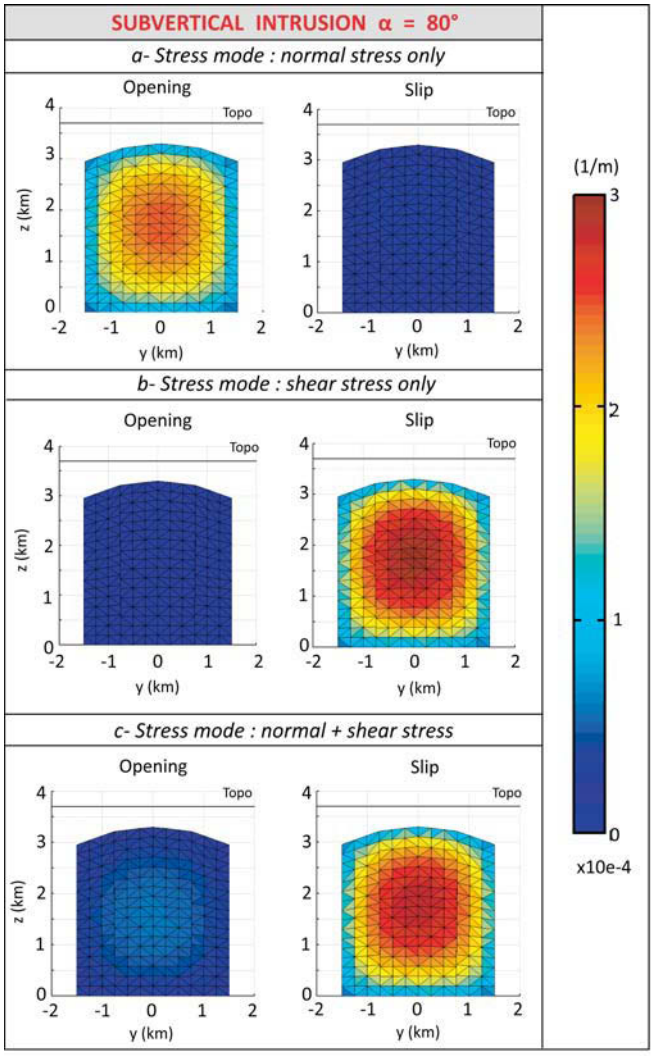

Figure 3.11: Normalized opening and slip (in m^{-1}) of a 80° subvertical fracture submitted to a- normal stress only, b- shear stress only or c- normal + shear stresses.

Models show two contrasting displacement patterns for normal, shear and mixed stress fields (Fig. 3.12). When the intrusion is submitted to normal stress only (i.e. the fracture is emplaced perpendicular to sigma 3 or the state of stress is isotropic), internal displacements are maximum at the center of the intrusion, where the opening is maximum. Internal displacements in the upper part of the edifice are upward and outward in the hanging wall and upward and inward in the footwall (Fig. 3.12a). Surface displacements of the fracture footwall show an upward movement, with a slight subsidence close to the intrusion while the hangingwall undergoes high amplitude upward displacements. In the horizontal plane, the hangingwall and footwall present opposite displacements. The former moves outward while the footwall moves inward (Fig. 3.12a). When studying surface vertical ratios, one can expect to get a positive ratio, while surface horizontal ratios will be negative (Table 3.1).

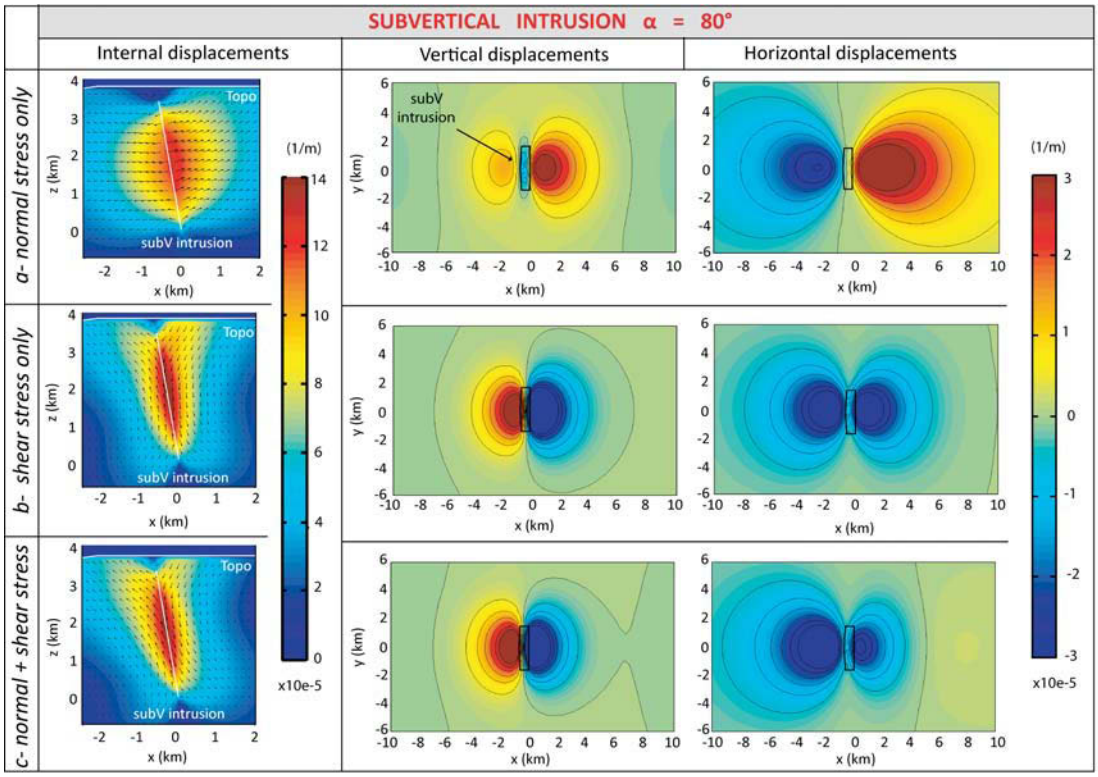

Figure 3.12: Internal and surface displacements associated with a subvertical plane (α = 80°) submitted either to a- normal stress only, b- shear stress only (k = 0.6), c- normal + shear stress (k = 0.6).

In the case of an anisotropic stress (i.e. shear stress only or combined normal and shear stresses), internal displacements maximum at the center of the intrusion but stronger than in the previous case (Fig. 3.12b and c). Internal displacements of the hanging wall are oriented inward and downward while the footwall is affected by inward and upward displacements. Vertically, the footwall undergoes an upward movement while the hangingwall undergoes a subsidence. Horizontally, both walls of the subvertical fracture undergo inward displacements (Fig. 3.12b and c). Surface vertical ratios are expected to be negative, while surface horizontal ratios will be positive. In the case of a subvertical fracture, maximum displacements are located in the summit area of the edifice.

3.4.1.2- Subhorizontal fracture (α = 10°)

Figure 3.13 presents the normalized opening and slip affecting a subhorizontal intrusion under various stress modes: a- normal stress only, b- shear stress only and c- a mixed mode of stress where normal and shear stresses occur. With normal stress only and shear stress only, results for a subhorizontal fractures are very similar to those obtained for a subvertical injection, although the maximum amplitudes of opening and slip are smaller than the ones obtained for a 80° dipping fracture. With a mixed mode of stress, similarly to the subvertical intrusion, the opening of the intrusion is small but amplitudes of opening in the center of the intrusion are higher for a subhorizontal intrusion, while the slip along the intrusion has a similar pattern but smaller amplitudes.

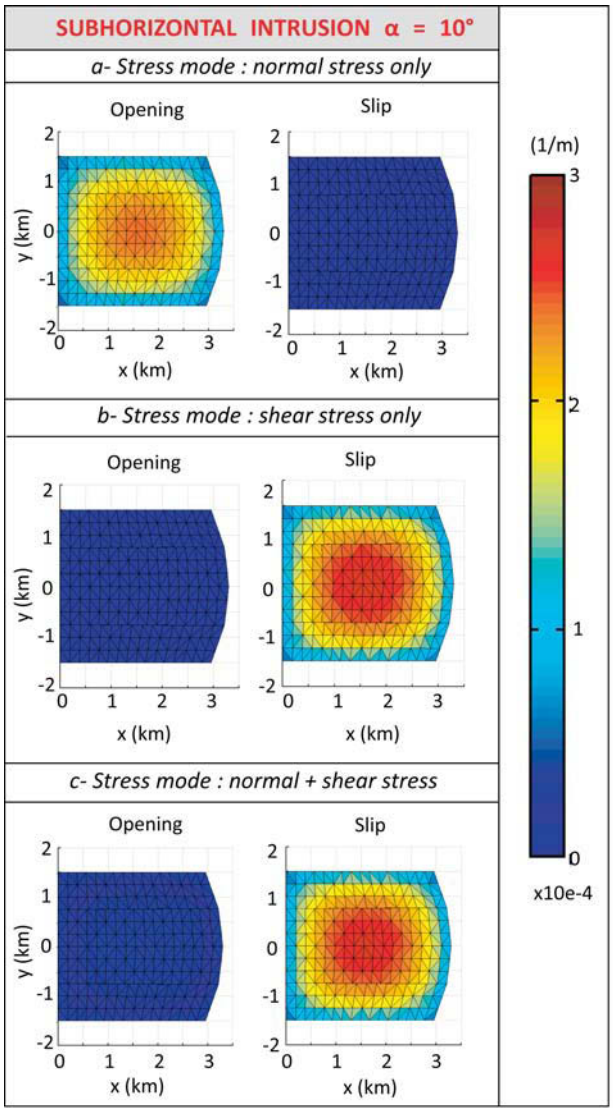

Figure 3.13: Normalized opening and slip (in m^{-1}) of a 10° subhorizontal intrusion submitted to a-normal stress only, b-shear stress only or c-normal + shear stresses.

In a way similar to subvertical fractures, the displacement fields related to subhorizontal fractures show striking differences (Fig. 3.14). When the intrusion is submitted to purely normal stresses (emplaced perpendicular to sigma 3 or in an isotropic stress field), internal displacements are sub-vertical, maximum on top of the intrusion and diverge from the fracture center. Thus they are oriented inward at the head of the intrusion and outward at the toe of the intrusion. Vertical displacements are symmetrical, exclusively oriented upward and reach a maximum on top of the intrusion, below the summit of the edifice. The head and the toe of the intrusion undergo opposite horizontal displacements, oriented inward for the head

and outward for the toe (Fig. 3.14a); we can expect to find positive vertical surface ratios and negative horizontal surface ratios. When the fracture is emplaced in an anisotropic stress field and at an angle from sigma 3 (shear stress only or mixed mode), internal displacements at the head, the center and the toe of the fracture are oriented outward, with maximum amplitudes at the center of the fracture. Vertical displacements are opposite: subsidence of the fracture head and uplift of the fracture toe; a negative vertical surface ratio is expected. Horizontal movements both are oriented outward at the head and toe; a positive horizontal surface ratio is expected. Internal and surface displacements affect the summit area and the flank of the edifice (Fig. 3.14b and c).

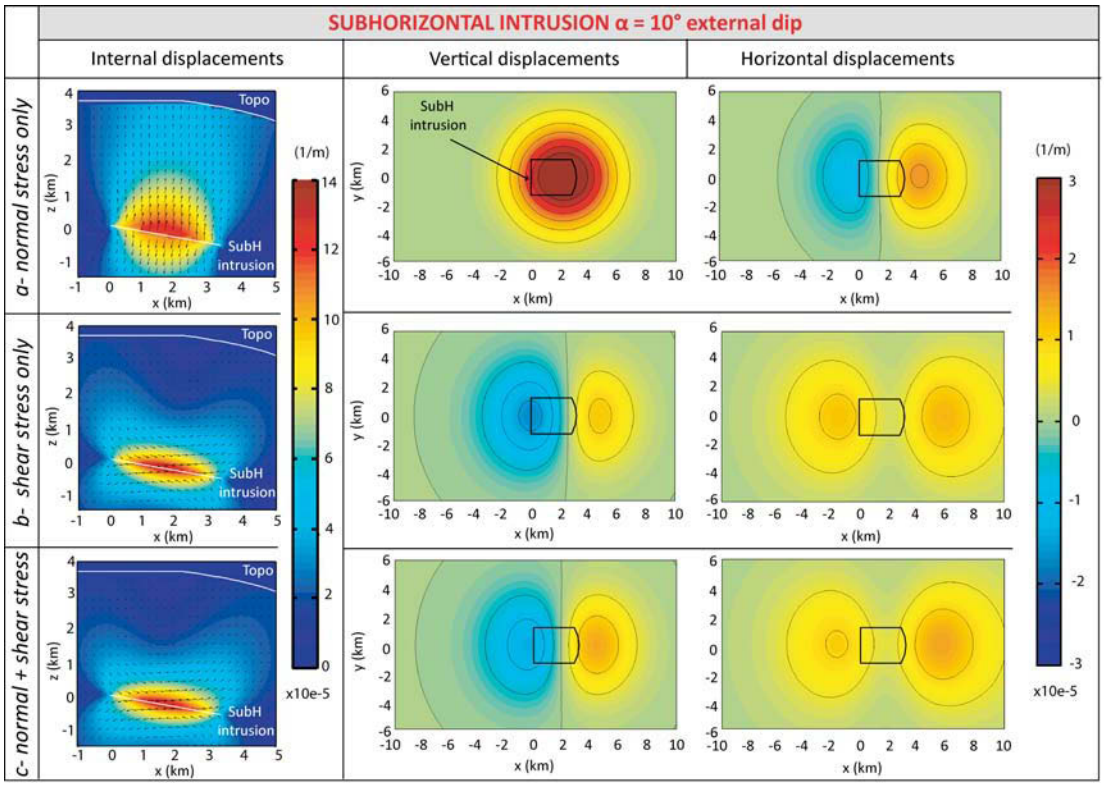

Figure 3.14: Internal and surface displacements associated with a subhorizontal plane (α = 10°) submitted either to a- normal stress only, or b- shear stress only (k = 0.6), or c- normal + shear stress (k = 0.6).

On the basis of the definitions of fig. 3.10 and the relative movements of high-angle and low-angle fractures compartments showed in fig. 3.12 and 3.14, the expected

amplitudes and signs of the ratios for both types of intrusions under various stress fields are summarised in Table 3.1.

Nature of stress field	Ratio	80° subvertical intrusion		10° subhorizontal intrusion	
		sign	amplitude	sign	amplitude
normal stress only	R(X)	negative	~ -1	negative	-1.5 to -1
	R(Z)	positive	> 1	positive	1
	R(X/Z)_hw or toe	positive	~ 1	positive	> 1
	R(X/Z)_fw or hd	negative	< -1	negative	-1 to 0
shear stress only*	R(X)	positive	~ 1	positive	~ 1
	R(Z)	negative	~ -1	negative	~ -1
	R(X/Z)_hw or toe	positive	~ 1	positive	> 1
	R(X/Z)_fw or hd	negative	< -1	negative	~ -1
normal + shear stresses	R(X)	positive	> 1	positive	> 1
	R(Z)	negative	< -1	negative	< -1
	R(X/Z)_hw or toe	positive	0 to 1	positive	~ 1
	R(X/Z)_fw or hd	negative	< -1	negative	~ -1

*Table 3.1: Signs and amplitudes of the displacements ratios for subvertical and subhotizontal fractures injected in an isotropic or an anisotropic stress field. R(X) = maximum horizontal displacements ratio, R(Z) = maximum vertical displacements ratio, R(X/Z)_hw or hd = maximum horizontal by vertical displacement ratio of the fracture hangingwall or head and R(X/Z)_fw or toe = maximum horizontal by vertical displacement ratio of the fracture footwall or toe. * signs and amplitudes of R(X) and R(Z) are opposite if the intrusion is shallow, has a low dip or k is high.*

3.4.2- Role of the fractures dips

The average openings and slips of a fracture are not only function of the normal and shear stresses at its surface but also depend on the dip of the fracture and the stress anisotropy. Here we analyze the relationships with dip, while that with anisotropy will be developed in section 3.5.3. When the stress mode involves

only normal stress, dips range from 0 to 30° for subhorizontal intrusions and from 60 to 90° for subvertical ones. However, if shear stress is involved (alone or combined to normal stress, 3.5.2.2 and 3.5.2.3), the specific cases of strictly horizontal (dip = 0°) and strictly vertical (dip = 90°). Indeed, being parallel to the principal stress orientations, these fractures are not submitted to shear stress and have the same behaviour as in an isotropic stress field (3.5.2.1)

3.4.2.1- Normal stress only

In the case of intrusions submitted to normal stress only (i.e. isotropic stress field) *k* is equal to 1. Thus, only movements of opening normal to the fracture surface occur. The normal stress applied to the fracture being assumed constant, the normalized average openings are almost constant, small variations are only due to the position of the fracture with respect to the topography.

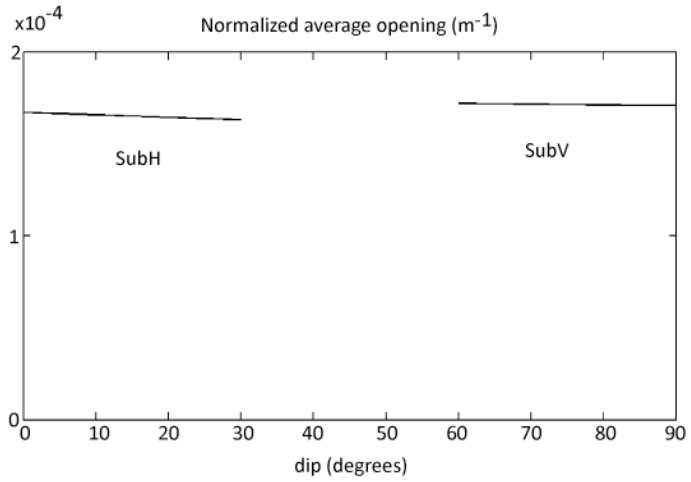

Figure 3.15: Variation of the normalized average openings (in m^{-1}) of the fractures as a function of their dip, with normal stress only. SubH = Subhorizontal intrusions; SubV = Subvertical intrusions.

In the case of subhorizontal intrusions, R(X) decreases when the dip increases as the maximum horizontal displacement associated with the toe of the intrusion decreases, while R(X) increases with the dip of subvertical intrusions until a value of -1 for a 90°-dipping intrusion, the displacement pattern being symmetrical on both sides of the fracture. R(Z) is almost constant for subhorizontal intrusions as the

surface vertical displacements are only made of one lobe with normal stress only (Fig. 3.14a). For subvertical intrusions, low dips correspond to low R(Z) due to strong asymmetry between the displacements of the hangingwall and the footwall of the intrusion (Fig. 3.12a). For dips close to 90°, the asymmetry decreses and R(Z) increases. R(Z) = 1 for dip = 90° as displacements are perfectly symmetrical, with the same amplitudes of opposite signs, the hangingwall being uplifted and the footwall subsided. $R(X/Z)_{hw,toe}$ have very similar evolution: they are always positive, increase with the dip of the intrusions, the $R(X/Z)_{hw}$ being superior to $R(X/Z)_{toe}$. $R(X/Z)_{toe}$ is inferior to 0.7 while $R(X/Z)_{hw}$ is superior to 0.7. $R(X/Z)_{hd}$ increases with the dips of the intrusions but are always negative, ranging between -1 and 0 for subhorizontal intrusions. For subvertical intrusions, $R(X/Z)_{fw}$ strongly varies with positive values for a dip between 60 and 75° and negative values for a dip between 75 and 90°.

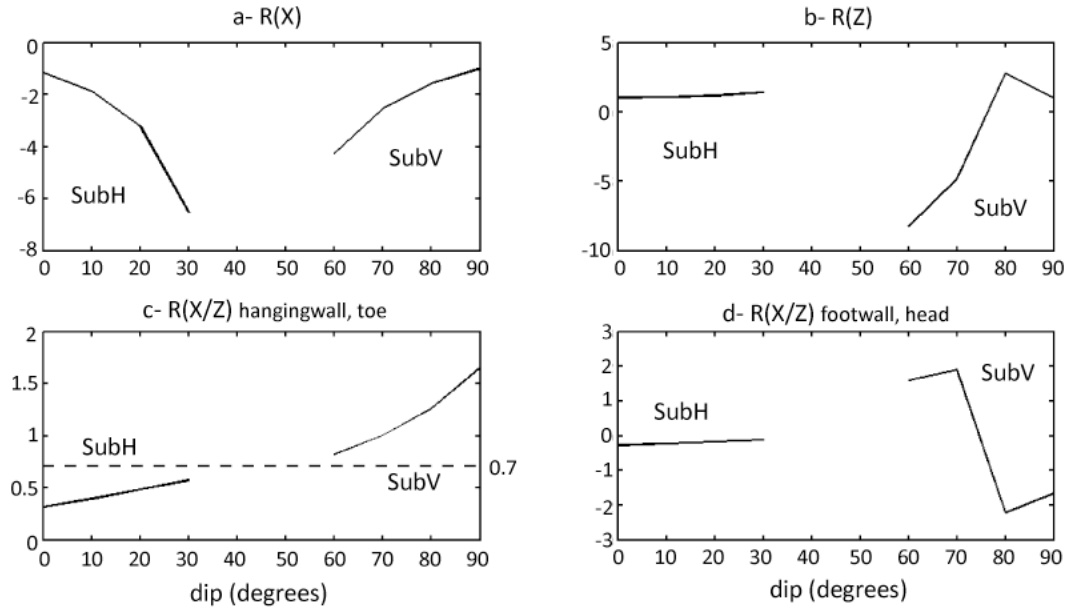

Figure 3.16: Influence of the dip of the intrusions on the surface displacements ratios when the intrusions are submitted to normal stress only: a- Variation of R(X); b- variation of the R(Z); c- variation of the R(X/Z) of the hangingwall (subvertical case) or the toe (subhorizontal case) of the fracture; d- variation of the R(X/Z) of the footwall (subvertical case) or the head (subhorizontal case) of the fracture. SubH = SubHorizontal intrusions; SubV = SubVertical intrusions.

The $R(X/Z)_{hw,toe}$ seems to be able to give interesting information in order to discriminate subvertical intrusions from subhorizontal ones, when emplaced with normal stress only. For other ratios, a given value can correspond to both subvertical

and subhorizontal intrusions, making impossible the distinction of the geometry of the intrusions in normal stress only

3.4.2.2- Mixed stress mode

In the mixed stress mode, the proportion of shear stress depends on the dip of the fracture/intrusion. It increases from 5 to 30° for subhorizontal intrusions and decreases when the intrusion tends to vertical (Fig. 3.17a). Although the applied normal stress is constant, the average opening for both types of intrusions varies with the dip angle (Fig. 3.17b). It is inversely proportional to the shear stresses. The larger the shear stress, the smaller the opening of the fracture. The dips of the intrusions have a small influence on the evolution of the average slip along the intrusions (Fig. 3.17c). The amplitudes of average slip is three times larger than the slip amplitudes for dips <= 10° and dips >= 80°, but become an order of magnitude larger than the average opening for dips > 10° and < 80°.

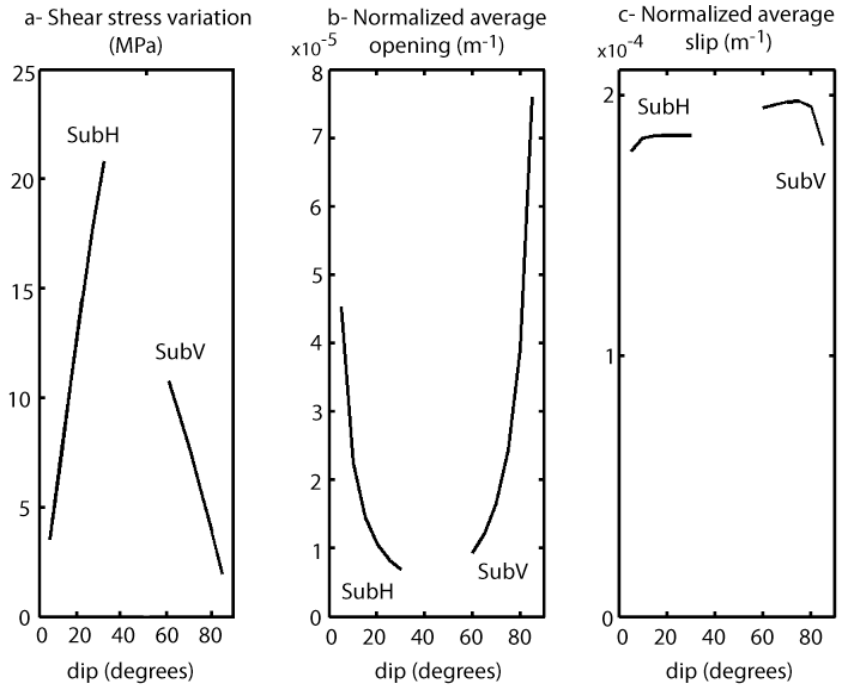

Figure 3.17: a- Variation of the shear stress (in Mpa) applied to fractures as a function of their dip; b- variation of the normalized average openings (in m^{-1}) of the fractures as a function of their dip; c- variation of the normalized average slips (in m^{-1}) along the fractures as a function of their dip. SubH = Subhorizontal intrusions; SubV = Subvertical intrusions. Stress mode = Normal + Shear stresses.

The study of surface displacements ratios shows a strong asymmetry of the surface horizontal displacements ratio R(X) between low-angle and high-angle fractures (Fig. 3.18a). R(X) decreases when the dip increases for both types of fractures, except for a 60°-dipping intrusion. However, the amplitudes of the ratios are not random as they are always superior to 0.8 for subhorizontal intrusions and always inferior to 0.8 for subvertical ones. When the intrusions are submitted to a mixed stress mode, R(X) are positive for all dips because the hangingwall/toe and footwall/head of the fractures undergo displacements oriented in the same direction (i.e. of same signs of the displacements). These general trends confirm the specific results obtained for the cases discussed in section 3.5.1 (Figs. 3.12 and 3.14). R(Z) has the same evolution for subhorizontal and subvertical intrusions: it increases with α (Fig. 3.18b). R(Z) is negative for all dips as the two sides of the fractures are affected by displacements in opposite directions (i.e. opposite signs). The variation is stronger in the case of subvertical intrusion due to the proximity with the topography. For what regards the surface horizontal/vertical displacements ratios R(X/Z), Fig. 3.18c indicates that $R(X/Z)_{hw}$ and $R(X/Z)_{toe}$ of the intrusions have a similar evolution whatever the type of intrusion and are always positive because both sides of the intrusions move towards the same direction. However, for subhorizontal intrusions, this ratio is superior to 0.6 while it is inferior to 0.6 in the case of subvertical intrusions. On the contrary, $R(X/Z)_{fw}$ and $R(X/Z)_{hd}$ have a similar evolution but are always negative because both sides of the intrusions move towards opposite directions (Fig. 3.18d), confirming again the results of Figs. 3.12 and 3.14.

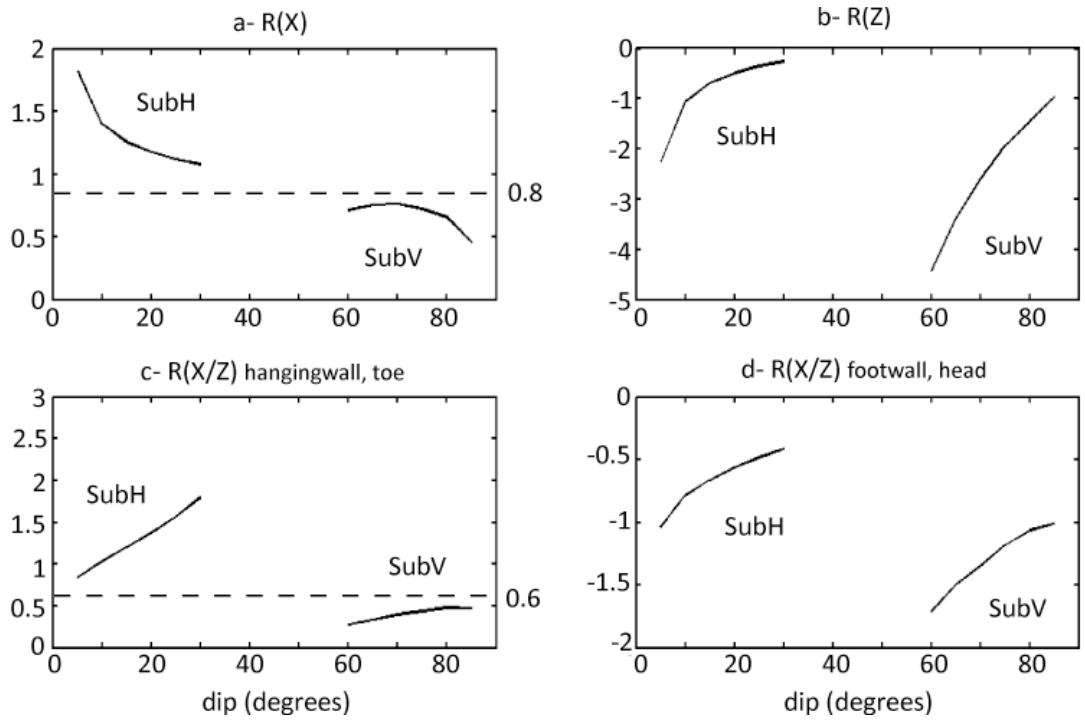

Figure 3.18: Influence of the dip of the intrusions on the surface displacements ratios when the intrusions are submitted to normal and shear stresses: a- Variation of R(X); b- variation of the R(Z); c- variation of the R(X/Z) of the hangingwall (subvertical case) or the toe (subhorizontal case) of the fracture; d- variation of the R(X/Z) of the footwall (subvertical case) or the head (subhorizontal case) of the fracture. SubH = SubHorizontal intrusions; SubV = SubVertical intrusions.

It appears from the analysis presented in Fig. 3.18 that RX (a) and $R(X/Z)_{hw,toe}$ (c) seem to be useful in order to discriminate subvertical from subhorizontal intrusions. The other ratios do not bring more information at this point.

3.4.2.3- Shear stress only

In the case of faults submitted to shear stress only, the internal overpressure of the faults is equal to 0 and k = 0.6. Thus, only movements of slip along the fractures occur. The shear stress variations for both types of fractures are very similar to those obtained with the mixed stress mode (section 3.5.2.2; Fig. 3.17a and 3.19a). Because of the normalization, the average slip along the faults is almost constant for both types of faults. The slight variation of slip for subvertical faults is related to the proximity of the topography (Fig. 3.19b).

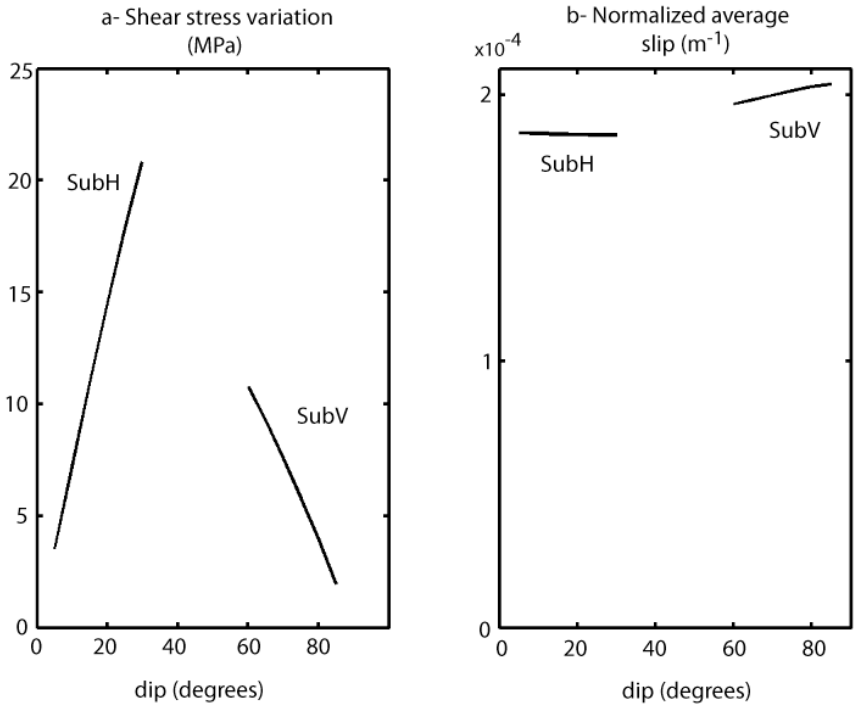

Figure 3.19: a- Variation of the shear stress (in MPa) applied to fractures as a function of their dip; b- variation of the normalized average slips (in m^{-1}) along the fractures as a function of their dip. SubH = Subhorizontal faults; SubV = Subvertical faults. Stress mode = Shear stress only.

The similarities between both stress modes (shear stress only and combined normal + shear stresses) are also visible on the evolutions of the surface displacement ratios (Fig. 3.20). However, some differences are remarkable: R(X) shows that the asymmetry between subvertical and subhorizontal faults is much less marked in the mode shear only than in the mixed mode (Fig. 3.20a). Moreover, R(X) for subhorizontal faults are superior to 1 while they are inferior to 1 for subvertical faults (Fig. 3.20a). Fig. 3.20c shows that the $R(X/Z)_{hw,toe}$ is always positive, superior to 0.8 for subhorizontal faults and inferior to 0.8 for subvertical faults. The evolution of other ratios is very similar to those of the mixed mode of stress.

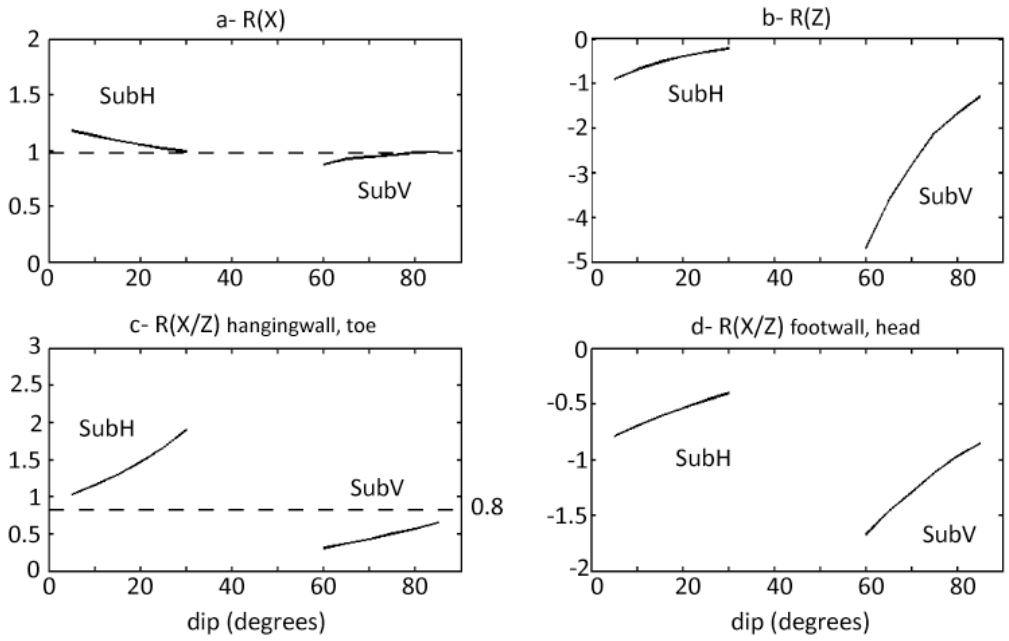

Figure 3.20: Influence of the dip of the faults on the surface displacements ratios when fault are submitted to shear stress only: a- Variation of the R(X); b- variation of the R(Z); c- variation of the R(X/Z) of the hangingwall (subvertical case) or the toe (subhorizontal case) of the fracture; d- variation of the R(X/Z) of the footwall (subvertical case) or the head (subhorizontal case) of the fracture. SubH = Subhorizontal faults; SubV = Subvertical faults.

Figs. 3.18 and 3.20 show that fractures submitted to normal and shear stresses and faults only affected by shear stress generate similar patterns of surface displacements and thus have the same contribution on the evolution of the geometry of the edifice. The comparison between the results obtained in the mixed mode of stress (fractures submitted to normal and shear stresses) and those obtained in a mode of shear stress only show that the R(X) and R(X/Z) (hangingwall and toe) can bring valuable information in order to distinguish subvertical from subhorizontal faults on the basis of surface recorded displacements. However, the study of the role of fault dips on the internal and surface displacements doesn't give strong insights that could help distinguish a mixed mode of stress from a shear only mode of stress due to the strong similarities in the evolution of the ratios in both stress modes.

3.4.3- Role of stress anisotropy

Here we investigate the influence of stress anisotropy on the average opening, average slip and surface displacement ratios for *k* ranging from 0.5 to 0.95. (*k* = 1 corresponding to an isotropic stress field is excluded).This influence has been tested for fixed dip values of 80° and 10° for subvertical and subhorizontal fractures respectively.

3.4.3.1- Mixed stress mode

By definition, for increasing values of *k*, the absolute values of shear stresses decrease (Fig. 3.21a).

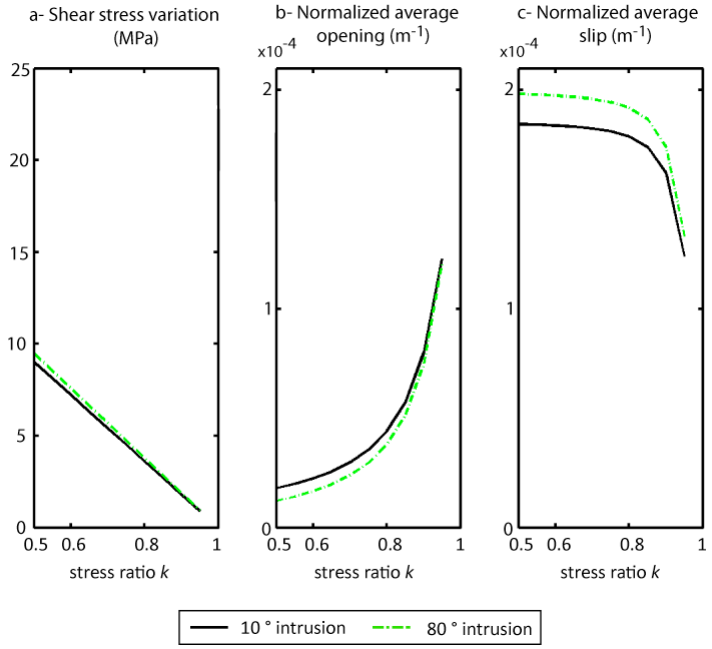

Figure 3.21: a- Variation of the shear stress (in MPa) applied to fractures as a function of the stress ratio k; b- variation of the normalized average openings (in m^{-1}) of the fractures as a function of the stress ratio k; c- variation of the normalized average slips (in m^{-1}) along the fractures as a function of the stress ratio k. Stress mode = Normal + Shear stresses.

The openings and slips have very similar values and evolutions for 10° and 80° fractures. The average openings for both types of intrusions increase while the stress anisotropy decreases. Indeed, when *k* reaches values close to 1, the stress field gets

closer and closer from an isotropic stress field where the intrusions are submitted to opening only (Fig. 3.21b). The average slips follow the same evolution as the shear stress and decrease when *k* increases (Fig. 3.21c). When *k* increases (from 0.5 to 1), R(X) for a subvertical intrusion decreases while it increases for a subhorizontal intrusion. The higher *k*, the stronger the contrast between R(X) for 10° and 80° intrusions. The ratio is superior to 1 for subhorizontal intrusions and inferior to 1 for subvertical intrusions (Fig. 3.22a). For $k > 0.92$, R(X) for a subvertical intrusion becomes negative as the hangingwall and the footwall of the fracture start to move in opposite directions (see Fig. 3.12 for details). $k = 0.92$ is the threshold from which the behaviour changes. R(Z) are very similar for both types of intrusions, except for $k > 0.9$, where the ratio reaches values much more negative for a subhorizontal intrusion (Fig. 3.22b). R(X/Z) for a subhorizontal intrusion are always larger than those for a subvertical intrusion (Fig. 3.22c), except for $k > 0.92$ for the footwall/head of the fracture (Fig. 3.22d).

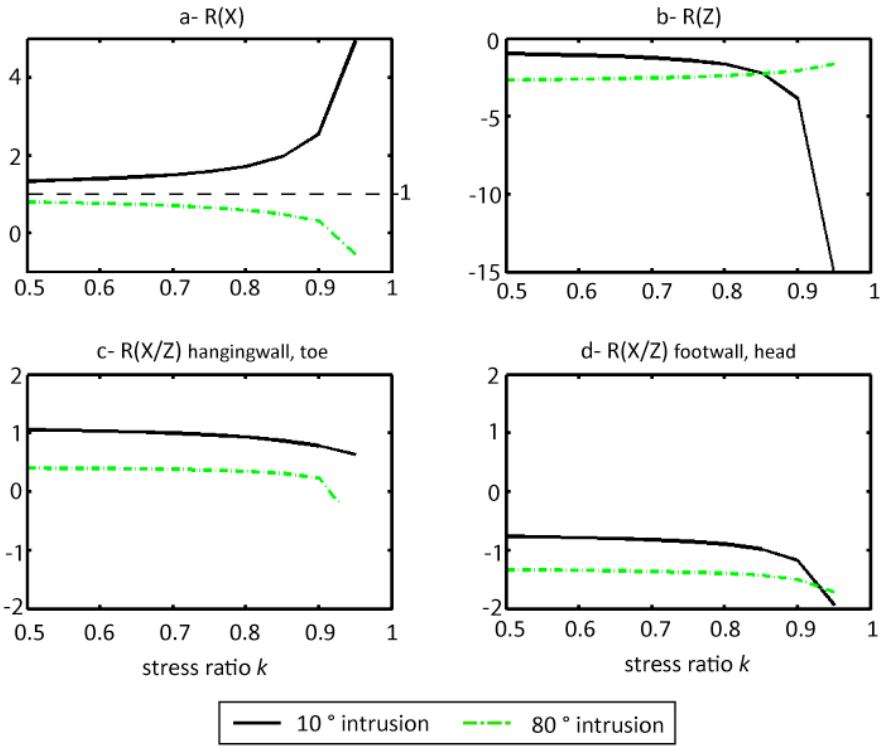

Figure 3.22: Influence of the stress anisotropy on the surface displacements ratios when intrusion are submitted to normal and shear stresses: a- Variation of the R(X); b- variation of the R(Z); c- variation of the R(X/Z) of the hangingwall (subvertical case) or the toe (subhorizontal case) of the fracture; d- variation of the R(X/Z) of the footwall (subvertical case) or the head (subhorizontal case) of the fracture.

The analysis of the influence of the stress anisotropy in a mixed mode of stress reveals once again that R(X) (Fig. 3.22a) and R(X/Z) (Fig. 3.22c) are the most valuable parameters that will allow us to discriminate subhorizontal from subvertical intrusions.

3.4.3.2- Shear stress only

Equation (9) indicates that the variation of the shear stress is a linear function of the stress ratio *k* (Fig.3.23a). The slip along the fault and the surface displacements are proportional to the total stress applied at the surface of the fracture. Here, the fracture is only submitted to shear stress so the displacements are normalized by the shear stress. Thus, the slips along the faults are not influenced by the value stress ratio *k* (Fig. 3.23b).

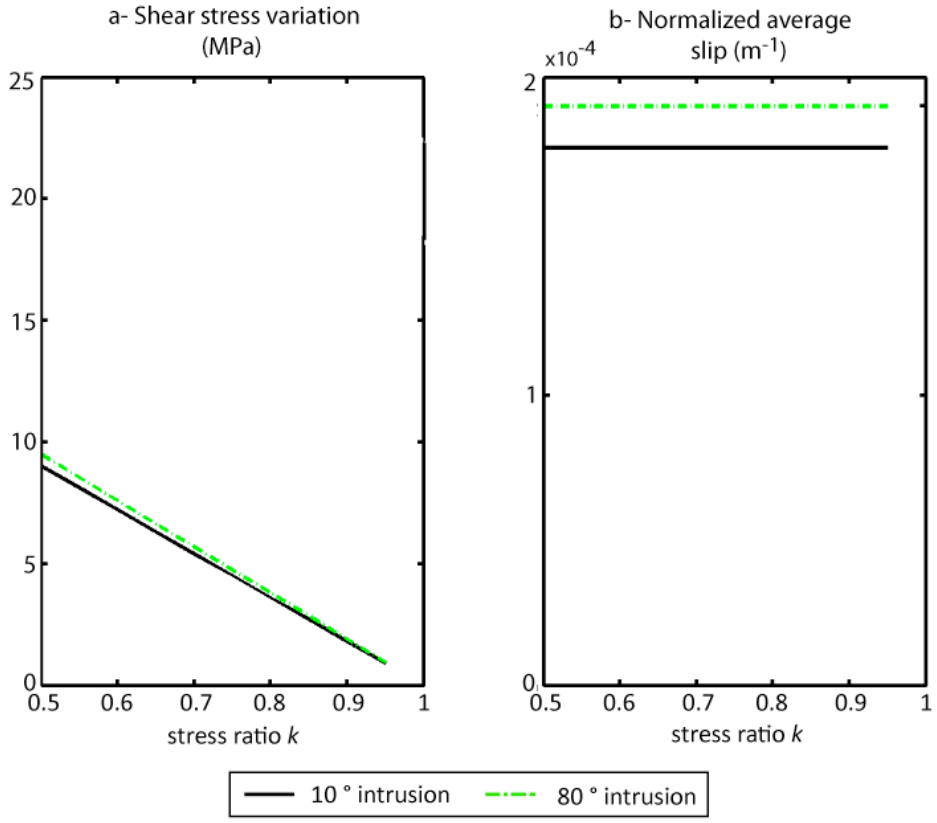

Figure 3.23: a- Variation of the shear stress (in MPa) applied to fractures as a function of the stress ratio k; b- variation of the normalized average slips (in m^{-1}) of the fractures as a function of the stress ratio k. Stress mode = shear stress only.

Similarly, the ratios of surface displacements are not dependent on the value of stress ratio *k*. It is worth noting that ratios for subhorizontal faults always are higher than for subvertical faults. However, although constant ratios are typical of a shear stress only mode, they will not allow an estimation of the value of the stress ratio *k*. In a shear stress only mode, surface displacements ratios only depend on the fault dip (Fig. 3.20).

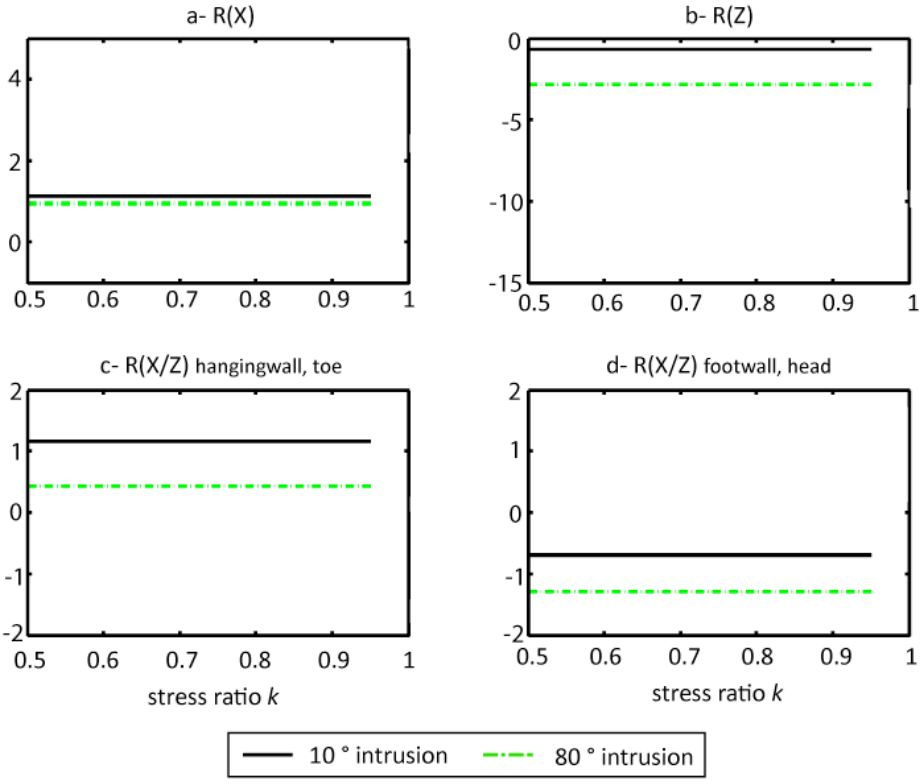

Figure 3.24: Influence of the stress anisotropy on the surface displacements ratios when fault are submitted to shear stresse only: a- Variation of the R(X); b- variation of the R(Z); c- variation of the R(X/Z) of the hangingwall (subvertical case) or the toe (subhorizontal case) of the fracture; d- variation of the R(X/Z) of the footwall (subvertical case) or the head (subhorizontal case) of the fracture.

3.4.4- Parameters controlling the evolution of displacement ratios with normal stress only and shear stress only

In the following, we test the influence of the topography, the height (length) of the subvertical (subhorizontal) fractures and their depth of emplacement on the displacement ratios generated in a normal only and shear only stress mode.

3.4.4.1- Role of topography

Results presented in this section, compare surface displacements ratios obtained for fractures emplaced below a 20° (black lines, reference case, Fig. 3.26 and 3.27) and 30° (red lines, Fig. 3.26 and 3.27) cone-shaped axi-symmetrical topography (Fig 3.25).

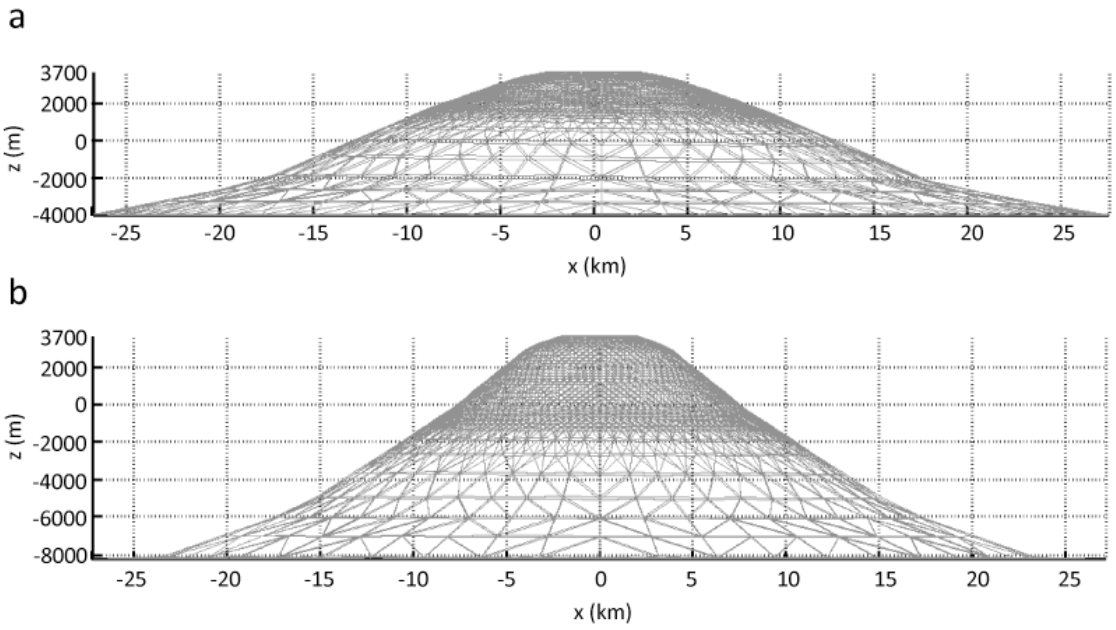

Figure 3.25: Geometry of the 20° (a) and 30° (b) cone-shaped axi-symmetrical topographies used in the model.

Normal stress only

Fig. 3.26 shows that the variations of the ratios are similar with only slight variations of the ranges when the topography is a 30° axi-symmetrical cone. Only R(X) for a dip = 30° is strongly modified below a 30°- sloped topography, being highly positive, while it is strongly negative for a 20°-sloped topography (Fig. 3.26a). Except for this value, it is reasonable to conclude that the nature of the topography has no major influence on the surface displacement ratios caused by intrusions emplaced in a normal stress field.

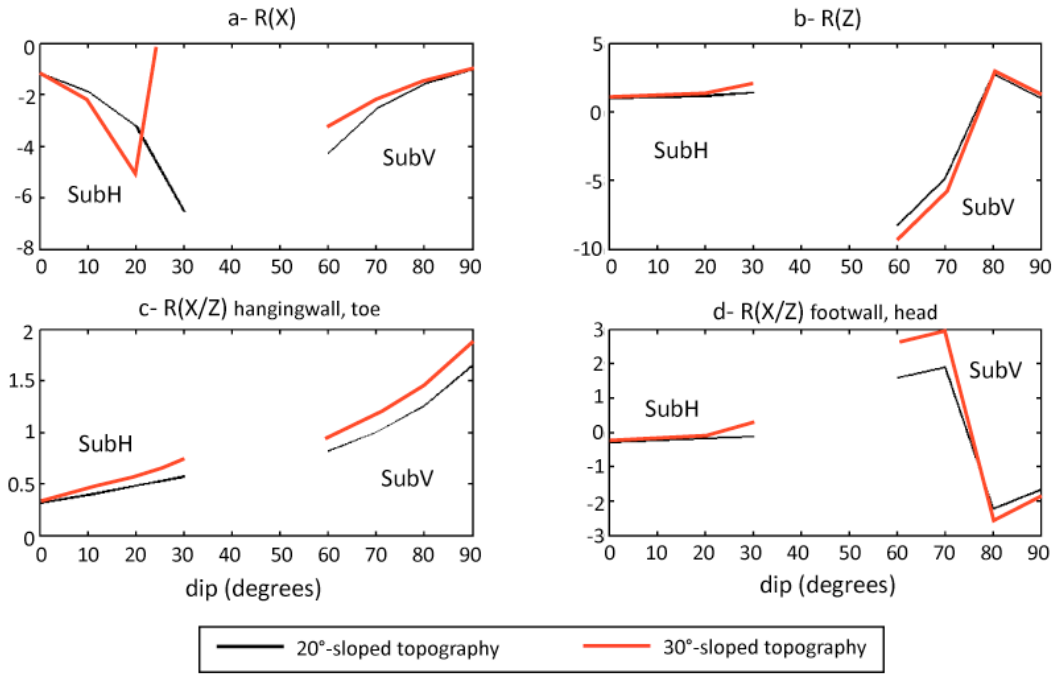

Figure 3.26: Role of the topography on the displacement ratios associated with subvertical and subhorizontal intrusions submitted to normal stress only within the edifice. Black lines represent results obtained for the reference case of a 20°-sloped topography (see Fig. 3.20) and red lines were correspond to a 30°-sloped topography.

Shear stress only

It is shown that the topography has no major influence on none of the surface displacement ratios with shear stress only: some small variations occur in the trends but the ranges of variations are similar between the reference case and results obtained for a 30°-sloped topography (Fig. 3.27). However, although the changes due to topography are minor, subhorizontal faults are more sensitive to the topography than subvertical ones, especially for horizontal displacements ratio R(X) (Fig. 3.27a). This is explained by the position of the faults within the edifice: subvertical faults are emplaced below the summit and are only affected by the top of the topography, which has a similar shape in every case (Fig. 3.25). Subhorizontal faults instead, are emplaced below the edifice flank which geometry is modified when the topography changes (Fig. 3.25). Moreover, with a 30°-sloped topography, displacements caused by a subvertical fault are more prone to affect the flank of the edifice than with a 20°-sloped topography.

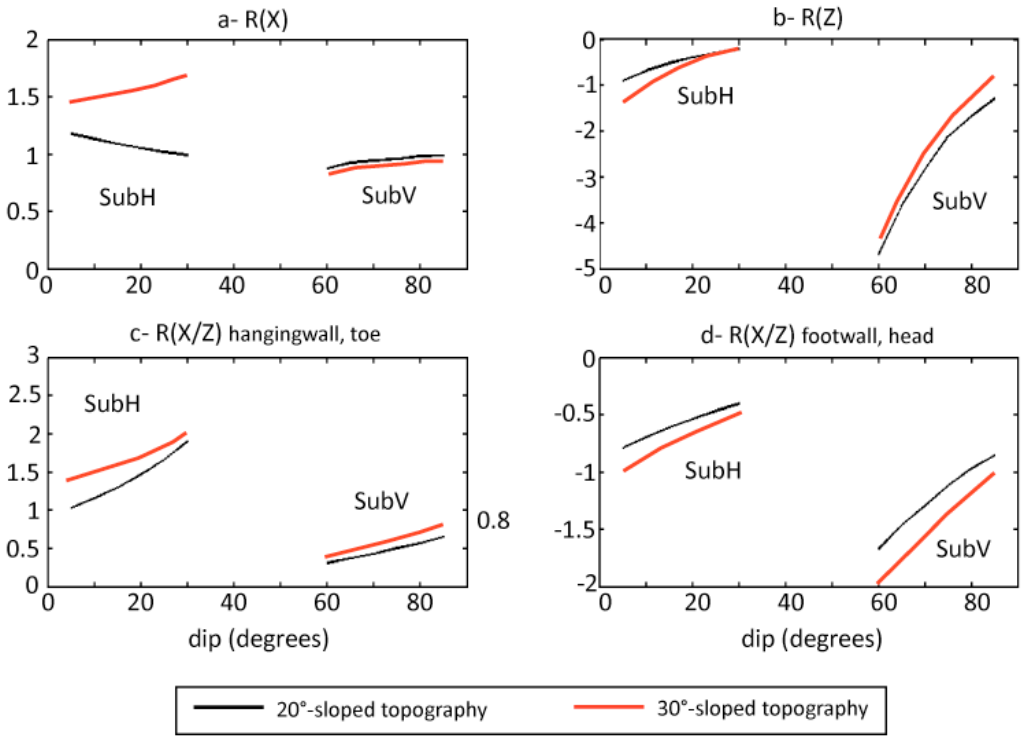

Figure 3.27: Role of the topography on the displacement ratios associated with subvertical and subhorizontal faults submitted to shear stress only within the edifice. Black lines represent results obtained for the reference case of a 20°-sloped topography (see Fig. 3.20) and red lines were correspond to a 30°-sloped topography.

3.4.4.2- Role of intrusion geometry

In this section, the influence of the height of high-angle and the length low-angle fractures (Fig. 3.28) on the surface displacement ratios is investigated.

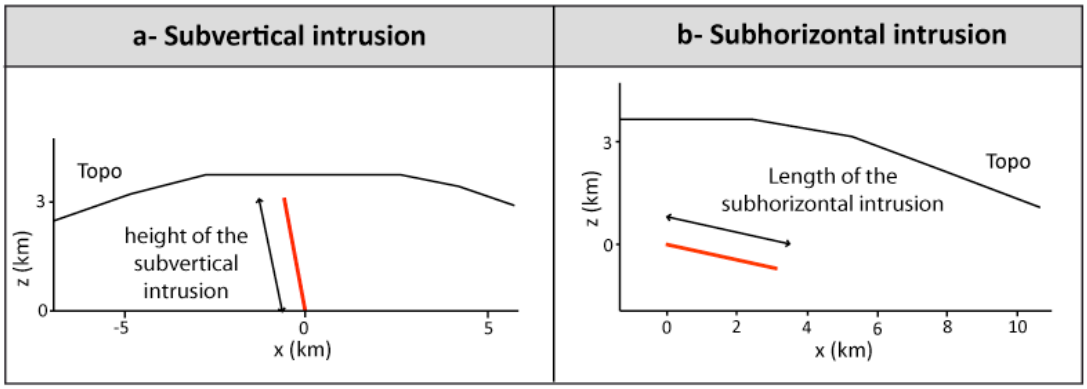

Figure 3.28: Definition of the height of subvertical fractures (a) and the length of subhorizontal fractures (b).

Normal stress only

It is clear from Fig. 3.29 that the geometry of both types of intrusions has no major influence on the surface ratios under normal stress only, which are almost the same as in the reference case (black lines).

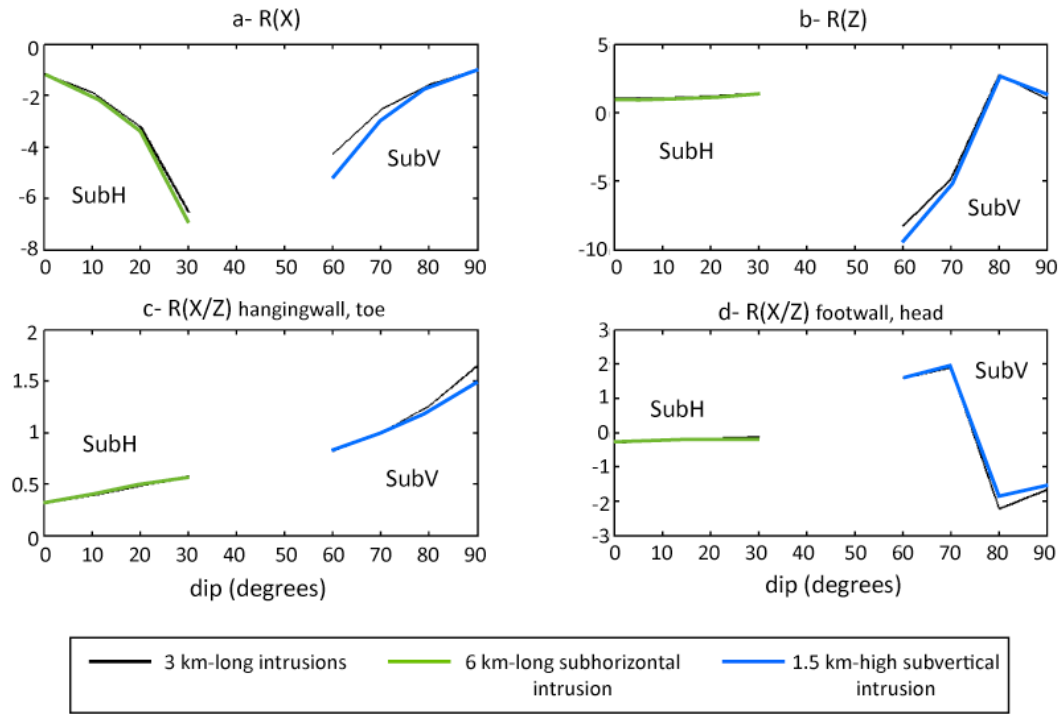

Figure 3.29: Role of the intrusion height/length on the surface displacement ratios under normal stress only. Black lines correspond to 3km-long subvertical and subhorizontal intrusions, blue lines correspond to 1.5 km-high subvertical intrusion and green lines to a 6 km-long subhorizontal intrusion.

Shear stress only

Reference height and length of the faults are assumed to be 3 km, as used in the reference case presented in Fig. 3.20. Here, we compare the reference results with results obtained for a 1.5 km-high subvertical fracture and a 6 km-long subhorizontal fracture (Fig. 3.30).

When the length of subvertical faults is the half of the height used in the reference case (1.5 km instead of 3 km), the evolution of the surface displacements ratios as a function of the dip of the high-angle fault remain similar to the reference case (blue

and black lines on Fig. 3.30). For what regards subhorizontal faults, if the length of the fracture is doubled (6 km instead of 3 km) the evolution of ratios presented in Fig. 3.30 (green and black lines) is also similar to the reference case. Thus, the height/length of the faults has no major effect on the ratios of displacements under shear stress only.

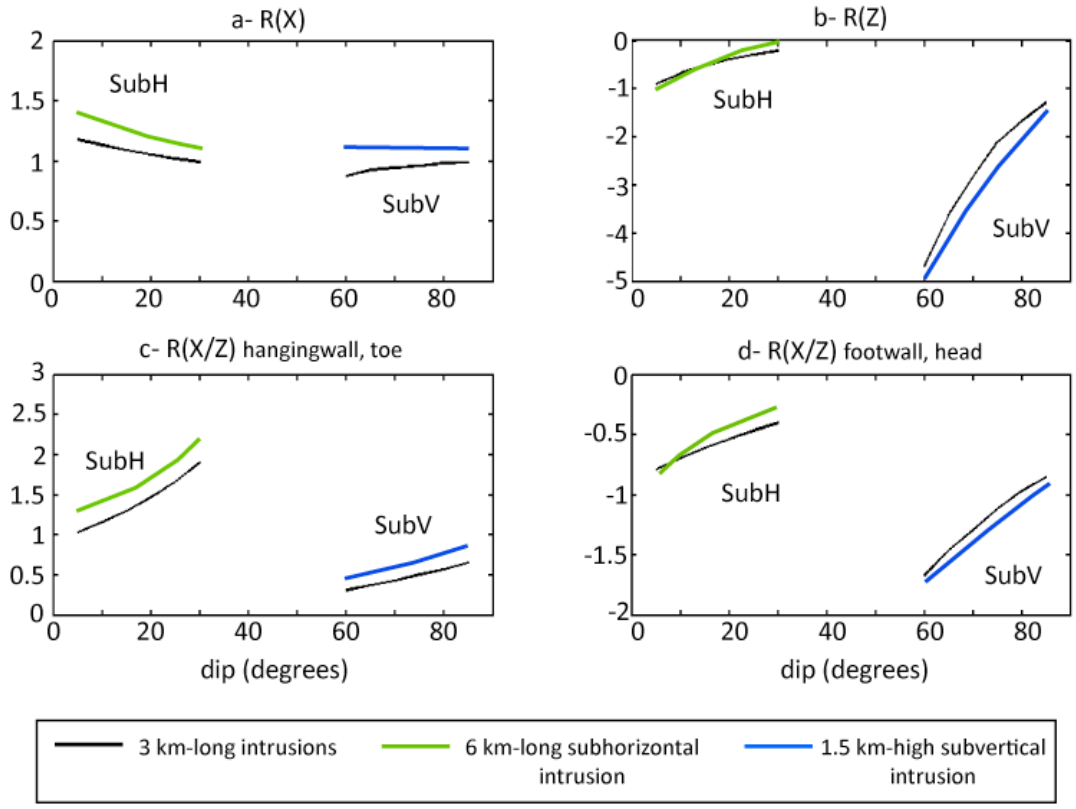

Figure 3.30: Role of the fault height/length on the surface displacement ratios under shear stress only. Black lines correspond to 3km-long subvertical and subhorizontal faults, blue lines correspond to 1.5 km-high subvertical fault and green lines to a 6 km-long subhorizontal fault.

3.4.4.3- Role of intrusion depth

Normal stress only

Under normal stress only, R(X) and $R(X/Z)_{hw,toe}$ remain similar for various depth to the ratios obtained for the reference case with intrusions emplaced at z = 0. For subhorizontal intrusions, R(Z) and $R(X/Z)_{hd}$ are not influence by the variations of the depth of intrusion. For subvertical intrusions, R(Z) and $R(X/Z)_{fw}$ are strongly

influenced by the intrusion depth for a dip of 70°. Amplitudes are the same but signs are opposite (with R(Z) = -5 for z = 0 and +5 for z = -3000, and $R(X/Z)_{fw}$ = 2 for z = 0 and -2 for z = -3000 m) while for dips of 60, 80 and 90°, no major modifications occur. However, the range of variation of R(Z) and $R(X/Z)_{fw}$ remain similar for all depths. It seems reasonable to conclude that the depth of emplacement has no major influence on the surface displacement ratios under normal stress only.

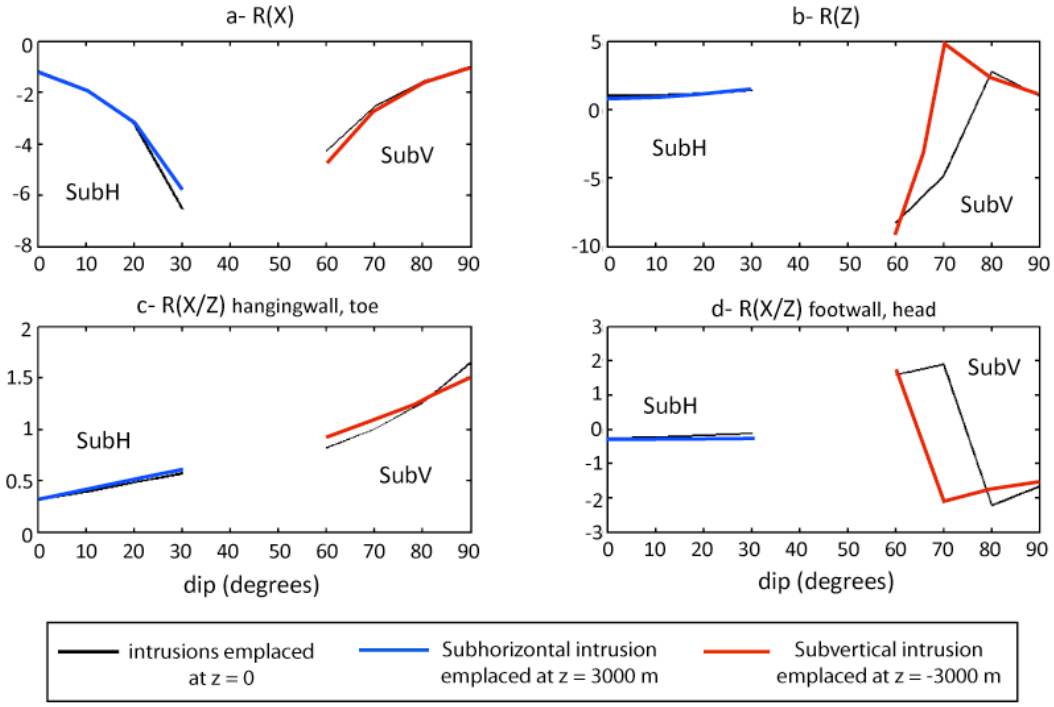

Figure 3.31: Role of the intrusion depth on the displacement ratios associated with subvertical and subhorizontal intrusions submitted to normal stress only within the edifice. Black lines correspond to fractures intruded at z = 0 m, red lines to subvertical intrusions emplaced at z = -3000 m and blue lines to subhorizontal intrusions emplaced at z = + 3000 m.

Shear stress only

Figure 3.32 evidences that the evolution trends of the ratios according to the dip of the faults, both for low-angle and high-angle faults, are not affected by a modification of their emplacement depth (in this case emplaced at z=-3000 m for subvertical faults and z =+3000m for subhorizontal ones, instead of z=0). The variations of the ratios are in the same range as the reference case, proving that when the faults are submitted to shear stress only, the surface displacement ratios

do not depend on the depth at which fractures are emplaced. $R(X/Z)_{toe}$ for a 30°-dipping shallow subhorizontal fault (Fig. 3.32c) is higher than the reference case, likely because of the decreasing influence of topography when dip increases for low-angle faults, creating smaller vertical displacements at the toe of the fault.

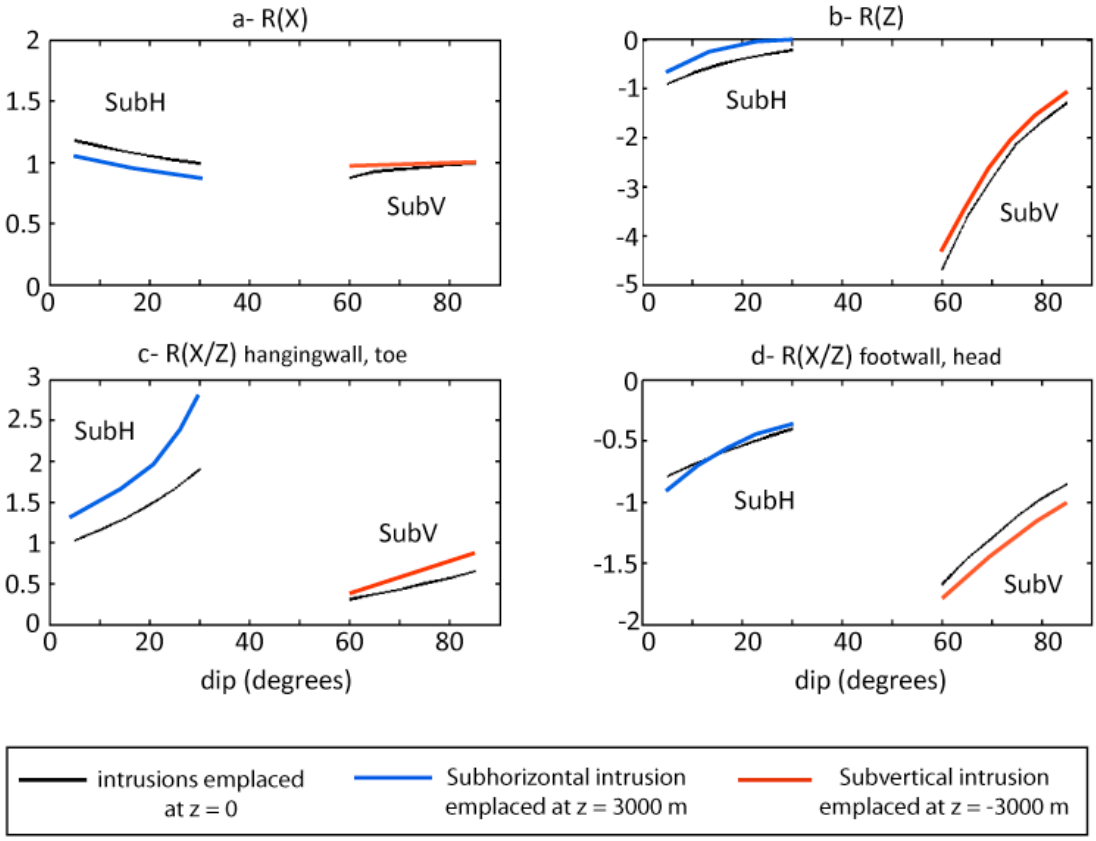

Figure 3.32: Role of the fault depth on the displacement ratios associated with subvertical and subhorizontal faults submitted to shear stress only within the edifice. Black lines correspond to fractures intruded at z = 0 m, red lines to subvertical faults emplaced at z = -3000 m and blue lines to subhorizontal faults emplaced at z = + 3000 m.

We showed that for normal stress only and shear stress only, surface displacement ratios are not dependent on the nature of the topography, the geometry of the fracture or the depth at which fracturess are emplaced, for both types of fractures.

3.4.5- Joint influence of the intrusion dips and stress anisotropy on the displacement ratios

In this section, the results are only discussed for the stress mode involving normal and shear stresses, where dips and *k* have an influence on the ratios of surface displacements. Indeed, we showed previously that when fractures are only submitted to shear stress, the ratios are independent from the stress ratio *k*.

3.4.5.1- Subvertical intrusions

Reference case

Figure 3.33 shows the evolution of the surface displacements ratios as a function of the dip of the fracture and the stress anisotropy in a case considered as a reference for 3 km-high subvertical intrusions emplaced at z = 0 below a 20°-sloped axi-symmetrical topography (Fig. 3.25a).

For a given value of R(X), the value of the intrusion dip widely evolves from 60 to 85°. Positive values of R(X) can be obtained from a wide range of combinations of *k* and dip. By contrast, negative values of R(X) are only met for *k* values larger than 0.9. In such a case, negative values of R(X) can give a good estimation the edifice stress ratio (Fig. 3.33a). Figure 3.30b reveals that R(Z) is mainly sensitive to the dip of the intrusion. This evolution is especially true for k<0.9, i.e. when R(X) is positive. Then using R(Z) enables the determination of the intrusion dip with an accuracy of around 5°. For instance, a R(Z) of - 1.5 corresponds to a dip ranging from 70 to 80°, and a R(Z) of - 4 corresponds to a dip between 60 and 65° (Fig. 3.33b). R(X/Z) do not bring more constraints on the intrusion dip or the value of the stress ratio (Fig. 3.33c and d).

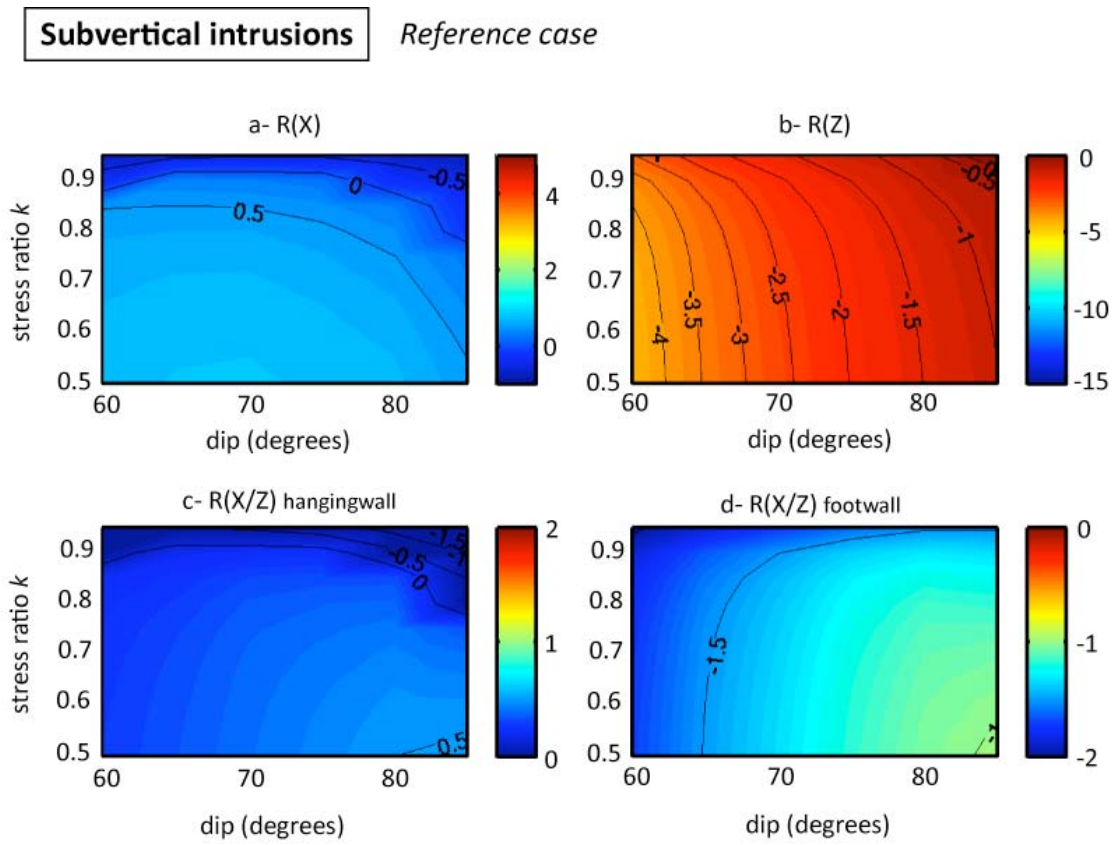

Figure 3.33: a- Influence of the intrusion dip and the stress ratio on a- the variation of the R(X); b- the variation of the R(Z); c and d- the variation of the R(X/Z) for subvertical intrusions. This case is the reference case: intrusions are 3 km high, quadrangular in shape, and emplaced at z = 0 below a 20° cone-shaped topography.

Role of the topography

The same ratios are studied in exactly the same conditions of intrusion geometries and depth. However, in the present case, the topography is made by a 30°-sloped axi-symmetrical cone (Fig. 3.25b). Figures 3.34a and b show that the conclusions drawn for the 20°-sloped axi-symmetrical cone on the evolution of R(X) and R(Z) remain. R(X/Z) show a stronger dependence on the nature of the topography, but this influence does not make the estimation of dips and *k* more accurate than the estimation from R(X) and R(Z) (Figs. 3.34c and d).

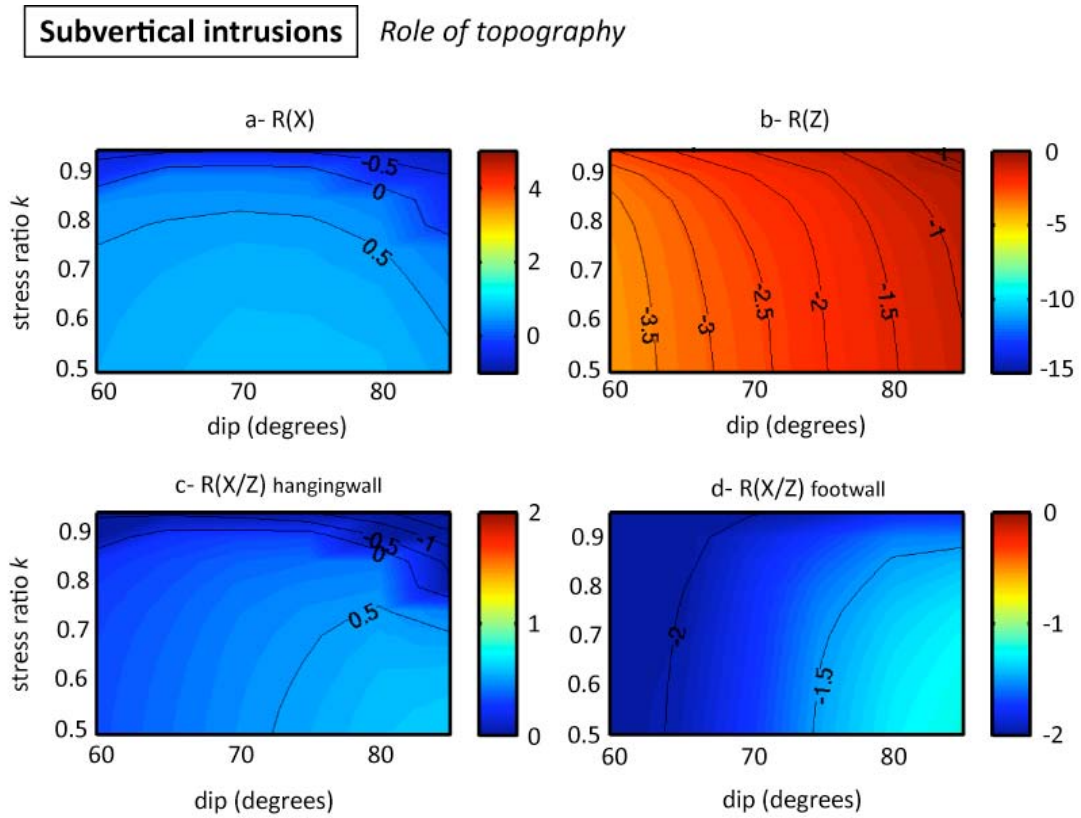

Figure 3.34: Role of the topography on a- the variation of R(X) with dip and k; b- the variation of R(Z) with dip and k; c and d- the variation of R(X/Z) with dip and k, for subvertical intrusions emplaced at z = 0 below a 30° cone-shaped topography.

Role of the intrusion height

Results for the horizontal and vertical surface displacement ratios obtained for subvertical intrusion of 1.5 km high instead of 3 km high (the shape of the intrusions remaining quadrangular) are presented in Figs. 3.35a and b. R(X) and R(Z) are not influenced by the height of subvertical intrusions. The comparison of the ratios R(X/Z) with the reference case (Figs. 3.33c and d) indicates that the intrusions height has no major effect on R(X/Z), especially on $R(X/Z)_{fw}$ (Figs. 3.35c and d).

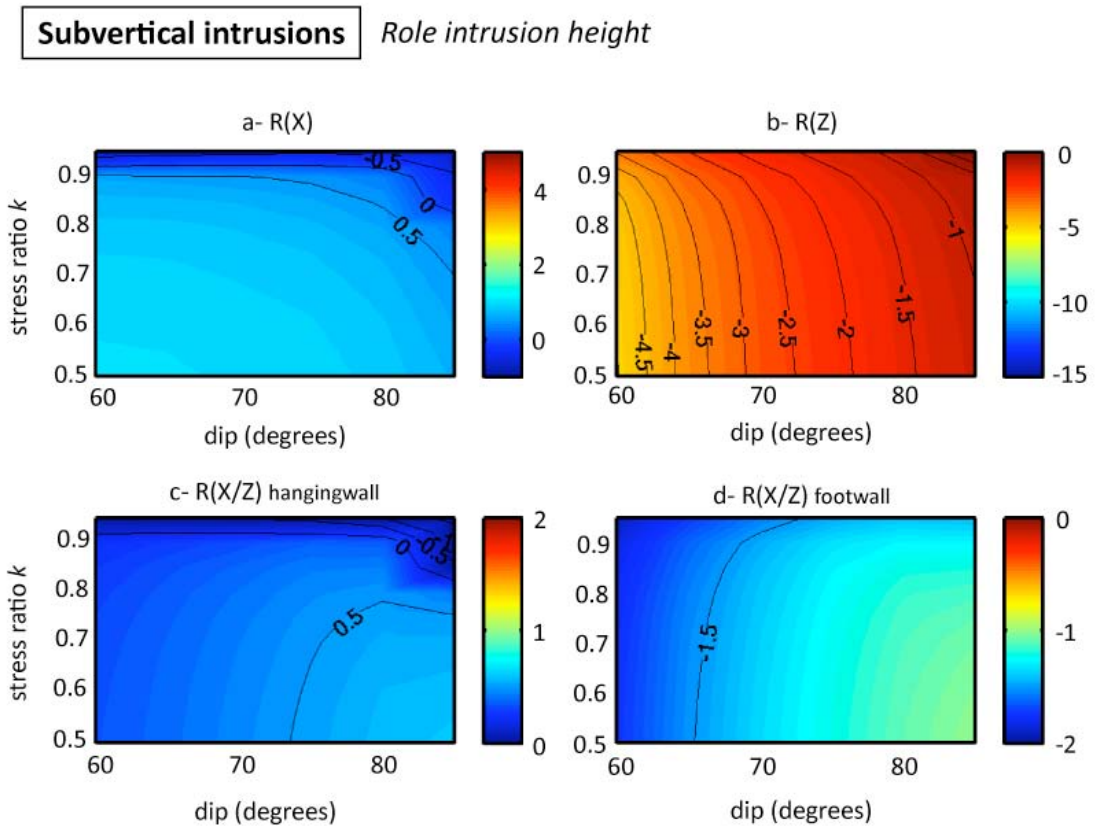

Figure 3.35: Role of the intrusion height on a- the variation of R(X) with dip and k; b- the variation of R(Z) with dip and k; c and d- the variation of R(X/Z) with dip and k, for subvertical intrusions. Here, subvertical intrusions are 1.5 km high, intruded at z = 0 below a 20°-sloped topography.

Role of the intrusion depth

We assume that subvertical intrusions are injected at z = - 3000 m and compare the behaviour of surface displacements ratios (Fig. 3.36) with respect to the reference case (Fig. 3.33) for z = 0. Similarly to previous parameters, R(Z) is not influenced by the depth at which subvertical intrusions are emplaced (Fig. 3.36b). However, the intrusion depth has an effect on the other surface displacement ratios. A given value of R(X) and $R(X/Z)_{hw}$ corresponds to wide range of stress ratio and dip (Figs. 3.36b and c) while $R(X/Z)_{fw}$ gives a good constraints on the intrusion dip. For example, for a $R(X/Z)_{fw}$ = - 1.5, the dip angle can be estimated between 65 and 70° (Fig. 3.36d).

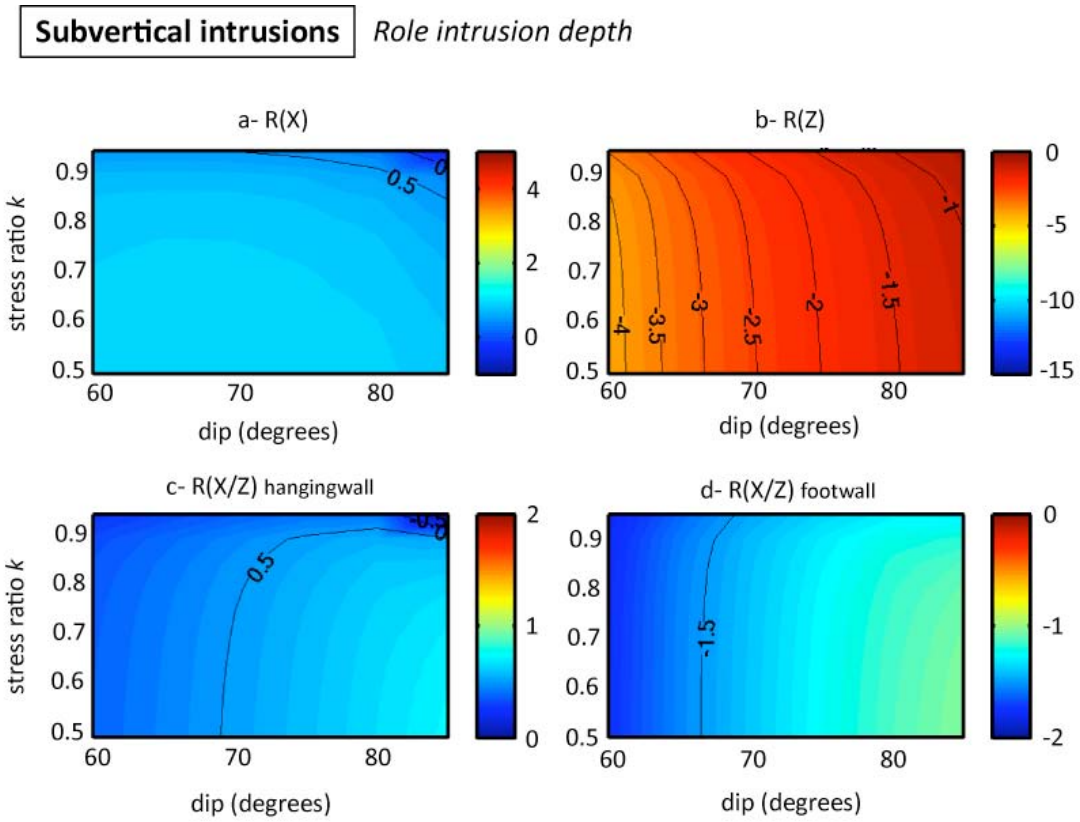

Figure 3.36: Role of the intrusion depth on a- the variation of R(X) with dip and k; b- the variation of R(Z) with dip and k; c and d- the variation of R(X/Z) with dip and k, for subvertical intrusions. Here, subvertical intrusions are intruded at at a depth of -3000 m below a 20°-sloped topography.

In order to try to estimate the depth of the intrusions from the surface displacements, we analyse the evolution of the maximum surface displacements gradient, corresponding to the point where the slope of the displacement curve (Fig. 3.10) along the profiles AB, CD, A'B', C'D' is maximum, with depth. Although this study doesn't indicate a precise intrusion depth, it is possible to distinguish a shallow intrusion from a deep intrusion as superficial fractures have smaller values of displacement gradient than deep intrusions. Moreover, shallow intrusions show large variations of the gradient with the dip and k while no variations are observed for deep intrusions (Fig. 3.37a and b).

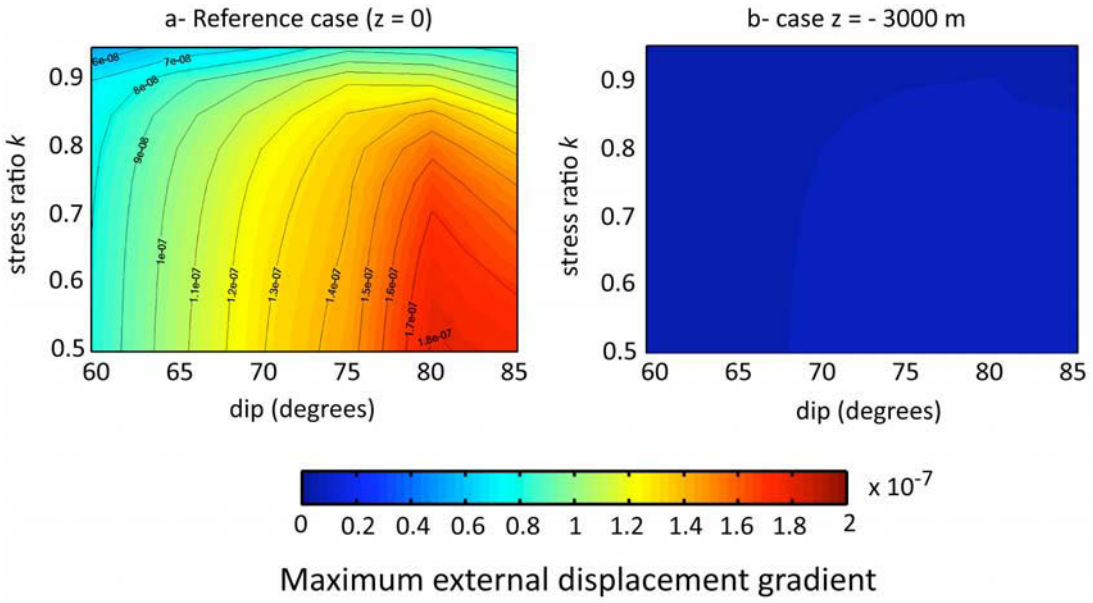

Figure 3.37: Maximum external displacement gradient associated with subvertical intrusions injected at z=0 (a) and at a depth of - 3000 m (b).

3.4.5.2- Subhorizontal intrusions

Reference case

Figure 3.38 shows the evolution of the surface displacements ratios as a function of the dip of the fracture and the stress anisotropy in a case considered as a reference for 3 km-long subhorizontal intrusions emplaced at z = 0 below a 20°-sloped axi-symmetrical topography.

Significant differences are observed between subvertical and subhorizontal intrusions: while R(X) could be positive or negative for subvertical intrusions, subhorizontal intrusions only generate positive R(X) (Fig. 3.38a). Moreover, Figs. 3.33a and 3.38a confirm the result deduced from Fig. 8a showing that R(X) is larger than 0.8 for subhorizontal intrusions and lower than 0.8 for subvertical intrusions. Here, a given R(X) corresponds to a wide range of stress ratios and intrusion dips, except for the ratios highest values which allow an estimation of *k* (Fig. 3.38a). Identical observations can be made for the R(Z), with similar amplitudes of the ratios for both subvertical and subhorizontal intrusions. Conversely to the analysis of ratios associated with subvertical intrusions, R(X) and R(Z) are not the most valuable

parameters to quantify the dip and stress ratio in the case of subhorizontal intrusions. Indeed, the R(X/Z) (Figs. 3.38c and d) allow to estimate the intrusion dip in an interval of 10°. For instance, a $R(X/Z)_{toe}$ of 1.5 and a $R(X/Z)_{hd}$ of - 0.5 correspond to displacements generated by a low-angle intrusion whose dip is comprised between 20 and 30°. The fact that $R(X/Z)_{toe}$ is larger than 0.6 for subhorizontal intrusions and lower than 0.6 for subvertical intrusions is confirmed by Figs. 3.33c and 3.38c. R(X) and R(X/Z) are much larger for subhorizontal intrusions than for subvertical ones. It remains however difficult to estimate precisely the stress ratio *k* from surface displacements ratios created by subhorizontal intrusions.

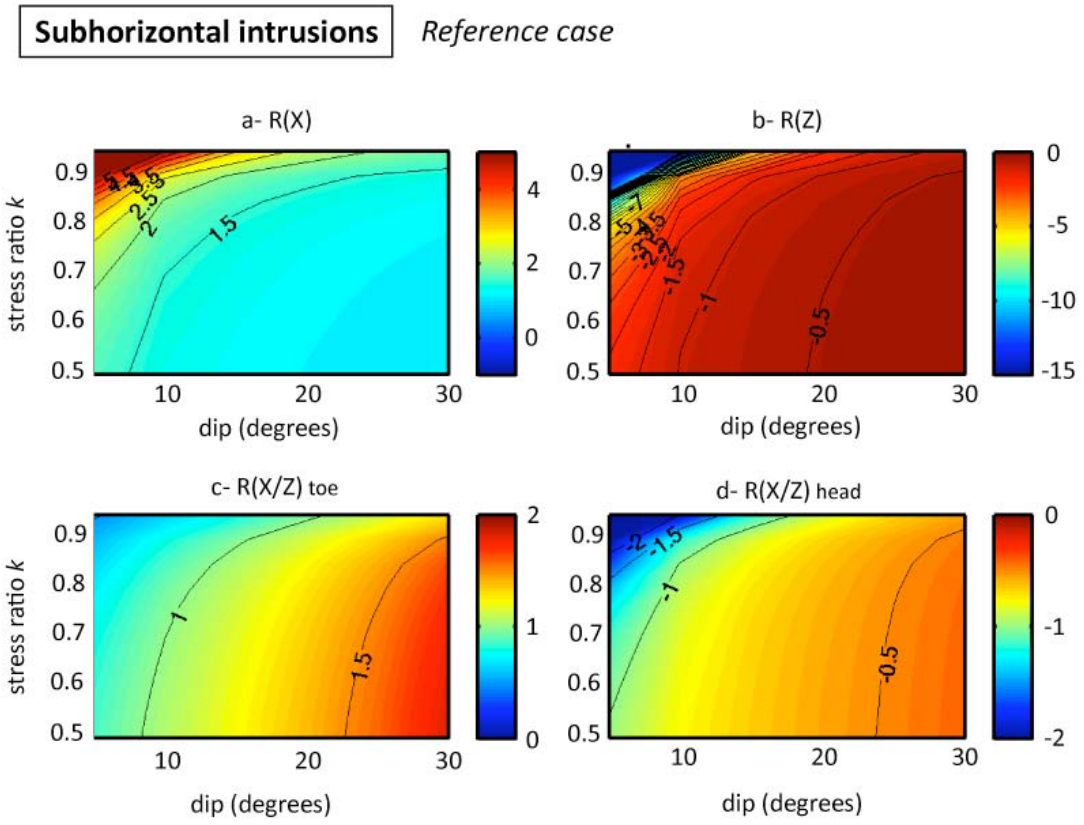

Figure 3.38: a- Influence of the intrusion dip and the stress ratio on a- the variation of the R(X); b- the variation of the R(Z); c and d- the variation of the R(X/Z) for subhorizontal intrusions. This case is the reference case: intrusions are 3 km long, quadrangular in shape, and emplaced at z = 0 below a 20° cone-shaped topography.

Role of the topography

The only ratios affected when the fracture is intruded below a 30° cone-shaped are R(X/Z). $R(X/Z)_{toe}$ reaches higher positive values and $R(X/Z)_{hd}$ reaches more negative values (Figs. 3.39c and d). Yet, a change in the topography does not improve the accuracy of the dip and stress ratios estimations.

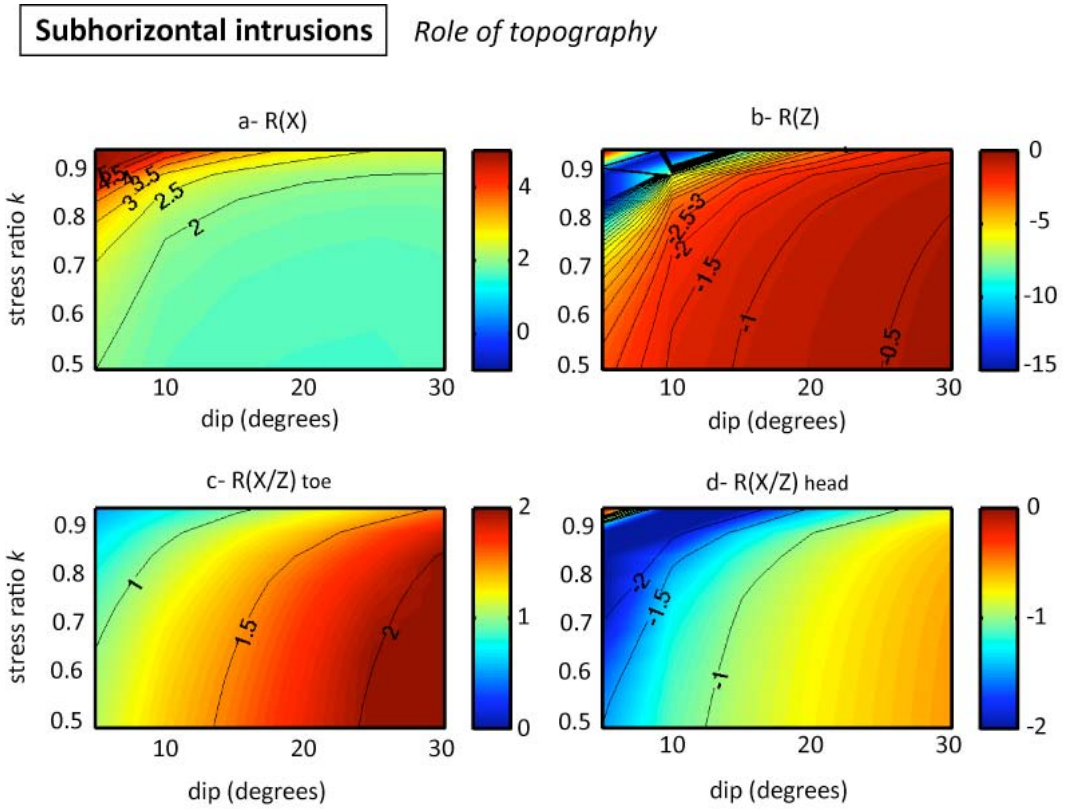

Figure 3.39: Role of the topography on a- the variation of R(X) with dip and k; b- the variation of R(Z) with dip and k; c and d- the variation of R(X/Z) with dip and k, for subhorizontal intrusions emplaced at z = 0 below a 30° cone-shaped topography.

Role of the intrusion length

For a 6 km long shallow-dipping fracture, the comparison with the reference case (Fig. 3.38) reveals that the length of the fracture is not a determining parameter in the nature of the surface displacements associated with subhorizontal intrusions as none of the ratios is influenced by a modification of the of its length (Fig. 3.40).

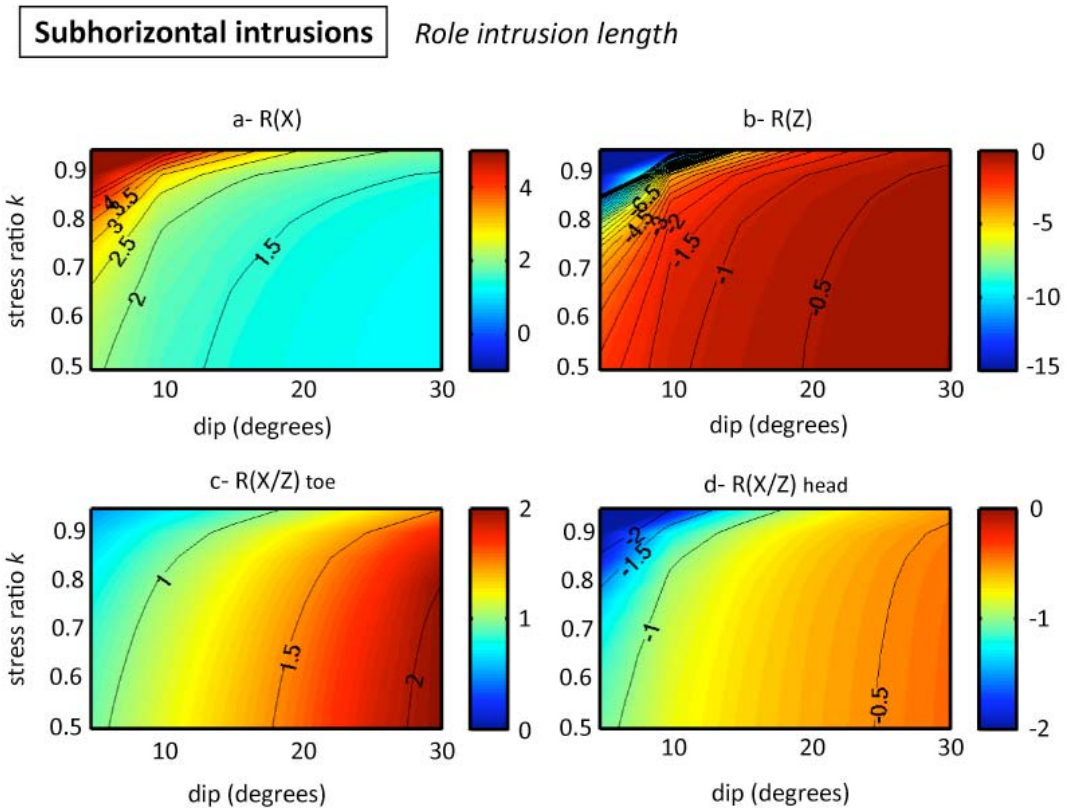

Figure 3.40: Role of the intrusion length on a- the variation of R(X) with dip and k; b- the variation of R(Z) with dip and k; c and d- the variation of R(X/Z) with dip and k, for subhorizontal intrusions. Here, fractures are 6 km long, intruded at z = 0 below a 20° cone-shaped topography.

Role of the intrusion depth

In order to test the role of the intrusion depth of low-angle fractures on the displacements ratios, we compare the ratios of the reference case (z = 0) with ratios obtained for a fracture intruded within the edifice at z = + 3000 m. Some values of the ratios are hidden because when a subhorizontal intrusion is emplaced at shallow depth, surface displacements can be made of a single "block", with a single component on the displacements (the behaviour in this case is similar to the behaviour of a subhorizontal intrusion in normal stress only) making difficult the estimation of the ratios for some values of dip. If we consider the evolution of the ratios on the dip ranges where the study is possible, the variations are close from those of the reference case with ratios having the same order of magnitudes magnitudes. Values of R(X) are however slightly higher, values of R(Z) slightly lower,

while values of R(X/Z) remain very similar (Fig. 3.41). The depth of subhorizontal intrusions has no major influence on the surface displacement ratios associated with these intrusions, at least for dips superior to 10°. For dips comprised between 5 and 10°, surface displacement patterns are not comparable with the reference case, no conclusions can be made about this specific case.

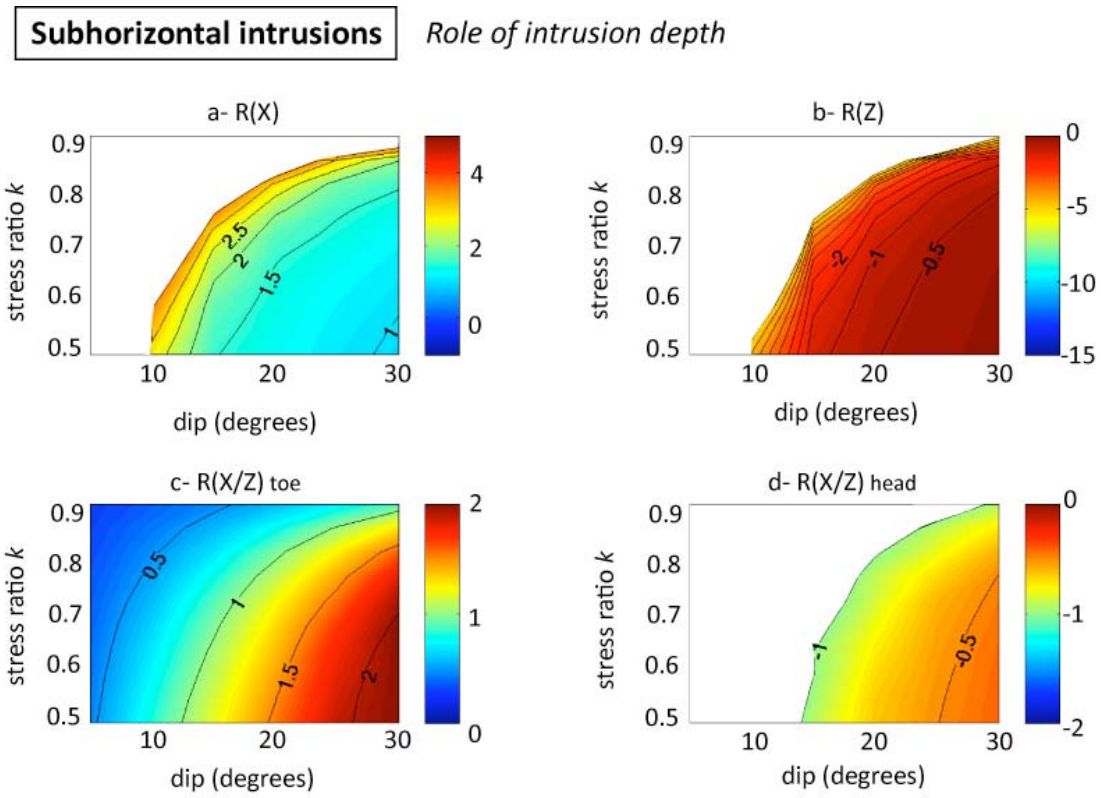

Figure 3.41: Role of the intrusion depth on a- the variation of R(X) with dip and k; b- the variation of R(Z) with dip and k; c and d- the variation of R(X/Z) with dip and k, for subhorizontal intrusions. Here, fractures are 3 km long, intruded at z = + 3000 m below a 20°-sloped topography.

Similarly to high-angle intrusions, the analyis of the maximum gradients (which are not represented as their patterns are similar to those for high-angle intrusions) permits to discriminate shallow subhorizontal intrusions from deep ones as they generate high values and wide variations of displacement gradients (Fig. 37a and b).

3.4.6- Detectability of low-angle intrusions within volcanic edifices: the example of Piton de la Fournaise volcano.

The study of the deformation fields associated to subhorizontal intrusions within basaltic volcanoes requires that the displacements generated by the intrusion is large enough to be recorded by the monitoring systems of the edifices, in order to compare modelling results with real (recorded) deformation. In this section, the detectability of subvertical intrusions is not studied as it is a recurrent, quite well constrained phenomenon at Piton de la Fournaise volcano. As subhorizontal injections are common within Piton des Neiges volcano at a depth larger than 1 km (section 3.2), it is reasonable to assume that low-angle intrusions also occur within the currently active volcano of La Reunion island, Piton de la Fournaise volcano (section 2.2.2), but they are not directly observed because the edifice is poorly eroded. As a consequence, we approach the question of the detectability of subhorizontal intrusions at Piton de la Fournaise whose summit and upper flanks are covered by a dense network of differential GPS. This network is able to record minimum vertical displacements of 1 cm and minimum horizontal displacements of 3 cm (Andrea Di Muro, pers. com.). The lower slopes of the edifice like the Grandes Pentes-Grand Brulé area on the eastern flank, are not covered by the GPS network but the deformation affecting this zone can by followed using InSAR data. InSAR can detect displacements of 1 cm in ground-satellite direction (ranging from 45° to 23° from the vertical), except in the Grandes-Pentes where precision is lower.

To remain consistent with geometries and parameters adopted in the model, we will investigate the detectability of a low-angle horizontal intrusion (dip = 10°), quadrangular in shape, with a length of 3 km, submitted to a mean overpressure of 1 MPa and injected below the realistic topography of Piton de la Fournaise volcano (Fig. 3.42). The depth of the intrusion will range between the level of the sea, considered as 0 m of depth (which is the assumed depth of the shallow magmatic chamber the volcano, Peltier et al., 2007 and 2008; Nercessian et al., 1996; Battaglia et al., 2005), and 1500 m above sea level (about 1100 m below the summit of Piton

de la Fournaise). The detectability of subhorizontal fractures at Piton de la Fournaise is investigated for an edifice loaded by:

1- normal stress only

2- shear stress only (k = 0.6)

3- a mixed mode of stress where normal and shears stresses are combined (k = 0.6).

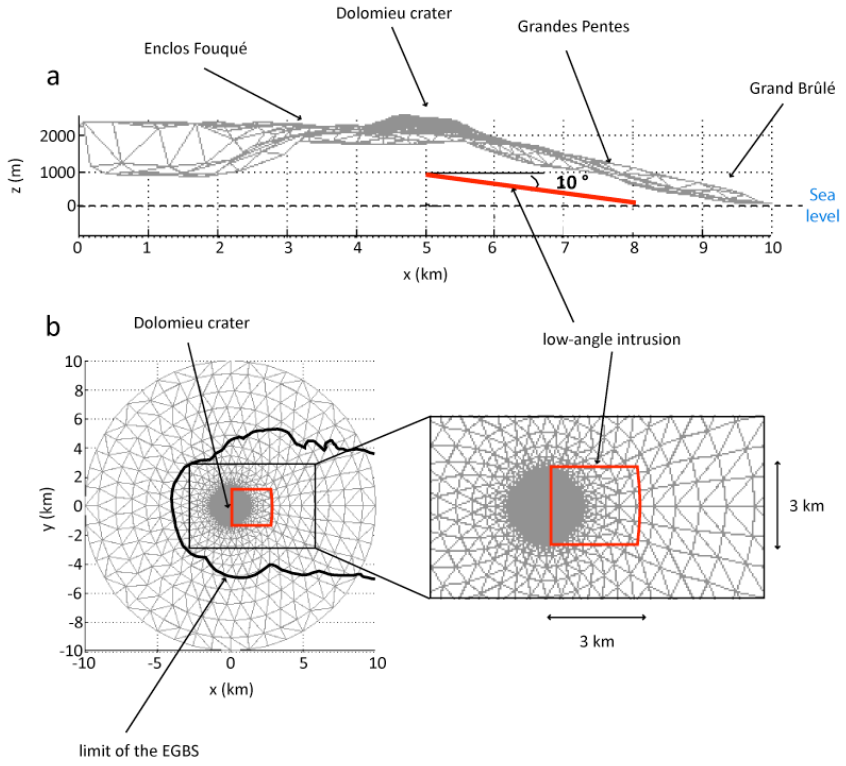

Figure 3.42: a- Real topography of Piton de la Fournaise volcano meshed by triangular elements, in lateral view; b- vertical view of the mesh of Piton de la Fournaise volcano with the geometry of the low-angle intrusion injected below the eastern flank of the edifice below the Grandes Pentes-Grand Brulé.

3.4.6.1- Detectability under normal stress only

At Piton de la Fournaise volcano, a 10°- dipping subhorizontal intrusion submitted to 1 MPa mean overpressure is affected by a maximum opening ranging between 1 m when intruded at z = 0 (sea level) and 2.5 m when intruded at an elevation of 1500 m (Fig. 3.43a). Figure 3.43b indicates that this opening is associated with a maximum vertical displacement at the edifice surface comprised

between 48 cm and 2.1 m.

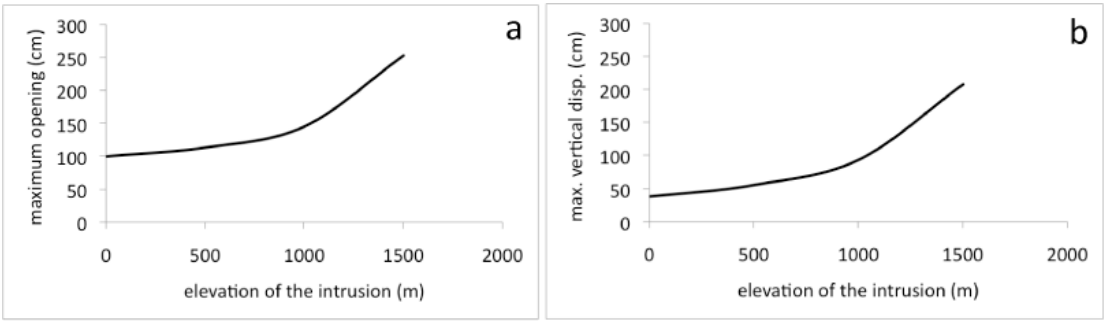

Figure 3.43: a- Influence of depth (m) on the maximum opening (cm) of subhorizontal intrusions emplaced under normal stress only within Piton de la Fournaise volcano; b- influence of depth (m) on the maximum vertical displacement (cm) due to horizontal intrusions at the surface of the edifice.

As the vertical limit of detection for vertical displacement by differential GPS measurements at Piton de la Fournaise volcano is 1 cm, a 1MPa overpressured low-angle intrusion should be instrumentally detected when injected within the edifice loaded by a normal stress field. Moreover, it has been estimated the minimum overpressure within the intrusion required to create 1 cm of vertical displacement at the surface of the volcano: it ranges from 0.005 to 0.027 MPa depending on the depth of the intrusion (Fig. 3.44b), which are plausible overpressure values for magmatic intrusions within basaltic volcanoes (see previous section). These overpressure values correspond to minimum required openings comprised between 1.3 and 2.7 cm, depending on the depth of intrusion (Fig. 3.44a).

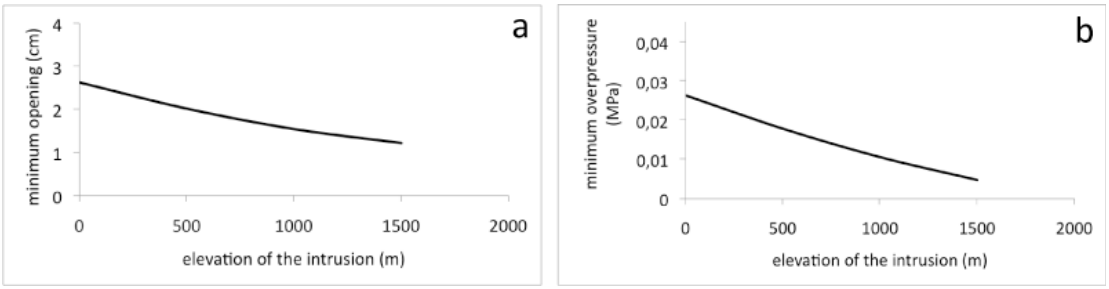

Figure 3.44: minimum openings (a) / overpressures (b) of subhorizontal intrusions required to generate 1cm of vertical displacement at the surface of the volcano for different depth of intrusion, under normal stress only.

3.4.6.2- Detectability under shear stress only

Under shear stress only, the maximum opening of the fault ranges between 10 cm at z = 0 and 40 cm at z = 1500 m (Fig. 3.45a). This amount of opening of the fracture is responsible for maximum vertical displacements of approximately 48 cm whatever the depth at which the fault is emplaced (Fig. 3.45b).

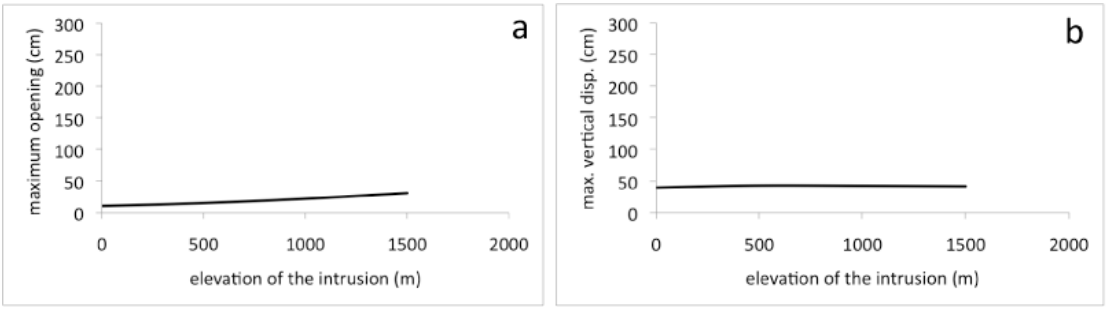

Figure 3.45: a- Influence of depth (m) on the maximum opening (cm) of subhorizontal faults emplaced under shear stress only within Piton de la Fournaise volcano; b- influence of depth (m) on the maximum vertical displacement (cm) due to horizontal faults at the surface of the edifice.

Under such a stress field, a vertical displacement of 1 cm at the surface of the edifice requires minimum overpressures of about 0.025 MPa at all depth (Fig. 3.46b), corresponding to minimum openings of 0.3 cm (z = 0) to 0.8 cm (z = 1500 m, Fig. 3.46a).

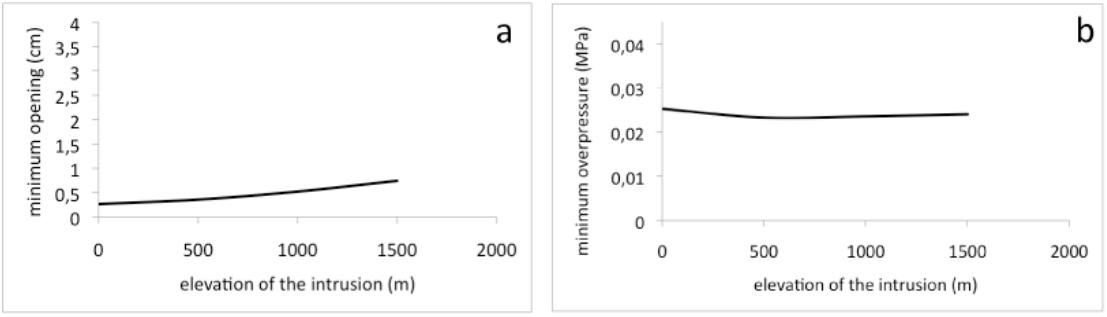

Figure 3.46: minimum openings (a) / overpressures (b) of subhorizontal faults required to generate 1cm of vertical displacement at the surface of the volcano for different depth of fault, under shear stress only.

3.4.6.3- Detectability under mixed stress

When the stress field combines normal and shear stresses, maximum openings of a 10° subhorizontal intrusion range from 1m to more than 2.5 m (Fig. 3.47a) while the maximum vertical displacements range from 60 cm to more than 2 m (Fig. 3.47b).

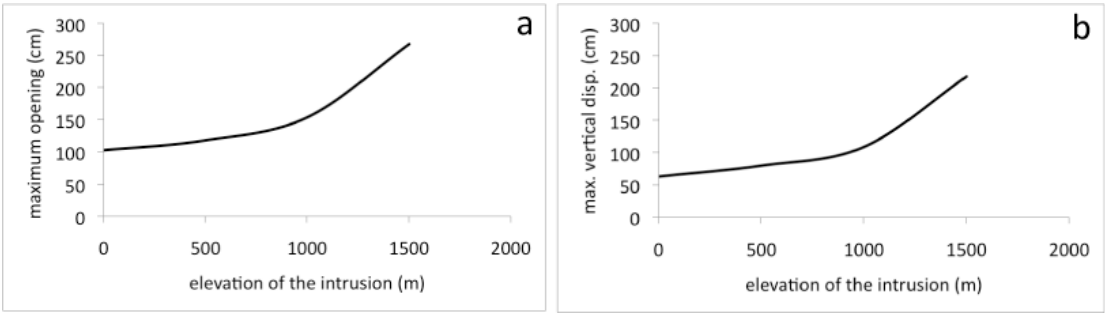

Figure 3.47: a- Influence of depth (m) on the maximum opening (cm) of subhorizontal intrusions emplaced under mixed stress within Piton de la Fournaise volcano; b- influence of depth (m) on the maximum vertical displacement (cm) due to horizontal intrusions at the surface of the edifice.

In this case, minimum openings comprised between 1.2 and 1.6 cm (Fig. 3.48a), corresponding to minimum overpressures of 0.005 to 0.018 MPa, are necessary to generate 1 cm of vertical displacement at the surface of the edifice (Fig. 3.48b).

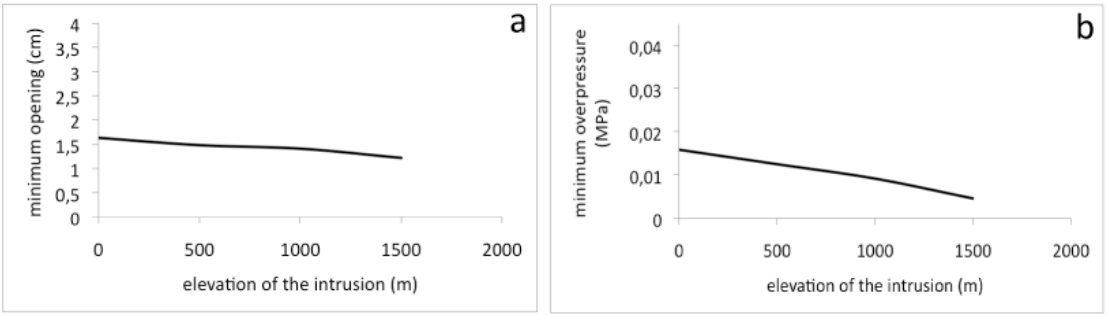

Figure 3.48: minimum openings (a) / overpressures (b) of subhorizontal intrusions required to generate 1cm of vertical displacement at the surface of the volcano for different depth of intrusion, under mixed stress.

For all stress fields, the minimum openings of a 10° subhorizontal intrusion required to create a detectable amount of vertical surface displacements range

between 0.3 and 3 cm, corresponding to minimum overpressures between 0.005 and 0.03 MPa. Previous studies carried out at Piton de la Fournaise (Fukushima, 2005; Fukushima et al., 2005; Peltier et al., 2007) showed that these values of overpressure are consistent with overpressures estimated from field displacements associated with regular subvertical intrusions within the volcano.

3.4.6.4- Influence of the fracture dips on their detectability

In this section, we study the influence of the fracture dips on the minimum openings and overpressures required to create 1 cm of vertical displacement at the surface of Piton de la Fournaise volcano.

Minimum openings

In normal stress only, when the intrusion dip increases, the minimum opening of the subhorizontal intrusion required to generate detectable vertical displacement increases. At z = 0, it ranges between 2,2 cm for dip = 0° and 3.8 cm for dip = 30°. At z = 1500 m, it ranges between 1 cm for dip = 0° and 1.7 cm for dip = 30° (Fig. 3.49a). Conversely, in shear stress only, the necessary minimum openings decrease when the fault dip increases, ranging from 0,03 cm for dip = 30° to 0.3 cm for dip = 10° at z = 0 and from 0.3 to 0.75 cm at z = 1500 m, respectively (Fig. 3.49b). Finally, in a mixed mode, the minimum openings globally increase when the dip increases, but values for a given dip are almost constant, ranging between 1.3 and 2 cm at all depth (Fig. 3.49c).

a- Normal stress only

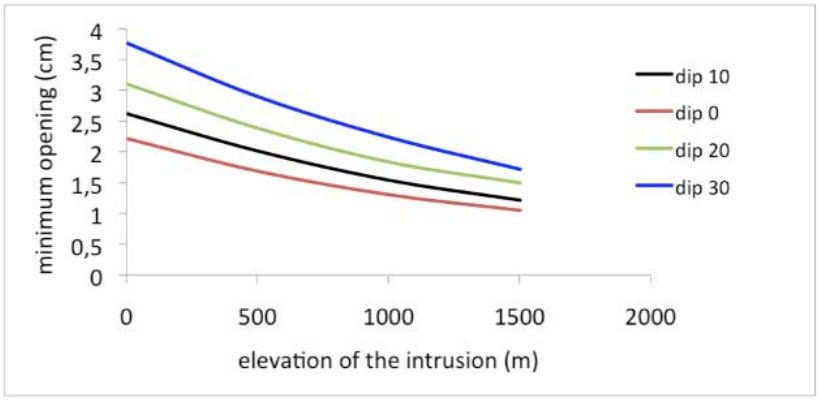

b- Shear stress only

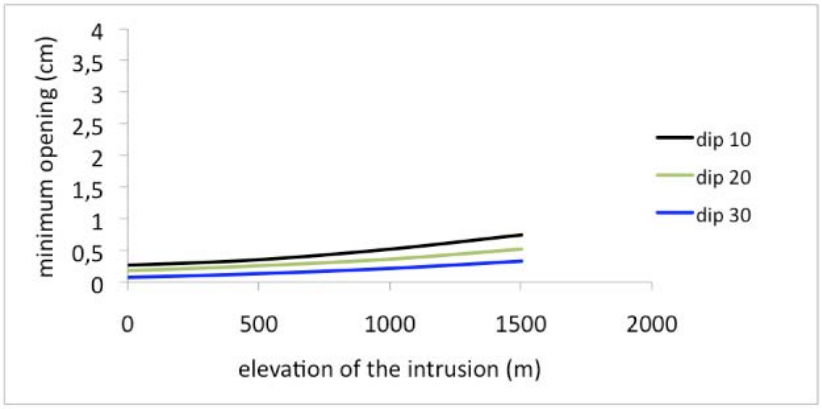

c- Mixed stress

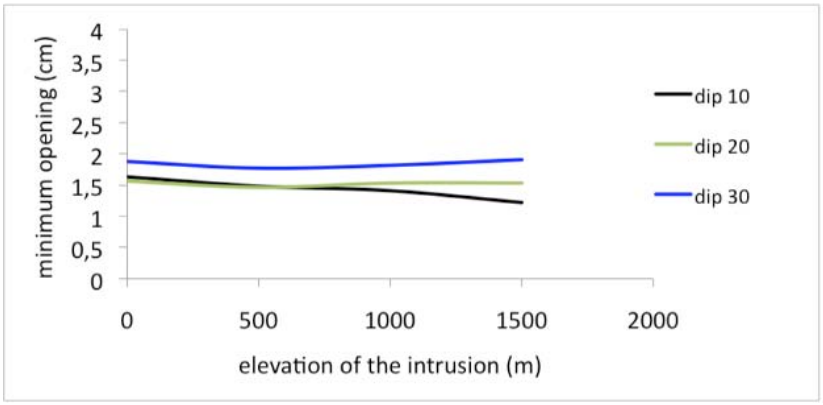

Figure 3.49: Influence of the subhorizontal fractures dips on the minimum values of openings required to create 1 cm of vertical surface displacement at Piton de la Fournaise volcano, for fractures emplaced in (a) a normal stress field, (b) a shear stress field and (c) a mixed stress field.

Minimum overpressures

The influence of the intrusion dips on the minimum overpressure is similar to that on the minimum openings, for all stress fields (Fig. 3.50). In normal stress only, minimum overpressures increase when the dip increases, from 0.02 MPa to 0.041 MPa at z = 0 and 0.002 to 0.02 at z = 1500 m (Fig. 3.50a). In shear stress only, minimum overpressure are almost constant for dip = 10° (0.022 MPa) and dip = 20° (0.025 MPa), while it slightly increases with depth for dip = 30°, from 0.027 at z = 0 to 0.034 at z = 1500 m (Fig. 3.50b). In a mixed mode of stress, minimum overpressures increase with the intrusion dips but for a given dip, they decrease when the emplacement elevation increases, ranging globally between 0.005 and 0.024 MPa (Fig. 3.50c).

a- Normal stress only

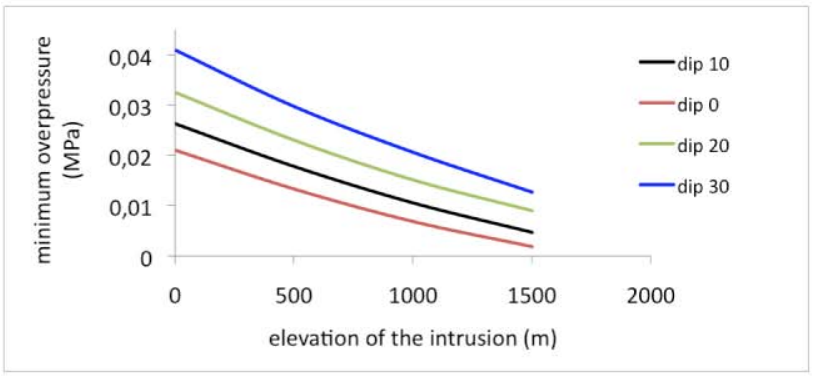

b- Shear stress only

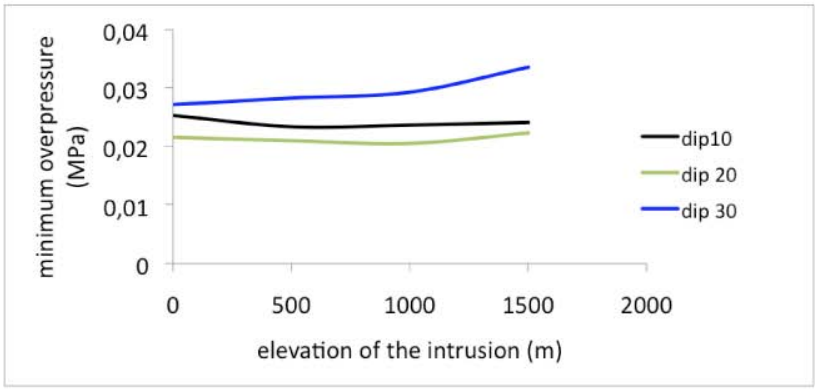

c- Mixed stress

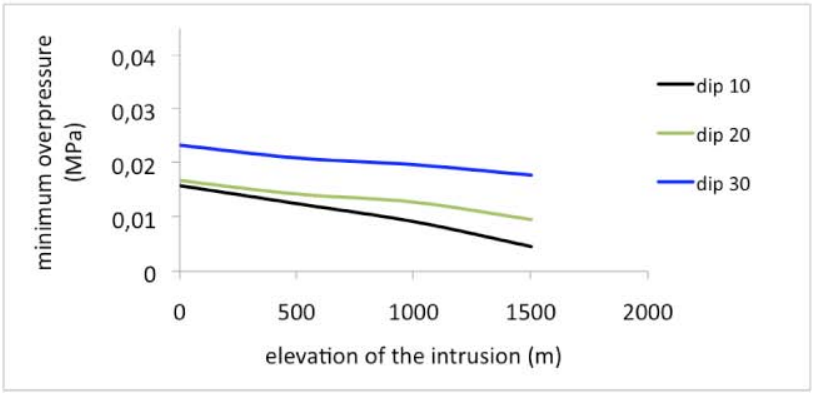

Figure 3.50: Influence of the subhorizontal fracture dips on the minimum values of internal overpressure required to create 1 cm of vertical surface displacement at Piton de la Fournaise volcano, for fractures emplaced in (a) a normal stress field, (b) a shear stress field and (c) a mixed stress field.

3.4.6.5- Influence of the stress anisotropy on the intrusion detectability

Here, the influence of the stress anisotropy on the minimum openings and overpressures required to create 1 cm of vertical displacement at the surface of Piton de la Fournaise volcano is investigated, in the case of shear stress only and mixed stress for a 10° subhorizontal fracture.

In shear stress only, the minimum opening is not affected by the stress anisotropy. For all stress ratios *k,* 0.3 cm of minimum opening is necessary to create 1 cm of vertical displacement. The minimum overpressures are constant for stress ratios between 0.5 and 0.77 (equal to 0.03 MPa) but increase 0.77 and 0.95 to reach 0.2 MPa. In a mixed stress, the minimum openings increase when the stress ratio increases (the anisotropy decreases, Fig. 3.51a), which is consistent with the fact that in normal stress only, minimum openings are higher than in a mixed mode (Fig. 3.44a and 3.48a). Minimum overpressures are constant, equal to 0.03 for a mixed stress for every values of *k.*

Thus, the stress anisotropy has no influence on the minimum openings of subhorizontal fractures emplaced in shear stress only and on the minimum overpressures of subhorizontal fractures emplaced in a mixed stress.

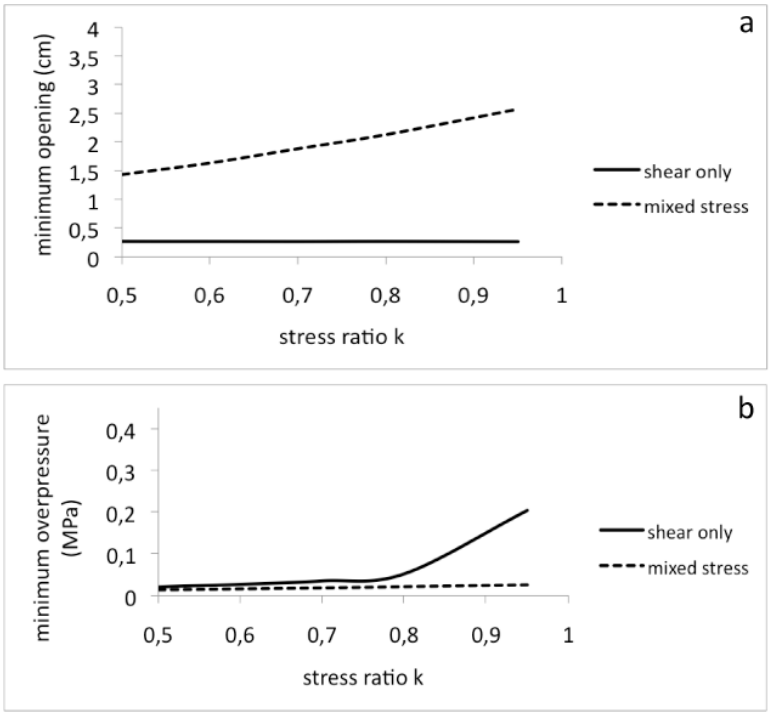

Figure 3.51: Influence of the stress anisotropy on the minimum values of opening (a) and internal overpressure (b) required to create 1 cm of vertical surface displacement at Piton de la Fournaise volcano, for fractures emplaced in a shear only stress field and a mixed stress field (dotted lines).

Assuming that subhorizontal intrusions is a plausible intrusive mechanism at

Piton de la Fournaise volcano, this study of detectability shows that the deformation fields associated to subhorizontal injections should be detected and recorded by the monitoring systems of the Volcanic Observatory (OVPF). Although the network of differential GPS is poorly developed on the lower slopes of Piton de la Fournaise volcano (in the Grandes Pentes area, Fig. 3.39a), the monitoring of the deformation can be carried out using remote sensing techniques like radar interferometry. However, this characterization of the detectability of subhorizontal intrusions only applies if we assume that Piton de la Fournaise volcano is a homogeneous and isotropic edifice whose behaviour is elastic. Moreover, the amplitude of surface displacements also depends on the surface of the sill. There is a minimum surface under which subhorizontal intrusions are not detected by GPS measurements but can be detected by InSAR measurements. The combination of GPS and InSAR is then a valuable method to determine the detectability of subhorizontal intrusions at Piton de la Fournaise volcano.

Chapter 4

Discussion

Most of the surface deformation of volcanic edifices reflects stress changes induced by magmatic processes occurring within the volcano, such as the growth of the magma chamber under internal pressure (Lundgren et al., 2003; Bonaccorso et al., 2005) and the injection of magmatic intrusions (Pollard et al., 1983; Sigmundsson et al., 1999; Fukushima et al., 2005). The intensity and the spatial distribution of the deformation depend partly on the depth and the shape of the source of pressure (Pollard et al., 1983) and partly on the rocks mechanical properties (Gudmundsson, 2003, 2006). This chapter discusses the theoretical results obtained from our modelling approach, in order to: 1- evidence the geometrical characteristics of magmatic intrusions within basaltic volcanoes (shield volcanoes and stratovolcanoes, the specific case La Reunion and Stromboli are taken as examples in section 4.1.2) combining field data (see also section 3.2) and modelling results; 2- define some criteria of identification of the nature of magmatic intrusions using surface displacements (section 4.1.3); 3- bring some insights on the nature of the stress field within basaltic volcanoes (section 4.2) and give some keys to characterize the stress field within a volcano based on the surface displacement pattern associated with intrusive activity, 4- study the role of shear stress and slip along the intrusions in the mechanism of lateral movements of volcanic flanks (section 4.2.3). Then, theoretical results will be applied to real cases of flank deformation (section 4.3). Finally, we will propose some further implications our study brings about modelling volcano deformation.

4.1- Geometry of magmatic intrusions within basaltic volcanoes

4.1.1- Occurrence of subhorizontal intrusions

A large variety of geometries of sheet intrusions has been documented through field observations (see section 3.2). In particular, field data collected in the inner structure of Piton des Neiges volcano (La Reunion Island) and studies on other deeply eroded basaltic volcanoes like La Palma and La Gomera in the Canary islands (Ancochea et al., 2008) show that an important part of magmatic intrusions is made of subhorizontal intrusions, especially in the deepest parts of the edifices. This fact points out a discrepancy that may occur studying young, poorly-eroded, or old, highly-eroded, basaltic volcanoes: when erosion gives access to the core of the edifice, measured deep intrusions (depth > 1 km) are mostly subhorizontal, while subvertical ones mostly occur at shallower levels (depth < 1 km). The transition between high-angle/low-angle intrusions seem to be dependent on the depth of magma injection within the edifice: the deeper the injection, the more frequent the subhorizontal geometry. However, the distribution of some intrusions cannot be simply explained by lateral propagation of magma at the Level of Neutral Buoyancy (Lister and Kerr, 1991).

The geometry of low-angle intrusions is commonly explained by topographical effects (Lister and Kerr, 1991; Rivalta et al., 2005; Kavanagh et al., 2006). Indeed, topographical effects related to the steep slopes of stratovolcanoes partly prevent the formation of low-angle intrusions at shallow levels as the effects of the vertical stress (load of the edifice) are dominant, favouring high-angle intrusions within the edifices. Deeper, arrested dikes can propagate laterally following heterogeneities and form horizontal magmatic bodies (Gudmundsson and Brenner, 2005).

A local rotation of the stress field due to the presence of mechanical heterogeneities is more likely at the origin of the observed intrusions geometries (Valentine and Krogh, 2006; Burchardt, 2008). Some authors (e.g., Gudmundsson, 2003) showed the importance of internal heterogeneities of a volcanic massif in the determination of the deformation at the surface and the geometry of its source, as

the presence of heterogeneities influences the stress distribution within the volcano. In our model, we assumed that, due to the presence of heterogeneities, subvertical and subhorizontal intrusions are not systematically emplaced perpendicular to $\sigma 3$, but the fractures can be intruded with an angle α from $\sigma 3$.

The presence of heterogeneities in a volcano can result from exogenous growth processes, which tend to accumulate stiff (with high Young's modulus) lava flows and soft (with low Young's modulus) pyroclastic and sedimentary layers (Lister and Kerr, 1991; Rivalta et al., 2005; Kavanagh et al., 2006). The contact between two lava flows or between lava and pyroclastic deposits is a mechanical interface through which magmatic intrusions can be emplaced. According to some field studies, in fact, low-angle intrusions preferentially intrude weak layers (Taisne and Jaupart, 2009. Endogenous processes, such as magmatic injections or the occurrence of active or ancient magma chambers, also create stiff heterogeneities (Gudmundsson, 2006; Famin and Michon, 2010) that may partly control the magma paths. Such heterogeneities may modify the state of stress in their surroundings during periods of unrest.

Besides heterogeneities, Gressier et al. (2010) showed that, in sedimentary basins, the depth of the transition subvertical/subhorizontal intrusions may be controlled by the pore fluid overpressure. Due to their low permeability rocks in sedimentary basins often contain fluids in overpressure. This condition encourages the formation of hydraulic fractures and the propagation of magmatic horizontal injections. The deep outcrops at Piton des Neiges volcano are mainly made of basic breccias, formed during the shield building stage of the edifice (Chevallier and Vatin-Perignon, 1982; Maillot, 1999). These breccias are highly altered by hydrothermal processes. The alteration tends to lower the permeability of the breccia, allowing the increase of the pore fluid pressure within the formation. The overpressure can also be favoured by the fact that, generally, breccia levels are stratigraphically located between levels of massive, several meters-thick lava flows, sealing the breccia. Thus breccia levels commonly found within basaltic volcanoes are likely to be in pore fluid overpressure conditions that, associated with heterogeneities (Gressier et al., 2010), can favour the formation of subhorizontal intrusions in the deepest part of the edifices. Moreover, in an anisotropic media (Kavanagh et al, 2006; Gressier et al,

2010 and this study), an excess in pore pressure (compared to hydrostatic value) is sufficient to enhance the formation of subhorizontal intrusions.

Although mechanical heterogeneities can occur both on shield volcanoes and stratovolcanoes, our field data from Piton des Neiges (Chaput et al., 2010) and previous data from La Gomera and La Palma (Cendrero, 1970; Ancochea et al., 2006 and 2008) evidenced subhorizontal within shield volcanoes only.

4.1.2- Cause of low-angle magmatic intrusions at La Reunion and Stromboli

The presence of low-angle intrusions is probably a common feature of many active volcanoes but very few examples were observed, mostly due to the low erosion of volcanic edifices. More field or geophysical works are needed to characterize more systematically magmatic intrusions within basaltic volcanoes and, particularly, to demonstrate if subhorizontal intrusions are more common than previously recognized. The presence or absence of low-angle magmatic intrusions at La Reunion and Stromboli, the two basaltic island systems subject of this study, is here shortly discussed according to recent interpretations.

4.1.2.1- Piton des Neiges volcano (La Reunion)

The existence of shallow-dipping intrusions in the inner structure of Piton des Neiges volcano has been shown by several studies (Chevallier, 1979; Maillot, 1999; Letourneur, 2008; Chaput et al., 2010; see chapter 2). They showed that subhorizontal intrusions generally occur as piles within the edifice, while individual intrusions are scarcer (Fig. 4.1). Sill clusters are composed of several parallel sills intruded at a geological contact characterized by a sharp lithological contrast, in this case where a low-rigidity layer (breccia) overlies a comparatively stiff layer (lava flows). The dip of the sills is that of the contact, which is usually gently sloping. Differently from what was inferred by Kavanagh et al. (2006) where subhorizontal intrusions may form at the interface between an upper rigid strata and a lower weaker strata, the structures we observe at Piton des Neiges indicate the opposite, as breccia levels are generally on top of the subhorizontal intrusions (Fig. 4.1a1).

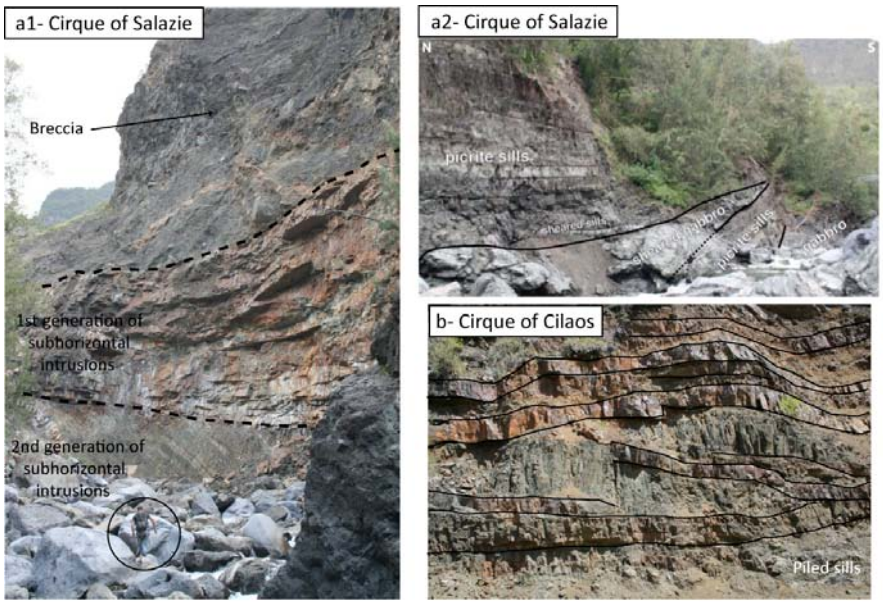

Figure 4.1: Piles of subhorizontal intrusions within Piton des Neiges volcano, in the Cirques of Salazie (a1 and a2) and Cilaos (b), pictures from Laurent Michon and Marie Chaput. See man for scale in Fig. a1.

However, the load of overlying lava flows may have sealed the breccia deposits, increasing their rigidity. According to the model proposed by Menand et al. (2008), we propose that the piles of subhorizontal intrusions occurring at Piton des Neiges volcano are formed by the emplacement of a first intrusion along a mechanical discontinuity (between upper breccia and lower lava flow), which provides favourable rigidity contrast for the emplacement of subsequent low-angle intrusions. Letourneur (2008) distinguished another group of subhorizontal intrusions within Piton des Neiges, whose emplacement is related to an increase of the gravitational stress field. With the increase of distance from the eruptive centre, in fact, these intrusions rotate and become sub-parallel to the near-surface stress field, unfavourable to dike injection. Maximum principal stress directions resulting from gravity-loaded models were shown to be parallel to the ground surface for the shallowest part of the edifice (Cayol and Cornet, 1998; Letourneur et al., 2008).

4.1.2.2- Piton de la Fournaise volcano (La Reunion)

As the volcano is young, active and poorly eroded, direct observations of the geometry of deep intrusions of the magmatic system of Piton de la Fournaise are not

possible.

The most recent model of formation of the Enclos-Grand Brulé Structure proposed by Michon and Saint-Ange (2008) suggests the existence of a discontinuity located below the Grand Brulé (Fig. 2.22), as did the model proposed by Merle and Lénat (2003). The drilling campaign carried out in the Grand Brûlé in 1986 (Rançon et al., 1989) did not permit the recognition of a possible "gliding horizon", as hypothesized by Merle and Lénat (2003) but a mechanical discontinuity was identified at a depth of 1000 m, at the interface between a dense, deeply-rooted body that was interpreted as the frozen reservoir of Les Alizés Volcano (Malengreau et al., 1999; Lénat et al., 2001, see section 2.3.2.2), and landslide-related deposits associated to recent lavas flows (Merle and Lénat, 2003). Rançon (1989) indicated that this depth corresponds to the presence of a laccolith of gabbro and intrusions of thin gabbro and picrite layers. The interface between the cumulative body and the overlying deposits, at 1000 m of depth beneath the Grand Brûlé, could have the rigidity contrast to allow the formation of intrusions. According to Menand (2008) and Kavanagh et al. (2006) the injection of a subhorizontal magmatic intrusion and its solidification may create conditions of rigidity favourable for the emplacement of subsequent low-angle intrusions and may account for the formation and growth of a laccolith by their vertical accumulation.

Despite the fact that the extension of this mechanical discontinuity is not constrained in the upper part of the edifice, especially in the Grandes Pentes area (Fig.2.22c), subhorizontal intrusions could be emplaced along this discontinuity also at shallower depth below the eastern flank of Piton de la Fournaise volcano.

4.1.2.3- Stromboli volcano

At Stromboli, active and poorly eroded volcano, recent field studies carried out by Corazzato et al. (2008) and Tibaldi et al. (2009) showed that low-angle intrusions are scarce in the upper part of the edifice. We propose that the three factors responsible here for the preferential emplacement of high-angle intrusions are: 1- the topography of the edifice, where the occurrence of steep slopes reinforce the effects of the vertical stress, favouring the formation of subvertical intrusions; 2-

the presence of a very superficial reservoir at an elevation of 500 m (see Fig.4.9) and 3- the relatively small scale of the edifice, the distance from the injection point being to short to enable a reorientation of the intrusions from subvertical to subhorizontal (see 4.1.1). However, as the core of the edifice is not accessible, no data are available on the nature of deep magmatic intrusions at Stromboli volcano, but because of the strong heterogeneity of the edifice, it is likely that deep subhorizontal intrusions, not directy observable, occur at Stromboli, similarly to Piton de la Fournaise volcano.

4.1.3- Identification of the geometry of magmatic intrusions from surface displacements

Our modelling results (Chapter 3) bring some indications to determine the geometry of magmatic intrusions using surface displacement ratios on volcanic edifices. It is important to keep in mind that the criteria exposed in this section refer exclusively to outward dipping fractures, as evidenced from field data (section 3.2). Indeed, inward dips could induce some differences in the geometries of the displacements. However, since to our knowledge this geometry was not observed in volcanic edifices, it was not investigated in our study.

4.1.3.1- Detection of subvertical or subhorizontal fractures

The determination of the geometry of a fracture is generally based on the deformation and seismic data recorded during the intrusive event. Pollard et al. (1983) carried out a theoretical analysis of the deformation fields in volcanic environment and described the relationships between the nature of surface displacements and the characteristics of the associated steeply-dipping fractures. Our modelling approach compares surface displacement fields caused by steeply-dipping and shallow-dipping fractures. It also gives some simple criteria for the recognition of the geometry of magmatic intrusions from surface displacements geometries, allowing the distinction between the effects of subvertical and subhorizontal fractures.

When the intrusions are emplaced in normal stress only:

- the distinction between the nature of the intrusions can be made on the basis of vertical displacement patterns, which is made of a unique lobe in the case of subhorizontal intrusions while several lobes are formed for subvertical intrusions (Fig. 3.12a and 3.14a).

- Using the surface ratios, the geometry of the intrusions can be identified thanks to $R(X/Z)_{hw,toe.}$ We showed that for both types of intrusions, their variations are similar (Fig. 3.16c) as they are always positive and increase with the dip of the intrusions. However, $R(X/Z)_{toe}$ is inferior to 0.7 while $R(X/Z)_{hw}$ is superior to 0.7, allowing the identification of the geometry of the intrusion from surface displacements in a normal stress only mode.

- Moreover, negative values of R(Z) exclusively correspond to subvertical intrusions (Fig. 3.16b). R(Z) is always positive for subhorizontal intrusions.

- Positive values of $R(X/Z)_{fw,hd}$ are only obtained for subvertical intrusions, while $R(X/Z)_{fw,hd}$ is always negative for subhorizontal intrusion (Fig. 3.16d).

Assuming that fractures along which the fractures occur are submitted to shear stress:

- The geometry of the fractures can also be distinguished on the basis of the horizontal and vertical displacements: for a subvertical fracture, horizontal movements are oriented inward and the hangingwall of the fracture is affected by subsidence while for a subhorizontal fracture, horizontal movements are oriented outward and the toe of the fracture is uplifted (Fig 3.12 and 3.14).

- the amplitudes of R(X) are always superior to 0.8 (1 if shear stress only) for subhorizontal fractures and always inferior to 0.8 for subvertical fractures (Fig. 3.18a and 3.20a).

- negative values of R(X) exclusively correspond to subvertical fractures (Fig. 3.33a). R(X) is always larger than 1 for subhorizontal fractures (Fig. 3.38a).

- for subhorizontal fractures, the $R(X/Z)_{toe}$ is larger than 0.6 (0.8 if shear stress only) while it is lower than 0.6 in the case of subvertical fractures (Figs. 3.18c and 3.20c).

- R(X) and R(X/Z) are much larger for subhorizontal fractures than for subvertical ones.

Table 4.1 summarizes the criteria we defined in order to discrimate subvertical from subhorizontal fractures.

stress field	intrusion	surface vertical displacements	surface horizontal displacements	R(X)	R(Z)	R(X/Z) hw,toe	R(X/Z) fw,hd
normal stress only	subH	1 lobe			> 0	< 0.7	< 0
	subV	2 or more lobes			can be < 0	> 0.7	> 0
shear stress only	subH	uplifted toe	Oriented outward	> 1		> 0.8	
	subV	subsided hangingwall	oriented inward	< 1		< 0.8	
mixed mode	subH	uplifted toe	oriented outward	> 0.8		> 0.6	
	subV	subsided hangingwall	oriented inward	< 0.8		< 0.6	

Table 4.1: Criteria of determination of the geometry of magmatic intrusions from surface displacement patterns and ratios on basaltic volcanoes.

4.1.3.2- Estimation of the fracture dip

Once the rough geometry (low-angle or high-angle) of the fracture has been determined, the ratios of surface displacements allow to quantify more precisely the dips of fractures submitted to normal stress only and to shear stress (alone or combined to normal stress), within the ranges defined in the model assumptions: 0 to 30° for low-angle fractures and 60 to 90° for high-angle fractures.

Under normal stress only, R(X) and $R(X/Z)_{fw,hd}$ do not allow the determination of the intrusion dip from a value of ratio as one value can correspond to several dips, both for subvertical and subhorizontal intrusions (Fig. 3.16a and c). On the other hand, a single value of $R(X/Z)_{hw,toe}$ correspond to a precise value of intrusion dip, either for a subvertical or a subhorizontal intrusion, without any ambiguity (Fig. 3.16c). Furthermore, for negative values of R(Z), it is possible to determine a single value of subvertical intrusion dip (Fig. 3.16b).

When shear stress is present, in the case of subvertical fractures, the variations of R(Z) bring interesting insight on the dip of an fracture as it permits its determination in an interval of 10° (Fig. 3.33b). The more negative the value of R(Z), the more accurate the estimation of the dip of the subvertical fracture. Similarly, based on $R(X/Z)_{fw}$, the deeper the subvertical fracture, the more accurate the estimation of its

dip (Fig. 3.36d). In the case of subhorizontal fractures, Figs. 3.38c and 3.38d indicate that an estimation of the fracture dip can be carried out in an interval of 10°, using the variations of both $R(X/Z)_{toe}$ and $R(X/Z)_{hd}$.

Table 4.2 summarizes the criteria we defined to estimate the fractures dips from the surface displacements.

stress field	intrusion	R(X)	R(Z)	R(X/Z)hw,toe	R(X/Z)fw,hd
normal stress only	subH		✔	✔	
	subV			✔	
shear stress (alone or mixed mode)	subH			✔	✔
	subV		✔		✔

Table 4.2: Summary of the valuable ratios in the estimation of the fractures dips from surface displacements.

4.1.3.3- Estimation of the fracture depth

Our results did not allow us to determine precisely the depth at which fractures are emplaced by a simple analysis of the surface displacements. However, a first approximation can be made studying the maximum external displacement gradients for diverse depth of fractures. It is possible to distinguish a shallow fracture as superficial fractures have higher values of maximum displacement gradient than for deep fractures. Moreover, deep fractures show large variations of the gradient with the dip and *k* while no variation is observed for shallow fractures (Figs. 3.37a and 3.37b). Thus, displacements gradients are valuable in the inference of fracture depth.

To conclude, this section 4.1.3 underlines that our results, in terms of surface displacement ratios and gradient, have a useful application in constraining the geometry and depth of magmatic intrusions submitted to normal, shear stress or mixed stress. Moreover, our results show that the topography has no major influence on the surface displacement ratios generated by both types of fractures

(section 3.5.4.1). As a consequence, the criteria of identification of the geometry of magmatic intrusions can be applied to any type of basaltic edifices, i.e. shield volcanoes and stratovolcanoes.

4.2- Nature of the stress field within basaltic volcanoes: insights from theoretical results.

The state of stress within a volcanic edifice is controlled by the mechanical properties of the material constituting the volcano and by the loading conditions (i.e. internal and external pressures applied to the edifice). Our study considers the influence of the nature of stress fields on the mechanical evolution of a volcanic edifice during magmatic fractures. Integration of anisotropic stress field allows integration of more realistic states of stress. Here, the intensity of the stress field anisotropy is defined by *k* as ratio between the load of the edifice (vertical stress) and the horizontal stress. Anisotropic stress field enables fractures to be submitted to both normal and shear stress, whereas normal stress solely acts on the fracture in isotropic stress field. Magmatic intrusions in basaltic volcanoes can be submitted to shear stress if they are injected in directions oblique to $\sigma 3$ for the reasons described in section 4.1. Topographical effects can also be responsible for shear stress at the surface of the fractures. We tested the influence of three stress fields on the surface displacements created by subvertical and subhorizontal fractures: a stress field where fractures are submitted to normal stress only (only opening of the fracture occurs), a stress field where fractures are submitted to shear stress only (only slip along the fracture occurs), a stress field where fractures are submitted to normal + shear stresses (opening of the fracture and slip along the fracture occur).

4.2.1- Determination of the stress field within an edifice

4.2.1.1- Presence of shear stress?

When intrusions are emplaced in a direction perpendicular to $\sigma 3$, it is possible to assume that they can be affected by normal stress only, favouring the

opening of the intrusion. The results presented in Figures 3.12 and 3.14 and in Table 3.1 give us first insights on how to discriminate subhorizontal from subvertical intrusions as well as intrusions submitted merely to normal stresses from intrusions submitted to mixed normal and shear stresses. Assuming that both subvertical and subhorizontal intrusions have outward dips, we can distinguish the stress mode under which an intrusion was injected. For a subvertical fracture, surface vertical displacements show that the hangingwall of the intrusion is uplifted if submitted to normal stress only while it is subsided if submitted to shear stress (only or combined to normal stress, Fig. 3.12). For a subhorizontal fracture, surface vertical displacements show a unique lobe if the intrusion is affected by normal stress only while 2 lobes are identified when shear occurs at the surface of the fracture (Fig. 3.14). R(Z) are expected to be positive when intrusions are submitted to normal stress only, while it is negative when faults are submitted to shear stress. However, these criteria are not sufficient to distinguish a mixed mode of stress (normal + shear stresses) from a stress mode made of shear only.

4.2.1.2- Shear stress only or mixed mode of stress?

The principal difference between a mixed stress mode and a shear stress only is that, in the latter, the ratios of surface displacements do not depend on the stress ratio *k*. If the role of the fracture dips on the surface displacements is only considered, a distinction between the mixed mode of stress and the shear only mode of stress can be made using R(X) and $R(X/Z)_{hw,toe}$. Indeed, despite similarities in the evolution of the ratios in both stress modes (Figs 3.18 and 3.20), in a mixed stress mode, values of 0.8 for R(X) and 0.6 for $R(X/Z)_{hw,toe}$ are discriminant for the geometry of the fractures while these values are 0.6 and 0.8 for R(X) and $R(X/Z)_{hw,toe}$, respectively, in a shear only stress mode (Fig. 3.18a and c, Fig. 3.20a and c). However, for low-angle fractures (fractures with values of dip lower than 20°), R(X) in a mixed stress mode are larger than 1.2 while they are lower than 1.2 in a stress mode involving shear stress only. This effect is reinforced when *k* increases. For what regards subvertical fractures, ratiosurfX are superior to 0.8 in shear only mode and inferior to 0.8 in a mixed mode of stress (Figs. 3.18a and 3.20a).

4.2.1.3- Estimation of the stress ratio

We showed that when a fracture is affected by shear stress only, no estimation of the stress ratio is possible from the different ratios of surface displacements as they are independent from *k.* In a mixed stress mode, negative values of R(X) associated with high-angle fractures can give a good estimation of the stress ratio (Fig. 3.33a). It is however difficult to estimate precisely the stress ratio *k* from surface displacements ratios created by subhorizontal fractures, as *k* strongly evolves for a given value of any ratio (Fig. 3.38a). It is important to notice that, similarly to what is observed for the identification of the fracture geometry (section 4.1.3.), the topography has no major influence on the determination of the nature of the stress field and on the estimation of the stress ratio. This observation can be applied to both basaltic shield volcanoes and stratovolcanoes.

4.2.2- Role of shear stress on flank displacements of basaltic volcanoes

Our theoretical results obtained for a 10° subhorizontal fracture and a 80° subvertical fracture show that, in an anisotropic stress field, the effect of shear stress favours slip movements along intrusions (Fig. 4.2).

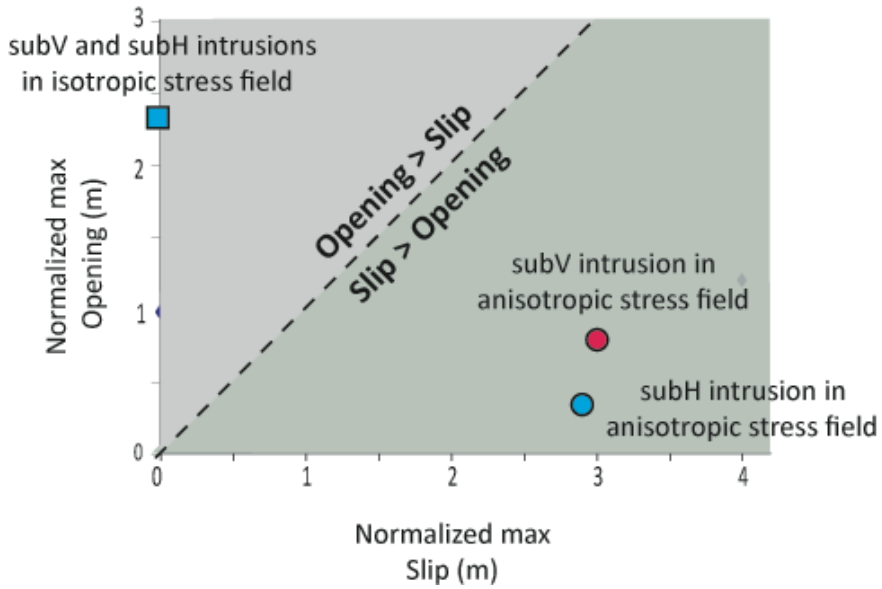

Figure 4.2: Maximum normalized opening and slip for 10° subhorizontal (subH) intrusion and 80° subvertical (subV) fracture in isotropic and anisotropic stress field (k = 0.6).

When the opening of the intrusions is combined to slip, a complex relationship occurs between opening/slip and deformation of the volcanic edifice. Our results with isotropic and anisotropic stress field prove that the shear stress creates the conditions that allow slipping along intrusions, generating large-scale deformation of the edifice. Outward displacements can be generated by a subhorizontal intrusion emplaced in an anisotropic stress field or a subvertical intrusion emplaced in an isotropic stress field. The shear stress affects both subvertical and subhorizontal intrusions. However, the internal and surface displacements generated by high-angle intrusions are localised in the summit area of the edifice and have a small lateral extension (Fig. 3.12). Conversely, low-angle intrusions are responsible for displacements affecting both the summit area and the flank of the edifice (Fig. 3.14). Moreover, while subvertical intrusion generates inward displacements in the summit area, subhorizontal intrusions favour large amplitude outward displacements of the flank and the summit of the edifice. The longer the subhorizontal intrusion, the wider the lateral extension of the flank displacements. The comparison between horizontal displacements for subhorizontal intrusion in an isotropic stress field and horizontal displacements in an anisotropic stress field, shows that slip along the intrusion favours the lateral extension of the flank displacements in the second case (Figs. 3.14 and 4.2). If one considers a mechanism of deformation where a single fracture is involved in an anisotropic stress field, subhorizontal intrusions have a far greater potential for flank-scale displacements than subvertical ones, possibly leading to lateral instability if the induced perturbation overcomes the threshold of stability of the volcanic flank.

4.3- Mechanisms of flank collapse on basaltic volcanoes: applications to real cases.

Historically documented events of volcano lateral collapse are rare. As a result understanding and assessing the processes involved in flank destabilization and flank movement are difficult. Thus, the few volcanoes identified as being structurally unstable are intensively monitored: the southern flank of Kilauea (Hawaii), the northern flank of Stromboli (Aeolian Islands), the eastern flank of Piton

de la Fournaise (Reunion Island) and the eastern flank of Mount Etna (Sicily). Several studies suggest that the occurrence of eruptions/intrusions, seismicity and flank destabilization of volcanic edifices are related (Dieterich, 1988; Iverson, 1995; Elsworth and Day, 1999) and that flank movement, in turn, influences magma propagation and the geometry of intrusive rift zones (Walter and Troll, 2003; Walter et al., 2005). Patterns of deformation at Etna and Kilauea volcanoes are interpreted as lateral movements of flanks combined with magmatic deformation (Bonforte and Puglisi, 2003; Delaney and Denlinger, 1999; Owen et al., 2000). At Piton de la Fournaise and Stromboli, asymmetric patterns of deformation are supposed to be entirely due to magmatic effects (Froger et al., 2004; Fukushima, 2005; Peltier et al., 2007). Flank instability seems to be independent from volcanoes composition, shape and geodynamic setting (see chapter 2). However, the study of volcanic flank behaviour is not limited to collapse phenomena. Understanding how magmatic intrusions can trigger flank-scale deformation (with or without collapse) on basaltic volcanoes is a key point in constraining two mechanisms: 1- the long-term evolution of basaltic edifices and 2 - the assessment of the potential for failure and associated hazards.

Although a lot of studies consider only the role of vertical intrusions as trigger of flank collapses on volcanoes (Dahlen, 1984; Dieterich, 1988; Iverson, 1995; Elsworth and Voight, 1995; Elsworth and Day, 1999; Walter et al. 2005), our theoretical results underline that high-angle intrusions alone are not the only way to generate flank-scale deformation. Another trigger has to be considered: subhorizontal intrusions below volcanic flanks. Piton des Neiges well illustrate the interaction between low-angle magmatic intrusion, slipping plane and large lateral displacements prone to enhance flank instability on basaltic volcanoes. The case discussed by Famin and Michon (2010) in the core of Piton des Neiges is the first observable outcrop where a detachment plane is in direct relationship with low-angle intrusions (section 4.1.2.1). Together with the submarine evidence offshore La Reunion (Oehler et al., 2004), these authors underline that this volcano experienced a major (long-term) destabilization of its northeastern flank (section 2.3.2.2, Figs. 2.23 and 2.26; section 3.1, Fig. 3.4). Low-angle injections have also been described on young, active and

poorly-eroded volcanoes.

In the following sections we discuss the interactions between magmatic intrusions and flank movements during several recent events: the April 2007 eruption of Piton de la Fournaise volcano, the March 2007 crisis at Stromboli volcano, the 2002-2003 events that occurred at Etna volcano and the 1995 eruption of Fernandina (Galapagos).

4.3.1- The April 2007 event at Piton de la Fournaise volcano

A recent episode of flank-scale deformation affected Piton de la Fournaise volcano during the April 2007 eruption. On February 26 the seismic activity began below the summit zone. It progressively increased and reached the value of more than 100 daily events on March 28 to 30. A seismic crisis started on March 30 at 16:25 UTM and the magma emission begun at 18:50 from an eruptive fissure located at 1900 m above sea level at the southeast of the central cone (Fig. 4.3a). The tremor ceased on March 31 at 05:15, after a first eruptive phase of less than 10 hours during which only a small volume of magma was emitted. The summit seismicity continued until the April 2 new eruptive phase, located in the Grand Brûlé at 600 m above sea level and 7 km away from the summit (Fig. 4.3a; Michon et al., 2009; Staudacher et al., 2009; Peltier et al., 2010). The large co-eruptive ground displacements that occurred during this event were recorded by radar interferometry (Fig. 4.3b, Froger et al., 2010). The distal event of April 2007 generated large-scale deformation that affected the eastern flank of Piton de la Fournaise volcano, as far as 6 km away from the summit area where regular eruptions generally are concentrated (Villeneuve and Bachèlery, 2006; Peltier et al., 2007).

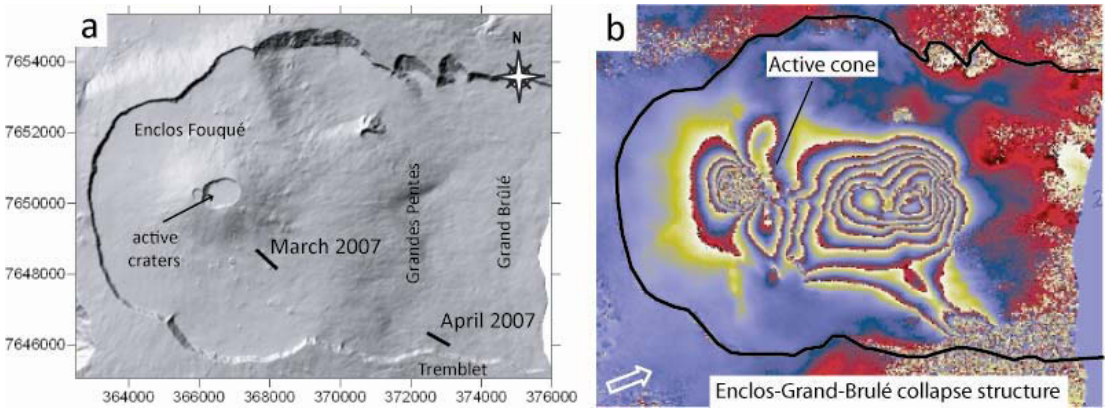

Figure 4.3: a- Location of the 2 eruptive fissures of March and April 2007 crisis; b- Ground displacements associated to these crisis, measured by ALOS-PALSAR radar (Froger et al., 2010).

The geometry, lateral extension of the deformed area and the intensity of the displacement were never been observed at Piton de la Fournaise volcano before 2007. They strongly contrast with the displacements associated with dike intrusions along the rift zones (Fukushima et al., 2005; Peltier et al., 2007).

Considering the geometry of the plumbing system in the Piton des Neiges volcano (i.e. shallow-dipping intrusions at depth), we interpret the deformation of the eastern flank of Piton de la Fournaise as the result of a subhorizontal intrusion. Two of the criteria defined for the identification of the geometry of the intrusions (section 4.1.3) suggest that a subhorizontal intrusion could be involved in the generation of this deformation pattern, as already suggested by Famin and Michon (2010). (1) In 2007, horizontal displacements are oriented eastward (equivalent to outward in the theoretical case) and vertical displacements show that the toe of the intrusion is uplifted (Fig. 4.6). (2) R(X) is positive (equals to 7), and larger than 1 while it would have been lower than 1 with a subvertical intrusion (Table 3.1 and Fig. 3.33a and 3.38a). We cannot derive more precise information about the possible dip of the intrusion as the R(X/Z) is difficult to estimate, given the complexity of the vertical pattern of displacements compared with the simple theoretical case we studied. Indeed, vertical displacements measured by radar interferometry for the 2007 eruption correspond to a finite deformation on a period of 35 days, making difficult to quantify the component of vertical displacement associated with the event of

intrusion itself. For that reason, it is also difficult to estimate the depth at which the intrusion might have been emplaced below the eastern flank. For what regards the nature of the stress field, R(X) being larger than 1.2, it is likely that the edifice is characterized by an anisotropic stress field based on the previously defined criteria (section 4.2) and the fact that several lobes can be identified on the vertical displacements, the subhorizontal intrusion should have been submitted to shear stress and, particularly, should have been emplaced in a mixed mode of stress (opening + shear stresses). No precise estimation of the stress ratio is instead possible.

Since the hypothesis of a shallow dipping intrusion below the flank of Piton de la Fournaise volcano during the April 2007 crisis seems realistic (although non exclusive), we tested it by using the numerical model described in the chapter 3, but under specific conditions:

1- Instead of applying the model to an ideal topography, we use the real topography of Piton de la Fournaise volcano (Fig. 3.42).

2- The geometry of the intrusion corresponds to a 6-km-long and 3-km-wide quadrangular. The eastward dip is fixed at 10° and the internal overpressure at 1 MPa. The intrusion is emplaced at an elevation of 1500 m, i.e. 1000 m below the summit of the edifice (Dolomieu crater).

3- The stress field within Piton de la Fournaise is assumed to be anisotropic, involving normal and shear stresses. As no precise estimation of the stress ratio is possible from the ratios of the displacements for subhorizontal intrusion (section 4.2.1.3), we assume k = 0.6.

The modelled opening and slip along the low-angle intrusion below the eastern flank of Piton de la Fournaise show that it is submitted to a maximum opening close to 2.4 m in the central part of the intrusion tip (Fig. 4.4a) while the slip reaches values larger than 3 m (Fig. 4.4b). The total surface of the intrusion is about 18 km^2, 25 % of which are affected by an opening larger than 2m, 45 % by a slip superior to 2.5 m and 12 % by a slip superior to 3.5 m. Figure 4.4c indicates that the internal displacements within the edifice reach a maximum value of 3 m in the Grandes Pentes area.

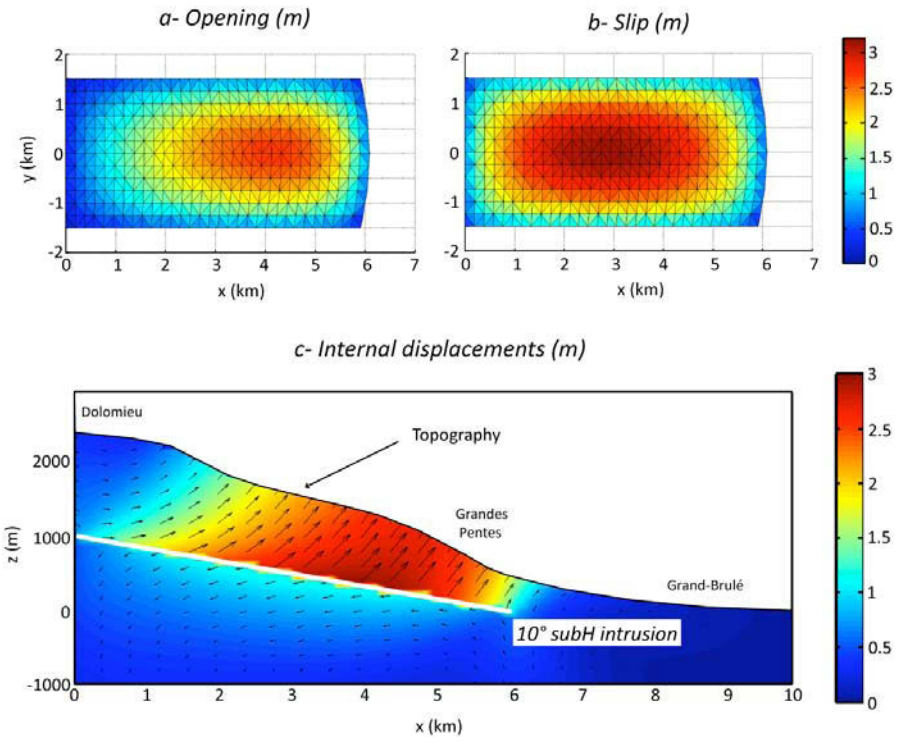

Figure 4.4: Opening (a) and Slip (b) of a 10° outward dipping intrusion injected below the eastern flank of Piton de la Fournaise volcano, and the generated internal displacements (c) within the edifice.

Displacement maps of the EGBS (Fig. 4.3) were built using the InSAR data collected by ENVISAT-ASAR and ALOS-PALSAR radars (Fig. 4.5). Figure 4.5 presents for comparative purposes the recorded vertical (Fig.4.5a) and eastward (Fig. 4.5b) co-eruptive ground displacements generated by the succession of events that occurred between March and May 2007 at Piton de la Fournaise volcano (Froger et al., 2010*)* and the modelled displacements caused by a 6 km long low-angle intrusions propagating eastward below the Grandes Pentes with an outward dip of 10°.

Recorded displacements

Recorded vertical displacements (Fig. 4.5a, top) show a complex pattern. The western part of the EGBS is affected by downward movements (subsidence) of 30 cm at the level of Bory crater and upward movement (uplift) of 10 to 30 cm East of it. On the eastern flank of the edifice, the recorded signal is more complicated with

areas affected by upward movements (maximum of 35 cm) and downward movements (maximum of 35 to 40 cm). Recorded displacements extend to the Grandes Pentes area.

Eastward recorded displacements (Fig. 4.5b, top) show another pattern of deformation: the western part of the active cone is submitted to low amplitude eastward movements, while the upper eastern flank is submitted to low amplitude westward movements. The lower eastern flank (base of the cone and Grandes Pentes area) is affected by a single pattern of eastward displacements reaching 1.4 m towards the sea.

Modelled displacements

Modelled eastward displacements (Fig. 4.5b, bottom) show strong similarities with the pattern recorded during the eruption. In the area of the base of the cone and Grandes Pentes, corresponding to the tip of the modelled intrusion, maximum eastward displacements are recorded, with the same geometry (lateral extension) and amplitudes than the recorded displacements. At the head of the intrusion, the western flank of the active cone is affected by the same eastward displacements of 0.2 m than the one observed in the recorded deformation. Away from the intrusion, the rest of the EGBS is affected by low-amplitude displacements oriented westward, both for the modelled and recorded deformation. There is a minor difference between the two signals: the upper eastern slopes of the active cone on the modelled displacements are not affected by low amplitude westward displacements, as observed on the recorded pattern (Fig. 4.5b, top).

For what regards the pattern of vertical displacements, recorded and modelled signals are strongly different (Fig. 4.5a). The area located above the tip of the modelled intrusion is affected by maximum uplift, similarly to the recorded signal, and the base of the eastern flank is uplifted of about 30 cm in both signals. However, the subsidence occurring in the Grandes Pentes area is not modelled, as uplift also occurs in this area on the pattern of modelled displacements. At the head of the intrusion, corresponding to the area of the active cone, only low-amplitude subsidence is modelled, while the recorded signal shows a general uplift East of the cone and subsidence to the West of it.

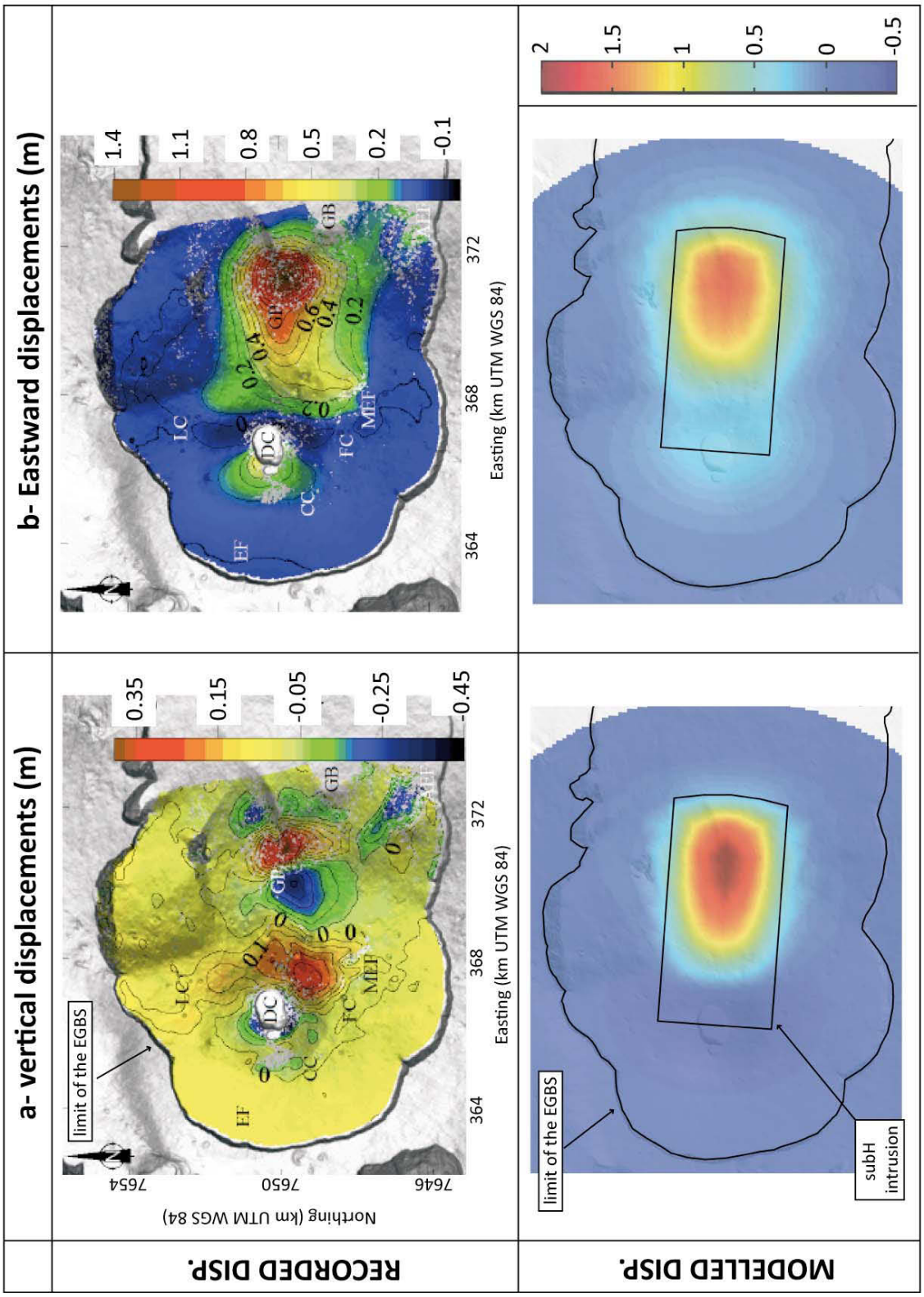

Figure 4.5: Recorded (period March-May 2007; Froger et al., 2010, appendix 5) and modelled displacements associated to the eruptive crisis at Piton de la Fournaise volcano. (a) vertical displacements in meters; (b) eastward displacements in meters.

The comparison between recorded and modelled eastward displacements indicates that the surfaces of displaced areas have comparable geometries, extensions and amplitudes. On the basis of the pattern of eastward displacements, the hypothesized dip and geometry for a low-angle intrusion seems to be a good (qualitative and quantitative) approximation of the source of observed deformations. However, the strong discrepancy between the recorded and modelled vertical displacements suggests that the assumed geometry is too simple to account for realistic displacements fields recorded during the April 2007 event at Piton de la Fournaise volcano. Several hypotheses can be made on the origin of the discrepancy we observe between the recorded and modelled displacements pattern:

1- In our model, we only take into account the contribution of a shallow-dipping intrusion injected below the eastern flank of Piton de la Fournaise, on the pattern of displacements associated to the 2007 crisis. However, the recorded displacements include the effects of the vertical intrusion of March 2007 (Michon et al., 2007; Michon et al., 2009; Peltier et al., 2009; Staudacher et al., 2009) that likely played a role on the nature and amplitude of the recorded displacements. Indeed, pattern observed in the area of the active cone could be strongly dependent on the March 2007 high- angle intrusion that occurred at the base of the cone.

2- We have chosen a simple geometry for the low-angle intrusion in our model, in order to check the hypothesis of a subhorizontal intrusions below the flank of Piton de la Fournaise during the 2007 crisis and to bring qualitative constraints on the geometry of the associated deformation pattern. This geometry could be refined in order to better fit the real data. Similarly, the nature of the stress field within Piton de la Fournaise volcano and the overpressure within the intrusion could be defined more accurately.

3- The constraints on the depth of the intrusion are missing. Indeed, high displacement gradients can correspond either to a superficial intrusion or to displacements associated a deep intrusion involving movements along lateral faults that would create high gradients.

4- The displacements we model correspond to movements that might occur immediately after the emplacement (co-eruptive displacements) of the intrusion while there is a time delay between the emplacement of the intrusion and the

recording of displacements using radar interferometry. This time delay, during which stress is released and mechanical adjustments begin, can be the origin of some of the differences between recorded and modelled displacements.

5- The eastern flank of Piton de la Fournaise volcano is likely to be affected by fractures, faults or others types of local discontinuities, which are not reproduced in the large-scale real topography of Piton de la Fournaise volcano we used in the model. The slope gradients map of the EGBS (Fig. 4.6a), for instance, exhibits a break-in-slope (area with lower gradients, i.e. between 5-10°, in blue in fig. 4.6a) between the steep eastern flank of the active cone and the Grandes Pentes. This discontinuity corresponds to an area where no vertical displacements have been measured (Figs. 4.5a and 4.6c). Other rectilinear break-in-slopes with very high gradients (>30°), with NNW-SSE and ENE-WSW orientations, are visible from the northwestern rim of the EGBS to the central sector of the Grandes Pentes (Fig. 4.7a). These main morphological features, already described by Michon and Saint-Ange (2008, Figs. 2.29, 4.6b and c), may control the pattern of vertical displacements affecting the Grandes Pentes area, likely due to the occurrence of three different “blocks”, moving independently and aligned along a fault oriented in the direction of the regional N75-80° structural trend (Michon and Saint Ange, 2008; Fig. 2.29, Fig. 4.6b and c). The central and the easternmost “blocks” (characterized by positive and negative vertical displacements, respectively, Fig. 4.6c) should be separated by a fault that could be in continuity with the vertical collapse structure identified on the northwestern rim of the EGBS. The westernmost “block” (showing a wide area affected by negative vertical displacements, Fig. 4.6c) could be separated from the central by a similar NNW-SSE oriented fault not visible at the surface.

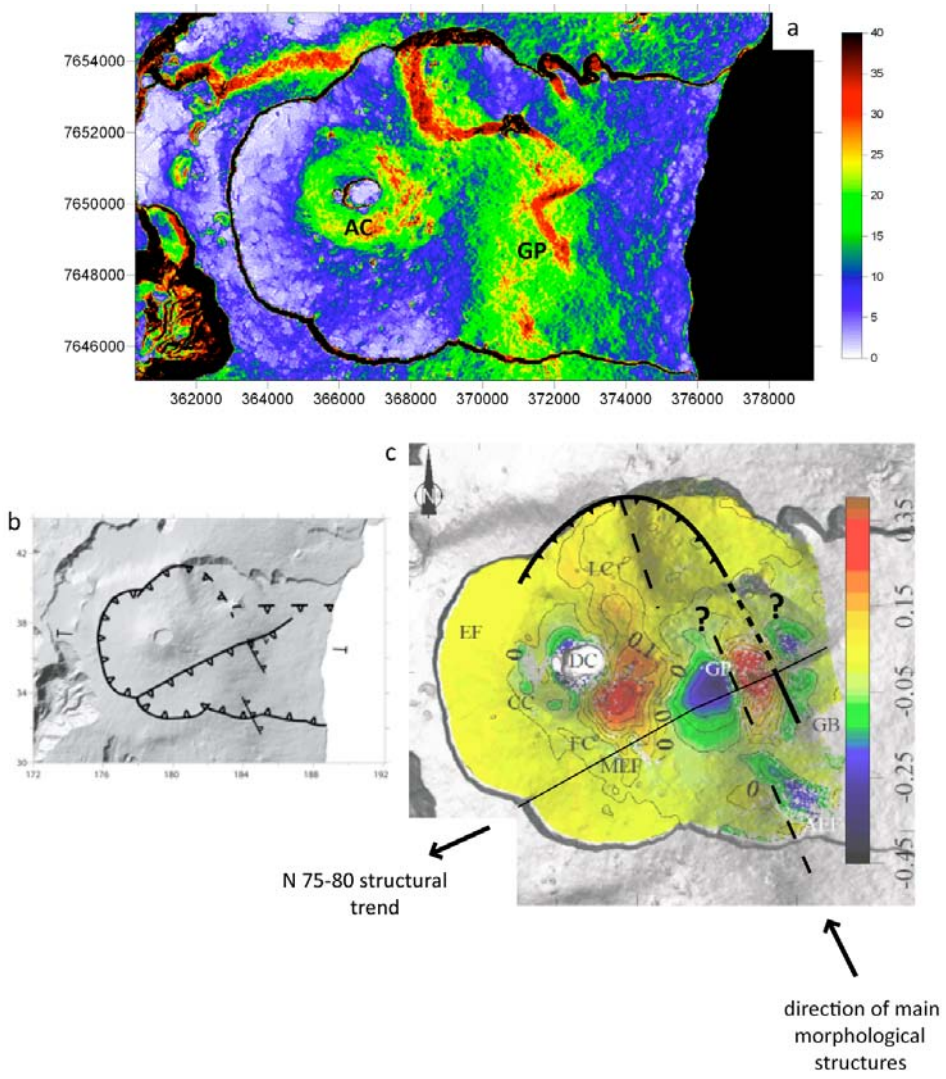

Figure 4.6: a- Slope gradients map of the Enclos-Grand Brulé Structure. AC: Active cone; GP: Grandes Pentes; b- Main tectonic structures of the EGBS proposed by Michon and Saint-Ange (2008); c- Vertical displacements during the 2007 eruption of Piton de la Fournaise and tectonic features of the EGBS (from Froger et al, 2010).

To conclude, we propose that the pattern of displacements recorded during the 2007 eruption at Piton de la Fournaise was generated by the emplacement of a subhorizontal intrusion below the eastern flank of the volcano (associated with a subvertical intrusion at the base of the cone, occurred in March 2007). The formation of this subhorizontal intrusion could be the consequence of the reorientation of a subvertical intrusion injected from the magmatic chamber located at the sea level of the sea, along an internal discontinuity within Piton de la Fournaise volcano. The elevation at which the subvertical intrusion is horizontalized is not well constrained, as information on the depth of the subhorizontal intrusion

below the flank is missing. The slip along the subhorizontal intrusion (due to shear stress) would be mainly responsible for lateral movements of the whole eastern flank, the intrusion acting as a detachment plane (Fig. 4.7). Opening normal to the subhorizontal intrusion might have favoured vertical movements of the eastern flank. It acted on superficial subvertical faults, triggering separate vertical movements (uplift/subsidence) of the blocks dissected by the faults (Fig. 4.7). The maximum uplift is observed in the area where opening of the intrusion is maximum (intrusion tip, Fig. 4.4a). In this model, the discrepancies observed between recorded and modelled vertical displacements might be thus due to the structural complexity of the Enclos-Grand Brulé structure. However, the deep geometry of these faults is not clearly constrained. Michon and Saint-Ange (2008) proposed a model of evolution of the Enclos-Grand-Brulé involving deep subvertical faults at the transition between the upper and lower parts of the structure (Fig. 2.22d). The two fault systems could be related but we have no information on the relationship between these deep faults and the superficial ones we propose in our model.

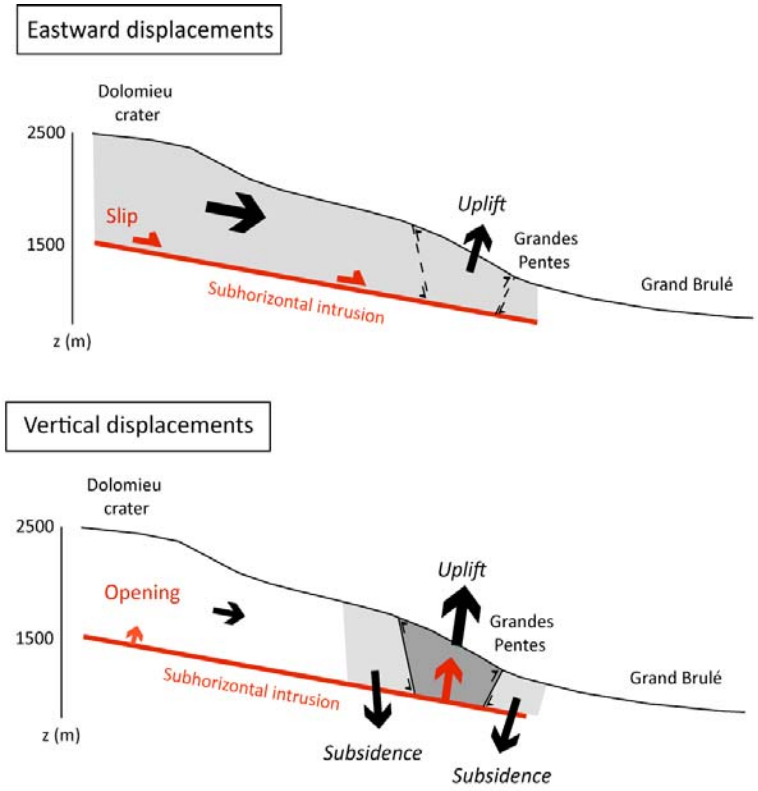

Figure 4.7: Possible mechanism explaining the occurrence of eastward and vertical displacements observed during the 2007 event at Piton de la Fournaise volcano.

4.3.2- The 2007 event at Stromboli volcano

The subaerial part of Stromboli edifice is a small-volume edifice characterised by steep slopes reaching 35° (see chapter 2) in the unstable area of the Sciara del Fuoco. Such morphological features, associated to the nature of the plumbing system of Stromboli, considered as made of 3 magmatic reservoirs whose shallower one is located only 500 m below the summit of the edifice (Fig. 4.8), are influent in the mechanism of flank displacements here. Slope instability phenomena at Stromboli are represented not only by large-scale gravitational collapse, as recognized in the past history of Stromboli (chapter 2), with mobilized volumes > 1km^3, but also by medium –scale landslides, involving masses in the order of some to tens Mm^3 (Tibaldi et al., 2008; Neri et al., 2008; Casalbore et al., 2010).

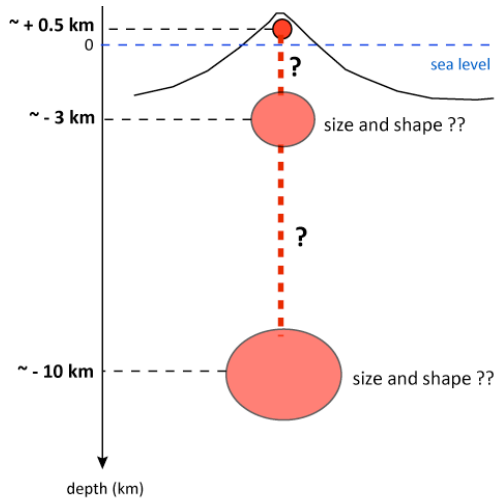

Figure 4.8: Plumbing system of Stromboli volcano (from Metrich et al., 2001; Bertagnini et al., 2003; Francalanci et al., 2004 and 2005);

Recent phases of flank deformation and/or collapses occurred in 2002-2003 (eruptive crisis associated to a tsunamigenic landslide of part of Sciara del Fuoco) and in 2007. The event of 2007 is well-documented in terms of deformation due to the improvement of the multi-parametric monitoring network that followed the 2002-2003 eruption and landslide at Stromboli (Bonforte et al., 2008). Before the onset of the 2007 eruption, measured deformations were usually of small magnitude

and related to the continuous settlement of Sciara del Fuoco after the landslide of December 2002 (Bonaccorso et al. 2009). Ground deformation signals associated to the 2007 eruption indicated the occurrence of rapid deflation at a shallow-intermediate (about 2.8 km depth below the crater area) magma storage as source mechanism.

As far as the Sciara del Fuoco is concerned, the observed deformations were confined only to the northern part of this depression (with the highest velocities recorded in the upper slope), without significant displacements in the central part (Bonforte et al., 2008; Bonaccorso et al., 2009). Casagli et al. (2009) modelled the ground displacements that occurred during the 2007 crisis based on interferometric radar (GB-InSAR, Fig. 4.9) monitoring of the upper slope of Sciara del Fuoco and structural geological field data.

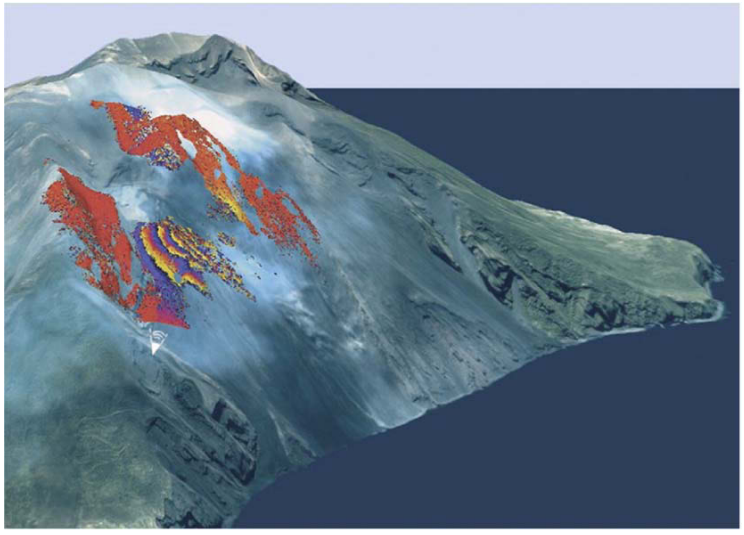

Figure 4.9: 3D model of the Stromboli Island (Sciara del Fuoco slope and NE crater) with the interferogram of 9/3/2007 obtained from the GB-InSAR (from Casagli et al., 2009). The position of the radar is shown with the white symbol.

Strain field evaluated from numerical modelling confirmed the hypothesis of two different types of intrusion that triggered different deformation patterns on the Sciara del Fuoco slope (Casagli et al., 2009):

1- vertical intrusion of magma at a shallow level in the summit area (Scarfi et al., 2010). NE-SW and NW-SE oriented eruptive fissures opened at 650-600 and 400 m

asl, respectively, as a consequence of the downward propagation of the dike downslope (Fig. 4.10; Neri and Lanzafame, 2009). The stress/strain analysis of Casagli et al. (2009) related to the lateral propagation of the intrusion in the NE-SW direction shows displacements in the order of half a meter, with the most deformed zone located in the northern, upper-central part of Sciara del Fuoco (Fig 4.12a).

2- injection of a sub-horizontal intrusion in the summit area starting from the dike and causing the formation of a bulge on the NW sector of Sciara del Fuoco. According to the model of Casagli et al. (2009), this intrusion has a small extension and generates localized displacements in the summit area. The maximum value of the shear strain increment should be located in correspondence with the position of an additional eruptive vent that opened at about 500 m asl just after this stage. According to Giordano and Porreca (2008) the intruding dike may have then diverted from the vertical shape and turned to inclined or subhorizontal, forming a temporary small reservoir, which was later largely emptied by the vent at 500 m a.s.l. Neri and Lanzafame (2009) interpreted the opening of this new vent as due to the lateral propagation of a sub-radial dike from the central conduit of the volcano.

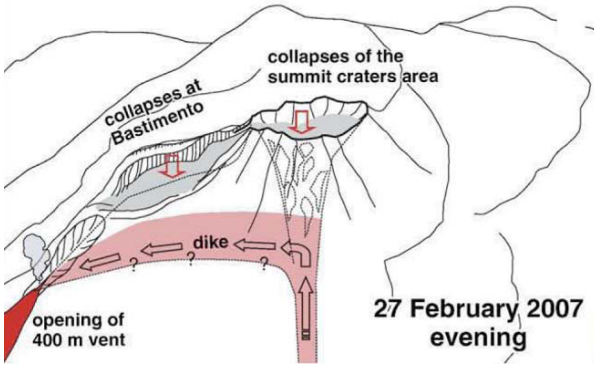

Figure 4.10: Model of lateral intrusion of a vertical dike from the central vent during the February 2007 eruptive crisis of Stromboli volcano, proposed by Neri and Lanzafame (2009).

Casagli et al. (2009) modelled the displacements associated with the lateral dike intrusion using a poro-elastic finite element model. With the MBEM used in this study, we modelled total displacements associated with the same intrusion (same geometry and depth of injection, Fig. 4.11, and submitted to 1 MPa overpressure)

and compare the results with the one obtained by Casagli et al. (2009; Fig. 4.12a and b). At Stromboli volcano, geotechnical studies showed that the Young's modulus of the edifice can be estimated at 2 GPa and the Poisson's ratio at 0.28 (Apuani et al., 2005a and b; Apuani and Corazzato, 2009). The density of the magma at Stromboli volcano is assumed to be 1900 kg.m^{-3} (Apuani and Corazzato, 2009; Tibaldi et al., 2009).

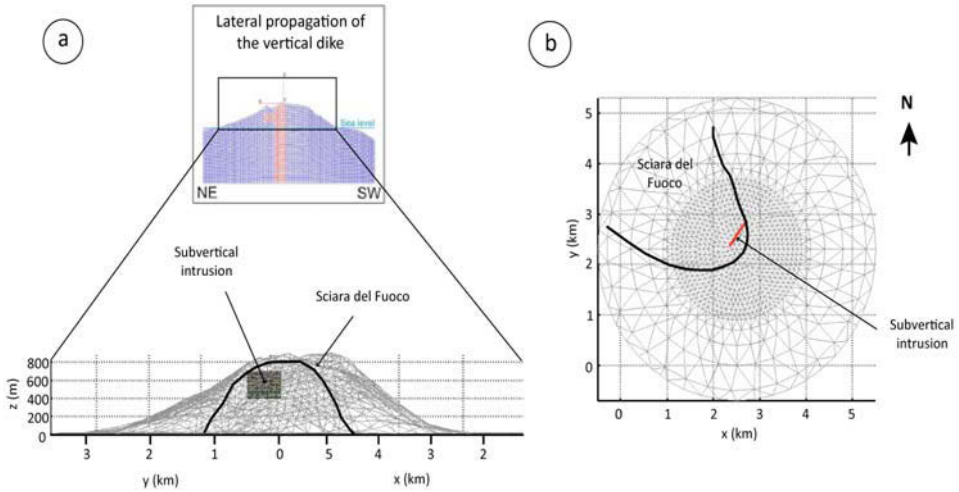

Figure 4.11: Lateral (a) and vertical (b) view of meshed topography of Stromboli volcano and the geometry of the modelled lateral dike in the northeastern part of Sciara del Fuoco associated with the 2007 Stromboli eruption.

The comparison of the modelled displacements reveals that with both models, the pattern of displacements of the Sciara del Fuoco slope is geometrically similar and extends on similar areas. However, the amplitudes of modelled displacements are quite different: in the model used by Casagli et al. (2009) total displacements range from 1 to 45 cm in the eastern upper slope of the Sciara del Fuoco, consistent with observed deformations, while with our model the Sciara del Fuoco is affected by small-amplitude displacements reaching a maximum of 2.2-2.5 cm in the upper eastern area. Several hypotheses can be made about the origin of these differences:

1 - The strong structural and mechanical heterogeneity of Stromboli volcano is modelled more realistically using a poro-elastic model (as Casagli et al., 2009 applied) than an elastic model.

2- Casagli et al. (2009) integrate the ground water conditions in their study, assuming that the volcanic edifice is saturated below sea level and dry above it, which is consistent with the absence of spring at Stromboli island. In our model, ground water conditions are not taken into account.

3- In the modelling proposed by Casagli et al. (2009) the simulation was implemented in successive stages, assuming the results of the previous stages as conditions for the next one. Considering that the lateral propagation of the subvertical dike is the fourth stage of this evolution, the modelled displacement field associated with this dike is influenced by the previous displacements related to the ascent of magma along the central vent of the edifice. In our model, instead, we only study the intrusion of this dike, without considering other sources of deformation.

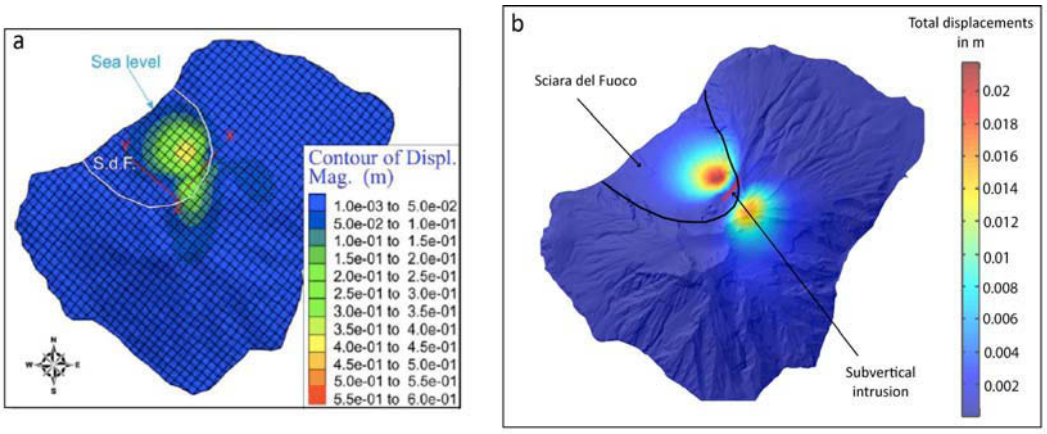

Figure 4.12: a- Displacements modelled by Casagli et al. (2009), associated with the lateral propagation of a vertical dike from the central vent during the 2007 Stromboli eruption; b- Displacements modelled with our MBEM for the same lateral intrusion at Stromboli volcano.

The emplacement direction of the 2007 vertical intrusion is consistent not only with the 2002–2003 event (Acocella et al., 2006), but also with the recent geological–structural history of the volcano, when magma was mostly injected along the main NE-trending weakness zone, with single dikes striking from NNE to E–W (Casagli et al., 2009). Field surveys at Stromboli revealed that the vertical dikes can abruptly bend into horizontal to sub-horizontal sills (Corazzato et al., 2008). This bending has been observed within a succession entirely made of scoria and breccia

deposits, a lithology similar to the one that composes the Sciara del Fuoco infill. Moreover, dike feeding into sill is a widespread phenomenon observed in several volcanoes (see Casagli et al., 2009 and references herein).

The possible "draining" effect exerted by the debuttressed zone of the Sciara del Fuoco depression on the magma rising into the cone was recently recognized (Tibaldi, 2004; Acocella and Tibaldi, 2005); this process in turn has the feedback effect of further enhancing slope instability. Modelling results obtained by Casagli et al. (2009) show that at Stromboli volcano vertical intrusions (possibly accompanied by small-scale subhorizontal intrusion) are capable of generating displacements of the northwestern flank of the edifice. Here, in fact, the extremely steep slope and the occurrence of lithological and mechanical heterogeneities in the Sciara del Fuoco (Tommasi et al., 2008) cause this sector to be prone to lateral destabilization. Conversely, according to numerical models (Apuani and Corazzato, 2009), gravity alone is not sufficient to affect the stability of the volcano slopes, but magma overpressure during feeding processes is the dominant cause in generating lateral instability at Stromboli (Tibaldi et al., 2009).

4.3.3- The 2002-2003 event at Etna volcano

Lateral spreading of the eastern and southern flanks of Etna volcano is a well-documented phenomenon involved in the dynamics of this volcano (Borgia et al., 1992; Borgia, 1994). InSAR data from Froger et al. (2001) allowed the recognition of 2 unstable sectors. The mobile eastern flank is much larger than the collapse scar of the Valle del Bove (Fig. 4.13) and is bounded by the E-W striking transtensive Pernicana Fault System, the N-S striking transtensive dextral Ragalna Fault System (Acocella and Neri, 2005; Fig. 4.13) and the North-east and South rift-zones (Froger et al., 2001). In this sector, structural features indicate on the whole eastward movements. The southern mobile sector (Fig. 4.13) slides southward along a basal decollement located 5 km below the edifice. The study of Froger et al. (2001) underlines the major role played by tectonic structures in the control of lateral movements affecting the eastern and southern flanks of Etna.

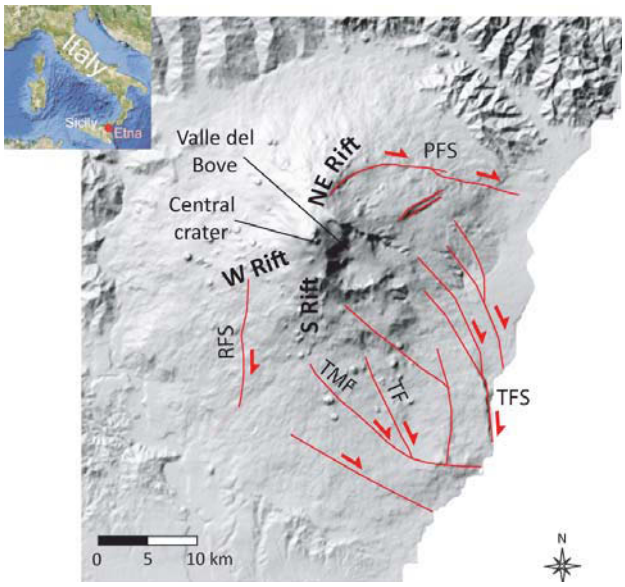

Figure 4.13: Geometry and structural features of the unstable flanks of Etna volcano (PFS = Pernicana Fault System; RFS = Ragalna Fault System; TFS = Timpe Fault System; TF = Trecastagni Fault; TMF = Tremestieri-Mascalucia Fault, from Rust and Neri, 1996; Neri et al., 2005; Falsaperla et al., 2010).

Recent eruptive crisis of 2001 and 2002-2003 were associated with major episodes of lateral displacements of the edifice and were both tectonically controlled. Neri et al. (2005) showed that the 2001 eruption was the result of the emplacements of a N-S oriented eccentric dike, consistent with the E-W regional extension, causing seaward movements of the edifice, while the 2002-2003 eruption was triggered by a flank slip of the eastern and southern sectors of the volcano. Puglisi et al. (2008) used GPS survey and interferometry data to study the 2001 eruption of Etna. They showed that the subvertical intrusion of 2001 caused the unbuttressed eastern flank to release the accumulated stress prior to the intrusion by propagating deformation towards the east, away from the source of the intrusion. This caused an acceleration of the sliding motion and an involvement of peripherical fault systems of the edifice like the TFS (Fig. 4.13). Their model also reveals that the *décollement* plane identified below the edifice extends beneath the whole eastern flank of the volcano.

Several studies indicated that a close relationship occurred between magmatic intrusions, tectonic activity along the major faults of the flanks of the edifice and lateral failure of the flanks. Acocella et al. (2003) propose a model of flank slip in the 2002-2003 crisis, in which the inception of the instability occurred in 3 stages: in the first one an earthquake occurred, secondly slip accelerated and the eruption started, while in the third phase the deformation propagated southward and eastward (Fig.

4.14a). According to Walter et al. (2005), the 2002-2003 slip event, involving an area of more than 700 km^2, was the result of a combined mechanism, 1- a pre-eruptive intrusion of magma and the inflation of the volcano, inducing 2- the movement of the eastern flank of Mount Etna along the Pernicana fault system (PFS in Fig. 4.13) and the basal *décollement*, which facilitated 3- subvertical intrusions along the NE and S rift zones and the onset of the eruption that was responsible for 4- the slip of the eastern and southern flanks of the edifice, involving the Trecastagni and other fault systems (Figs. 4.13 and 4.14b).

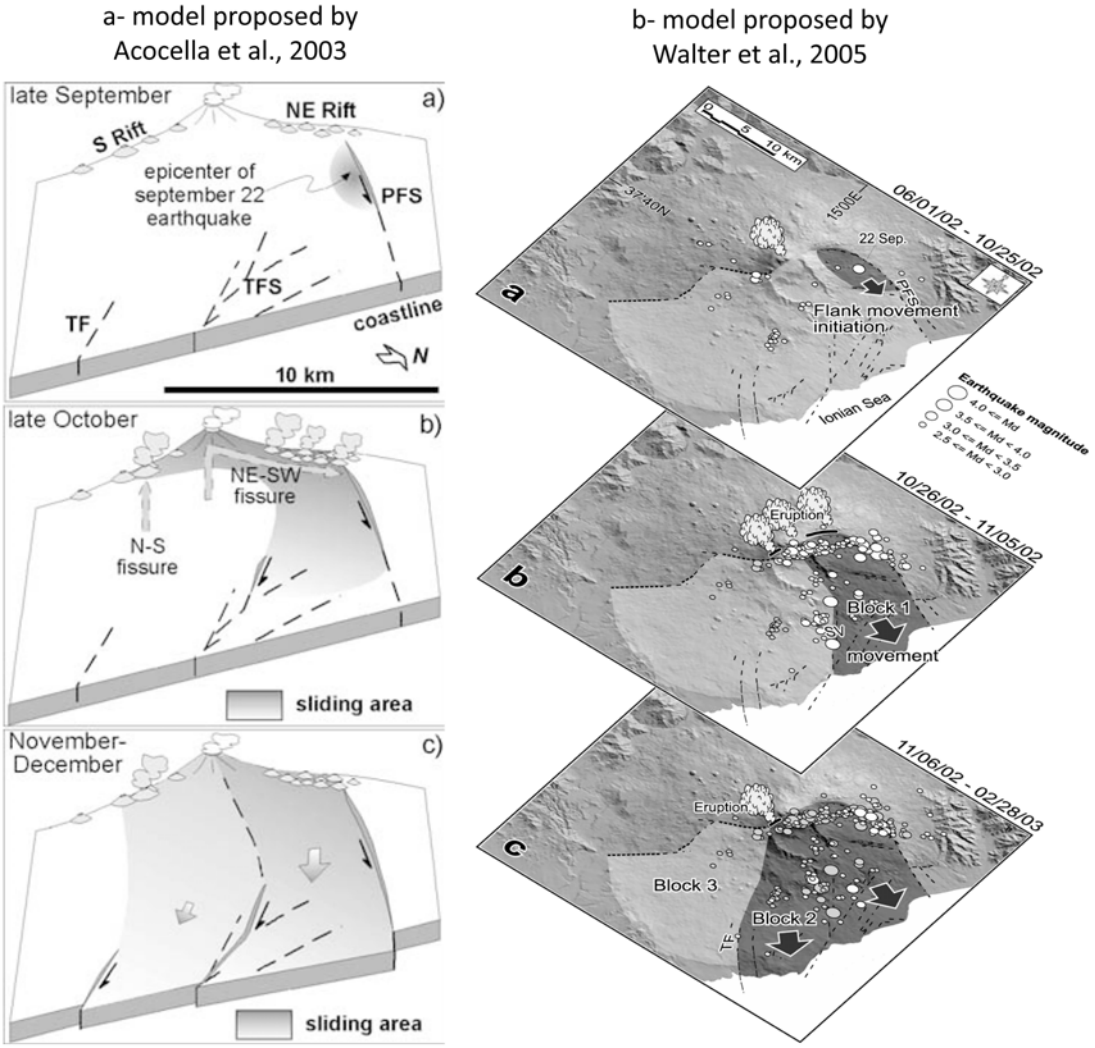

Figure 4.14: Models of evolution of the mobile flank of Mount Etna during the 2002-2003 crisis. Both models propose a common mechanism of flank instability in 3 stages involving magmatic intrusion, fault activity and lateral movements of the flanks (from a- Acocella et al., 2003; b- Walter et al., 2005).

According to Neri et al. (2004), during the 2002–2003 event, extension along the Northeast Rift Zone was accommodated by left-lateral motion along the Pernicana Fault, whereas deformation of this area triggered faulting on the eastern flank of the volcano. According to the authors, the inception of instability in the eastern flank of Etna is related to eruptions in the NE rift zone, triggering large, short-lived movements along the western portion of the Pernicana fault system and small, long-lived displacements along the eastern portion. The surface deformation might then migrate southward and eastward, reactivating other fault systems and triggering lateral instability of a larger portion of the edifice.

From the model of flank instability at Piton des Neiges volcano (Famin and Michon, 2010), we propose that subhorizontal intrusions could be emplaced along the basal *décollement* at Mount Etna, triggering increments of lateral movements of the eastern flank (as occurred in 2002-2003, steps 1 and 2 in the model of Walter et al., 2005) and extension in the upper part of the edifice. These conditions may enhance the injection(s) of subvertical intrusions along the rift zones (step 3), leading to the slip of a larger sector of the edifice involving lateral faults systems, and possibly lateral collapse of the eastern and southern flanks of the volcano.

4.3.4- Principal mechanisms of flank instability in basaltic volcanoes

The review of the dynamics of unstable flanks movements we carried out in this section permits to distinguish two principal mechanisms causing flank-scale displacements and/or lateral collapse on basaltic volcanoes.

Case 1: Gentle-sloped large-scale volcanic edifices where flank dynamics is controlled by basal failure planes.

At Piton de la Fournaise and Etna volcanoes, we propose that the emplacement of subhorizontal intrusions in a basal detachment/*décollement* plane is a possible mechanism triggering lateral flank movements (Fig. 3.2a). While at Piton de la Fournaise volcano the subhorizontal intrusion appears to be responsible for the majority of the deformation affecting the flank, we suggest that at Mount Etna,

subhorizontal intrusions only initiate flank instability through movements along the basal failure surface. The slip movement is then amplified as initial lateral movements favour subvertical intrusions along the rift zones, involving the fault systems of the eastern and southern flanks of Mount Etna. Vertical pattern of displacements recorded at Piton de la Fournaise shows that lateral faults also play a role in the mechanical behaviour of the eastern flank of the edifice.

At Kilauea, the fault system forming the Hilina slump is connected to a deep basal *décollement* (chapter 1 and 3; Fig. 3.2b) so that movements along the normal faults coincide with movement along the basal plane (Dvorak et al., 1994; Denlinger and Okubo, 1995) favouring lateral displacements of the south flank of Kilauea volcano. Dvorak (1994) and Owen et al. (2000) showed that the movements along the subhorizontal *décollement* at the base of the edifice were correlated to intrusions along the east rift-zone. Some authors proposed a different model where the Hilina slump would be rooted in a detachment located at 3-4 km of depth (Morgan et al., 2003). In this case, subhorizontal intrusions con occur along this detachment plane, triggering lateral displacements of the flank and movements along the Hilina fault system.

Famin and Michon (2010) proposed that the northeastern flank of Piton des Neiges volcano was undergoing large-scale movements through a combined mechanism of deformation associated with repeated subhorizontal intrusions within a pre-existing detachment fault. Indeed, hydrothermal alteration due to the heat of cooling injections could be responsible for a slow inter-intrusion deformation of the flank while the subhorizontal intrusions themselves would trigger rapid co-intrusive slip along the detachment fault (section 4.1.2.1). This reveals an incremental mechanism of long-term deformation associated with intrusion-related slow and rapid displacements

At Fernandina volcano (Galapagos), the study of INSAR data from the eruption of 1995 revealed that a shallow-dipping intrusion below the western flank of the edifice created flank-scale ground displacements (Jonsson et al., 1999, Fig. 4.15) of the edifice. However, no tectonic system (lateral faults, detachment/*décollement)* seems to play a role in the flank displacements observed at Fernandina volcano.

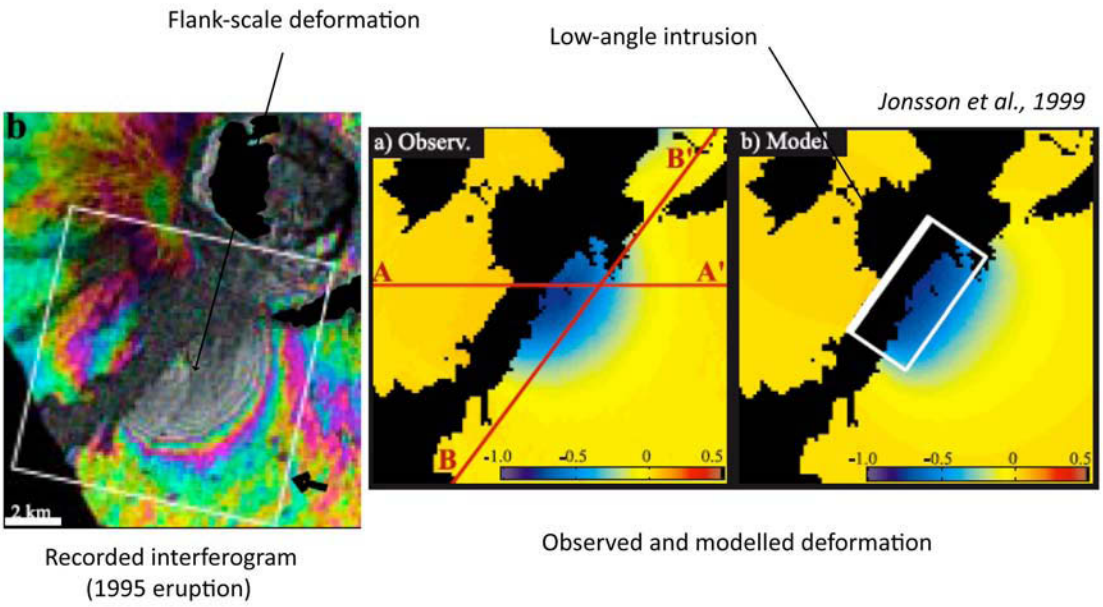

Figure 4.15: Flank-scale deformation related to shallow-dipping intrusion during the 1995 eruption of Fernandina volcano, revealed by InSAR data (modified from Jonsson et al., 1999).

Case 2: Flank instability on steep-sloped small-scale basaltic volcanic edifices

This mechanism applies to small-scale edifices affected by lateral instability like Stromboli volcano, the submarine Monowai cone in the Kermadec arc (Wright et al., 2008; Chadwick et al., 2008) or Oshima Oshima volcano. For this type of edifice, which are basaltic stratovolcanoes, given the size of the edifice, a subvertical intrusion may be able to generate flank-scale deformation (see the case of Stromboli, 4.3.2). Due to their common steepness, it is likely to imagine that the slopes of stratovolcanoes can be prone to lateral failure associated with a subvertical intrusion.

These two different cases reveal that among the parameters involved in the control and/or the trigger of lateral instability on basaltic volcanoes we defined in chapter 1, some have a major role in inducing the phenomenon, such as the volume and the nature of the edifices, their slopes, the presence of internal heterogeneities (basal sliding surfaces) and the regional tectonics, controlling the influence of fault systems on the mobility of volcanic flanks. The examples of Piton de la Fournaise, Etna, Kilauea and Stromboli emphasize the importance of the relationship between

magmatism and flank instability on basaltic volcanoes. We underline from field data and modelling results that magmatic intrusion is often the key process that triggers flank displacements likely to enhance lateral failure on basaltic volcanoes.

4.4- Further implications

4.4.1- Some insights into the nature and geometry of the superficial plumbing system of Piton de la Fournaise volcano

The low-angle intrusion we modelled at Piton de la Fournaise for the April 2007 crisis (section 4.3.1) has a volume of 47 10^6 m^3 and should be injected from the magmatic chamber below Piton de la Fournaise, whose volume has been estimated between 0.1 and 0.35 km^3 (Albarède, 1993; Sigmarsson et al., 2005; Peltier et al., 2007). However, there is a large discrepancy with the total volume of magma emitted during the eruption of April 2007, reaching 230 10^6 m^3 (Bachèlery et al, 2010, appendix 7).

The modelling results of pre-eruptive phases from Peltier et al. (2007) reveals the presence of a magmatic chamber at sea level. According to Battaglia et al. (2005), below Piton de la Fournaise a geological discontinuity should be located at sea level, where the density of the magma is equal to the density of surrounding rocks, favouring the accumulation of magma. Our data do not bring new information on the existence and nature of this reservoir and we have no reason to disagree with this assumption.

However, we are able to make some hypothesis on the nature of the plumbing system overlying the sea level reservoir, at a depth of 1-2 km below the summit of the volcano. We propose that subhorizontal injection of magma (together with subvertical injections) is a recurrent mechanism affecting the central area of Piton de la Fournaise volcano. This process should be responsible for magma storage within the edifice and could be an argument to explain the continuous magma inflation observed at Piton de la Fournaise volcano, as already proposed by Lénat and Bachèlery (1990) and Prono et al. (2009). According to those authors, in fact, the shallow magmatic system at Piton de la Fournaise was made of a dense network of

interconnected subvertical and subhorizontal intrusions. However, the storage capacities of the edifice are limited. We consequently suggest that the uncommon lateral injection of magma below the unbuttressed eastern flank of the volcano in April 2007 acts as a "pressure valve" that permitted the edifice to accommodate a new injection of magma. Lateral injections of magma trough subhorizontal intrusions may bring the edifice to a mechanical equilibrium and could favour the withdrawal of large volumes of magma, explaining the discrepancy between the intruded/emitted magma volumes observed during the 2007 eruption.

4.4.2- Modelling of volcanic deformation processes

A first general implication of our modelling results is that the length/height of the fractures and the topography have no major influence on the ratios of surface displacements. As a consequence, these indications can be easily generalised to any kind of topography and fracture geometry. However, the criteria we proposed from our models are based on the detection of surface displacements associated with single intrusive events, involving fractures which geometry is relatively simple. Deformation patterns recorded during real intrusive episodes are usually much more complicated as they can involve several fractures with complex geometries. In this case, long and complex data inversion is needed in order to infer the characteristics of the source of deformation.

Although being based on simple cases, our results can give first insights on the source of a displacements field and yield very interesting constraints on the initial stress field within volcanic edifices (the existence of anisotropy), information of prime importance for modelling. Indeed, while most inversions carried out from geodetic data, considering a dislocation as the source of the displacement, are performed taking into account the opening of the fracture and assuming that no slip occurs, the criteria we presented firstly focus on whether shear stress is involved or not in the mechanical behaviour of an overpressured fracture. If the role of shear stress in triggering large-scale lateral displacements on basaltic volcanoes is determined, the component of displacement associated with the slip along the fractures has to be also taken into account in the inversion processes used in

quantitative modelling of volcano deformation.

4.4.3- Improvement of the model

As it is well known, the modelling of natural process involves simplifications of phenomena. In order to simplify a complex mechanism, some assumptions have to be made. We studied displacement fields generated by fractures submitted to different stress fields using a model where the medium is assumed to be homogeneous and isotropic. The application of our theoretical results to Piton de la Fournaise volcano showed that despite these assumptions, the displacements we modelled were in good quantitative and qualitative agreement with the recorded displacements, at least regarding the horizontal ones. However, the discrepancy between modelled and recorded vertical displacements evidenced that these assumptions could be source of approximations in the results. We hypothesized that discrepancies were probably related to the fact that our model does not allow to consider mechanical heterogeneities within the medium (i.e. portions were elastic parameters vary, like rift zones) neither the presence of fractures and faults, common in a realistic volcanic edifice. Further work needs to be done in order to integrate heterogeneities in the model, as did Letourneur et al. (2008) for Piton de la Fournaise volcano.

Moreover, in our model the medium is assumed to be elastic, as displacements are linearly related to the stresses applied to the fracture (Hooke's law). This assumption implies some limitations of the model, which could be overcome using a visco-plastic model. Indeed, magmatic intrusions are modelled as fractures submitted to overpressure, but physical properties of the magma within the intrusions should be also considered. In order to study more accurately the interactions between the intrusions and the medium (and the stress field) in which they are emplaced, a model in which parameters like magma viscosity within the intrusion is required. Moreover, the evolution of the mechanical state of an edifice over time is not taken into account in our model. If one wants to study the influence of repeated intrusions over time, mechanical perturbations related to each intrusion have to be added in time. The example of Stromboli volcano (section 4.3.2) showed

that a poro-elastic model could be more adapted for the study of intrusion-related field displacements on basaltic volcanoes. In their model, Casagli et al. (2009) consider the parameter of the ground water conditions of Stromboli island. This factor has an influence on the pore pressure within the edifice (Iverson, 2000; Gressier et al., 2010) but is not taken into account in our model, although most of the basaltic volcanoes are island volcanoes.

Finally, the study of intrusion-related displacements fields could be coupled with a mechanical study of flank stability in order to better constrain the mechanical conditions (referred to as “threshold of stability” in this discussion) under which the flanks of a basaltic volcano might fail. This is a major issue in the assessment of the risk associated with landslide-related tsunamis on island volcanoes (see prospects for the examples of La Reunion and Stromboli).

General conclusions

Active basaltic volcanoes are revealed to be dynamically evolving structures, the growth and development of which are characteristically punctuated by episodes of instability and structural failure occurring instantaneously or over a long period of time. Multiple destabilization processes operate simultaneously, in response to a perturbation of the mechanical equilibrium of an edifice, producing events of varying magnitudes and frequencies. Some volcanoes appear to have a far greater potential for failure than others. The study of nature and evolution of basaltic volcanoes showed that among the factors of instability, involved in long-term instability and/or sudden failure events, some are clearly identified and their role well-constrained while the influence of other parameters remains poorly understood.

In particular, the comparative description of geological settings and of the morphological and structural features of two end-member basaltic edifices, La Reunion shield edifice and Stromboli stratovolcano, revealed that :

1- these two volcanic systems are located in different geodynamic settings, a tectonically active subduction setting at Stromboli while La Reunion is a hotspot-related edifice in an inactive area.

2- the systems are made of several coalesced volcanoes.

3- the nature and volumes and the edifices are not comparable, Stromboli representing 0.7 % of La Reunion.

4- the evolution of the edifices occurred on different time spans.

However, La Reunion and Stromboli present some similarities:

1- they experimented a similar evolution made of recurrent flank collapses.

2- they both are affected by an intense intrusive activity along rift zones controlled by regional tectonics and the geometry of collapse structures.

It appears that the geodynamic context is probably not a first-order factor of control of the process of lateral instability of basaltic volcanoes. Conversely, the examples of La Reunion and Stromboli illustrate that intrusive activity is likely to play a major role in the evolution of basaltic edifices.

Subsequent work has been dedicated to the numerical study of the relationship between magmatic intrusions and deformation of basaltic volcanoes through a Mixed Boundary Element Method, combined to new field data on the Piton des Neiges volcano (La Reunion Island). We emphasize the major importance of field studies carried out in the internal structure of eroded volcanoes in order to understand the mechanisms of eruptions on active volcanoes. Such studies also allow the exploration of the origin of observed structures, their geometry and their structural relationship with the host formations. Our results from numerical modelling bring new insights on the contribution of magmatic intrusions in the process of volcano flank instability. The statistical study of the populations of basaltic intrusions from published data and recent measurements on basaltic volcanoes show that not only the role of subvertical but also of subhorizontal intrusions has to be considered in the morpho-structural evolution of basaltic volcanoes, principally in the process of flank instability. The quantitative importance of low-angle intrusions is reinforced by the theoretical analysis we carried out using a MBEM. On the basis of surface displacements generated by overpressured fractures, we introduce some criteria of detection of the geometry of magmatic intrusions and determination of the stress field within volcanic edifices. Our study reveals a new model of interaction between intrusions and flank-scale movements: the co-intrusive shear stress creating slip along subhorizontal intrusions in an anisotropic stress field leads to flank-scale displacements of basaltic edifices, likely to trigger large sector collapses of the edifices if mechanical conditions favourable for failure are reached. Moreover, applications of theoretical results to basaltic volcanoes like Stromboli, Piton de la Fournaise or Etna permitted to propose mechanisms of flank destabilizations where magmatic intrusions have major influence on the stability of the edifices. However, no general model emerges as the diversity of geometries (and structures) of basaltic volcanoes and their magmatic systems leads to a diversity of mechanisms of flank instability.

The results we present have more general implications on the modelling of deformation processes of volcanoes: we showed that the existence of shear stress within volcanoes is a key factor to take into account in future models, in order to achieve more realistic studies of volcanoes behaviour and deformation, leading to a

better understanding of the processes involved in their evolution. This is a challenging issue for the scientific community as most of the unstable basaltic edifices worldwide are island volcanoes where flank failure is prone to cause catastrophic tsunamis.

Flank collapses on basaltic volcanoes and associated tsunami hazard. The examples of La Reunion and Stromboli.

Flank destabilisation on basaltic volcanoes is generally the consequence of a combination of processes involving intrusive and/or extrusive magmatic activity, movements of large volumes of volcanic material along faults or sliding planes, seismic activity linked to these movements or rock fracturing. This diversity of phenomena implies a diversity of hazards associated to flank instability on basaltic volcanoes.

The 2002-2003 eruption of Mount Etna volcano is a good illustration of the relationships that occur between classical magmatic activity and slipping of a volcanic flank. Walter et al. (2005) studied the feedback processes magmatic processes and lateral collapse during this eruption and showed that a complex mechanism affected the volcano.

A close interrelation between magmatic processes and flank movements can occur and generate several types of hazards associated to seismic activity along the major faults involved in the slipping of the flank, lava flows and ash fallout directly related to eruptive activity and possible landslide-generated tsunami waves.

Lateral failure of volcanic edifices produces landslides ranging enormously in terms of volume (McGuire, 1996). When they occur on volcanic islands, these landslides are prone to generate tsunamis of variable sizes, representing a major threat to the populations of these islands. About 5 % of all tsunamis are thought to have been formed by volcanic activity and at least a fifth of these results from volcanically induced landslides (Smith and Shepherd, 1996). Keating and McGuire (2000) did a review of the main landslides and tsunamis associated to failure of volcanic island edifices. This chapter is dedicated to the study of tsunamis generated by flank collapse at La Reunion island and Stromboli island.

1- Landslide-generated tsunamis at La Reunion island

During its evolution, the La Reunion island and its 3 volcanic edifices were the location of numerous voluminous landslides (Fig. 1). At least 50 major events were recognised in the last 2 Myrs, from the identification of submarine debris avalanche deposits on the flanks of the island (Labazuy, 1996; Oehler et al, 2008, Fig. 2.26), giving a recurrence interval of one major landslide every 40 000 years. Some smaller landslides also occurred during the growth of the island. The last lanslide that affected Piton de la Fournaise volcano is related to the formation of the Enclos-Grand-Brûlé depression, about 4500 years ago (Bachèlery and Mairine, 1990).

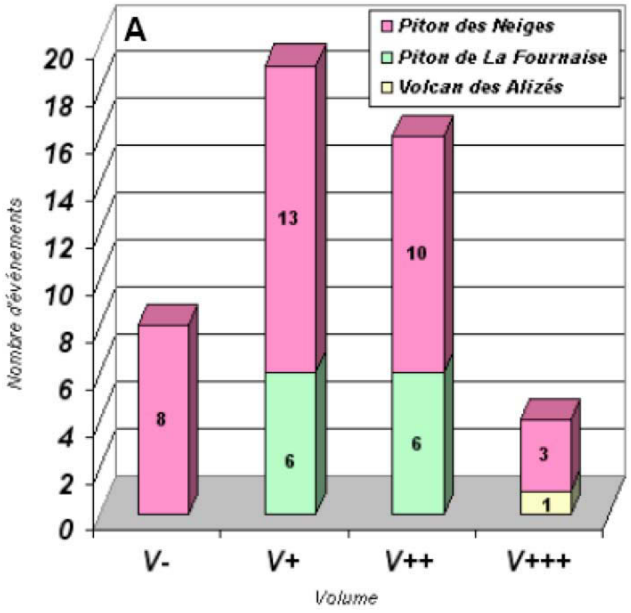

Figure 1: Number of landslides and their volumes for the 3 edifices of La Reunion island (Piton de la Fournaise, Piton des Neiges and Les Alizés). The volumes correspond to V- < 1 km^3; 1 < V+ < 10 km^3; 10 < V++ < 100 km^3; V+++ > 100 km^3 (From Oehler, 2005).

These landslides can be subaerial or submarine and it is likely that some of them were associated to tsunamis that damaged the coasts of La Reunion. Although major collapse events have a recurrence time that make them negligible at human scale, it is important to consider smaller volumes destabilization, whose recurrence interval is probably shorter, in the mitigation of tsunami hazards at La Reunion island (and other volcanoes), although few evidence of tsunami-related deposits are available on the island. La Reunion presents a high vulnerability to tsunamis due to several factors:

1- its population, about 800 000 inhabitants, is gathered on the main cities all spread along the coast of the island, like the capital Saint-Denis and its 150 000 inhabitants.
2- The important demographic growth of the island, whose population could reach the million of inhabitants in the next decade.
3- All the main infrastructures of the island (airport, main roads, economic and industrial centers…) are directly concerned as they are on the coasts, or at very low altitude.

Based on the study of inland debris avalanche deposits related to the destruction of Piton des Neiges volcano, Bret et al. (2003) identified 3 main risk scenarios, depending on the volume of the removed material, from minor rock falls to major debris flows. His study doesn't consider the submarine component of these collapses but it is easy to understand that major subaerial destabilization has the power to trigger tsunamis.

The first study of the formation, propagation and impact of tsunami waves related to a lateral instability of Piton de la Fournaise was carried out by Kelfoun et al. in 2010 (Fig. 2). These authors used a new numerical model to discuss the consequences of a tsunami generated by the collapse of part of the eastern flank of Piton de la Fournaise within the Enclos-Grand-Brûlé structure. A simulated landslide of 10 km^3 (Fig. 2a) spreads in 2 main lobes (Fig. 2b) due to the presence of a submarine relief in front of the Enclos scar, called the Eastern Submarine Buldge by Oehler (2007). It travels up to 45 km from its source and creates a deposit with a mean thickness of 20 m, reaching more than 50 m at the front (Fig. 2b).

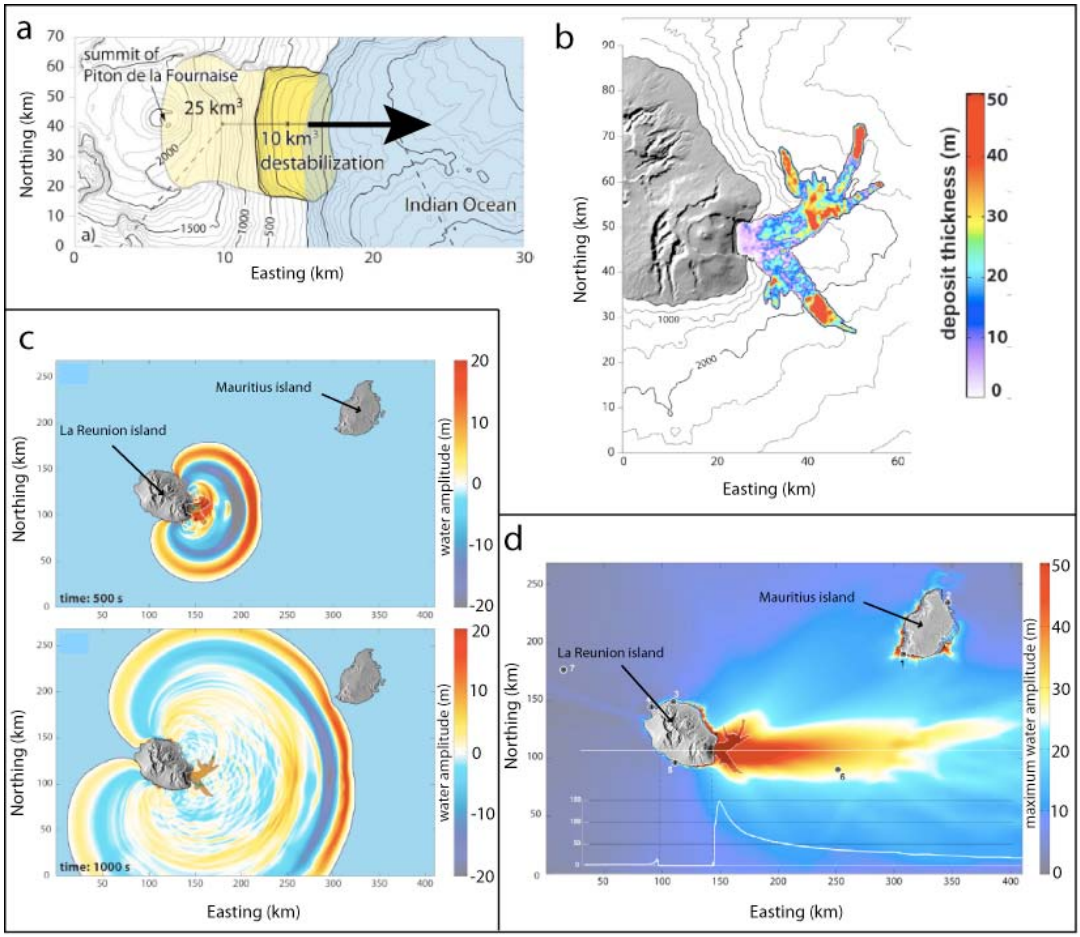

Figure 2: Geometry of a 10 km^3 landslide affecting the eastern flank of Piton de la Fournaise volcano (a), and the numerical results of the morphology of the associated deposit (b), the propagation of the landslide-generated tsunami-waves (c) and the maximum amplitude of the waves hitting the coast of La Reunion and Mauritius islands (d), modified from Kelfoun et al., 2010.

The interaction between ocean water and the landslide generates a succession of waves that propagates and hits the coast of La Reunion island, with a maximum wave amplitude of more than 50 m on the NE and SE coasts (Fig. 2c and d). The model of Kelfoun et al. (2010) shows that the capital of the island (Saint-Denis) is hit by a first 10 m high wave 12 minutes only after landslide while a second wave of 25 m reaches the city 18 minutes after the landslide. The island of Mauritius is also affected by large amplitude waves (Fig. 2d).
This kind of tsunami leads to evacuation times as small as 2 minutes before the first wave reaches the nearest coast, and 10 to 20 minutes for the island to be encircled.

This study reveals that the consequences of a 10 km^3 landslide of the eastern flank of Piton de la Fournaise volcano are dramatic on a local scale (Mascareignes Plateau) but smaller on a regional scale (Indian Ocean). For what regards the evacuation plan at La

Reunion, a program called “Plan de Secours Spécialisé Tsunami” was created after the tsunami that affected La Reunion in 2004 after the December 2004 Andaman earthquake (Indonesia). However, this plan only concerns seismic-related tsunamis and there is no plan dedicated to the prevention of damages caused by landslide-related tsunamis at La Reunion island.

Although the hazard associated to this kind of landslide is very small on human scale (low recurrence time and large volume), this first risk scenario gives first insight on the consequences of a landslide in terms of tsunami and damages. It clearly indicates that less voluminous events are to be considered in the evaluation of the risk associated to flank instability at La Reunion island and the creation of an adapted plan of risk assessment.

2- Landslide-generated tsunamis at Stromboli island

Although the inhabited areas of the Island are located in safe parts, they remain under the threat of hazards related to paroxysmal activity and tsunamis. The low stability of present day Sciara del Fuoco, whose subaerial part, made of loose clastic material, grew on steep unbuttressed slopes, represents a major potential hazard.

According to historical reports in the last century, the Stromboli coast was struck by six local tsunamis, most of them likely generated by submarine landslides (Maramai et al., 2005). The formation of the Sciara del Fuoco depression 5000 years ago (Pasquarè et al., 1993; Tibaldi, 2001) is thought to have been the source of a South-Tyrrhenian-wide tsunami (Tinti et al., 2000). Tanner and Calvari (2004) identified a brecciated deposit that could be linked to the tsunami caused by the formation of Sciara del Fuoco collapse.

The submarine continuation of the Sciara del Fuoco scar is covered by a major fan deposit as far as 20 km from the coast of the island, down to more than 2600 m b.s.l., representing 28 % of the whole volcano surface (Bosman et al., 2009). The estimated volume of the Sciara del Fuoco last collapse ranges from 0.97 to 1.81 km^3 according to Kokelaar and Romagnoli (1995) and is close to 0.73 ± 0.22 km^3 for Tibaldi (2001). A least 2 other Sciara del Fuoco-like collapses occurred in the last 13 kyrs, giving a recurrence time of about 4.3 kyrs for landslide events comparable to the 1 km^3 collapse of the Sciara del Fuoco. The modelling results of Tinti et al. (2000) showed that a landslide of 1 km3 generates tsunami waves that form a circular wave system with amplitude ranging from 10 to 40 m in front of the Northern coast,

near Ficogrande where the village of Stromboli lies close to the sea. The waves reach the most part of the island 200 seconds after the initiation of the landslide and larger effects are produced after 300 seconds. However, this type of voluminous landslide is not the most frequent at Stromboli island but has to be considered as an extreme scenario in the hazards associated to flank collapse at Stromboli.

Based on bathymetrical data and morphological features of the submarines flanks of Stromboli island, Casalbore et al. (2010) underlined that the island has a great potential for repeated submarine medium-scale tsunamigenic landslides. The recent occurrence of the landslide-tsunami event that affected the NW flank of Stromboli volcano on December 30th, 2002 showed that a medium-scale submarine mass failure may represent a significant and not infrequent source of hazard (Tommasi et al., 2008; Chiocci et al., 2008). The volume of the collapse was estimated at about 28.10^6 m^3 (Chiocci et al., 2008). The landslide of December 2002, the propagation of the tsunami and its consequences were modelled numerically by Tinti et al. (2005). The results show that medium-scale submarine landslides at Stromboli are a major threat as they can hit the whole in less than 4 minutes after the initiation of the collapse. Moreover, the most affected area is the northern coast where the Stromboli village lies, where waves as high as 5 to 10 meters can struck the shoreline (Fig. 3 and 4).

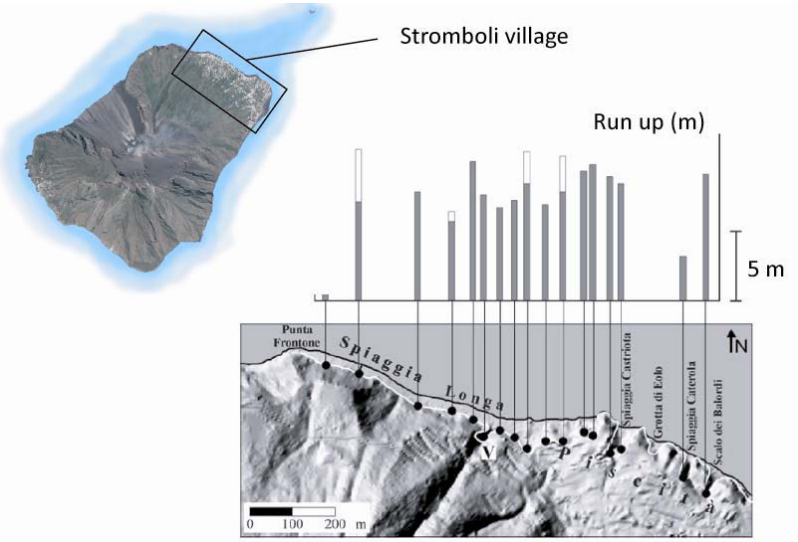

Figure 3: Run up of the tsunami waves associated to the December 2002 collapse of a portion of the Sciara del Fuoco that struck the northern coast of Stromboli island (modified from Tinti et al., 2005).

Given the instability of Sciara del Fuoco, recurrent medium-scale events of destabilization have to be taken into account as they are able to generate destructive tsunamis affecting the most habited area of the island, with a recurrence time certainly much smaller than the 4.3 kyrs estimated for Sciara del Fuoco-like collapses and associated tsunamis.

Figure 4: Northeastern coast of Stromboli island, showing the maximum run up of the December 2002 tsunami (red dashed line) and the operative center (COA) created by the italian civil protection after the crisis of 2002-2003 (from Bertolaso et al., 2009).

In the days that followed the December 2002 tsunami, surveys were carried out on the Aeolian islands and the surrounding coast in order to measure the run ups of the waves, evaluate the damages and gather information from the local populations (Maramai et al, 2005b). After the 2002-2003 crisis at Stromboli, and the dramatic impact of the tsunami on the inhabitants and the public opinion, the Italian government together with the civil protection created an operative center (COA, Fig. 6.4) whose objective was to monitor continuously the volcano and the associated hazards (Bertolaso et al., 2009). An alert system was created in order to warn the population in case of tsunami and shelters were installed in the higher parts of the island to protect the populations.

While deformation of basaltic volcanoes related to magmatic processes like intrusions or reservoir inflation can affect an edifice over long time spans, the collapse of a volcano flank is usually an instantaneous phenomenon leading to catastrophic damages

related to landslide-generated tsunamis. It appears very difficult to forecast instantaneous flank failures and the examples of La Reunion and Stromboli islands clearly show that the hazards associated to medium-scale instabilities on the flanks of the edifices is not negligible and has to be considered in the creation (La Reunion) or improvement (Stromboli) of evacuation and protection plans.

References

A

Acocella, V., Behncke, B., Neri, M., D'Amico, S., 2003. Link between large-scale flank slip and 2002–2003 eruption at Mt. Etna (Italy). *Geophysical Research Letters,* 30 (24), 2286.

Acocella, V., 2005. Modes of sector collapse of volcanic cones: Insights from analogue experiments. *Journal of Geophysical Research,* VOL. 110, B02205, doi:10.1029/ 2004JB003166.

Acocella, V. and Neri, M., 2005. Structural features of an active strike-slip fault on the slidingflank of Mt. Etna (Italy). *Journal of Structural Geology*, 27, 343–355. doi:10.1016/ j.jsg.2004.07.006.

Acocella, V. and A. Tibaldi, 2005. Dike propagation driven by volcano collapse: A general model tested at Stromboli, Italy. *Geophysical Research Letters*, Volume 32, Issue 8.

Aiuppa, A., 2008. Degassing of halogens from basaltic volcanism: Insights from volcanic gas observations*, Chemical Geology*, doi:10.1016/j.chemgeo.2008.08.022.

Albarède, F., 1993. Residence time analysis of geochemical fluctuations in volcanic series.*Geochemica and Cosmochemica Acta* 57, 615-621.

Allard, P., Carbonelle, J., Métrich, N., Loyer, H., and Zettwoog P., 1994. Sulphur output and magma degassing budget of Stromboli volcano. *Nature,* 368, 326–330.

Allard, P., 1997. Endogenous magma degassing and storage at Mount Etna. *Geophysical Research Letters,* 24, 2219–2222.

Ancochea E., Hernan, F., Huertas, M.J, Brandle, J.L., Herrera, R., 2006. A new chronostratigraphical and evolutionary model for La Gomera: Implications for the overall evolution of the Canarian Archipelago. *Journal of Volcanological and Geothermal Research,* 157, Issue 4, 271-293.

Ancochea, E., Brandle, J.L., Huertas, M.J., Hernan, F., Herrera, R., 2008. Dike-swarms, key to the reconstruction of major volcanic edifices: The basic dikes of La Gomera (Canary Islands). *Journal of Volcanological and Geothermal Research*, 173, 207-216.

Anderson, E. M., 1938. The dynamics of sheet intrusion. *Proc. R. Soc. Edinburgh*, 58, 242–251.

Anderson, H., and J. Jackson, 1987. The deep seismicity of the Tyrrhenian sea, Geophys. *J. R. Astron. Soc.*, 91 613 – 637.

Annen, C., Lénat, J.-F. and Provost, A., 2001. The long-term growth of volcanic edifices: numerical modelling of the role of dyke intrusion and lava-flow emplacement. *Journal of Volcanology and Geothermal Research*, 105: 263-289.

Apuani, T., Corazzato, C., Cancelli, A., Tibaldi, A., 2005a. Stability of a collapsing volcano (Stromboli-Italy): limit equilibrium analysis and numerical modelling. In:

Gudmundsson, A., Acocella, V. (Eds.), The Tectonics and Physics of Volcanoes. *Special Issue, Journal of Volcanology and Geothermal Research*, vol. 144, 1–4, pp. 191-210.

Apuani, T., Corazzato, C., Cancelli, A., Tibaldi, A., 2005b. Physical and mechanical properties of rock masses at Stromboli: a dataset for volcano instability evaluation. *Bulletin of Engineering Geology and Environment*, 64, 419-431.

Apuani, T. and C. Corazzato, 2009. Numerical model of the Stromboli volcano (Italy) including the effect of magma pressure in the dyke system. *Rock Mechanics and Rock Engineering*, 43, 53-72.

B

Bachèlery, P., 1981. Le Piton de la Fournaise (Ile de la Réunion). Etude volcanologique, structurale et pétrologique, Ph.D. thesis, 215 pp., Univ.Clermont-Ferrand II, Clermont-Ferrand, France.

Bachelery, P., and P. Mairine, 1990. Evolution volcano-structurale du Piton de la Fournaise depuis 0.53 Ma. In : JF Lénat (eds) Le volcanisme de La Réunion, *monography*.

Bachèlery, P., Saint-Ange, F., Villeneuve, N., Savoye, B., Normand, A., Le Drezen, E., Barrère, A., Quod, J.P., Deplus, Ch., 2010. Huge lava flows into the sea and caldera collapse, April 2007, Piton de la Fournaise volcano. IAVCEI Third Workshop on Collapse Calderas, La Réunion, abstract.

Barberi, F., F. Innocenti, G. Ferrara, J. Keller, and L. Villari, 1974. Evolution of Eolian Arc volcanism (Southern Tyrrhenian Sea). *Earth and Planetary Science Letters*,21, 269-276.

Battaglia, J., Ferrazzini, V., Staudacher, T., Aki, K., Cheminée, J.L., 2005. Pre-eruptive migration of earthquakes at the Piton de la Fournaise volcano (Réunion Island). *Geophysical Journal International*, 161, 549–558.

Beauducel, F. and F.-H. Cornet, 1999. Collection and three-dimensional modeling of GPS and tilt data at Merapi volcano, Java. *Journal of Geophysical Research*, 104, 725–736.

Bertagnini, A., N. Métrich, P. Landi, and M. Rosi, 2003. Stromboli volcano (Aeolian Archipelago, Italy): An open window on the deep-feeding system of a steady state basaltic volcano. *Journal of Geophysical Research*, 108(B7), 2336, doi:10.1029/2002JB002146.

Bertolaso, G., De Bernardinis, B., Bosi, V., Cardaci, C., Ciolli, S., Colozza, R., Cristiani, C., Mangione, D., Ricciardi, A., Rosi, M., Scalzo, A., Soddu, P., 2009. Civil protection preparedness and response to the 2007 eruptive crisis of Stromboli volcano, Italy. *Journal of Volcanology and Geothermal Research*, vol. 182, issue 3-4, pp. 269-277.

Billard G. and Vincent P.-M., 1974. Cartes géologiques de la France – La Réunion – 4 feuilles 1/50.000è.

Boccaletti, M., R. Nicolich, and L. Tortorici, 1984. The Calabrian arc and the Ionian sea in the dynamic evolution of the central Mediterranean. *Marine Geology*, 55, 219-245.

Bonaccorso, A., Cianetti, S., Giunchi, C., Trasatti, E., Bonafede, M. and Boschi, E., 2005. Analytical and 3-D numerical modelling of Mt. Etna (Italy) volcano inflation. *Geophysical Journal International*, 163, 852-862.

Bonaccorso, A., Bonforte, A., Gambino, S., Mattia, M., Guglielmino, F., Guglisi, G., Boschi, E., 2009. Insight on recent Stromboli eruption inferred from terrestrial and satellite ground deformation measurements. *Journal of Volcanological and Geothermal Research*, 182, 172-181.

Bonforte, A. And G. Puglisi, 2003. Magma uprising and flank dynamics on Mount Etna volcano, studied using GPS data (1994-1995). *Journal of Geophysical Research*, Vol. 108, Issue B3, pp. ECV 3-1, CiteID 2153, DOI 10.1029/2002JB001845.

Bonforte, A., Aloisi, M., Antonella, G., Casagli, N., Fortuny-Guash, J., Guerri, L., Nunnari, G., Puglisi, G., Spata, A., Tarchi, D., 2008. Movements of the Sciara del Fuoco. *Geophysical Monograph*, vol. 182, 183-199.

Borgia, A., Ferrari, L., Pasquarè, G., 1992. Importance of gravitational spreading in the tectonic and volcanic evolution of Mount Etna. *Nature*, 357: 231-235.

Borgia, A., 1994. Dynamic basis of volcanic spreading. *Journal of Geophysical Research,* VOL. 99, N°. B9, p. 17,791-17,804.

Borgia, A., Delaney, P.T. and R.P. Denlinger, 2000. Spreading volcanoes. *Annual Review of Earth And Planetary Sciences*, Volume 28, pp. 539-570.

Bosman, A., F.L. Chiocci, C. Romagnoli, 2009. The geology of the submarine portion of Stromboli volcano, revealed by high-resolution bathymorphological and backscatter data. *Bulletin of Volcanology*, 71, 9, 1007-1019.

Bret L., Fevre Y., Join J.-L., Robineau B. and Bachelery P., 2003. Deposits related todegradation processes on Piton des Neiges Volcano (Réunion Island): Overview and geological hazard. *Journal of Volcanological and Geothermal Research,* 123, 25–41.

Brenguier, F., Shapiro, N.M., Campillo, M., Ferrazzini, V., Nercessian, A., Coutant, O., Duputel, Z., 2007. Seismic imaging and monitoring of Piton de la Fournaise volcano from ambient seismic noise correlations. *Geophysical research abstracts*, 9, 01326.

Burchardt, S., 2008. New insights into the mechanics of sill emplacement provided by field observations of the Njardvik Sill, Northeast Iceland. *Journal of. Volcanological and Geothermal Research*, 173, *3-4*,280-288.

C

Calvari, S., and H. Pinkerton, 2004. Birth, growth and morphologic evolution of the ‘‘Laghetto’’ cinder cone during the 2001 Etna eruption. *Journal of Volcanological and Geothermal Research*, 132, 225 – 239, doi:10.1016/S0377- 0273(03)00347-0.

Carminati, E., M.J.R. Wortel, W. Spakman, and R. Sabadini, 1998. The role of slab detachment processes in the opening of the western-central Mediterranean basins: Some geological and geophysical evidence. *Earth Planetary Science Letters*, 160, 651-665.

Carracedo, J.C., 1994. The Canary Islands: an example of structural control on the growth of large oceanic-island volcanoes. *Journal of Volcanology and Geothermal Research,* 60, 225-241.

Carracedo, J.C., 1996. A simple model for the genesis of large gravitational landslide hazards in the Canary Islands. In: McGuire, Jones, Neuberg_Eds.., Volcano Instability on the Earth and Other Planets. *Geological Society of London Special Publications,* 110: 125–135.

Carracedo, J.C., 1999. Growth, structure, instability and collapse of Canarian volcanoes and comparisons with Hawaiian volcanoes. *Journal of Volcanology and Geothermal Research Special Issue*, v. 94, p. 1–19.

Casagli, N., Tibaldi, A., Merri, A., Del Ventisette, C., Apuani, T., Guerri, L., Fortuny-Guasch, J., Tarchi ,D., 2009. Deformation of Stromboli Volcano (Italy) during the 2007 eruption revealed by radar interferometry, numerical modelling and structural geological field data. *Journal of Volcanological and Geothermal Research,* 182, 3-4, 182-200.

Casalbore, D., Romagnoli, C., Bosman, A., Chiocci, F., 2010. Potential tsunamigenic landslides at Stromboli Volcano (Italy): Insight from marine DEM analysis. *Geomorphology,* doi: 10.1016/j.geomorph.2010.10.026.

Cayol, V. and F. H. Cornet, 1997. 3D mixed boundary elements for elastostatic deformation fields analysis. *Int. J. Rock Mech. Min. Sci. Geomech. Abstr.*, 34, 275–287.

Cayol, V. and F.H. Cornet, 1998. Three-dimensional modelling of the 1983-1984 eruption at Piton de La Fournaise Volcano, Reunion Island. *Journal of Geophysical Research*, 103, n°B8: 18025-18037.

Cayol, V., Dieterich, J.H., Okamura, A.T., Miklius, A., 2000. High magma storage rates before the1983 eruption of Kilauea, Hawaii, *Science,* 288: 2343–2346.

Cendrero, A., 1970. The volcano plutonic complex of La Gomera, *Bulletin of Volcanol*ogy, 34:537–561.

Chadwick, W. W., and J. H. Dieterich, 1995. Mechanical modeling of circumferential and radial dike intrusion on Galapagos volcanoes, *Journal of Volcanological and Geothermal Research*, *66*, 37–52.

Chadwick, W. W., Jr., I. C. Wright, U. Schwarz-Schampera, O. Hyvernaud, D. Reymond, and C. E. J. de Ronde, 2008. Cyclic eruptions and sector collapses at Monowai submarine volcano, Kermadec arc: 1998–2007, *Geochemistry Geophysics and Geosystems,* 9, Q10014, doi:10.1029/ 2008GC002113.

Chaput, M., Famin, V., Michon, L., and T. Catry, 2010. Large-scale destabilization of a basaltic shield volcano (Piton des Neiges volcano, La Réunion Island). IAVCEI Third Workshop on Collapse Calderas, La Réunion, abstract.

Charvis, P., Laesanpura, A., Gallart, J., Hirn, A., Lepine, J., de Voogd, B., Minshull, T.A., Hello, Y. et B. Pontoise, 1999. Spatial distribution of hotspot material added to the lithosphere under La Réunion, from wide-angle seismic data. *Journal of Geophysical Research,* B104,(2): 2875-2893.

Cheng, C.H. and D.H. Johnston, 1981. Dynamic and static moduli. *Geophysical Research Letters*, 8, 39-42.

Chevallier L., 1979. Structure et évolution du volcan "Piton des Neiges", Ile de La Réunion. Leurs relations avec les structures du bassin des Mascareignes – Océan Indien Occidental. Thèse de doctorat de l'Université de Grenoble.

Chevallier, L., Vatin-Perignon, N., 1982. Volcano-structural evolution of Piton des Neiges, Reunion Island, Indian Ocean. *Bulletin of Volcanology,* Volume 45, Issue 4, pp.285-298.

Chiocci, F.L., Romagnoli, C., Bosman, A., 2008. Morphologic resilience and depositional processes due to the rapid evolution of the submerged Sciara del Fuoco (Stromboli Island) after the December 2002 submarine slide and tsunami*. Geomorphology*, Vol. 100, no. 3-4, pp. 356-365.

Chiocci, F.L., Coltelli, M., Bosman, A., Cavallaro, D*., in press*. Continental Margin Large-Scale Instability Controlling the Flank Sliding of Etna Volcano. *Earth and Planetary Science letters.*

Clague, D.A. and Denliguer, R.P., 1994. Role of olivine cumulates in destabilizing the flanks of Hawaiian volcanoes. *Bulletin of Volcanology*, 56:425-434.

Clague, D.A. and J.G. Moore, 2002. The proximal part of the giant submarine Wailau landslide, Molokai, Hawaii. *Journal of Volcanological and Geothermal Research*, 113:259-287.

Courtillot, V., D. Besse, D. Vandamme, R. Montigny, J.J. Jaegger, and H. Capetta, 1986. Deccan flood basalts at the Cretaceous/Tertiary boundary? *Earth and Planetary Science Letters*, 80, 361–374.

Corazzato C., L. Francalanci, M. Menna, C.M. Petrone, A. Renzulli, A. Tibaldi, L. Vezzoli, 2008. What controls sheet intrusion in volcanoes? Structure and petrology of the Stromboli sheet complex, Italy. *Journal of Volcanological and Geothermal Research*, 173:26-54.

Courtillot, V., J. Besse, D. Vandamme, R. Montigny, J.-J. Jaeger, H. Cappetta, 1986. Deccan flood basalts at the Cretaceous-Tertiary boundary?, *Earth and Planetary Science Letters*, *80*, 361–374.

Crouch, S.L., 1976. Solution of plane elasticity problems by the displacement discontinuity method*. Int. J. Numer. Meth. Engng.,* 10, 3001-3433.

Curran, J.H., Corkum, B.T., Shah, S., 1994. COMPUTE3D BEM, Version 2.23. *Rock Engineering Group*, Department of Civil Engineering, University of Toronto.

Currie K.L. and J. Ferguson, 1970. The mechanism of intrusion of lamprophyre dikes indicated by 'Offsetting' of dikes. *Tectonophysics*, 9, Issue 6, 525-535.

D

Dahlen, F.A., 1984. Noncohesive Critical Coulomb Wedges: An Exact Solution. *Journal of Geophysical Research*, Vol. 89,No. B12, 10125-10133.

Day, S.J., 1996. Hydrothermal pore fluid pressure and the stability of porous, permeable volcano. In: McGuire WJ, Jones AP, Neuberg J. (eds), Volcano Instability on the Earth and Other Planets. *Geological Society Special Pubications. London*, 110:77-93.

Day, S.J., Carracedo, J.C., Guillou, H., Gravestock, P., 1999. Recent structural evolution of the Cumbre Vieja volcano, La Palma, Canary Islands: volcanic rift zone reconfiguration as a precursor to volcano flank instability? *Journal of Volcanological and Geothermal Research*, 94, 135-167.

De Astis, G., Ventura, G., Vilardo, G., 2003. Geodynamic significance of the Aeolian volcanism (Southern Tyrrhenian Sea, Italy) in light of structural, seismological, and geochemical data. *Tectonophysics,* vol. 22, n° 4, 1040.

Delaney, P.T., Miklius, A., Arnadottir, T., Okamura, T. and M.K. Sako, 1993. Motion of Kilauea volcano during sustained eruption from the Puu'Oo and Kupaianaha vents, 1983-1991. *Journal of Geophysical Research*, 98, 17,801-17,820.

Delaney, P.T. and Denlinger, R.P., 1999. Stabilization of volcanic flanks by dike intrusion: an example from Kilauea. *Bulletin of Volcanology*, 61, 356-362.

Del Negro, C. and R. Napoli, 2002. Ground and marine magnetic surveys of the lower eastern flank of Etna volcano (Italy). *Journal of Volcanology and Geothermal Research*, Vol. 114, No. 3, 357-372.

Deniel, C., G. Kieffer, and J. Lecointre, 1992. New ^{230}Th and ^{238}U and ^{14}C age determinations from Piton des Neiges volcano, Reunion: A revised chronology for the differenciated series. *Journal of Volcanology and Geothermal Research*, 51, 253–267.

Denlinger, R.P. and Iverson, R.M., 1990. Limiting equilibrium and liquefaction potential of infinite submarine slopes. *Marine Geotechnologies*, vol. 9, pp. 299–312.

Denlinger, R.P., Okubo, P., 1995. Structure of the mobile south flank of Kılauea volcano, Hawaii. Journal of Geophysical Research, 100, 24499– 24507.

Deplus, C., Le Friant, A. and Boudon, G., 2001. Submarine evidence for large-scale debris avalanches in the Lesser Antilles Arc. *Earth and Planetary Sciences Letters*, 192(2), 145–157.

De Voogd, B., S. Pou Palomé, A. Hirn, P. Charvis, J. Gallart, D. Rousset, J. Danobeitia, and H. Perroud, 1999. Vertical movements and material transport during hotspot activity: Seismic reflection profiling offshore la Réunion, *Journal of Geophysical Research*, 104, 2855–2874.

Dieterich, J. H., 1988. Growth and persistence of Hawaiian volcanic rift zones. *Journal of Geophysical Research*, 93,4258–4270.

Dieterich, J.H., Cayol, V., Okubo, P., 2000. The use of earthquake rate changes as a stress meter at Kilauea volcano. *Nature*, *408* , 457-460.

Donnadieu, F., Merle, O., Besson, J.C., 2001. Volcanic edifice stability during cryptodome intrusion. *Bulletin of Volcanology*, 63:61-72.

Driad, L., 1997. Structure profonde de l'Edifice volcanique de la Réunion (océan Indien) par sismique réfraction grand-angle, PhD, 179 pp., Univ. de Paris 7, Paris.

Duffield, W., 1982. Huge landslide blocks in the growth of Piton de la Fournaise, La Réunion, and Kilauea volcano, Hawaii. *Journal of Volcanology and Geothermal Research*, vol. 12, issue 1-2, pp. 147-160.

Duncan, R.A., J. Backman, and A. McDonald, 1989. Reunion hotspot activity through Tertiary time: Initial results from Ocean Drilling Program Leg 115, *Journal of Volcanological and Geothermal Research*, 36, 193-198.

Dvorak, J., 1994. An earthquake cycle along the south flank of Kilauea volcano, Hawaii, *Journal of Geophysical Research*, 99, 9533-9541.

Dvorak, J. J., Klein, F.W. and D. A. Swanson, 1994. Relaxation of the south flank after the 7.2-magnitude Kalapana earthquake, Kilauea volcano, Hawaii, *Bull. Seismol. Soc. Am.*, 84, 133-141.

E

Elsworth D. and B. Voight, 1995. Dike intrusion as a trigger for large earthquakes and the failure of volcano flanks. *Journal of Geophysical Research,* 100, 6005-6024.

Elsworth D. and S.J. Day, 1999. Flank collapse triggered by intrusion: the Canarian and Cape Verde Archipelagoes. *Journal of Volcanology and Geothermal Research,* 94, 323-340.

F

Faccenna, C., Molin, P., Orecchio, B., Olivetti, V., Bellier, O., Funiciello, F., Minelli, L., Piromallo, C., Billi, A., 2011. Topography of the Calabria subduction zone (southern Italy): Clues for the origin of Mt. Etna. *Tectonics*, Vol. 30, Issue 1, doi:10.1029/2010TC002694.

Famin, V. and L. Michon, 2010. Volcano destabilization by magma injections in a detachment. *Geology,* 38*,* 3, 219-222.

Falsaperla, S., G. Lanzafame, V. Longo, and S. Spampinato, 1999. Regional stress field in the area of Stromboli (Italy): Insights into structural data and crustal tectonic earthquakes, *Journal of Volcanological and Geothermal Research*, 88, 147-166.

Falsaperla, S., Cara, F., Rovelli, A., Neri, M., Behncke, B., Acocella, V., 2010. Effects of the 1989 fracture system in the dynamics of the upper SE flank of Etna revealed by volcanic tremor data: The missing link? *Journal of Geophysical Research*, Vol. 115, B11306, doi:10.1029/2010JB007529

Fernández, C., De la Nuez, J., Casillas, R., García, E., 2002. Stress fields associated with the growth of a large shield volcano (La Palma. Canary Islands). *Tectonics*, 20,

367–384.

Ferrari, L., and P. Manetti, Geodynamic framework of the Tyrrhenian volcanism: A review, *Acta Vulcanologica*, 3, 1-10, 1993.

Finizola, A., Sortino, F., Lenat, J.F., Valenza, M., 2002. Fluid circulation at Stromboli volcano (Aeolian Islands, Italy) from self-potential and CO2 surveys. *Journal of Volcanological and Geothermal Research,* 116, 1-18.

Finizola, A., Sortino, F., Lènat, J.F., Aubert, M., Ripepe, M., Valenza, M., 2003. The summit hydrothermal system of Stromboli. New insights from self-potential, temperature, CO2 and fumarolic fluid measurements, with structural and monitoring implications. *Bulletin of Volcanology,* 65, 486-504.

Fiske, R.S. and Jackson, E.D., 1972. Orientation and growth of Hawaiian volcanic rifts: The effects of regional structure and gravitational stresses*. Proc. R. Soc. London Ser.* , A 329: 299-326.

Francalanci, L., Tommasini, S., Conticelli, S., 2004. The volcanic activity of Stromboli in the 1906-1998 AD period: mineralogical, geochemical and isotope data relevant to the understanding of the plumbing system. *Journal of Volcanology and Geothermal Research*, vol. 131, issue. 1-2, 179-211.

Francalanci, L., Davies, G.R., Lustenhouwer, W., Tommasini, S., Mason, P.R.D.,Conticelli, S., 2005. Intra-Grain Sr Isotope Evidence for Crystal Recycling and Multiple Magma Reservoirs in the Recent Activity of Stromboli Volcano, Southern Italy *Journal of Petrology*, Vol. 46, Issue 10, pp. 1997-2021.

Fretzdorff, S., Stoffers, P., Devey, C.W. and Munschy, M., 1998. Structure and morphology of submarine volcanism in the hotspot region around Reunion Island, western Indian Ocean. *Marine Geology*, 148(1-2): 39-53.

Froger, J.L., Merle, O., Briole, P., 2001. Active spreading and regional extension at Mount Etna imaged by SAR interferometry*. Earth and Planetary Science Letters,* 187, 245–258.

Froger, J.-L., Fukushima, Y., Briole, P., Staudacher, T., Souriot, T., Villeneuve, N., 2004. The deformation field of the August 2003 eruption at Piton de la Fournaise, Reunion Island, mapped by ASAR interferometry. *Geophysical Research Letters*, 31, L14601, doi:10.1029/ 2004GL020479.

Froger, J.L., Augier, A., Cayol, V., Souriot, T., 2010. Some considerations about the April 2007 eruption at Piton de la Fournaise suggested by InSAR data. IAVCEI Third Workshop on Collapse Calderas, La Réunion, abstract.

Fukushima, Y., 2005. Transferts de magma au volcan du Piton de La Fournaise déterminés par la modélisation 3D de données d'interférométrie radar entre 1998 et 2000, Thèse de doctorat, Université de Clermont Ferrand.

Fukushima, Y., Cayol, V. and P. Durand, 2005. Finding realistic dike models from interferometric synthetic aperture radar data: The February 2000 eruption at Piton de la Fournaise. *Journal of Geophysical Research*, 110, B03206, doi:10.1029/2004JB003268.

Fukushima, Y., Cayol, V., Durand, P., Massonnet, D., 2010. Evolution of magma conduits during the 1998–2000 eruptions of Piton de la Fournaise volcano, Réunion Island.

Journal of Geophysical Research, 115, B10204, doi:10.1029/2009JB007023.

G

Gailler L.-S., Lénat J.-F., Lambert M., Levieux G., Villeneuve N. and Froger J.-L., 2009. Gravity structure of Piton de la Fournaise volcano and inferred mass transfer during the 2007 crisis. *Journal of Volcanological and Geothermal Research,* 184, 31–48.

Gallart, J., L. Driad, P. Charvis, M. Sapin, A. Hirn, J. Diaz, B. de Voogd, and M. Sachpazi, 1999. Perturbation to the lithosphere along the hotspot track of La Rdunion from an offshore-onshores eismic transect. *Journal of Geophysical Research*, vol. 104, n° B2, pages 2895-2908.

Gamberi, F., Marano, M., Savelli C., 1997. Tectonic, volcanic and hydrothermal features of a submarine portion of the Aeolian arc (Tyrrhenian Sea). *Marine Geology* 140, 167-181.

Gamberi, F. and Marani, M., 2007. Downstream evolution of the Stromboli slope valley (southern Tyrrhenian sea). *Marine Geology* 243, 180-199.

Gillot P.-Y. and Nativel P., 1982. K-Ar chronology of the ultimate activity of Piton des Neiges Volcano, Reunion Island, Indian Ocean. *Journal of Volcanological and Geothermal Research,* 13, 131–146.

Gillot P.-Y., Nativel P. and Condomines M., 1990. Geochronology of Piton de la Fournaise. In: J. F. Lénat (ed.) *Le Volcanisme de la Réunion, Monogr.* pp. 243–256. Cent. De Rech. Volcanol.: Clermont-Ferrand, France.

Gillot, P.Y., Keller, J., 1993. Radiochronological dating of Stromboli. *Acta Vulcanologica* 3, 69-77.

Gillot, P-Y., Lefevre, J-C.,Nativel, P-E., 1994. Model for the structural evolution of the volcanoes of Reunion Island. *Earth and Planetary Science Letters*, vol. 122, no. 3-4, p. 291-302.

Giordano, G., and M. Porreca, 2008. Field observations on the initial lava flow and fracture system developed during the early days of the Stromboli 2007 eruption. *Journal of Volcanological and Geothermal Research*, 182, 145-154.

Goes, S., Giardini, D., Jenny, S., Hollenstein, C., Kahle, H.-G., Geiger, A., 2004. A recent tectonic reorganization in the South-Central Mediterranean. *Earth and Planetary Science Letters* 225, 335–345.

Got, J.L., Monteiller, V., Monteux, J., Hassani, R., Okubo, P., 2008. Deformation and rupture of the oceanic crust may control growth of Hawaiian volcanoes. *Nature*, 451, 453-456.

Gressier, J.B, Mourgues, R., Bodet, L., Matthieu, J.Y., Galland, O., Cobbold, P., 2010. Control of pore fluid pressure on depth of emplacement of magmatic sills: An experimental approach. *Tectonophysics*, 489, 1-4, 1-13.

Gudmundsson, A., 1983. Form and dimensions of dykes in eastern Iceland. *Tectonophysics,* 95, 295– 307.

Gudmundsson, A., 2003. Surface stresses associated with arrested dykes in rift zones. *Bulletin of Volcanology*, 65: 606-619.

Gudmundsson, A., 2005. The effects of layering and local stresses in composite volcanoes on dyke emplacement and volcanic hazards. *Comptes Rendus Geosciences*, vol. 337, issue 13, pp. 1216-1222.

Gudmundsson, A. and S.J. Brenner, 2005. On the conditions of sheet injections and eruptions in stratovolcanoes. *Bulletin of Volcanology*, 67, 768-782.

Gudmundsson, A., 2006. How local stresses control magma-chamber ruptures, dyke injections, and eruptions in composite volcanoes*. Earth Science Reviews*, v. 79, iss. 1-2, p. 1-31.

Gvirtzman, Z. and A. Nur, 1999. The formation of Mount Etna as the consequence of slab rollback*. Nature*, Vol. 401, Nº 6755, pp. 782-785.

Gvirtzman, Z. and Nur, A., 2001. Residual topography, lithospheric structure and sunken slabs in the central Mediterranean. *Earth and Planetary Science Letters* Volume 187, Issues 1-2, Pages 117-130.

H

Hampton, M. A., H. J. Lee, and J. Locat, 1996. Submarine Landslides. *Reviews of Geophysics, 34(1),* 33-59.

Hayashi, J.F. and S. Self, 1992. A comparison of pyroclastic flow and debris avalanche mobility. *Journal of Geophysical Research,* Vol. 97, No. B6, pp. 9063-9071.

Holcomb, R.T., Searle, R.C., 1991. Large landslides from oceanic volcanoes. *Marine Geotechnics,* 10, 19-32.

Hurlimann, M., Turon, E. and J. Marti, 1999. Large Landslides Triggered by Caldera Collapse Events in Tenerife, Canary Islands. *Physics and Chemistry of the Earth (A),* Vol. 24, No. 10, pp. 921-924.

Hurlimann, M., Marti, J., Ledesma, A., 2004. Morphological and geological aspects related to lerge slope failures on oceanic islands. The huge La Orotava landslides on Tenerife, Canary Islands. *Geomorphology*, Volume 62, Issues 3-4, Pages 143-158.

I

Iverson, R.M., 1995. Can magma-injection and groundwater forces cause massive landslides on Hawaiian volcanoes? *Journal of Volcanological and Geothermal Research,* 66, 295-308.

Iverson, R.M., 2000. Landslide triggering by rain infiltration. *Water Resources*, v. 36, p. 1897– 1910, doi: 10.1029/2000WR900090.

J

Jaeger, J. C., and N. G.W. Cook, 1979. *Fundamentals of rock mechanics*, Chapman and Hall, London, 3rd ed.

Jenny, S., Goes, S., Giardini, D., Kahle, H-G., 2006. Seismic potential of southern Italy. *Tectonophysics*, 415, 81–101.

Jonsson, S., Zebker, H., Cervelli, P., Segall, P., Garbeil, H., Mouginis-Mark, P., Rowland, S., 1999. A Shallow-Dipping Dike fed the 1995 Flank Eruption at Fernandina Volcano, Galapagos, Observed by Satellite Radar Interferometry. *Geophysical Research Letters*, Vol. 26, No. 8, 1077-1080.

K

Kavanagh, J. L., Menand, T., Sparks, R.S.J, 2006. An experimental investigation of sill formation and propagation in layered elastic media. *Earth and Planetary Science Letters,* 245*,* 799–813.

Keating, B.H. and W.J. McGuire, 2000. Island edifice failures and associated tsunami hazards. *Pure Applied Geophysics* 157, 899-955.

Kelfoun, K., Giachetti, T., Labazuy, P., 2010. Landslide-generated tsunamis at Réunion Island. *Journal of Geophysical Research*, vol. 115, issue 4, 17 pp.

Kluska J. M., 1997. Evolution magmatique et morpho-structurale du Piton des Neiges (Ile de la Réunion) au cours des derniers 500000 ans. Thèse de l'Université Paris XI, Orsay.

Kokelaar, P., Romagnoli, C., 1995. Sector collapse, sedimentation and clast population evolution at an active island-arc volcano: Stromboli, Italy. *Bulletin of Volcanology* 57, 240-262.

Krastel, S., Schmincke, H.-U., Jacobs, C.L., Rihm, R., Le Bas, T.P., Alibes, B., 2001. Submarine landslides around the Canary Islands*. Journal of Geophysical Research* 106, 3977-3997.

L

Labazuy, P., 1996. Recurrent landslides events on the submarine flank of Piton de la Fournaise volcano (Reunion Island). In: Mc Guire, W.J., Jones, A.P., Neuberg, J. (Eds.), Volcano Instability on the Earth and Other Planets. *Journal of Geological Society London*, pp. 295–306.

Lagmay, A. M. F., B. van Wyk de Vries, N. Kerle, and B. D. M. Pyle, 2000. Volcano instability induced by strike-slip faulting. *Bulletin of Volcanology*, 62, 331–346.

Le Bas, T.P. and D. C. Mason, 1996. Automatic Registration of TOBI Side-Scan Sonar and

Multi-Beam Bathymetry Images for Improved Data Fusion. *Marine Geophysical Researches,* 19: 163–176.

Le Friant, A., Boudon, G., Deplus, C. & Villemant, B., 2003. Large scale flank-collapse events during the activity of Montagne Pele´e, Martinique, Lesser Antilles. *Journal of Geophysical Research*, 108, B1, 2055.

Lénat, J.F., Vincent, P., Bachèlery, P., 1989. The off-shore continuation of an active basaltic volcano: Piton de La Fournaise (Reunion island, Indian Ocean); structural and geomorphological interpretation from sea beam mapping. *Journal of Volcanological and Geothermal Research* 36, 1-36.

Lénat, J.-F. and P. Bachèlery, 1990. Structure and dynamics of the central zone of Piton de la Fournaise volcano, in Le Volcanisme de la Réunion, Monogr. Cent. De Rech. Volcanol., edited by J-.F. Lénat, pp. 257– 296, Cent. De Rech. Volcanol., Clermont-Ferrand, France.

Lénat, J.F. and Labazuy, P., 1990. Morphologies et structures sous-marines de la Réunion. Dans: J.F. Lénat (Ed), Le volcanisme de la Réunion. Monographie. Centre de Recherches Volcanologiques, Clermont-Ferrand, pp. 43-74.

Lénat, J.-F., B. Gibert-Malengreau, and A. Galdéano, 2001. A new model for the evolution of the volcanic island of Réunion (Indian Ocean). *Journal of Geophysical Research*, 106, 8646– 8663.

Lénat, J.-F., Boivin, P., Deniel, C., Gillot, P.-Y., Bachèlery, P. and Team Fournaise-2, 2009. Age and nature of lavas on the submarine flanks of Piton de la Fournaise (Reunion island). *Journal of Volcanological and Geothermal Research*, 184: 199-207.

Letourneur, L., 2008. Structure and Dynamics of Plumbing Systems of Oceanic Shield Volcanoes: An Example from Réunion Island. PhD thesis, University of Gottingen (Germany).

Letourneur L., Peltier A., Staudacher T. and Gudmundsson A., 2008. The effects of rock heterogeneities on dyke paths and asymmetric ground deformation: The example of Piton de la Fournaise (Réunion Island). *Journal of Volcanological and Geothermal Research,* 173, 289-302.

Levieux, G., 2004. Synthèse géophysique de la zone de forage de reconnaissance géothermique du Piton de la Fournaise, DEA, Univ. Blaise Pascal, Clermont-Ferrand, 65 pp.

Lipman, P.W. and D.R. Mullineaux, 1981. The 1980 eruptions of Mount St. Helens, *Washington. U.S. Geological Survey Professional Paper,* 1250.

Lister, J.R. and R.C. Kerr, 1991. Fluid-mechanical models of crack propagation and their application to magma transport in dykes. *Journal of Geophysical Research,* **96***,* 10049–10077.

Lonsdale, P., 1989. A geomorphological reconnaissance of the submarine part of the East Rift Zone of Kilauea Volcano, Hawaii. *Bulletin of Volcanology*, Volume 51, Issue 2, pp.123-144.

Lundgren, P., Berardino, P., Coltelli, M., Fornaro, G., Lanari, R., Puglisi, G., Sansosti, E. Tesauro, M., 2003. Coupled magma chamber inflation and sector collapse slip

observed with synthetic aperture radar interferometry on Mt. Etna volcano. *Journal of Geophysical Research*, Vol. 108, Issue B5, Doi 10.1029/2001JB000657.

M

Maccaferri, F., Bonafede, M., Rivalta, E., 2010. A numerical model of dyke propagation in a layered elastic media. *Geophysical Journal International*, 180, 1107-1123.

Mahoney, J. J., Duncan, R. A., Khan, W., Gnos, E. and G.R. Mc Cormick, 2002. Cretaceous volcanic rocks of the South Tethyan suture zone, Pakistan: implications for the Réunion hotspot and Deccan Traps. *Earth and Planetary Science Letters*, Volume 203, Issue 1, p. 295-310.

Maillot, E., 1999. Les systèmes intrusifs des volcans boucliers océaniques: Ile de la Réunion (Océan Indien). Approche structurale et expérimentale. PhD Thesis, Université de la Réunion.

Malengreau, B., J.-F. Lénat, and J.-L. Froger, 1999. Structure of the Réunion Island (Indian Ocean) inferred from the interpretation of gravity anomalies. *Journal of Volcanological and Geothermal Research*, 88, 131-146.

Maramai, A., Graziani, L., Tinti, S., 2005a. Tsunamis in the Aeolian Islands (southern Italy): a review. *Marine Geology*, vol. 215, n°1-2, pp. 11-21.

Maramai, A., Graziani, L., Alessio, G., Burrato, P., Colini, L., Cucci, L., Nappi, R., Nardi, A., Vilardo, G., 2005b. Near- and far-field survey report of the 30 December 2002 Stromboli (Southern Italy) tsunami. *Marine Geology,* doi: 10.1016/ j.margeo.2004.11.009.

Marinoni, L.B. and A. Gudmundson, 2000. Dykes, faults and paleostresses in the Teno and Anaga massifs of Tenerife (Canary Islands). *Journal of Volcanological and Geothermal Research,* 103*,* 83-103.

Marti, J., Hurlimann, M., Ablay, G.J., Gudmundsson, A., 1997. Vertical and lateral collapses on Tenerife (Canary Islands) and other volcanic ocean islands. *Geology,* 25, 879-882.

Masson, D.G., Watts, A.B., Gee, M.J.R., Urgeles, R., Mitchell, N.C, Le Bas, T.P., Canals, M., 2002. Slope failures on the flanks of the western Canary Islands. *Earth-Science Reviews*, 57:1–35

McDonald, G.A, and R. Abbott, 1970. Volcanoes in the sea. *Univ. of Hawaii Press*, Honolulu, 441 pp.

McDonald, G., 1972. Volcanoes. *Prentice-hall, inc.*, Englewood cliffs, New Jersey. 510 pp.

McDougall I., 1971. The geochronology and evolution of the young volcanic Island of Réunion, Indian Ocean. *Geochimica Cosmochimica Acta,* 35, 261–288.

McGuire, W.J., 1996. Volcano instability: a review of contemporary themes, From McGuire, W.J., Jones, A.P. and Neuberg, J. (eds), Volcano Instability on the Earth

and Other Planets. *Geological Society of London Special Publications* No. 110, pp.1-23.

McGuire, W.J. and Pullen, A.D., 1989. Location and orientation of eruptive fissures and feeder-dykes at Mount Etna: influence of gravitational and regional tectonic stress regimes. *Journal of Volcanological and Geothermal Research,* 38, 325–344.

Menand, T., 2008. The mechanics and dynamics of sills in layered elastic rocks and their implications for the growth of laccoliths and other igneous complexes. *Earth and Planetary Science Letters*, 267, 93-99.

Menand T., 2009. Physical controls and depth of emplacement of igneous bodies: A review. *Tectonophysics*, in press, DOI:10.1016/j.tecto.2009.10.016.

Menand, T., Daniels, K.A., Benghiat, P., 2010. Dyke propagation and sill formation in a compressive tectonic environment. *Journal of Geophysical Research*, 115, No. B8, B08201.

Menard, H. W., 1983. Insular Erosion, Isostacy and Subsidence*. Science,* 220, 913–918.

Merle, O. and A. Borgia, 1996. Scaled experiments of volcanic spreading. *Journal of Geophysical Research* 101:13805-13817.

Merle, O., Vidal, N., van Wyk de Vries, B., 2001. Experiments on vertical basement fault reactivation below volcanoes. *Journal of Geophysical Research* ,106:2153-2162.

Merle, O., and J. Lénat, 2003. Hybrid collapse mechanism at Piton de la Fournaise volcano, Reunion Island, Indian Ocean. *Journal of Geophysical Research*, 108(B3), 2166, doi:10.1029/2002JB002014.

Merle, O., Barde Cabusson, S., Maury, R., Legendre, C., Guille, G., Blais, S., 2006. Volcano core collapse triggered by regional faulting. *Journal of Volcanological and Geothermal Research,* 158:269–280.

Merle O., Mairine P., Michon L., Bachèlery P. and Smietana M., 2010. Calderas, landslides and paleo-canyons on Piton de la Fournaise volcano (La Réunion Island, Indian Ocean). *Journal of Volcanological and Geothermal Research* 189, 131–142.

Metrich, N., Bertagnini, A:, Landi, P., Rosi, M., 2001. Crystallization Driven by Decompression and Water Loss at Stromboli Volcano (Aeolian Islands, Italy). *Journal of Petrology*, vol. 42, No. 8, 1471-1490.

Michon, L., F. Saint-Ange, P. Bachelery, N. Villeneuve, and T. Staudacher, 2007a. Role of the structural inheritance of the oceanic lithosphere in the magmato-tectonic evolution of Piton de la Fournaise volcano (La Réunion Island). *Journal of Geophysical Research*, 112, B04205, doi:10.1029/2006JB004598.

Michon, L., Staudacher, T., Ferrazzini, V., Bachèlery, P. and J. Marti, 2007b. April 2007 collapse of Piton de la Fournaise: a new example of caldera formation. *Geophysical Research Letters*, vol. 34, L21301, doi:10.1029/2007GL031248.

Michon, L. and F. Saint-Ange, 2008. Morphology of Piton de la Fournaise basaltic shield volcano (La Réunion Island): Characterization and implication in the volcano evolution. *Journal of Geophysical Research,* Vol. 113, B03203, doi:10.1029/2005JB004118.

Michon L., Cayol V., Letourneur L., Peltier A., Villeneuve N. & Staudacher T., 2009a. Edifice growth, deformation and rift zone development in basaltic setting: Insights from Piton de la Fournaise shield volcano (Réunion Island). *Journal of Volcanological and Geothermal Research,* 184, 14–30.

Michon L., Villeneuve N., Catry T. and Merle O., 2009b. How summit calderas collapse on basaltic volcanoes: New insights from the April 2007 caldera collapse of Piton de la Fournaise volcano. *Journal of Volcanological and Geothermal Research,* 184, 138–151.

Milano, G., Vilardo, G., Luongo,G., 1994. Continental collision and basin opening in southern Italy: A new plate subduction in the Tyrrhenian Sea? *Tectonophysics*, 230, 249-264.

Mitchell, N.C., Masson, D.G., Watts, A.B., Gee, M.J.R., Urgeles, R., 2002. The morphology of the submarine flanks of volcanic ocean islands. A comparative study of the Canary and Hawaiian hotspot islands. *Journal of Volcanology and Geothermal Research,* 115:83-107.

Moore, J. G., 1964. Giant submarine landslides on the Hawaiian ridge. *U.S. Geological Survey Professional Paper*, 501-D, 95–98.

Moore, J.G., Clague, D.A., Holcomb, R.T., Lipman, P.W., Normark, W.R. and Torresan, M.E., 1989. Prodigious submarine landslides on the Hawaiian ridge. *Journal of Geophysical Research*, vol. 94, n° B12, 17,465-17,484.

Moore, J.G. and Normark, W.R., 1994. Giant Hawaiian landslides. *Annual Review of Earth and Planetary Sciences*, 22:119-44.

Morgan, J.K., Moore, J.G., Clague, D.A., 2003. Slope failure and volcanic spreading along the submarine south flank of Kilauea volcano, Hawaii. *Journal of Volcanology and Geothermal Research*, Vol. 108, No. B9, 2415.

Morgan, J.K. and P.J. McGovern, 2005a. Discrete element simulations of gravitational volcanic deformation: 1. Deformation structures and geometries. *Journal of Geophysical Research,* vol. 110, B05402, doi:10.1029/2004JB003252.

Morgan, J.K. and P.J. McGovern, 2005a. Discrete element simulations of gravitational volcanic deformation: 2- Mechanical analysis. *Journal of Geophysical Research,* vol. 110, B05403, doi:10.1029/2004JB003253

Morgan, J.K., 2006. Volcanotectonic interactions between Mauna Loa and Kilauea: Insights from 2-D discrete element simulations. *Journal of Volcanology and Geothermal Research,* 151, 109-131.

Mulder, T., Cochonet, P., 1996. Classification of offshore mass movements. *Journal of Sedimentary Research*, vol. 66, n° 1, p. 43-57.

Murray, J.B., 1988. The influence of loading by lavas on the siting of eruption vents on Mount Etna. *Journal of Volcanological and Geothermal Research*, 35, 121–139.

N

Naumann, T., and D. Geist, 2000. Physical volcanology and structural development of

Cerro Azul Volcano, Isabela Island, Galápagos: implications for the development of Galápagos-type shield volcanoes. *Bulletin of Volcanology*, Volume 61, Issue 8, pp. 497-514.

Nercessian, A., Hirn, A., Lepine, J.C., Sapin, M., 1996. Internal structure of Piton de la Fournaise volcano from seismic wave propagation and earthquake distribution. *Journal of Volcanological and Geothermal Research*, 70, 123–143.

Neri, M., Acocella, V., Behncke, B., 2004. The role of the Pernicana Fault Systemin the spreading ofMt.Etna (Italy) during the 2002–2003 eruption. *Bulletin of Volcanology*, 66, 417–430, doi: 10.1007/S00445-003-0322-X.

Neri, M., Acocella, V., Behncke, B., Maiolino, V., Ursino, A., Velardita, R., 2005. Contrasting triggering mechanisms of the 2001 and 2002–2003 eruptions of Mount Etna (Italy). *Journal of Volcanological and Geothermal Research*, 144, 235–255. doi:10.1016/j.jvolgeores.2004.11.025.

Neri, M., Lanzafame, G., Acocdella, V., 2008. Dyke emplacement and related hazard in volcanoes with sector collapse: the 2007 Stromboli (Italy) eruption. *Journal of the Geological Society*, vol. 165, 883-886.

Neri, M. and G. Lanzafame, 2009. Structural features of the 2007 Stromboli eruption. *Journal of Volcanological and Geothermal Research,* 182, 137-144.

O

Oehler, J.-F., P. Labazuy, and J.-F. Lénat, 2004. Recurrence of major flank landslides during the last 2 Ma-history of Réunion Island. *Bulletin of Volcanology*, 66, 585–598.

Oehler, J.-F., 2005. Les déstabilisations de flanc des volcans de l'Ile de la Réunion (Océan Indien): Mise en évidence, implications et origines, Ph.D. thesis, 422 pp., Univ. Clermont-Ferrand II, Clermont-Ferrand, France.

Oehler, J.-F., B. Van Wyk de Vries, and P. Labazuy, 2005. Landslides and spreading of oceanic hot-spot and arc shield volcanoes and Low Strength Layers (LSLs): An analogue modelling approach. *Journal of Volcanological and Geothermal Research*, 144, 169–189.

Oehler, J.-F., P. Labazuy and J.-F. Lénat, 2008. Growth and collapse of La Reunion Island volcanoes. *Bulletin of Volcanology*, 70:717–742.

Owen, S., Segall, P., Lisowski, M., Miklius, A., Denlinger, R. and M. Sako, 2000. Rapid deformation of Kilauea Volcano: Global positioning system measurements between 1990 and 1996. *Journal of Geophysical Research*, 105, 18,983–18,998.

Owen, S.E. and R. Burgmann, 2006. An increment of volcano collapse: Kinematics of the 1975 Kalapana, Hawaii, earthquake. *Journal of Volcanological and Geothermal Research*, 150, 163–185.

P

Pareschi, M.T., Boschi, E., Mazzarini, F. and M. Favalli, 2006. Large submarine lanslides offshore Mt. Etna. *Geophysical Research letters*, vol. 33, L13302, doi:10.1029/2006GL026064.

Pasquarè, G., Francalanci, L., Garduno, V.H., Tibaldi, A., 1993. Structure and geological evolution of the Stromboli volcano, Aeolian Islands, Italy. *Acta Vulcanologica* 3:79–89.

Peltier A., Staudacher T. and Bachèlery P., 2007. Constraints on magma transfers and structures involved in the 2003 activity at Piton de La Fournaise from displacement data. *Journal of Geophysical Research* 112.

Peltier, A., Famin, V., Bachèlery, B., Cayol, V., Fukushima, Y., Staudacher, T., 2008. Cyclic magma storages and transfers at Piton de la Fournaise volcano (La Réunion hotspot) inferred from deformation and geochemical data. *Earth and Planetary Science Letters*, 270, 3-4, 180–188.

Peltier A., Staudacher T., Bachèlery P. and V. Cayol, 2009. Formation of the April 2007 caldera collapse at Piton de la Fournaise volcano: insights from GPS data. *Journal of Volcanological and Geothermal Research,* 184, 152-163.

Peltier A., Staudacher T. and Bachèlery P., 2010. New behaviour of the Piton de La Fournaise volcano feeding system (La Réunion Island) deduced from GPS data: Influence of the 2007 Dolomieu caldera collapse. *Journal of Volcanological and Geothermal Research,* 192, 48-56.

Peterson, D. W. & Moore, J. G. 1987. Geologic history and evolution of geologic concepts, Island of Hawaii. *United States Geological Society Professional Paper,* 1350, 149-189.

Pollard, D.D., Delaney, P.T., Dufield, W.A., Endo, E.T., Okamura, A.T., 1983. Surface deformation in volcanic rift zones. *Tectonophysics*, 94, 541-584.

Prono, E., Battaglia, J., Monteiller, V., Got, J.L., Ferrazzini, V., 2009. P-wave velocity structure of Piton de la Fournaise volcano deduced from seismic data recorded between 1996 and 1999.*Journal of Volcanological and Geothermal Research,* 184*, 1-2, Recent advances on the geodynamics of Piton de la Fournaise volcano*, 49-62.

Puglisi, G., Bonforte, A., Ferretti, A., Guglielmino, F., Palano, M. and C. Prati, 2008. Dynamics of Mount Etna before, during, and after the July–August 2001 eruption inferred from GPS and differential synthetic aperture radar interferometry data, *Journal of Geophysical Research*, 113, B06405, doi:10.1029/2006JB004811.

Q

R

Rancon, J. P., Lerebour, P., Auge, T., 1989. The Grand Brûlé exploration drilling: new data on the deep framework of the Piton de la Fournaise volcano. I: Lithostratigraphic units and volcanostructural implications. *Journal of Volcanology and Geothermal Research*, vol. 36, n°1-3, pp. 113-127.

Reid M.E., Sisson T.W., Brien D.L., 2001. Volcano collapse promoted by hydrothermal alteration and edifice shape, Mount Rainier, Washington. *Geology*, 29:779-782.

Richards, M.A., Duncan, R.A and V.E. Courtillot, 1989. Flood Basalts and Hot-Spot Tracks: Plume Heads and Tails. *Science*, Vol. 246 no. 4926 pp. 103-107.

Rizzo, F.J., 1967. An integral equation approach to boundary value problems of classical elastostatics. *Quart. Appl. Math*, 25, 83-95.

Rivalta, E., Bottinger, M., Dahm, T., 2005. Buoyancy-driven fracture ascent: Experiments in layered gelatine. *Journal of Volcanology and Geothermal Research,* 144, 273-285.

Roeloffs, E., 1996. Poroelastic Techniques in the Study of Earthquake-Related Hydrologic Phenomena, In: Renata Dmowska and Barry Saltzman, Editor(s). *Advances in Geophysics,* 37, Pages 135-195.

Romagnoli, C., Kokelaar, P., Rossi, P.L., Sodi, A., 1993. The submarine extension of Sciara del Fuoco feature (Stromboli Island): morphologic characterisation. *Acta Vulcanologica* 3:91–98.

Romagnoli, C., Casalbore, D., Chiocci, F.L., Bosman, A., 2009a. Offshore evidence of largescale lateral collapses on the eastern flank of Stromboli, Italy, due to structurally controlled, bilateral flank instability. *Marine Geol*ogy, 262 (1–4), 1–13.

Romagnoli, C., Kokelaar, P., Casalbore, D., Chiocci, F.L., 2009b. Lateral collapses andactive sedimentary processes on the northwestern flank of Stromboli volcano. Italy. *Marine Geology,* 265, 101–119.

Rosi, M., Bertagnini, A., Landi, P., 2000. Onset on the persistent activity at Stromboli volcano (Italy). *Bulletin of Volcanology*, Volume 62, Numbers 4-5, p. 294-300.

Rowland, S.K., and H. Garbeil, 2000. Slopes of oceanic basalt volcanoes. *In* Mouginis Mark, P.J.C.J.A.F.J.H., ed., Fall Meeting of the American-Geophysical Union: San Francisco, Ca, *American Geophysical Union*, p. 223-247.

Ruch, J., Acocella, V., Storti, F., Neri, M., Pepe, S., Solara, G., Sansosti, E., 2010. Detachment depth revealed by rollover deformation:an integrated appraoch at Mount Etna. *Geophysical Research Letters*, vol. 37, L16304, doi:10.1029/2010GL044131.

Russo, G., Giberti, G. and Giovanni Sartoris, 1996. The influence of regional stresses on the the mechanical stability of volcanoes; Stromboli (Italy) (*in* Volcano instability on the Earth and other planets), *Geological Society Special Publications*, 110 65-75.

Rust, D. and M. Neri, 1996. The boundaries of large-scale collapse on the flanks of Mount Etna, Sicily, in: McGuire, W.J., Jones, A.P., Neuberg, J. (Eds.), Volcano

Instability on the Earth and Other Planets*, Geological Society of London Special Publication*, 110, pp. 193–208.

S

Satake, K. and Y. Kato, 2001. The 1741 Oshima-Oshima eruption: extent and volume of submarine debris avalanche. *Geophysical research Letters*, vol. 28, 3, 427-430.

Satake, K., 2007. Volcanic origin of the 1741 Oshima-Oshima tsunami in the Japan Sea. *Earth Planets Space*, 59, 381–390.

Scarfi, L., Zuccarello, L., Patanè, D., 2010. Magma dynamics of 2007 Stromboli effusive eruption as revealed by high precision location of seismic events. . *Journal of Volcanology and Geothermal Research,* 198, 405-415.

Schlich, R., Dyment, J., Munschy M., 1990. Structure and age of the Mascarene and Madagascar basins. *In Abstr. Volcanisme Intraplaque*. Le point-chaud de la Réunion. Réunion Nov. 1990.

Segall, P., Grasso, J.R., Mossop, A., 1994. Poroelastic stressing and induced seismicity near the Lacq gas field, southwestern France. *Journal of Geophysical Research,* 99, 15,423-15,438.

Segall, P., Desmarais, E., Shelly, D., Miklius, A., Cervelli, P., 2006. Earthquakes triggered by silent slip events on Kilauea volcano, Hawaii. *Nature*, 442.

Servadio Z., Villeneuve N., Gladys A., Staudacher T., Urai M., 2008. Preliminary results of lava flow mapping using remote sensing in Piton de la Fournaise, La Réunion island. *Workshop on the "Use of Remote Sensing Techniques for Monitoring Volcanoes and Seismogenic Areas*", abstract, IEEE Naples.

Siebert, L., 1984. Large volcanic debris avalanches: characteristics of source areas, deposits, and associated eruptions. *Journal of Volcanology and Geothermal Research,* 22, 163-197.

Sigmarsson, O., Condomines, M., Bachèlery, P., 2005. Magma residence time beneath the Piton de la Fournaise Volcano, Reunion Island, from U-series disequilibria, *Earth and Planetary Science Letters*, 234, 223–234.

Sigmundsson, F., Durand, P., Massonnet, D., 1999. Opening of an eruptive fissure and seaward displacement at Piton de la Fournaise volcano measured by RADARSAT satellite radar interferometry, *Geophysical Research Letters*, 26, 533–536.

Smietana, M., Bachèlery, P. and Hémond, C., 2010. Heterogeneity in the mantle source of La Réunion Island, Goldschmidt conference abstract 2010, *Geochimica Cosmochima Act*a, 74, 12, suppl. 1, A972.

Smith, M.S. and J.B. Shepherd, 1996. Tsunami waves generated by volcanic landslides: an assessment of the hazard associated with Kick 'em Jenny *Geological Society London Special Publications,* v. 110, p. 115-123.

Smith, J. R., Jr., and P. Wessel, 2000. Isostatic Consequences of Giant Landslides on the Hawaiian Ridge, *Pure applied geophys*ics, 157, 899–955.

Staudacher, T., Ferrazzini, V., Peltier, A., Kowalski, P., Boissier, P., Catherine, P., Lauret, F., Massin, F., 2009. The April 2007 eruption and the Dolomieu crater collapse, two major events at Piton de la Fournaise (La Réunion Island, Indian Ocean). *Journal of Volcanology and Geothermal Research,* 184, 126-137.

Staudigel H. and Schmincke H. U., *1984*. The Pliocene Seamount series of La Palma, Canary Islands. *Journal of Geophysical Research*, 83,11195-11215.

Stein, R.S., King, G.C.P, Lin, J., 1992. Change in Failure Stress on the Southern San Andreas Fault System Caused by the 1992 Magnitude = 7.4 Landers Earthquake. *Science,* 258 (5086), 1328. [DOI: 10.1126/science.258.5086.1328].

Swanson, D.A., Duffield, W.A., Fiske, R.S., 1976. Displacement of the south flank of Kilauea Volcano: The result of forceful intrusion of magma into the rift zones : interpretation of geodetic and geologic information leads to a new model for the structure of Kilauea Volcano. *U.S. Govt. Print. Off.* (Washington), 101-676-452.

T

Taisne, B., and C. Jaupart, 2009. Dike propagation through layered rocks. *Journal of Geophysical Research*, 114, B09203, doi:10.1029/2008JB006228.

Tanner, L. H. and Calvari, S., 2004. Unusual sedimentary deposits on the SE side of Stromboli volcano, Italy: products of a tsunami caused by the ca. 5000 years BP Sciara del Fuoco collapse? *Journal of Volcanology and Geothermal Research*, v. 137, iss. 4, p. 329-340.

Tibaldi, A., Pasquaré, G., Francalanci, L., Garduño, V.H., 1994. Collapse type and recurrence at Stromboli volcano, associated volcanic activity, and sea level changes. *Accademia dei Lincei, Atti dei Convegni Lincei, Roma* 112, 143–151.

Tibaldi A., 1996. Mutual influence of diking and collapses at Stromboli volcano, Aeolian Arc, Italy. *Geological Society of London Special Publication,* 110:55-63.

Tibaldi A, 2001. Multiple sector collapses at Stromboli volcano, Italy: how they work. *Bulletin of Volcanology* 63:112-125.

Tibaldi, A., 2003. Influence of cone morphology on dykes, Stromboli, Italy. *Journal of Volcanological and Geothermal Research,* 126, 1-2, 79-95.

Tibaldi, A., Corazzato, C., Apuani, T., Cancelli, A., 2003. Deformation at Stromboli volcano (Italy) revealed by rock mechanics and structural geology. *Tectonophysics* 361, 187–204.

Tibaldi, A., 2004. Major changes in volcano behaviour after a sector collapse: insights from Stromboli, Italy. *Terra Nova*, 16, 2–8.

Tibaldi, A., Bistacchi, A., Pasquarè, F., Vezzoli, L., 2005. Extensional tectonics and volcano lateral collapses: insights from Ollagüe volcano (Chile) and analogue modelling. *Terra Nova* 18, 282–289.

Tibaldi, A. and Lagmay, A.F.M., 2006. Interaction between volcanoes and their basement. *Journal of Volcanology and Geothermal Research,* Vol. 158, issues 1-2 , Pages 1-5.

Tibaldi, A., Corazzato, C., Kozhurin, A., Lagmay, A.F.M., Pasquarè, F.A., Ponomareva, V., Rust, D., Tormey, D., Vezzoli, L., 2007. Influence of substrate tectonic heritage on the evolution of composite volcanoes: Predicting sites of flank eruption, lateral collapse, and erosion. *Global and Planetary Change,* Volume 61, Issues 3-4, Pages 151-174.

Tibaldi, A., Corazzato, C., Marani, M., Gamberi, F., 2009. Subaerial-submarine evidence of structures feeding magma to Stromboli Volcano, Italy, and relations with edifice flank failure and creep. *Tectonophysics*, v. 469, iss. 1-4, p. 112-136.

Tilling, R.I. and J.J Dvorak, 1993. Anatomy of a basaltic volcano. *Nature*, 363, 125-132.

Tinti, S., Bortoluzzi, E., Romagnoli, C., 2000. Computer simulations of tsunamis due to sector collapse at Stromboli, Italy. *Journal of Volcanology and Geothermal Research*, vol. 96, issue 1-2, pp. 103-128.

Tinti, S., Maramai, A., Armigliato, A., Graziani, L., Manucci, A., Pagnoni, G., Zaniboni, F., 2005. Observations of physical effects from tsunamis of December 30, 2002 at Stromboli volcano, southern Italy. *Bulletin of Volcanology,* Vol. 68, Issue 5, pp.450-461.

Tommasi, P., Baldi, P., Chiocci, F., Coltelli, M.,Marsella, M., Romagnoli, C., 2008. Slope Failures Induced by the December 2002 Eruption at Stromboli Volcano. *Geophysical Monograph*, vol. 182, pp. 129-145.

Townsend, J., and M. D. Zoback, 2000. How faulting keeps the crust strong. *Geology*, 28(5), 399– 402.

Tryggvason, E., 1984. Widening of the Krafla fissure swarm during the 1975-1981 volcano-tectonic episode. *Bulletin of Volcanol*ogy, 47: 47-69

U

Upton B. G. J. and Wadsworth W. J., 1965. Geology of Reunion Island, Indian Ocean. *Nature,* 207, 151–154.

Upton B. G. J. and Wadsworth W. J., 1972. Aspect of magmatic evolution of Réunion Island. *Phil. Trans. R. Soc. London A,* 271, 105–130.

V

Valentine, G.A. and K.E.C. Krogh, 2006. Emplacement of shallow dikes and sills beneath a small basaltic volcanic center – The role of pre-existing structure(Paiute Ridge, southern Nevada, USA). *Earth and Planetary Science Letters,* 246, 217-230.

van Wyk de Vries, B. and Borgia, A., 1996. The role of basement in volcano deformation. In: Mc Guire, W.J., Jones, A.P., Neuberg, J. (Eds.), Volcano Instability on the Earth and Other Planets. *Journal of Geological Society London*, pp 95-110.

van Wyk de Vries B and P.W. Francis, 1997. Catastrophic collapse at statovolcanoes induced by gradual volcano spreading. *Nature*, 387:387-390.

van Wyk de Vries B and R. Matela, 1998. Styles of volcano-induced deformation: numerical models of substratum flexure, spreading and extrusion. *Journal of Volcanological and Geothermal Research* 81:1-18.

van Wyk de Vries, B., Self, S., Francis, P.W., Keszthelyi, L., 2001. A gravitational spreading origin for the Socompa deb-ris avalanche. *Journal of Volcanological and Geothermal Research* 105:225-247.

Vidal, N. and O. Merle, 2000. Reactivation of basement faults beneath volcanoes: a new model of flank collapse. *Journal of Volcanological and Geothermal Research,* 99:9-26.

Villeneuve, N. and P. Bachèlery, 2006. Revue de la typologie des éruptions au Piton de La Fournaise, processus et risques volcaniques associés. *European Journal of Geography*, No. 336.

Voight, B., Glicken, H., Janda, R.J., Douglass, P.M., 1981. Catastrophic rockslide avalanche of May 18. *In*: Lipman PW, Mullineaux DR (eds), The 1980 eruptions of Mount St. Helens, Washington. *U.S. Geological Survey Professional Pap*er 1250:347-377.

W

Walker, G.P.L., 1986. Koolau dike complex, Oahu: Intensity and origin of a sheeted dike complex high in a Hawaiian volcanic edifice. *Geology*, 14, p. 310–313.

Walker, G.P.L., 1987. The dike complex of the Koolau volcano, Oahu: internal structure of a Hawaiian rift zone. In: R.W. Decker, T.L. Wright and P.H. Stauffer (Editors), Volcanism in Hawaii, *U.S. Geological Survey Professional Paper,* 1350.

Walker, G.P.L., 1993. Basaltic-volcano systems. *In* Prichard, H. M., Alabaster, T., Harris, N. B. W. & Neary, C. R. (eds), *Magmatic Processes and Plate Tectonics, Geological Society Special Publication* No. 76, 3-38.

Walker, G.P.L. and P.G. Eyre, 1995. Dyke complexes in American Samoa. *Journal of Volcanological and Geothermal Research, 69*, 241–254.

Walker, G.P.L., 1999. Volcanic rift zones and their intrusion swarms. *Journal of Volcanology and Geothermal Research*, 94: 21-34.

Walter, T.R. and Troll, V.R., 2003. Experiments on rift zone evolution in unstable volcanic edifices. *Journal of Volcanology and Geothermal Research,* Volume 127, Issues 1-2, Pages 107-120.

Walter, T.R, Acocella, V., Neri, M., Amelung, F., 2005. Feedback processes between magmatic events and flank movement at Mount Etna (Italy) during the 2002-2003 eruption. *Journal of Geophysical Research*, 110, B10205, doi:10.1029/ 2005JB003688.

Watanabe,T., Masuyama,T., Nagaoka,K. and T. Tahara, 2002. Analog experiments on magma-filled cracks: Competition between external stresses and internal pressure. *Earth Planets Space*, Vol. 54 (No. 12), pp. 1247-1261.

Welsch, B., 2010. Signification des Océanites dans le fonctionnement du Piton de la

Fournaise, Île de La Réunion. Thèse de l'Université de la Réunion, 308 pp.

White, R.S. and D. McKenzie, 1995. Mantle plumes and flood basalts. *Journal of Geophysical Research*, vol. 100, no. B9, pp. 17,543-17,585.

Wright, I. C., Chadwick Jr. W. W., de Ronde, C. J., Reymond, D., Hyvernaud, O., Gennerich, H. H., Stoffers, P., Mackay, P., Dunkin, M. and S. C. Bannister, 2008. Collapse and reconstruction of Monowai submarine volcano, Kermadec arc, 1998–2004. *Journal of Geophysical Research*, 113, B08S03, doi:10.1029/ 2007JB005138.

X

Y

Z

Zbinden, E.A. and J.M. Sinton, 1988. Dikes and the petrology of Waianae volcano, Oahu. *Journal of Geophysical Research*, 93, 14,856-14,866.

Appendix

Appendix 1

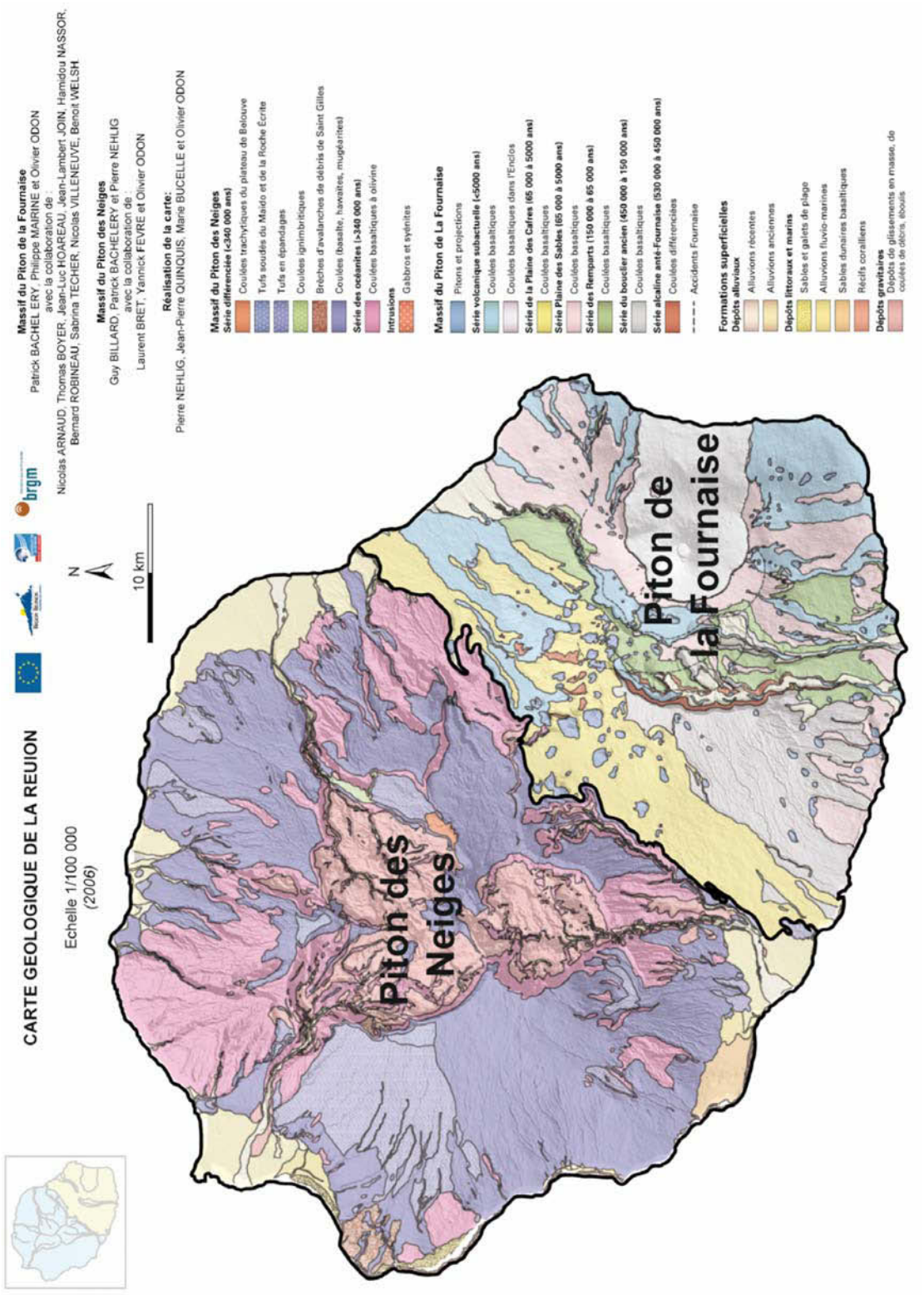

Simplified geological map of La Reunion island (from BRGM, 2006)

Appendix 2

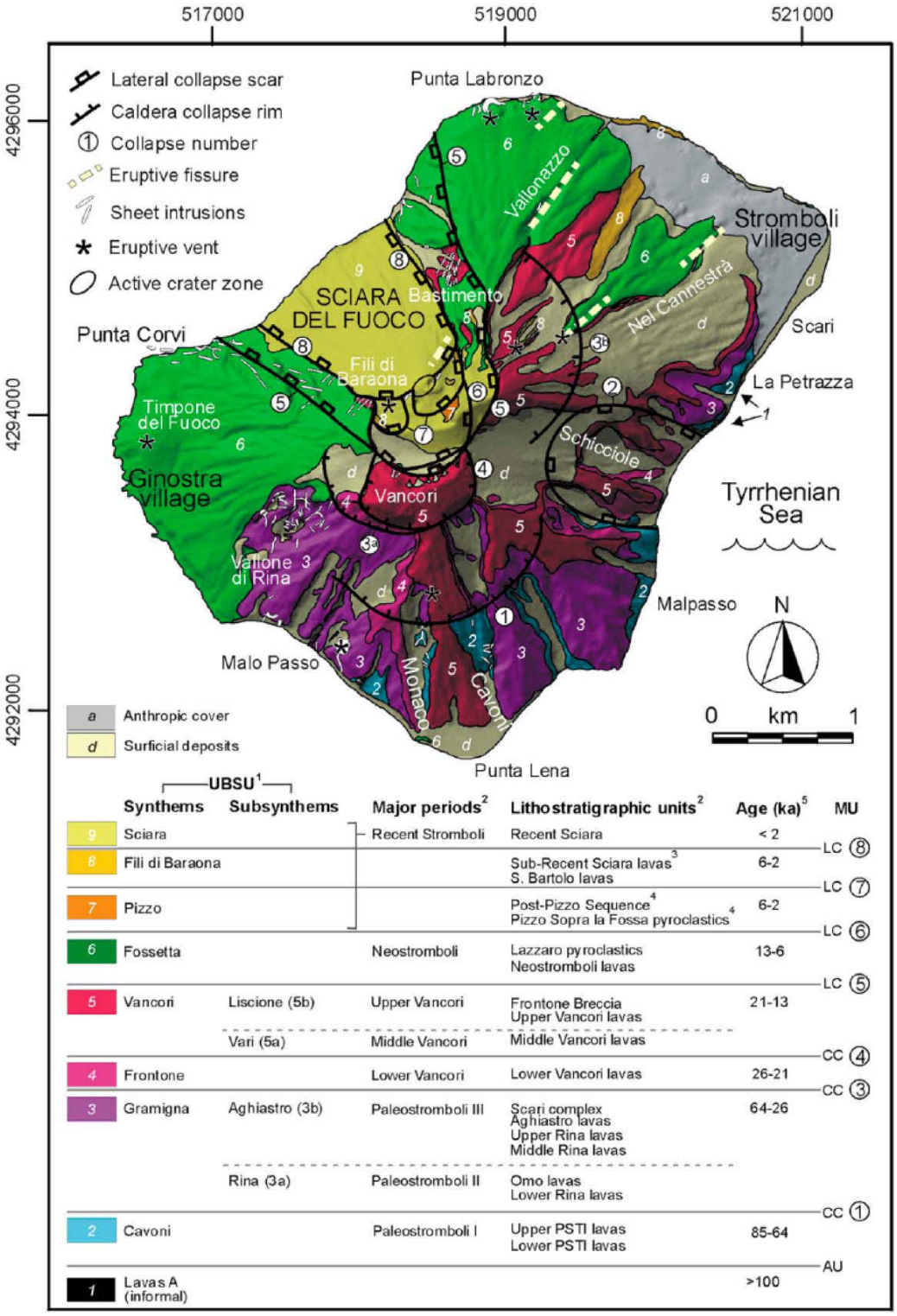

UBSU[1] Synthems	Subsynthems	Major periods[2]	Lithostratigraphic units[2]	Age (ka)[5]	MU
9 Sciara		Recent Stromboli	Recent Sciara	< 2	
					LC ⑧
8 Fili di Baraona			Sub-Recent Sciara lavas[3] S. Bartolo lavas	6-2	
					LC ⑦
7 Pizzo			Post-Pizzo Sequence[4] Pizzo Sopra la Fossa pyroclastics[4]	6-2	
					LC ⑥
6 Fossetta		Neostromboli	Lazzaro pyroclastics Neostromboli lavas	13-6	
					LC ⑤
5 Vancori	Liscione (5b)	Upper Vancori	Frontone Breccia Upper Vancori lavas	21-13	
	Vari (5a)	Middle Vancori	Middle Vancori lavas		
					CC ④
4 Frontone		Lower Vancori	Lower Vancori lavas	26-21	
					CC ③
3 Gramigna	Aghiastro (3b)	Paleostromboli III	Scari complex Aghiastro lavas Upper Rina lavas Middle Rina lavas	64-26	
	Rina (3a)	Paleostromboli II	Omo lavas Lower Rina lavas		
					CC ①
2 Cavoni		Paleostromboli I	Upper PSTI lavas Lower PSTI lavas	85-64	
					AU
1 Lavas A (informal)				>100	

Simplified geological map of Stromboli Island (from Corazzato et al., 2008)

Appendix 3

Catry, T., V. Cayol, L. Michon, M. Chaput, V. Famin and C. Romagnoli, Cointrusive shear stress triggers flank collapse on basaltic volcanoes, *Journal of Volcanological and Geothermal Research*, **submitted** (November 2010).

Elsevier Editorial System(tm) for Journal of Volcanology and Geothermal Research
Manuscript Draft

Manuscript Number:

Title: Cointrusive shear stress triggers flank collapse on basaltic volcanoes

Article Type: Research Paper

Keywords: dike, sill, volcano destabilization, numerical modelling

Corresponding Author: Mr thibault catry,

Corresponding Author's Institution: University of Bologna

First Author: Thibault Catry

Order of Authors: Thibault Catry; Valérie Cayol; Laurent Michon; Marie Chaput; Vincent Famin; Claudia Romagnoli

Abstract: Most basaltic volcanoes are affected by lateral instabilities of their flank during their evolution. Classical models consider the relationship between vertical intrusions of magma and flank movements along a preexisting sliding surface. A set of published and new field data allowed us to recognize the role of subhorizontal intrusions in the process of flank instability and to characterize the geometry of both subvertical and subhorizontal intrusions within basaltic volcanoes. This study compares the results of numerical modelling of the displacements associated to high-angle and low-angle intrusions within basaltic volcanoes. We use a Mixed Boundary Element Method to investigate the mechanical response of an edifice to the injection of magmatic intrusions in different stress fields. Our results indicate that the anisotropy of the stress field favours the slip along the intrusions due to cointrusive shear stress, generating flank-scale displacements of the edifice, especially in the case of subhorizontal intrusions, capable of triggering large-scale flank collapses on basaltic volcanoes. Apart from previous models of subvertical intrusions-related mechanism of collapse, our field study combined to theoretical approach confirms the importance of shallow-dipping intrusions in the morphostructural evolution of basaltic volcanoes with particular regards to flank instability.

Suggested Reviewers: Virginie Pinel
LGIT, Université de Savoie
Virginie.Pinel@univ-savoie.fr

Thomas Walter
Volcanotectonics lab, GeoForschungsZentrum
twalter@gfz-postdam.de

Eumenio Ancochea
istituto de Geologia Economica, CSIC Universidad Complutense
geodec@geo.ucm.es

Alessandro Tibaldi
Dipartimento di SCienze Geologiche e Geotechnologie, Università di Milano Bicocca
alessandro.tibaldi@unimib.it

Research highlights

> This study compares the results of numerical modelling (MBEM) of the displacements associated to high-angle and low-angle intrusions within basaltic volcanoes.
> Our results indicate that the anisotropy of the stress field favours the slip along the intrusions due to cointrusive shear stress.
> Slip along subhorizontal intrusions induces flank-scale displacements of the edifice capable of triggering large-scale flank collapses on basaltic volcanoes.
> Our study confirms the importance of shallow-dipping intrusions in the morphostructural evolution of basaltic volcanoes with particular regards to flank instability.

coverletter
Click here to view linked References

DIPARTIMENTO DI SCIENZE DELLA TERRA
E GEOLOGICO AMBIENTALI

Submission of research article: "Co-intrusive shear stress triggers flank collapse on basaltic volcanoes" by Catry et al. to *Journal of Volcanology and Geothermal Research*

Dear Editor,
the article we submit deals with the study of deformation associated with subvertical and subhorizontal intrusions below the flanks of a volcanic edifice. It represents an original contribution, based on numerical modelling (trough a Mixed Boundary Element Method) and on some new field data collected on a highly eroded basaltic volcano (Piton des Neiges, La Reunion Island). The latter data suggest that the occurrence of subhorizontal intrusions in basaltic volcanoes may be frequently underestimated.

In the article we propose that subhorizontal intrusions play a not less important role than subvertical ones in the morphostructural evolution of basaltic volcanoes and, particularly, in promoting large-scale flank collapses. The results from numerical modelling show, in fact, that within an edifice loaded by an anisotropic stress field, the co-intrusive shear stress creating slip along subhorizontal intrusions can be an efficient mechanism of high-amplitude deformation on volcano flanks.

We guess that the article we submit fits the topics of *Journal of Volcanology and Geothermal Research* because:

1) a synthetic comparison between data from literature on sheet intrusions geometry and size in basaltic volcanoes and field observation is made, and the relative occurrence of subhorizontal vs. subvertical intrusions in poorly- or highly-eroded volcanoes is discussed;
2) it is suggested that model involving magmatic intrusions should better take into account their realistic geometries, possibly deduced from field observations;
3) the quantitative importance of low-angle intrusions in volcanic flank instability is reinforced by the obtained results of numerical modelling.

Best regards,

Bologna, XX/11/2010 Thibault Catry

ALMA MATER STUDIORUM - UNIVERSITÀ DI BOLOGNA
PIAZZA DI PORTA SAN DONATO, 1 - 40126 BOLOGNA - ITALIA - TEL. 051-2094900 - FAX 051-2094904 info@geomin.unibo.it

Co-intrusive shear stress triggers flank collapse on basaltic volcanoes

T. Catry (1,2), V. Cayol (3), L. Michon (2), M. Chaput (2), V. Famin (2), C. Romagnoli (1)

(1) Dipartimento di Scienze della Terra e Geologico-Ambientali, Università di Bologna, 1 Piazza di Porta San Donato 40127 Bologna, Italy (catry.thibault2@unibo.it), (2) Laboratoire Géosciences Réunion, UMR CNRS 7154 IPGP, Université de la Réunion , Saint-Denis, France (tcatry@univ-reunion.fr), (3) Laboratoire Magmas et Volcans, UMR 6524, CNRS-IRD-Université Blaise Pascal, 5 rue Kessler, 63038 Clermont-Ferrand, France.

Abstract

Most basaltic volcanoes are affected by lateral instabilities of their flank during their evolution. Classical models consider the relationship between vertical intrusions of magma and flank movements along a preexisting sliding surface. A set of published and new field data allowed us to recognize the role of subhorizontal intrusions in the process of flank instability and to characterize the geometry of both subvertical and subhorizontal intrusions. This study compares the results of numerical modelling of the displacements associated to high-angle and low-angle intrusions within basaltic volcanoes. We use a Mixed Boundary Element Method to investigate the mechanical response of an edifice to the injection of magmatic intrusions in different stress fields. Our results indicate that the anisotropy of the stress field favours the slip along the intrusions due to cointrusive shear stress, generating flank-scale displacements of the edifice, especially in the case of subhorizontal intrusions, capable of triggering large-scale flank collapses on basaltic volcanoes. Apart from previous models of subvertical intrusions-related mechanism of collapse, our field study combined to theoretical approach confirms the importance of shallow-dipping intrusions in the morphostructural evolution of basaltic volcanoes with particular regards to flank instability.

1- Introduction

Besides erosion, flank collapse is the main cause of destruction of volcanic edifices (e.g. Moore, 1964). A longstanding problem in volcanology is to explain why flank collapse often coincides with periods of enhanced magmatic activity. In a first category of proposed explanations, the flanks of a volcano could slide on a basal shear plane dipping outward (i.e. a detachment) or landward (i.e. a decollement), pushed by recurrent subvertical magma injections (i.e. dikes) into the rift zones (Swanson et al., 1976; Dieterich, 1988; Iverson, 1995; Elsworth and Voight, 1995). However, this model requires an unrealistic amount of intrusions of reasonable dimensions to yield the observed surface deformations of volcano flanks (Iverson, 1995). An alternative end-member model has been recently proposed, in which the injection of subhorizontal intrusions (i.e. sills) in planes of weakness activates flank sliding by the sole action of gravity (Famin and Michon, 2010). The mechanical ability of such low-dipping intrusions to destabilise a volcanic edifice remains to be tested.

In this paper, we investigate how planar intrusions can induce or enhance flank collapse in a volcano, depending on their geometry. To do so, we first provide a review of the most commonly observed intrusion geometries in basaltic volcanic edifices undergoing recurrent collapses. Using a numerical Boundary Element Method, we then evaluate the pattern of co-intrusive strains related to each intrusion geometry and the associated stress field. This relationship between geometry of intrusions and deformation is investigated in the case of an edifice loaded by either an isotropic or an anisotropic stress field. Our numerical study not only shows that some intrusion geometries generate larger deformations and more flank collapse than others; it also provides keys to identify these geometries from the

73 pattern of surface edifice deformations. These theoretical results could be applied to
74 evaluate the destabilisation hazard of an eruptive crisis, provided that the surface
75 deformations are monitored in real time.

76
77

78 **2- Sheet intrusions within basaltic edifices**

79 In basaltic setting, magma is injected in the edifice as sheet intrusions rooted in a
80 magma reservoir. Field analyses carried out on active and extinct basaltic volcanoes
81 in Hawaii, American Samoa, Fogo, Tenerife, Stromboli and La Réunion have revealed
82 that steeply-dipping intrusions (70-90°, Table 1) are dominant in the upper part of
83 the edifices (< 1 km depth) (Walker, 1986; Zbinden and Sinton, 1988; Walker and
84 Eyre, 1995; Day et al., 1999; Marinoni and Gudmundsson, 2000; Tibaldi, 2003;
85 Letourneur et al., 2008). These intrusions are concentrated along preferential
86 pathways (the rift zones).

87 A strikingly different geometry have been described for the intrusive complex
88 injected in the lowermost units of the volcanic edifice of La Gomera (Canary
89 archipelago), where most of the sheet intrusions present outward shallow dips
90 ranging 0° to 30° (Cendrero, 1970, Ancochea et al., 2008). These intrusions are
91 related to the development of a shield volcano that underwent successive flank
92 collapses (Ancochea et al., 2006). Then, the volcano was cut by sub-vertical dikes
93 related to the younger edifice (Ancochea et al. 2006). Finally, abundant shallow
94 dipping intrusions also developed in the submarine sequence of La Palma (Canary
95 archipelago), above the plutonic complex (Staudigel and Schmincke, 1984;
96 Fernandez et al., 2002). In a similar way to La Gomera, shallow-dipping intrusions are

97 cut by subvertical dikes related to the younger edifice (Staudigel and Schminke,
98 1984).

99 In the southern part of Piton des Neiges volcano, the deeply incised extinct volcano
100 of La Réunion, about 60% of sheet intrusions have a dip lower than 40°. These
101 intrusions, which display radial outward dip directions (Fig. 1), are either scattered in
102 the lava pile or concentrated in narrow deformation zones. On the northern flank of
103 Piton des Neiges, the majority of sheet intrusions also dip outward at low angle (≤
104 30°), and are injected in a detachent (Famin and Michon, 2010).

105 Thus, besides subvertical intrusions, subhorizontal magma injections may occur in
106 basaltic volcanoes. The difference in the structural level cut by each intrusion
107 geometry, i.e. in subsurface for subvertical intrusions and at depth for subhorizontal
108 ones, suggests that magma is injected subhorizontally at depth and subvertically in
109 the upper part of the edifice. We consequently aim at understanding with a
110 numerical Boundary Element Method the role of subvertical or subhorizontal magma
111 injections in the volcano stability.

112

113 **3- Numerical modelling of sheet intrusions**

114

115 Theoretical studies indicate that magma should intrude perpendicular the least
116 principal stress (Anderson, 1938). If the intrusion intrudes a preexisting fracture or
117 fault (Currie and Ferguson, 1970; Gudmundsson, 1983), or is guided by a rheological
118 contrast (Kavanagh et al., 2006; Menand, 2009; Maccaferri et al., 2010), the intrusion
119 might be emplaced in a direction oblique to the minimum principal stress, resulting
120 in normal and shear displacements as preexisting shear stresses are relaxed to zero

121 as the fracture opens.

122

123 3.1 Model description

124 In order to study the response of a volcano to such an intrusion, we use a Mixed
125 Boundary Elements numerical Method (MBEM) (Cayol and Cornet, 1997) for linear
126 elastic, homogeneous and isotropic media.

127 The MBEM is a fully three dimensional method which considers realistic
128 topographies as well as any number and geometry of sources, such as magma
129 reservoir, intrusions or faults. Boundary conditions are stresses. Here, perturbations
130 (driving stresses) of the initial state of stress are calculated and applied to the
131 fractures in order to investigate the resulting displacement field. Our model is static,
132 as we are interested in the final deformation produced by the intrusion.

133 A Young's modulus E = 5GPa and a Poisson's ratio υ = 0.25 were inferred from
134 seismic velocities at Piton de la Fournaise neighbour volcano (Nercessian et al., 1996;
135 Brenguier et al., 2007; Prono et al., 2009), corrected by a factor of 0.25 to account
136 for the difference between dynamic and static moduli at a low confining pressure
137 (Cheng and Jonston, 1981).

138 The topography and the fractures (sheet intrusions) are meshed by triangular
139 elements. Mesh density increases in areas where deformation gradients are
140 expected to be the largest and decreases further (Fig.2). Slopes of basaltic volcanoes
141 usually range from few degrees to 12° (Rowland and Garbeil, 2000) although some
142 volcanic edifices, such as Piton de la Fournaise and Stromboli, have unusual slopes
143 locally reaching 20 to 35°. An axial-symmetrical cone-shaped topography with 20°
144 slopes is thus used (Fig.2). As the slope of the edifice has little influence on

displacements if it is not steeper than 20° (Cayol and Cornet, 1998), this assumption seems reasonable.

3.2 Intrusions geometry

Since the geometry of subhorizontal intrusions is poorly-constrained by field data, we assumed both kind of intrusions are planar and have a trapezoidal shape (Fig.3a). Indeed, at Piton de la Fournaise volcano, the inversion of Insar and GPS data showed that the geometry of intrusions that occurred in the 1998-2005 period (Fig.5a, Fukushima et al., 2010; Peltier et al., 2007; Peltier et al, 2008) was very often trapezoidal . Here, the size of the intrusions is such that both sills and dikes have the same area. Following field studies, we assume that subvertical intrusions have dips ranging from 60 to 90° and that subhorizontal intrusions have dips ranging from 180° to 200° (Fig.3b).

The intrusions are assumed to be injected from a reservoir located at 2.5-3 km below the summit of the edifice, corresponding to the level of neutral buoyancy in basaltic edifices (Tilling and Dvorak, 1993). Neutral buoyancy is the level where magma density equal density of the surrounding rocks. This depth is the depth of the top of summit reservoir determined at Kilauea, Mauna Loa, Krafla (Tryggvason, 1984) and Piton de la Fournaise (Peltier et al., 2007 and 2008; Nercessian et al., 1996; Battaglia et al., 2005). As the modelled edifice is 2.5 km high, in our models, the top of the subhorizontal intrusions and the bottom of the subvertical intrusions are located at sea level, beneath the axis of symmetry of the topography.

170 3.3 Principal stresses in the edifice

171 Initial principal stresses in the elastic medium are assumed to be parallel to the
172 geographic axis at the location of the intrusions. Indeed, maximum principal stress
173 directions resulting from gravity-loaded models, were shown to be subvertical
174 except for the shallowest part of the edifice where they become parallel to the
175 ground surface (Cayol and Cornet, 1998; Letourneur et al, 2008). These principal
176 stresses will be refered to as σ_v and σ_h, for the vertical and horizontal principal
177 stresses, respectively.

178 We define the stress ratio *k* as

179 $$k = \sigma_h / \sigma_v \qquad (1)$$

180 In this study, displacements associated to injections in edifices loaded by two
181 different initial state of stress are compared. (I) the initial stress is assumed to be
182 isotropic with terms equal to the weight of rocks such that the ratio *k* is 1 (ii) the
183 initial stress is assumed to be anisotropic, such that the maximum principal stress is
184 vertical and the ratio *k* is <1.

185 A crude estimate of the crust stress ratio *k* is given by considering a half-space
186 deforming uniaxially under its own weight (no horizontal extension). For this special
187 case, the stress ratio is determined to be (Jaeger and Cook, 1979):

188 $$k = \frac{\sigma_h}{\sigma_v} = \frac{\upsilon}{(1-\upsilon)} = 1/3 \text{ for } \upsilon = 0.25 \qquad (2)$$

189 This loading neglect pore fluids and that fact that the state of stress in a edifice
190 results from the successive episodes of tectonic loading and faulting. There are
191 several evidence that the crust is critically stressed. In volcanic islands as well as
192 continental crust, stress changes created by fluids movement, whether magmatic

(Dieterich et al., 2000), acqueous or gasous (Roeloffs, 1996; Segall et al., 1994) or resulting from fault motions (Stein et al., 1992; Segall et al., 2006), trigger seismicity. In situ stress measurements in deep wells and Boreholes worldwide (Townsend and Zoback, 2000) show that Coulomb failure theory, using friction coefficients, μ, in the range of 0.6-1, give predictions that are consistent with the measurements. These studies also indicate that pore pressures are close to hydrostatic. Assuming the crust is in a state of failure equilibrium, we can compute the stress ratio *k* of a fluid saturated crust as :

$$\frac{\sigma_h}{\sigma_v} = \frac{\sqrt{1+\mu^2}-\mu}{\sqrt{1+\mu^2}+\mu} + 2\frac{\rho_w}{\rho_r}\frac{\mu}{\sqrt{1+\mu^2}+\mu} \qquad (3)$$

where, ρ_w and ρ_r are the density of water and the bulk density of volcanic rock, respectively. Taking = 2700 kg/m3 and considering friction coefficients corresponding to extreme values of laboratory experiments (0.6-1), we get ratios of σ_h / σ_v ranging from $\sigma_h / \sigma_v = 0.5$ for = 1 to $\sigma_h / \sigma_v = 0.9$ for = 0.6.

Here, we have chosen to investigate the displacements induced by stress anisotropy such that: $0{,}6 < k < 1$ (4)

3.4 Applied traction perturbation

At the fracture surface (see Figure 4 for a description of the model parameters), the stress perturbations tensor corresponding to the intrusion of magma in the elastic rock matrix is defined as :

$$\Delta\sigma(z) = \begin{bmatrix} P_m(z)-k\sigma_v(z) & 0 & 0 \\ 0 & P_m(z)-k\sigma_v(z) & 0 \\ 0 & 0 & P_m(z)-\sigma_v(z) \end{bmatrix} \qquad (5)$$

where $P_m(z)$, the magma pressure is created by the magma density, ρ_m,

in the inclined fracture with its top at z_0, and an constant overpressure ΔP_0, inherited from the magmatic source:

$$P_m(z) = \rho_m g(z_0 - z) + \Delta P_0 \qquad (6)$$

We asume that, in the edifice, the maximum principal stress σ_v is lithostatic. It is given by

$$\sigma_v(z) = \rho_r g(z_{surf} - z) \qquad (7)$$

Here, ρ_r is the bulk density of rocks and z_{surf} is the elevation of the surface above each fracture element.

Normal stress change, $\Delta\sigma_n(z)$, and shear stress change, $\Delta\tau(z)$, resolved on the fracture, dipping at an angle α, can be computed from equation (5) and are given as:

$$\Delta\sigma_n(z) = P_m(z) - \sigma_v(z)(k\sin\alpha^2 + \cos\alpha^2) \qquad (8)$$

and

$$\Delta\tau(z) = \sigma_v(k-1)\cos\alpha\sin\alpha \qquad (9)$$

Practically, in our boundary element code, we apply tractions vectors, T, to each triangular element of the fractures corresponding to:

$$\mathrm{T} = \Delta\sigma(z)n, \qquad (10)$$

where $\Delta\sigma(z)$ is given by (5) and $n = (\sin\alpha, 0, \cos\alpha)^{\mathrm{T}}$ is the unit normal vector to the fracture.

In the calculations, we the take the same bulk density of rocks as used for defining ranges of stress ration = 2700 kg/m3. The picritic magma density is taken as ρ_m= 3200 kg.m^{-3}. We also compute the value of so that the mean value of the normal stress change corresponds to normal stress change generally inferred for intrusions. From the inversion of GPS and InSAR displacements associated to recent eruptions of Piton de la Fournaise volcano (Peltier et al, 2007;

2008; Fukushima et al., 2010), values of overpressure were determined to range from 0.3 to 6 MPa.

At Stromboli volcano, using ground-based InSAR displacements and forward numerical modelling, Casagli et al. (2009) estimated overpressures of 0 to 1 MPa for the pre-effusive displacements of the 2007 eruption.. At Sierra Negra volcano (Galapagos Island), a sill overpressure of 4.5 MPa was estimated at a depth of 2 km from the inversion of InSAR data. In our models, we assume a mean value of normal stress change of $\overline{\Delta\sigma_n(z)}$= 1 MPa.

4- Results

Modelling results for several dip angles of subhorizontal and subvertical intrusions are first presented at the beginning of the section then 2 cases are discussed : 1- a75°-dip intrusion, as described in Oahu Island (Walker, 1986) and determined from Piton des Neiges data and 2- a 10°-dip intrusion, as determined for sills at Piton des Neiges. We compare the maximum opening and slip at the intrusion surface and surface displacement of the edifice , for stress fields having different stress anisotropies *k* and dip angles.

Dip of the intrusion (Fig. 5)

In an anisotropic stress field, the opening of the subhorizontal intrusion increases when the dip increases due to the decreasing effect of $\sigma_{vertical}$ when the inclination of the sill gradually reaches 200°. The opening is then facilitated in the direction of the smallest stress. The case of the subvertical intrusion is more complex: one can intuitively expect that when the subvertical intrusion becomes vertical, the opening

264 is higher than for a intrusion inclined of 60° because of the decreased influence of
265 the vertical stress. However, the opening of the intrusion increases when its dip
266 decreases. The behaviour of the opening of the subvertical intrusion can be
267 explained by the fact that the slip increase (Fig. 5b), which facilitates the opening in a
268 direction normal to the intrusion, balancing the effect of the vertical stress. The
269 opening of the intrusions in an anisotropic stress field is therefore influenced by the
270 dip of the intrusion and the shear stress creating slip along the intrusion.
271 Figure 7b shows that in isotropic conditions there is no slip along the intrusions,
272 whatever their dip, while in anisotropic stress field an increase of the dip of a
273 subhorizontal intrusion creates an increase of the slip along it because the shear
274 stress is stronger when the obliquity towards σ3 (= $\sigma_{horizontal}$) increases. The slip along
275 the subvertical intrusion increases with the decrease of the dip due to stronger
276 influence of $\sigma_{vertical}$ (load of the edifice).
277 The fact that in isotropic stress field, the dip has no influence on the slip along the
278 intrusions which is always close to 0 (Fig. 5b) and poor influence on the opening of
279 the intrusions (Fig. 5a) results in small-amplitude surface displacements (Fig. 5c and
280 d). On the contrary, the fact that an anisotropic stress field favours the increase of
281 opening and slip due to dip variations creates large amplitude displacements at the
282 surface of the edifice (Fig. 5c and d).
283 Large scale deformation events seem to require a combination of opening of the
284 intrusions and slip along the intrusions, enhanced by the anisotropy of the stress
285 field loading the edifice.
286
287 *Anisotropy* (Fig. 6)

This section investigates the role of the anisotropy on the opening, slip, and surface displacements. This has been tested for dip values fixed at 75° and 190° for the subvertical and subhorizontal intrusions, respectively (Fig. 5b).

When the anisotropy raises (*k* from 1 to 0.6) the opening of the intrusions increases because the horizontal component of the stress is smaller and smaller compared to the vertical stress. Normal opening in the direction of the the horizontal stress is thus favoured. This increase is larger for high-angle intrusion than for low-angle one because this latter is submitted to stronger effects of the edifice load (Fig. 6a). The increase of the anisotropy ratio facilitates the slip along the intrusions because σ3 (= $\sigma_{horizontal}$) is lower and lower compared to $\sigma_{vertical}$ (= σ1), increasing the shear stress (Fig 6b). Finally, since a low value of anisotropic stress field encourages the combined effects of opening and slip, it creates large amounts of internal and eastward surface displacements of the edifice (Fig. 6c and d), confirming the previous results of figure 5.

Opening and slip

In this and in the following section, the results obtained for a 75°-dipping and 190°-dipping intrusions are taken into account in case of isotropic and anisotropic stress field, respectively. In our model, all magmatic bodies are intruded at the level of the sea. An internal overpressure of 1 MPa in a subvertical intrusion (75°) creates, in an isotropic stress field, a maximum opening (thickness) reaching 1 m at the center of the intrusion (Fig.7a1). Because of the isotropic stress field, the intrusion is not submitted to shear stress and the slip along it is equal to 0 (Fig. 7a3). The geometry of a subhorizontal intrusions, in the same conditions of overpressure and stress field,

313 shows that the maximum opening is about 1 m in the center and the head of the
314 fracture (fig. 7a2). As for a subvertical intrusion, when the intrusion is not submitted
315 to shear stress the slip along it is null (fig. 7a4). The opening is clearly predominant
316 over the slip if the sheets intrude in an isotropic stress field. As defined in the
317 previous section, the anisotropic stress field implies a ratio $k \neq 1$. Here, we have
318 chosen to display the case of $\sigma_{horizontal} / \sigma_{vertical} = 0.8$. Apart from the nature of the
319 stress field, all other parameters remain the same as in the case of an isotropic stress
320 field (geometry of the intrusions, overpressure of 1MPa, etc.). Because of
321 topographical effects and the structure of a natural edifice (with variations of
322 volcanic products in space and time, existence of rift-zones and fractures, etc.) a
323 model where the edifice is loaded by an anisotropic stress field seems more realistic
324 to investigate its mechanical response to magmatic intrusions.
325 Figure 7b shows that when a subvertical intrusion occurs in an anisotropic stress
326 field, unlike the previous case, the geometry of the intrusion is controlled both by
327 the opening and the slip due to shear stress. In this case, the opening is 2.5 times
328 stronger than in an isotropic stress field (Fig. 7b1), and the slip appears to be as high
329 as the opening (Fig. 7b2). As for the subhorizontal intrusion, the opening is of the
330 same order as in isotropic stress field (Fig. 7b3) with a maximum value of 1m (the
331 effect of the topography is much stronger in this case, partly preventing the normal
332 opening of the intrusion) while the slip becomes predominant reaching 4m (Fig.7b4).
333 In anisotropic stress field thus, the opening and the slip both play a role in the
334 mechanical effects of a magmatic intrusion on the edifice.
335
336 *Surface displacements* :

For what regards the surface deformation in isotropic stress field, the results show that :

- an outward 75°-dip intrusion submitted to 1 MPa overpressure creates outward displacements of small amplitude, with a maximum value of 0.3 m (Fig.8a). Vertical displacements reach 0.15 m (Fig. 9a). The surface displacements exhibit an area of maximum deformation circular in shape, reaching around 0.25 m of maximum displacements but limited in the summit area of the volcano (few kilometers from the top of the cone). At the periphery of the edifice apex, the surface displacements decrease strongly and are close to 0 (negative values correspond to inward or downward movements, Fig.8a and 9a).

- in the case of a subhorizontal intrusion (8 km long), the displacements remain of small amplitude (Fig. 8a and 9a on the right), similar to that due to high-angle intrusions (Fig. 8a and 9a on the left). The deformation is located below the flank of the edifice, with a vertical and an outward component. The maximum surface displacements area is located above the head of the intrusion, on the volcano flank between 8 to 12 km from the summit and displacements reach 0.2 - 0.3 m.

In an anisotropic stress field, the patterns of internal displacements and surface deformation are similar to those obtained in isotropic stress field but the amplitudes of displacements strongly increase (Fig 8b and 9b). The area affected by intrusions is still located below the summit and the flank of the edifice respectively, but the 0.8/0.6 m (instead of 0.3/0.15 m) at the surface (Fig. 8 and 9). The directions of

displacements indicate that for a subhorizontal intrusion submitted to shear stress, the outward movements are stronger than in the case of isotropic stress field reaching 0.5 m against 0.15 m (Fig. 8b).

5- Discussion

5.1- Occurrence of subhorizontal intrusions within basaltic edifices

A large variety of geometries of sheet intrusions has been documented through field observations (see section 2). Field data collected in the inner structure of Piton des Neiges volcano (La Reunion Island) point out a discrepancy that may occur studying young, poorly-eroded, or old, highly-eroded, basaltic volcanoes: when the erosion gives access to the core of the edifice, measured intrusions are mostly subhorizontal, while subvertical ones mostly occur at shallower levels. The distribution of intrusions and the transition between high angle/low angle intrusions seem to be controlled by the depth of injection within the edifice. The deeper the injection, the more frequent are subhorizontal intrusions. Other basaltic volcanoes like La Palma and La Gomera in the Canary islands (Ancochea et al., 2008) show that an important part of magmatic intrusions is made of subhorizontal intrusions, espaecially in the deepest parts of the edifices corresponding to the early stages of the construction of the volcanoes.

According to some field studies, low-angle intrusions preferentially intrude weak layers (Taisne and Jaupart, 2009; Famin and Michon, 2010). In particular, the

386 geometry of low-angle intrusions is commonly explained by topographical effects
387 and the occurrence of heterogeneities such as the interface between two volcanic
388 deposits with different physical properties (Lister and Kerr, 1991; Rivalta, 2005;
389 Kavanagh et al., 2006) in the volcanic edifice. Moreover, the distribution of some
390 intrusions can not be simply explained by lateral propagation of magma at the Level
391 of Neutral Buoyancy (Lister and Kerr, 1991). A local rotation of the stress field due to
392 the presence of heterogeneities is more likely at the origin of the observed
393 geometries (Valentine and Krogh, 2006; Burchardt, 2008).

394 Gressier et al. (2010) showed that, in sedimentary basins, the depth of the
395 transition subvertical/subhorizontal intrusions may be controlled by the pore fluid
396 overpressure. Due to their low permeability, in fact, rocks in sedimentary basins
397 often contain fluids in overpressure and this condition encourages the formation of
398 hydraulic fractures and the propagation of magmatic injections. The deep outcrops
399 at Piton des Neiges volcano (400-1500 m) are mainly made of primitive basic
400 breccias, formed during the first stage of the volcano-structural evolution of the
401 edifice (Chevallier and Vatin-Perignon, 1982; Maillot, 1999). These breccias are
402 highly altered by hydrothermal processes due to the circulation and accumulation of
403 fluids. The alteration tends to lower the permeability of the breccia, allowing the
404 increase of the pore fluid pressure within the formation. The overpressure can also
405 be favoured by the fact that, generally, breccia levels are stratigraphically located
406 between levels of massive, several meters-thick lava flows, sealing the breccia. In
407 Piton des Neiges volcano, the breccia commonly lies on differentiated lava flows and
408 is covered by the same lava flows.

409 Breccia levels commonly found within basaltic volcanoes thus are likely to be

410 in pore fluid overpressure conditions that, associated to heterogeneities (Gressier et
411 al., 2010), can favour the formation of subhorizontal intrusions in the deepest part of
412 the edifices, like at Piton des Neiges volcano. In addition, in an anisotropic media
413 (Kavanagh et al, 2006; Gressier et al, 2010 and this study), an excess in pore pressure
414 (compared to hydrostatic value) is sufficient to enhance the formation of
415 subhorizontal intrusions.
416 Low-angle injections have also been described on young, active and poorly-eroded
417 volcanoes. At Piton de la Fournaise volcano, as already suggested by Famin and
418 Michon (2010), the recently observed deformation of the eastern flank could be
419 linked to the injection of a subhorizontal intrusion below the flank of the edifice.
420 Drillings carried out in 1989 in the Grand-Brûlé area (lowest part of the Enclos-
421 Grand-Brûlé-Structure, Michon et al., 2008) identified levels of piled thin « layers » of
422 picritic basalts (Rançon et al., 1989) at the contact between a frozen magmatic
423 chamber and superficial lava flows. These layers could have played the same role as
424 the subhorizontal intrusions described by Famin and Michon (2010) in the Cirque de
425 Salazie (Piton des Neiges volcano), where picritic sills triggered the reactivation of a
426 preexisting detachment fault involved in the large-scale flank destabilization of the
427 Northeastern flank of the edifice.
428 Future studies on other basaltic volcanoes could reveal that subhorizontal intrusions
429 are common in the deep parts of the edifices, emphasizing their role in the morpho-
430 structural evolution of basatic volcanoes.
431
432
433

5.2- Large scale flank displacements enhanced by shear stress on basaltic volcanoes

Our results indicate that an increase in the ratio of anisotropy generates an increase of internal and surface deformation, by favouring the slip along the intrusions in an anisotropic stress field (Fig. 10), especially in the case of subhorizontal intrusions.

5.2.1- origin of the anisotropic stress field

The conditions of formation and/or propagation/arrest of magmatic intrusions within volcanoes depend on the state of stress of the edifice. The state of stress is controlled itself by the mechanical properties of the material constituting the volcano and by the loading conditions (i.e. internal and external pressures applied to the edifice). Our study considers the influence of an anisotropic stress field on the mechanical evolution of an edifice associated to magmatic intrusions, in order to account for more realistic state of stress within basaltic volcanoes. This aspect is often described at stratovolcanoes where internal heterogeneities are common due to the variety of activity and eruptive products.The anisotropic stress field loading basaltic volcanoes can have several origins like topographical effects, heterogeneities in the edifice (presence of rift-zones, fractures, interface between layers with different mechanical properties), buttressed/unbuttressed flanks.

Gressier (2010) confirmed experimentally that an anisotropic stress field favours the formation of subhorizontal intrusions within volcanic edifices.

459

460 5.2.2- Role of shear stress in the displacements fields on basaltic volcanoes

461 In an anisotropic stress field the shear stress creating slip along the subhorizontal
462 intrusions favours the lateral displacement of the flank of the edifice. The slip has
463 also an influence on the opening of the intrusion, which is increased when combined
464 to slip so that a complex relationship occurs between opening/slip and deformation
465 of the edifice.

466 Combined to the data obtained for an isotropic stress field where smal amplitude of
467 displacements are observed, our results prove that the shear stress occurring in
468 anisotropic stress field creates the conditions that allow slipping along intrusions
469 generating large-scale deformation of the edifice. The shear stress affects both
470 subvertical and subhorizontal intrusions. However, this effect is very localised on
471 high-angle intrusions where around 2 % of the surface of the intrusion is affected by
472 maximum slip of 2.6 m (Fig. 7) while it concerns the whole surface of the low-angle
473 intrusion reach 4 m of slip (Fig. 7). This is due to the fact that in the case of
474 subhorizontal intrusion, the maximum principal stress σ1 (vertical stress) has a
475 stronger influence, the load of the edifice leading to lateral slip in the direction of the
476 minimum principal stress σ3 (less constrained direction) and high amplitude
477 displacements , located below the flank of the edifice. In the case of subvertical
478 intrusions, High amplitude displacmements are generated by the combination of
479 localised opening (in the direction of σ3) + slip affecting a smaller area of the apex of
480 the edifice (Fig. 8 and 9).

481

482 Our theoretical results evidence a new mechanism of large-scale flank collpase on

483 basaltic volcanoes: the co-intrusive shear stress creating slip along subhorizontal
484 intrusions in an anisotropic stress field leads to flank-scale deformation of basaltic
485 edifices, likely to trigger large sector collapses of the edifices.
486
487 The case discussed by Famin and Michon (2010) in the core of Piton des Neiges
488 volcano is the first observable outcrop where a detachment plane is in direct
489 relationship with low-angle intrusions. Together with the submarine evidence
490 offshore La Reunion (Oehler et al., 2004), these authors underline that this volcano
491 experimented a major (long-term) destabilization of its northeastern flank. The
492 repeated low-angle intrusions should have reactivated a preexisting slip surface,
493 generating large movements of the unbuttressed flank of the volcano towards the
494 North. Some other examples of basaltic volcanoes underline a probable role of
495 subhorizontal intrusions in the deformation of the edifice like at Stromboli volcano
496 (Casagli et al., 2009) or Piton de la Fournaise volcano (Famin and Michon, 2010). At
497 mount Etna, Walter et al. (2005) studied the interplay between subvertical intrusions
498 and flank movements based on numerical modelling (BEM). They showed that the
499 flank-scale movements at Etna can be triggered by subvertical injections on magma
500 when combined to movements along major faults (Pernicana, Trescastagni, Ragana
501 and Santa Venerina fault systems and basal detachment) favouring outward slip of
502 the whole flank. Although a lot of studies consider the role of vertical intrusions as
503 trigger of flank collapses on volcanoes (Dahlen, 1984; Dieterich, 1988; Iverson, 1995;
504 Elsworth and Voight, 1995; Elsworth and Day, 1999), our theoretical results and the
505 example of mount Etna underline that high-angle intrusions alone are not the only
506 way to generate flank-scale deformation triggering sector collapses on basaltic

volcanoes. Another trigger has to be considered : subhorizontal intrusions in pre-existing detachments below edifices flanks. Piton des Neiges, Piton de la Fournaise and Etna well illustrate the interaction between magmatic intrusion, slipping plane and flank failure on volcanoes.

6- Conclusion

Our study based on the combination of new field data on the Piton des Neiges volcano (La Reunion Island) and results from numerical modelling brings new insights on the contribution of magmatic intrusions in the process of volcano flank instability. The statistical study of the populations of basaltic intrusions from published data and recent measurements on basaltic volcanoes show that not only the role of subvertical but also subhorizontal intrusions have to be considered in the morpho-structural evolution of basaltic volcanoes. The quantitative importance of low-angle intrusions is reinforced by the theoretical analysis we carried out using a MBEM. A new model of interaction between intrusions and flank-scale movements is evidenced : within an edifice loaded by an anisotropic stress field, it appears that the co-intrusive shear stress creating slip along subhorizontal intrusions is an efficient mechanism of high-amplitude deformation of volcano flanks, triggering large-scale sector collpases on basaltic volcanoes.

References

Ancochea E., Hernan, F., Huertas, M.J, Brandle, J.L., Herrera, R., 2006. A new chronostratigraphical and evolutionary model for La Gomera: Implications for the overall evolution of the Canarian Archipelago. *J. Volcanol. Geotherm. Res.,* **157**, Issue 4, 271-293.

Ancochea, E., Brandle, J.L., Huertas, M.J., Hernan, F., Herrera, R., 2008. Dike-swarms, key to the reconstruction of major volcanic edifices: The basic dikes of La Gomera (Canary Islands). *J. Volcanol. Geotherm. Res*., **173**, 207-216.

Anderson, E. M., 1938. The dynamics of sheet intrusion. *Proc. R. Soc. Edinburgh*, **58**, 242–251.

Battaglia, J., Ferrazzini, V., Staudacher, T., Aki, K., Cheminée, J.L., 2005. Pre-eruptive migration of earthquakes at the Piton de la Fournaise volcano (Réunion Island). *Geophys. J. Int.*, **161**, 549–558.

Brenguier, F., Shapiro, N.M., Campillo, M., Ferrazzini, V., Nercessian, A., Coutant, O., Duputel, Z., 2007. Seismic imaging and monitoring of the Piton de la Fournaise volcano from ambient seismic noise correlations. *Geophysical Research Abstracts*, **9**, 01326.

Burchardt, S., 2008. New insights into the mechanics of sill emplacement provided by field observations of the Njardvik Sill, Northeast Iceland. *J. Volcanol. Geotherm. Res.*, **173**, *3-4*,280-288.

Casagli, N., Tibaldi, A., Merri, A., Del Ventisette, C., Apuani, T., Guerri, L., Fortuny-Guasch, J., Tarchi ,D., 2009. Deformation of Stromboli Volcano (Italy) during the 2007 eruption revealed by radar interferometry, numerical modelling and structural geological field data. *J. Volcanol. and Geotherm. Res.,* **182,** 3-4, 182-200.

Cayol, V. and F. H. Cornet, 1997. 3D mixed boundary elements for elastostatic déformation fields analysis. *Int. J. Rock Mech. Min. Sci. Geomech. Abstr.*, **34**, 275–287.

Cayol, V. and F.H. Cornet, 1998. Three-dimensional modelling of the 1983-1984 eruption at Piton de La Fournaise Volcano, Reunion Island. *J. Geophys. Res*, **103**, n°B8: 18025-18037.

Cendrero, A., 1970. The volcano plutonic complex of La Gomera, *Bull. Volcanol*., **34**:537–561.

Cheng, C.H. and D.H. Johnston, 1981. Dynamic and static moduli. *Geophys. Res. Left*., **8**, 39-42.

Chevallier L. and N. Vatin-Pérignon, 1982. Volcano-structural evolution of Piton des Neiges, Reunion Island*. Indian Ocean. Bull. Volc*., **45**:285-298.

Currie K.L. and J. Ferguson, 1970. The mechanism of intrusion of lamprophyre dikes indicated by 'Offsetting' of dikes. *Tectonophysics*, **9**, Issue 6, 525-535.

Day, S.J., Carracedo, J.C., Guillou, H., Gravestock, P., 1999. Recent structural evolution of the Cumbre Vieja volcano, La Palma, Canary Islands: volcanic rift

zone reconfiguration as a precursor to volcano flank instability? *J. Volcanol. Geotherm. Res.*, **94**, 135-167.

Dieterich, J. H., 1988. Growth and persistence of Hawaiian volcanic rift zones. *J. Geophys. Res.*, **93**,4258–4270.

Dieterich, J.H., Cayol, V., Okubo, P., 2000. The use of earthquake rate changes as a stress meter at Kilauea volcano. *Nature* , **408** , 457-460.

Elsworth D. and B. Voight, 1995. Dike intrusion as a trigger for large earthquakes and the failure of volcano flanks. *J. Geophys. Res.,* **100**, 6005-6024.

Elsworth D. and S.J. Day, 1999. Flank collapse triggered by intrusion: the Canarian and Cape Verde Archipelagoes. *J. Volcanol. Geotherm., Res.* **94**, 323-340.

Famin, V. and L. Michon, 2010. Volcano destabilization by magma injections in a detachment. *Geology,* **38***,* 3, 219-222.

Fernández, C., De la Nuez, J., Casillas, R., García, E., 2002. Stress fields associated with the growth of a large shield volcano (La Palma. Canary Islands). *Tectonics*, **20**, 367–384.

Fukushima, Y., Cayol, V., Durand, P., Massonnet, D., 2010. Evolution of magma conduits during the 1998–2000 eruptions of Piton de la Fournaise volcano, Réunion Island. *J. Geophys. Res.,* **115**, B10204, doi:10.1029/2009JB007023.

Gressier, J.B, Mourgues, R., Bodet, L., Matthieu, J.Y., Galland, O., Cobbold, P., 2010. Control of pore fluid pressure on depth of emplacement of magmatic sills: An experimental approach. *Tectonophysics***, 489**, 1-4, 1-13.

Gudmundsson, A., 1983. Form and dimensions of dykes in eastern Iceland. *Tectonophysics,* **95**, 295– 307.

Iverson, R.M., 1995. Can magma-injection and groundwater forces cause massive landslides on Hawaiian volcanoes? *J. Volcanol. Geotherm. Res.,* **66**, 295-308.

Jaeger, J. C., and N. G.W. Cook, 1979. *Fundamentals of rock mechanics*, Chapman and Hall, London, 3rd ed.

Kavanagh, J. L., Menand, T., Sparks, R.S.J, 2006. An experimental investigation of sill formation and propagation in layered elastic media. *Earth Planet. Sci. Lett.,* **245***,* 799–813.

Letourneur, L., Peltier, A., Staudacher, T., Gudmundsson, A., 2008. The effects of rock heterogeneities on dyke paths and asymmetric ground deformation: The example of Piton de la Fournaise (Reunion Island*). J. Volc. Geotherm. Res.,* **173***, 3-4*, 289-302.

631 Lister, J.R. and R.C. Kerr, 1991. Fluid-mechanical models of crack propagation and
632 their application to magma transport in dykes. *J. Geophys. Res.,* **96***,* 10049–
633 10077.
634
635 Maccaferri, F., Bonafede, M., Rivalta E., 2010. A numerical model of dyke
636 propagation in layered elastic media. *Geophys. J. Int.,* **180,** 1107–1123.
637
638 Maillot, E., 1999. Les systèmes intrusifs des volcans boucliers océaniques: Ile de la
639 Réunion (Océan Indien), *thèse de doctorat, Université de la Réunion*.
640
641 Marinoni, L.B. and A. Gudmundson, 2000. Dykes, faults and paleostresses in the
642 Teno and Anaga massifs of Tenerife (Canary Islands). *J. Volc. Geotherm. Res.,*
643 **103***,* 83-103.
644
645 Marinoni, L.B., 2001. Crustal extension from exposed sheet intrusions: a review and
646 method proposal. *J. Volc. Geotherm. Res.,* **107***,* 27-46.
647
648 Menand T., 2009. Physical controls and depth of emplacement of igneous bodies: A
649 review. *Tectonophysics*, in press, DOI:10.1016/j.tecto.2009.10.016.
650
651 Menand, T., Daniels, K.A., Benghiat, P., 2010. Dyke propagation and sill formation in
652 a compressive tectonic environment. *J. Geophys. Res***.**, **115**, No. B8, B08201.
653
654 Moore, J. G., 1964. Giant submarine landslides on the Hawaiian ridge. *U.S. Geol.Surv.*
655 *Prof. Pap.*, **501-D**, 95–98.
656
657 Nercessian, A., Hirn, A., Lepine, J.C., Sapin, M., 1996. Internal structure of Piton de la
658 Fournaise volcano from seismic wave propagation and earthquake distribution.
659 *J.Volcanol. Geotherm.Res.*, **70**, 123–143.
660
661
662 Oehler, J.F., Labazuy, P., Lénat, J.F, 2004. Recurrence of major flank landslides during
663 the last 2-Ma-history of Reunion Island*. Bull. Volc.,* **66***,* 585–598.
664
665 Peltier, A., Staudacher, T., Bachèlery, P., 2007. Constraints on magma transfers and
666 structures involved in the 2003 activity at Piton de La Fournaise from
667 displacement data. *J. Geophys. Res*, **112**, B03207, doi:10.1029/2006JB004379.
668
669 Peltier, A., Famin, V., Bachèlery, B., Cayol, V., Fukushima, Y., Staudacher, T., 2008.
670 Cyclic magma storages and transfers at Piton de la Fournaise volcano (La
671 Réunion hotspot) inferred from deformation and geochemical data. *Earth*
672 *Planet. Sci. Lett*., **270**, 3-4, 180–188.
673
674 Prono, E., Battaglia, J., Monteiller, V., Got, J.L., Ferrazzini, V., 2009. P-wave velocity
675 structure of Piton de la Fournaise volcano deduced from seismic data recorded
676 between 1996 and 1999.*J. Volcanol. Geotherm. Res.,* **184***, 1-2, Recent advances*
677 *on the geodynamics of Piton de la Fournaise volcano*, 49-62.

Rancon, J.P., Lerebour,P., Augé, T., 1989. The Grand Brule exploration drilling : new data on the deep Framework of the Piton de la Fournaise volcano. Part 1 : lithostratigraphic units and volcanostructural implications. *J. Volcanol. Geotherm. Res*., **36**, issues 1-3, 113-127.

Rivalta, E., Böttinger, M., Dahm, T., 2005. Buoyancy-driven fracture ascent: Experiments in layered gelatine. *J. Volcanol. Geotherm. Res.,* **144**, 273–285.

Roeloffs, E., 1996. Poroelastic Techniques in the Study of Earthquake-Related Hydrologic Phenomena, In: Renata Dmowska and Barry Saltzman, Editor(s). *Advances in Geophysics,* **37**, Pages 135-195.

Rowland, S.K., and H. Garbeil, 2000. Slopes of oceanic basalt volcanoes, *in* Mouginis Mark, P.J.C.J.A.F.J.H., ed., Fall Meeting of the American-Geophysical Union: San Francisco, Ca, Amer Geophysical Union, p. 223-247.

Segall, P., Grasso, J.R., Mossop, A., 1994. Poroelastic stressing and induced seismicity near the Lacq gas field, southwestern France. *J. Geophys. Res.,* **99**, 15,423-15,438.

Segall, P., Desmarais, E., Shelly, D., Miklius, A., Cervelli, P., 2006. Earthquakes triggered by silent slip events on Kilauea volcano, Hawaii. *Nature*, **442**.

Staudigel H. and Schmincke H. U., 1984. The Pliocene Seamount series of La Palma, Canary Islands. *J. Geophys. Res.*, **83**,11195-11215.

Stein, R.S., King, G.C.P, Lin, J., 1992. Change in Failure Stress on the Southern San Andreas Fault System Caused by the 1992 Magnitude = 7.4 Landers Earthquake. *Science* **258** (5086), 1328. [DOI: 10.1126/science.258.5086.1328].

Swanson, D.A., Duffield, W.A., Fiske, R.S., 1976. Displacement of the south flank of Kilauea Volcano: The result of forceful intrusion of magma into the rift zones : interpretation of geodetic and geologic information leads to a new model for the structure of Kilauea Volcano. *U.S. Govt. Print. Off.* (Washington), 101-676-452.

Taisne, B., and C. Jaupart, 2009. Dike propagation through layered rocks. *J. Geophys. Res*., **114**, B09203, doi:10.1029/2008JB006228.

Tibaldi, A., 2003. Influence of cone morphology on dykes, Stromboli, Italy. *J. Volcanol. Geotherm. Res.,* **126**, 1-2, 79-95.

Tilling, R.I. and J.J Dvorak, 1993. Anatomy of a basaltic volcano. *Nature*, **363**, 125-132.

Townsend, J., and M. D. Zoback, 2000. How faulting keeps the crust strong. *Geology*, **28**(5), 399– 402.

Tryggvason, E., 1984. Widening of the Krafla fissure swarm during the 1975-1981 volcano-tectonic episode. *Bull. Volcanol*., **47**: 47-69.

Valentine, G.A. and K.E.C. Krogh, 2006. Emplacement of shallow dikes and sills beneath a small basaltic volcanic center – The role of pre-existing structure (Paiute Ridge, southern Nevada, USA). *Earth Planet. Sci. Lett.*, **246**, 217–230.

Walker, G.P.L., 1986. Koolau dike complex, Oahu: Intensity and origin of a sheeted dike complex high in a Hawaiian volcanic edifice. *Geology*, **14**, p. 310–313.

Walker, G.P.L. and P.G. Eyre, 1995. Dyke complexes in American Samoa. *J. Volcanol. Geotherm. Res., **69**,* 241–254.

Walter, T.R., Acocella, V., Neri, M., Amelung, F., 2005. Feedback processes between magmatic events and flank movement at Mount Etna (Italy) during the 2002–2003 eruption. *J. Geophys. Res*., **110,** B10205, doi:10.1029/2005JB003688.

Zbinden, E.A. and J.M. Sinton, 1988. Dikes and the petrology of Waianae volcano, Oahu. *J. Geophys. Res*., **93**, 14,856-14,866.

Figure captions

Table 1: Max range of dip and mean dip of shallow intrusions within several poorly-eroded basaltic volcanoes.

Figure 1: Rose diagram showing the dip directions of subhorizontal intrusions in the Cirque of Cilaos (Piton des Neiges volcano).

Figure 2: Geometry and mesh of the topography in map view. The mesh is denser in the summit part, above the area where magmatic intrusions is located.

Figure 3: a- Geometries of subVertical (subV) and subHorizontal (subH) intrusions considered in the model and b- the range of assumed dips. These representations are not at scale. Both type of intrusions have the same area in the model.

Figure 4: Main parameters involved in the calculation of the displacements associated to a suvertical or subhorizontal (this sketch) intrusion.

Figure 5: Influence of the dip of subvertical and subhorizontal intrusions on the maximum opening of the intrusion (a), the maximum slip along the intrusion (b), the maximum internal displacements within the edifice (c) and the maximum outtward surface displacements (d). The role of the dip is tested in an isotropic stress field and in an anisotropic stress field (k = 0.8).

Figure 6 : Influence of the anisotropy of the stress field loading the edifice on the maximum opening of the intrusions (a), the maximum slip along the intrusions (b), the maximum internal displacements within the edifice (c) and the maximum outward surface displacements (d). SubV = subvertical ; subH = subhorizontal intrusions.

Figure 7: a- modelled opening (a1 and a3) and slip (a2 and a4) of a sectorial, 75°-outward dipping and 190°-outward dipping intrusions within an edifice loaded by an isotropic stress field; b- - modelled opening (a1 and a3) and slip (a2 and a4) of a sectorial, 75°-outward dipping and 190°-outward dipping intrusions within an edifice loaded by an anisotropic stress field (k = 0.8).

Figure 8: a- Modelled outward displacements associated to subvertical (75°) and subhorizontal (190°) intrusions in an isotropic stress field ; b- Modelled outward displacements associated to subvertical (75°) and subhorizontal (190°) intrusions in an anisotropic stress field (k = 0.8).

Figure 9: a- Modelled vertical displacements associated to subvertical (75°) and subhorizontal (190°) intrusions in an isotropic stress field ; b- Modelled vertical displacements associated to subvertical (75°) and subhorizontal (190°) intrusions in an anisotropic stress field (k = 0.8).

Figure 10: Relationship between slip and opening of subvertical (subV) and subhorizontal (subH) intrusions, submitted either to isotropic or anisotropic stress field.

808

Table

Click here to download Table: table1.doc

Volcano	Max range	Mean dip	Reference
Teno	80-85°	82°	Marinoni and Gudmundsson (2001)
Anaga	82-87°	78°	Marinoni and Gudmundsson (2001)
Koolau	75-80°	80°	Walker (1986)
Ofu-Olosega	70-80°	70°	Walker and Eyre (1995)
Stromboli	70-80°	74°	Tibaldi (2003)
Tutuila	70-75°	73°	Wlaker and Eyre (1995)
Wainaea	70-90°	65°	Zbinden and Sinton (1988)
Piton de la Fournaise	85-90°	80°	Letourneur et al. (2008)

Figure
Click here to download high resolution image

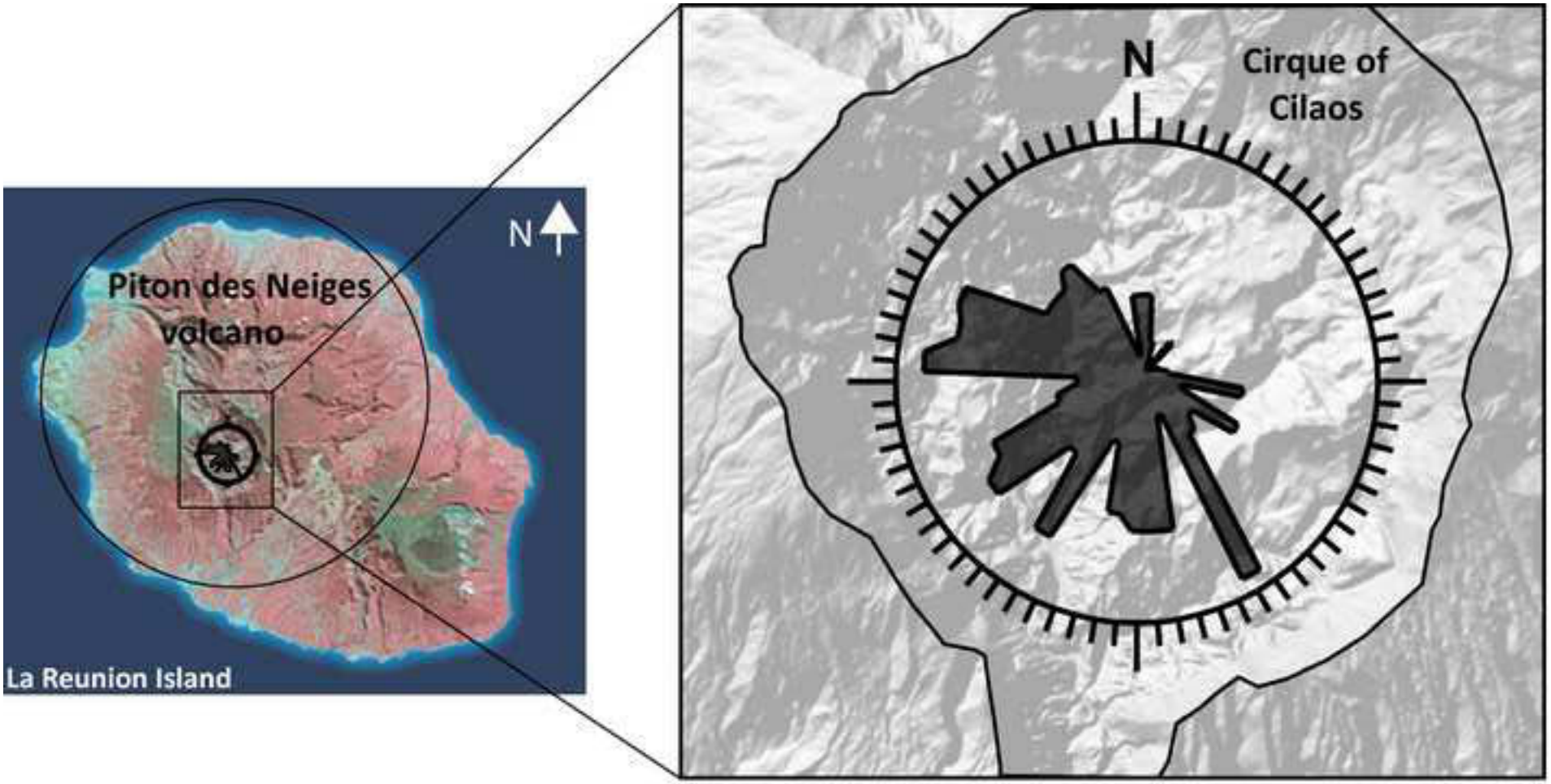

Figure
Click here to download high resolution image

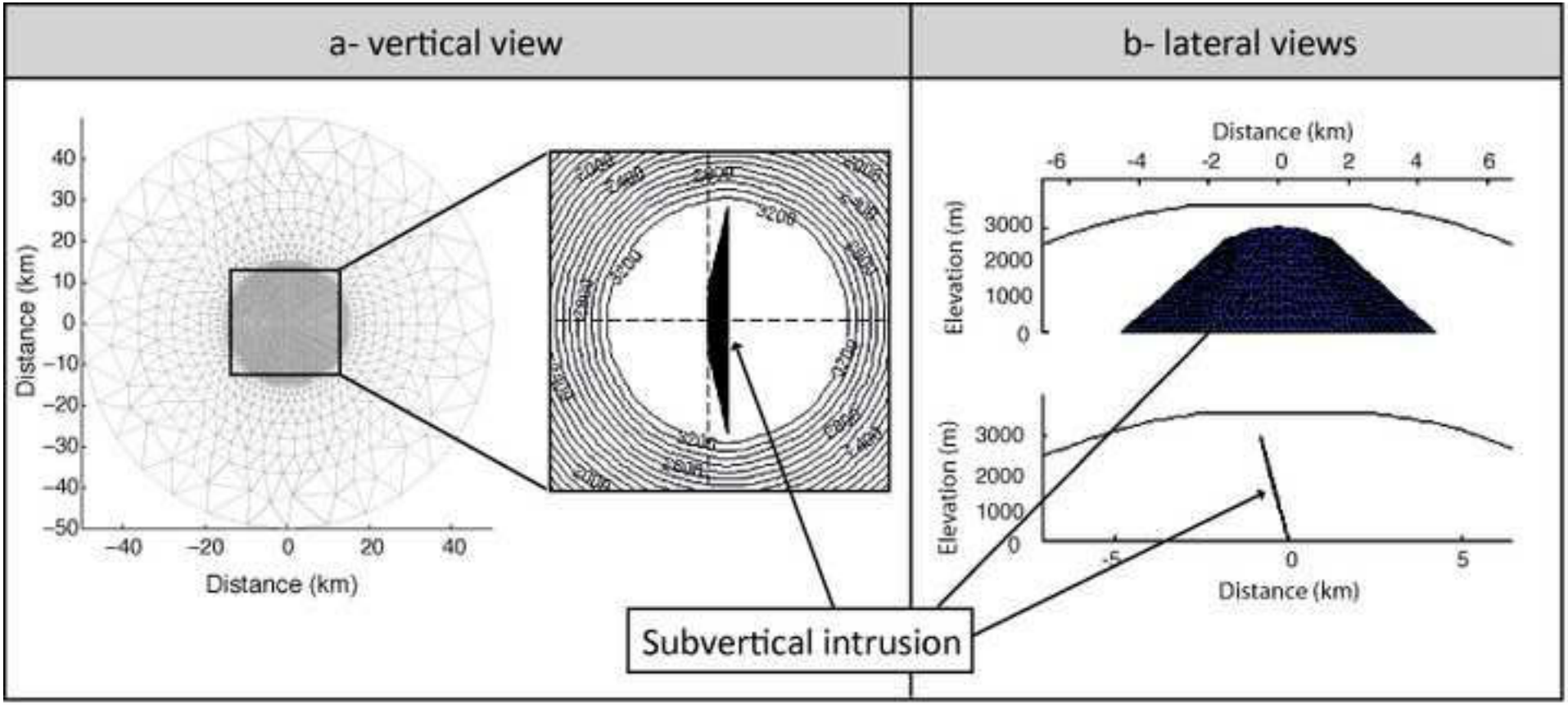

Figure

Click here to download high resolution image

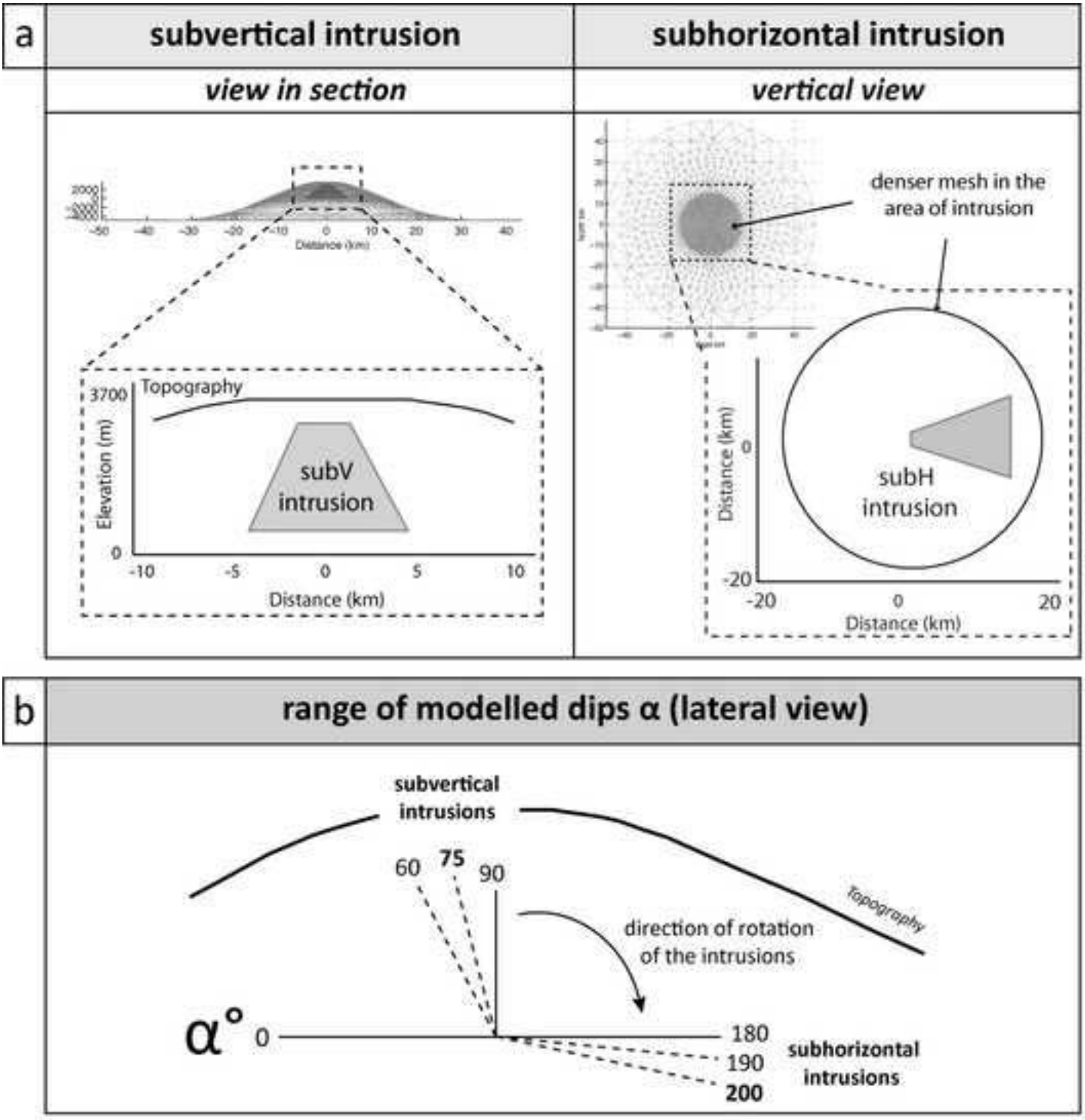

Figure

Click here to download high resolution image

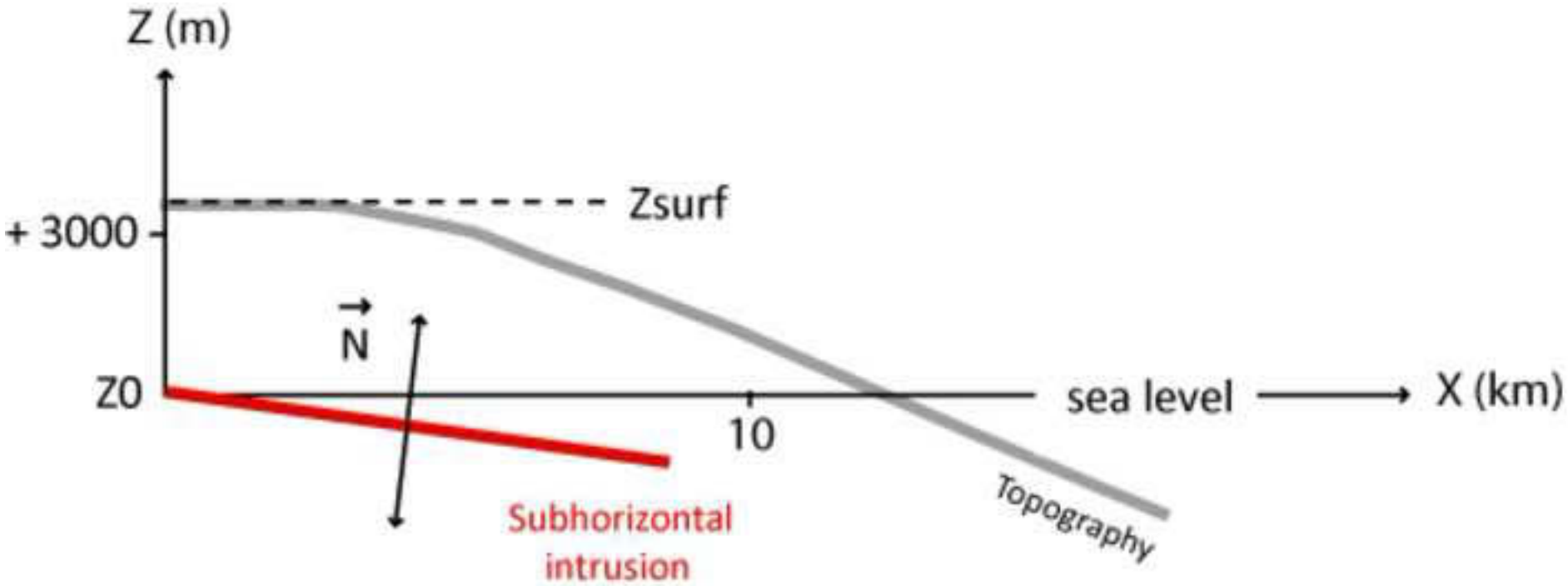

Figure

Click here to download high resolution image

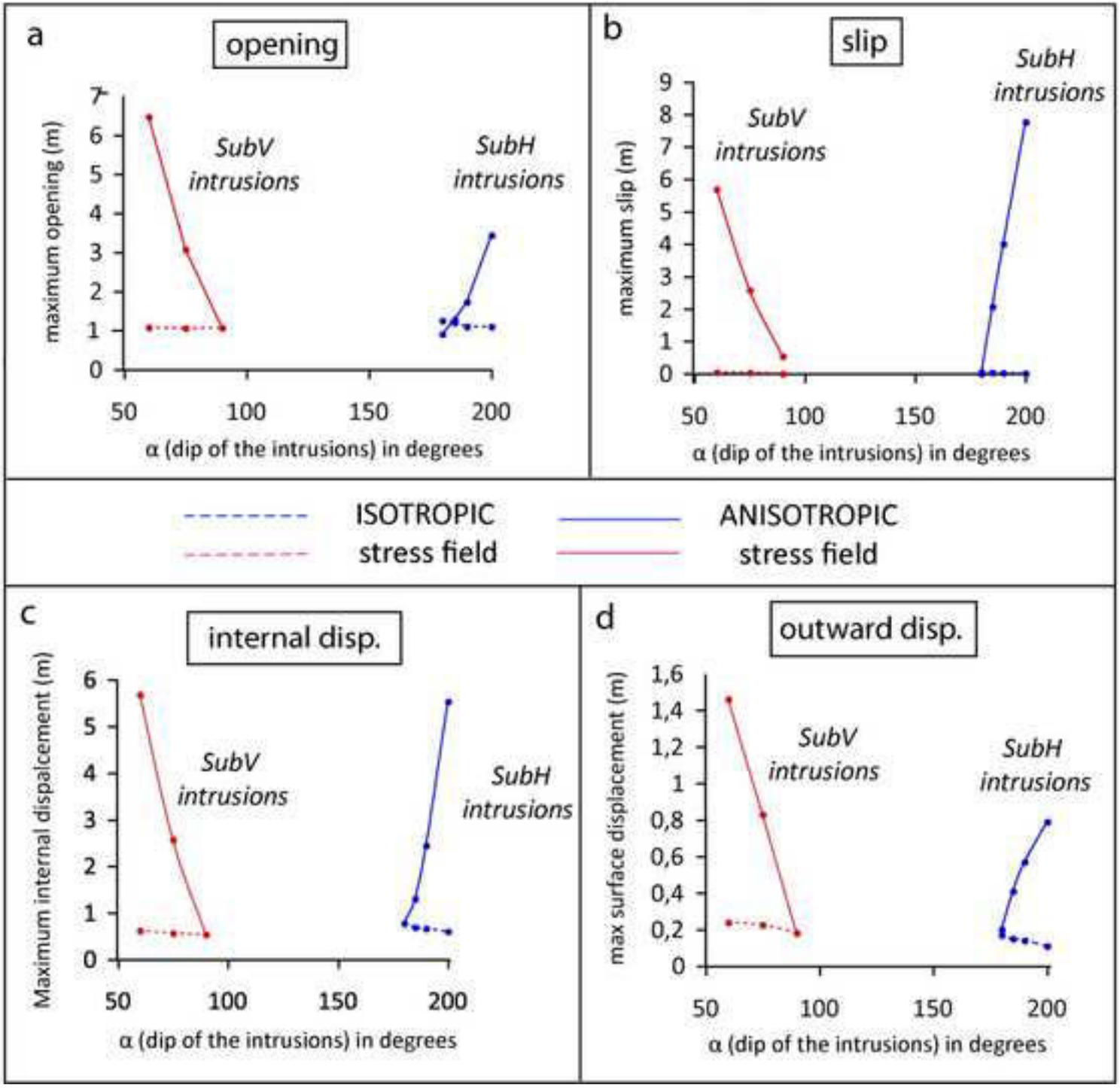

Figure

Click here to download high resolution image

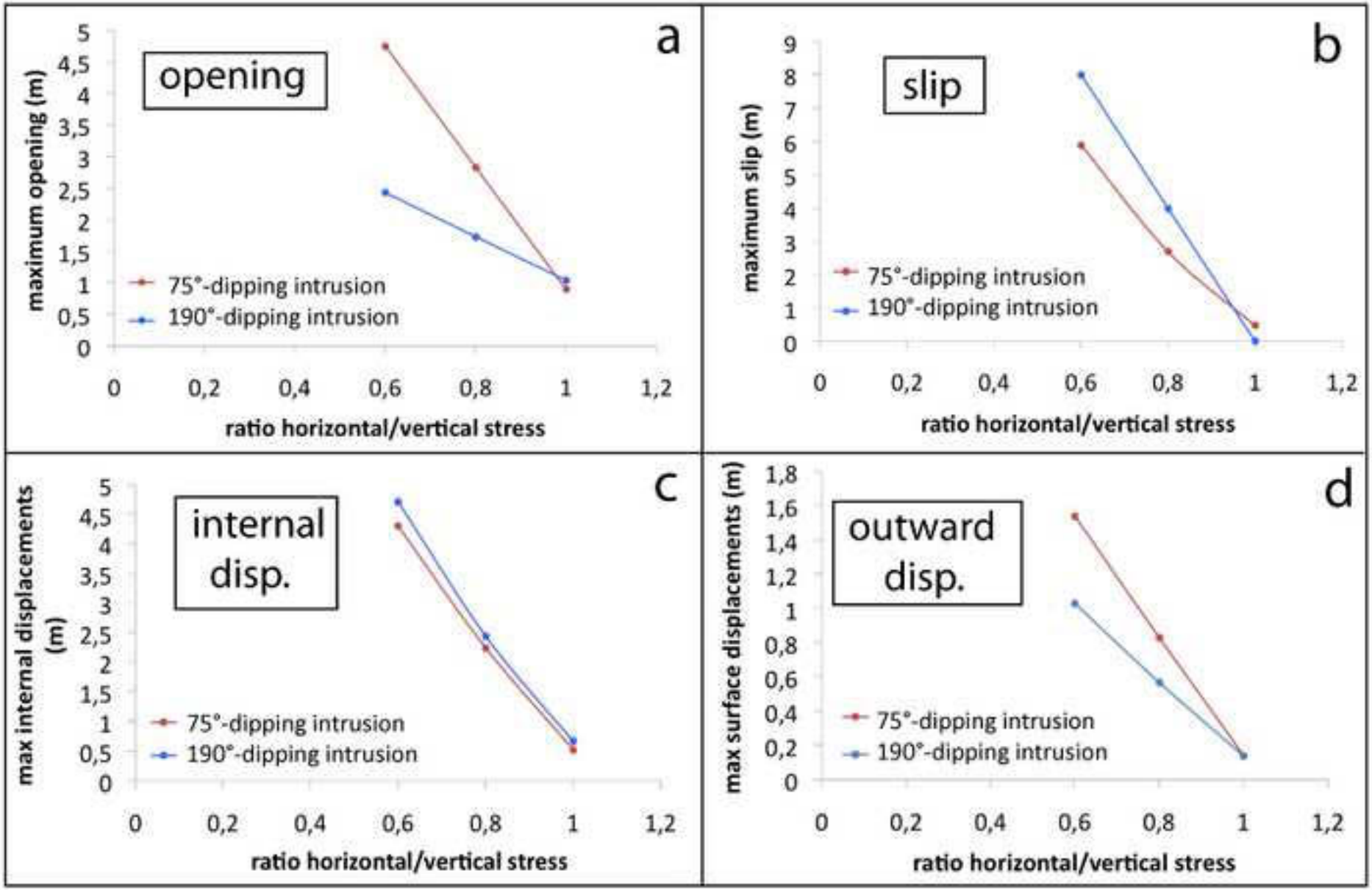

Figure

Click here to download high resolution image

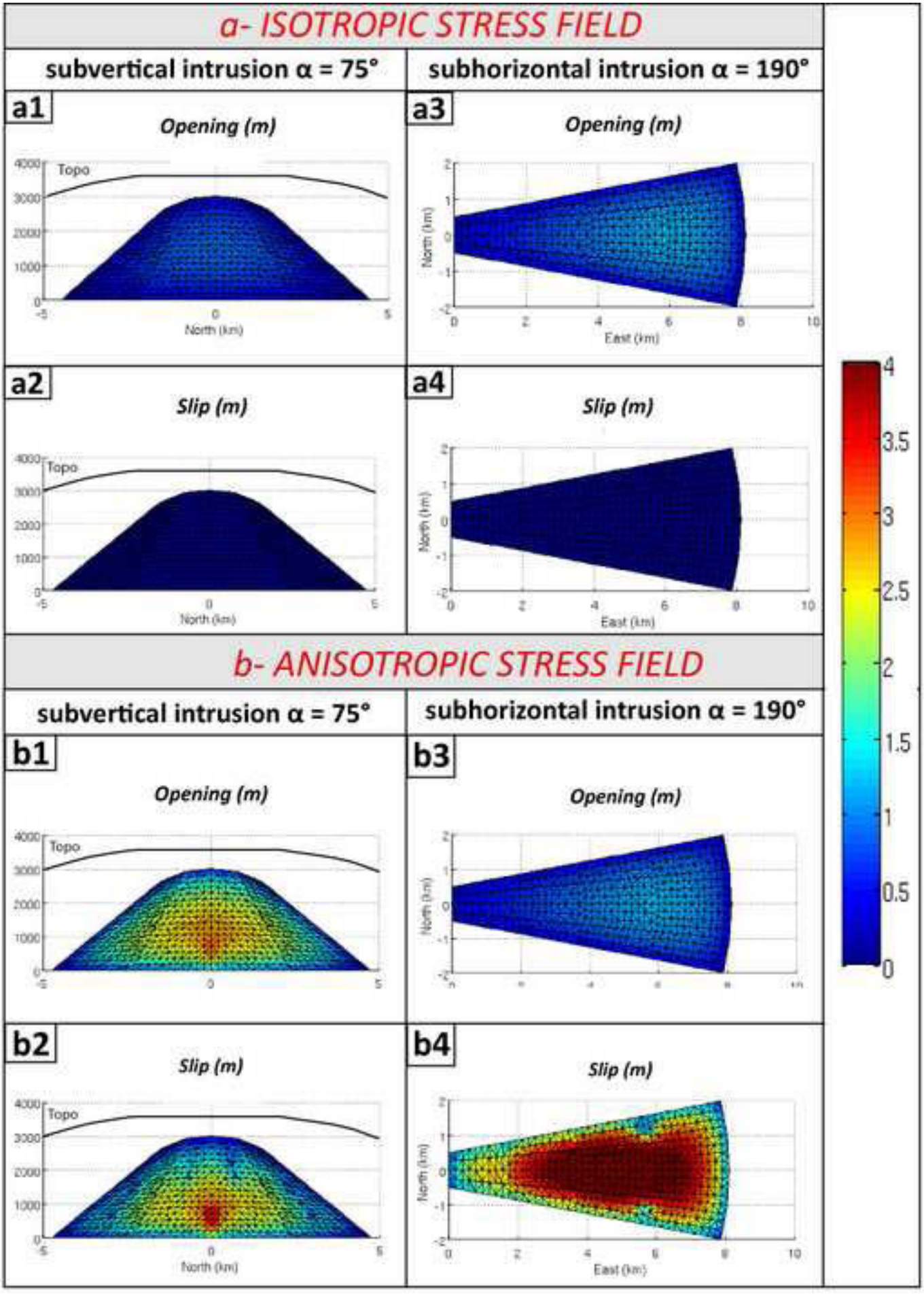

Figure

Click here to download high resolution image

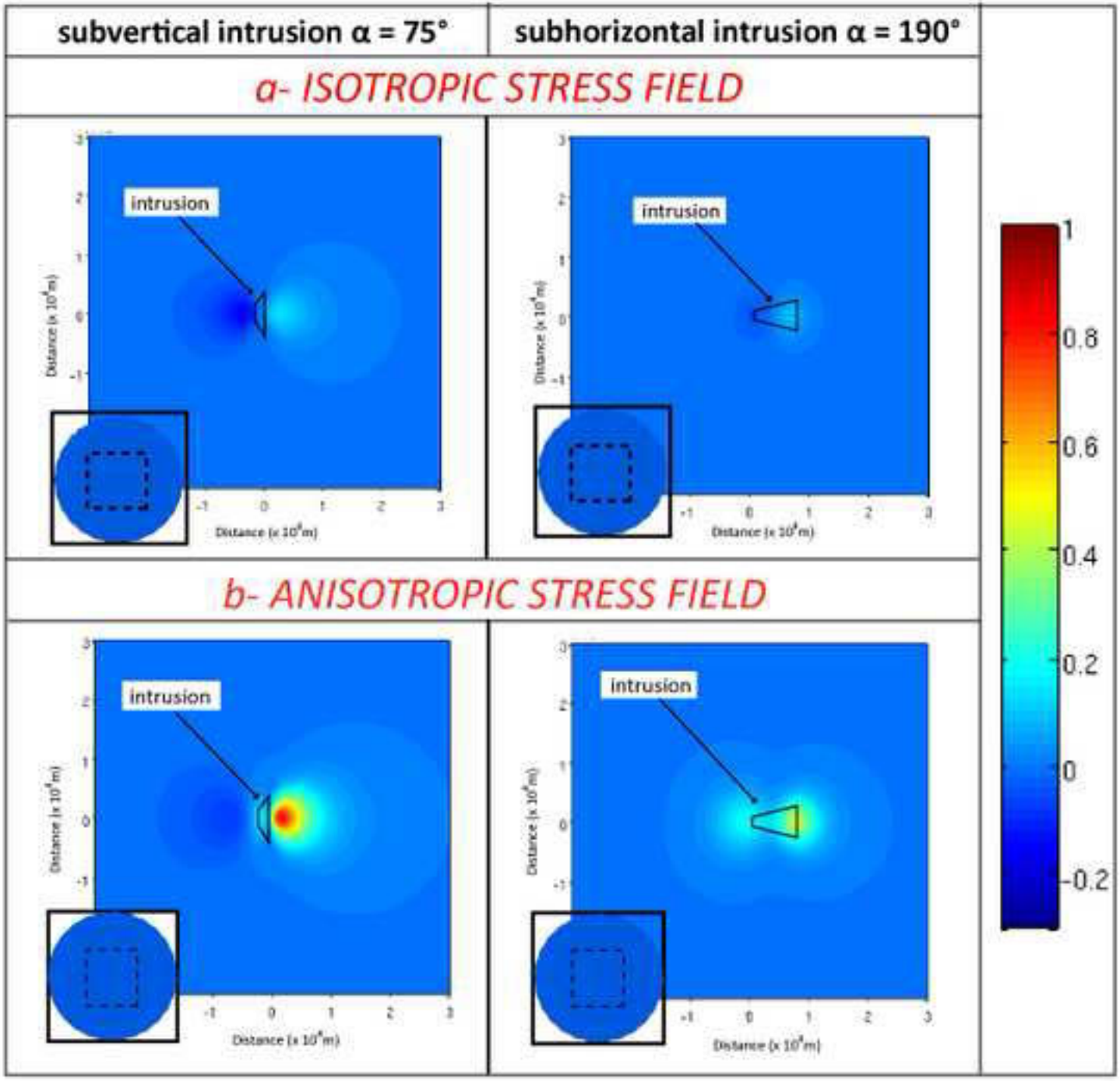

Figure

Click here to download high resolution image

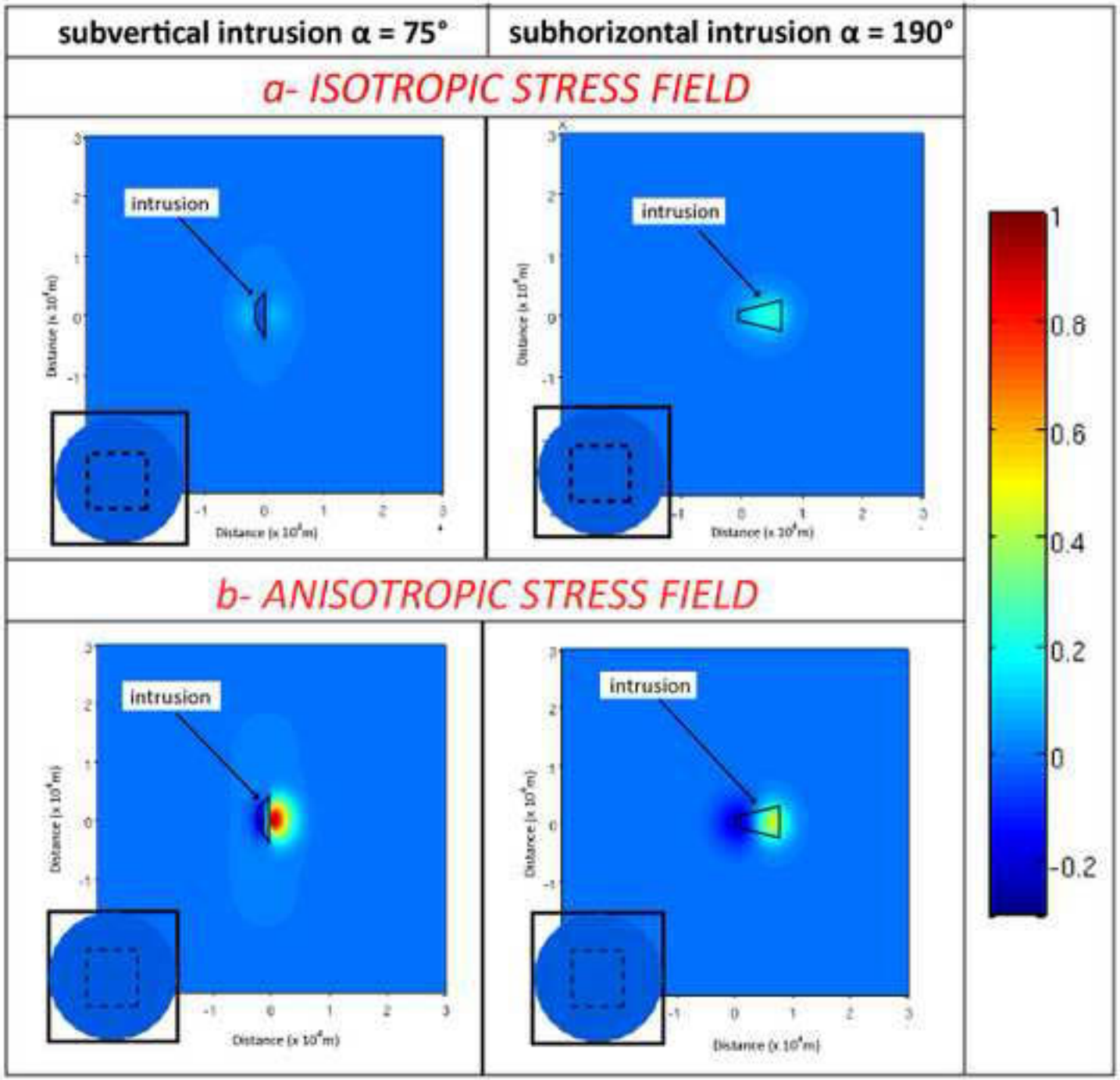

Figure
Click here to download high resolution image

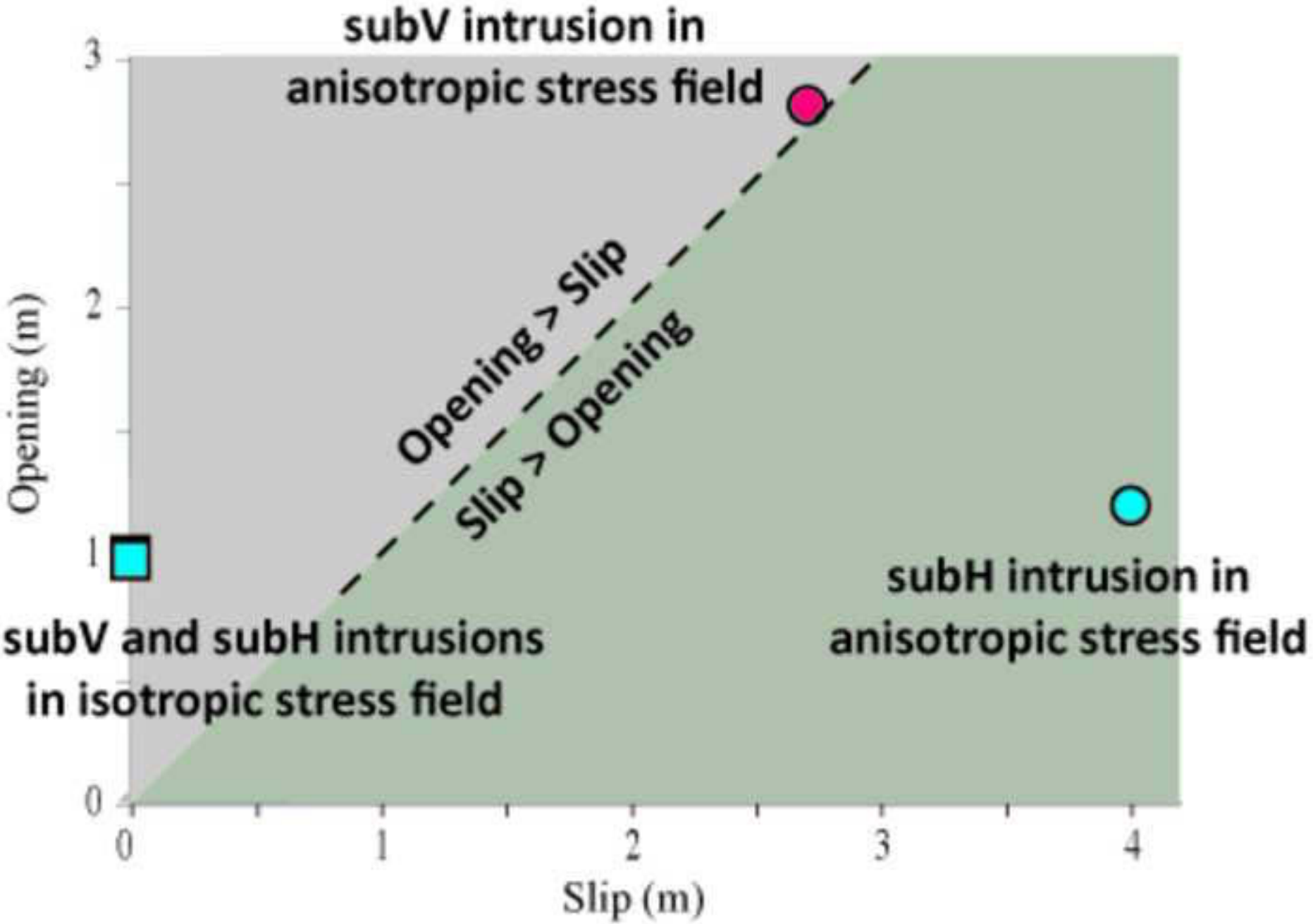

Appendix 4

Chaput, M., Famin, V., Michon, L. and T. Catry, 2010. Large-scale destabilization of a basaltic shield volcano (Piton des Neiges volcano, La Reunion Island). IAVCEI third Workshop on Caldera Collapse, La Reunion, abstract.

Large-scale destabilization of a basaltic shield volcano (Piton des Neiges volcano, La Réunion Island)

Marie Chaput[1], Vincent Famin[1], Laurent Michon[1], Thibault Catry[1, 2]

[1] Laboratoire Géosciences Réunion - IPGP, UMR CNRS 7154, Université de la Réunion, 15 Avenue René Cassin, 97715 Saint Denis messag Cedex 9, France, marie.chaput@univ-reunion.fr
[2] Dipartimento di Scienze della Terra e Geologico-Ambientali, Università di Bologna, 1 Piazza di Porta San Donato 40127 Bologna, Italy

Keywords: volcano destabilization, sills, Piton des Neiges, La Réunion

Piton des Neiges is a highly extinct shield volcano eroded by three deep depressions (Cirques) surrounding the summit of the edifice. Within the Cirques are exposed old basic products from the volcano shield building stage (>2,1Ma – 430 ka). We carried out a structural investigation in the basic deposits of the Cirque of Cilaos (south of Piton des Neiges summit) to constrain the destabilization processes that affected the edifice during its early aerial phase of construction.

The internal structure of the cirque of Cilaos is made of piled basic lava flows and breccias, capped by lavas from the differentiated stage (< 350 ka). The breccias mainly consist in debris avalanche deposits and debris flows containing only basic elements. Two kinds of debris avalanche breccias can be distinguished: the “lower” breccia, with a consolidated green-dark matrix, is widely zeolitised, chloritized and serpentinized and is crosscut by many intrusions (dikes and sills). The “upper” breccia presents a light brown zeolitized matrix, poorly consolidated and poorly intruded. Both avalanches display jigsaw-cracked blocks, up to a few tens of meters in diameter.

Several evidences of brittle deformation (faults and/or intrusions) were recorded within the breccias and the basic lava flows. Paleo-stresses reconstructed from deformation data allow the recognition of two successive episodes of deformation (Figure 1):

- The first, older step of deformation is extensional with a minimum principal stress σ_3 oriented N-S. It is recorded within the “lower” breccia and the underlying zeolitized lava flows which are assumed to be the oldest formations of the Cirque.
- The second, later step of deformation is extensional with σ_3 oriented NW-SE. It is widely expressed in all basaltic formations (lavas and breccias) of the Cirque. It is coeval with strike-slip faulting whose minimum principal stress is also oriented NW-SE. Shear structures and beddings dips within the breccia suggest a runout toward the NW. Intrusions from the basic stage, striking N20-N40 and dipping NW, are also consistent with a flank destabilization toward the NW.

These results in Cilaos show that the dismantling of Piton des Neiges volcano is the consequence of both slow and rapid destabilizations that occurred in at least two episodes:

(1) a N-S destabilization during the initial eruptive history of the volcano, whose related deposits, zeolitized and chloritized, are still visible at the bottom of the Cirque, in riverbeds.
(2) a NW rapid collapse producing debris avalanche deposits (that currently cover the main part of the Cirque of Cilaos), accompanied by slow internal deformation that affected the whole stratigraphic sequence.

The temporal evolution of the stress fields recorded in Cilaos can also be observed north of Piton des Neiges, in the Cirque of Salazie. A recent study within debris avalanche deposits attests that the northern flank of the edifice was affected by an extensional deformation (rapid failure combined with slow deformation) in a N-S direction (Famin and Michon, 2010). New deformation data, collected in overlying pahoehoe lava flows (in the northern scarp of the Cirque of Salazie), evidence that this flank undergone a later stage of slow internal deformation in a NW-SE direction.

The combined study of cirques of Cilaos and Salazie reveals that (1) dismantling events on Piton des Neiges volcano are characterized by the combination of episodic catastrophic flank collapses and slow deformation, (2) the stress field evolved from a N-S- to a NW-SE-oriented extension during the shield building stage, perhaps as a consequence of the nearby growth of the Alizés or and/or Piton de la Fournaise volcanoes, and (3) this evolution was a large-scale process that affected the whole edifice.

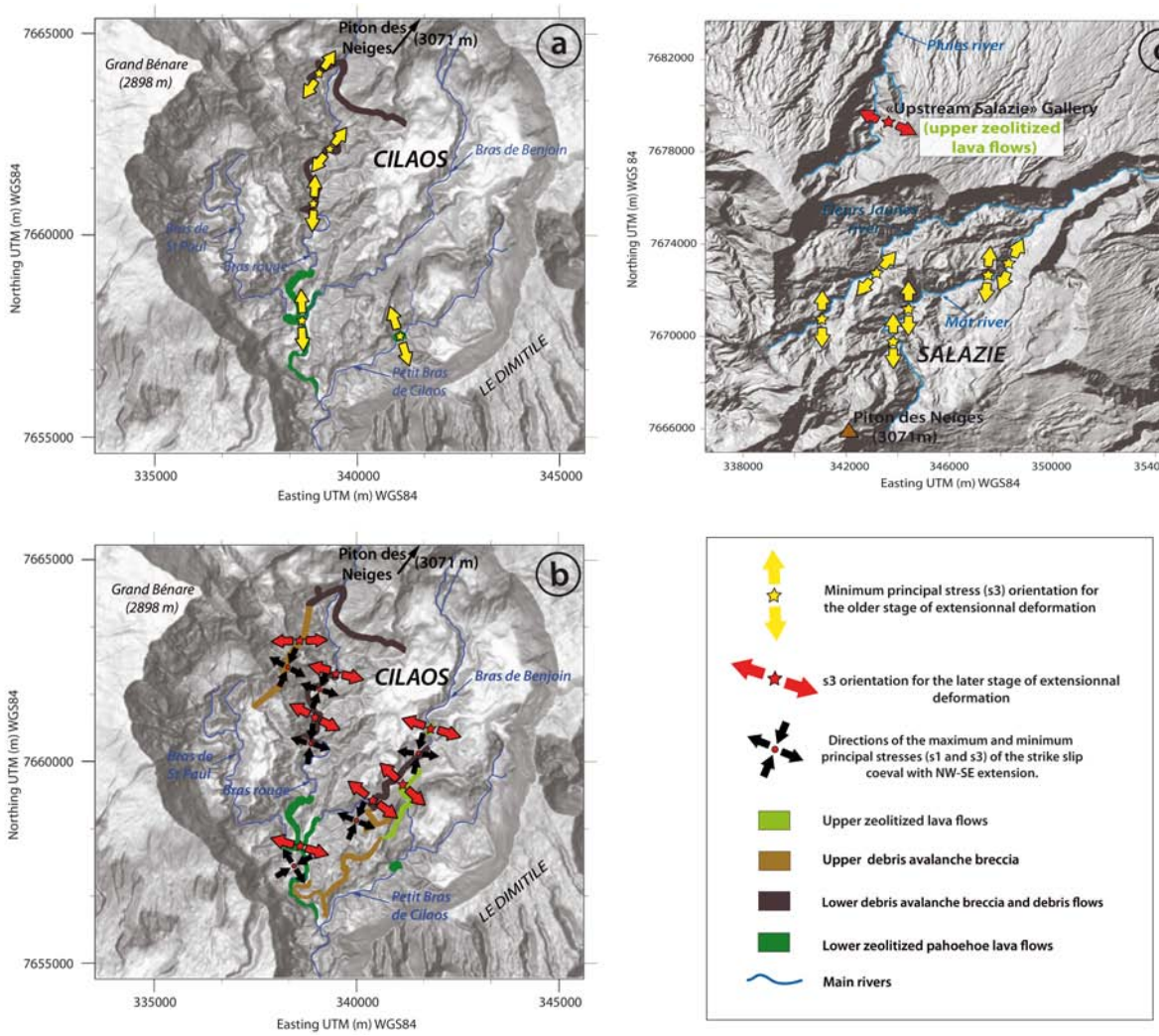

Fig. 1: Successive steps of destabilization of the southwestern and northern flanks of Piton des Neiges volcano, inferred from microstructural studies. a. Older phase of deformation oriented N-S in the Cirque of Cilaos. b. Later phase of deformation oriented NW-SE in the Cirque of Cilaos and coeval with strike-slip faulting. c. Similar N-S to NW-SE stress field evolution in the cirque of Salazie (modified from Famin and Michon, 2010).

1 Famin, V. & Michon, L. Volcano destabilization by magma injections in a detachment. *Geology* **38**, 219-222 (2010).

Appendix 5

Froger, J.L., Augier, A., Cayol, V., Souriot, T., 2010. Some considerations about the April 2007 eruption at Piton de la Fournaise suggested by InSAR data. IAVCEI Third Workshop on Collapse Calderas, La Réunion, abstract.

Some considerations about the April 2007 eruption at Piton de la Fournaise suggested by InSAR data.

J.-L. Froger, A. Augier, V. Cayol, T. Souriot)

[1] Laboratoire Magmas et Volcans UMR 6524, CNRS-IRD-Université Blaise Pascal, 5 rue Kessler 63 038 Clermont-Ferrand, France, J.L.Froger@opgc.univ-bpclermont.fr

Keywords : Caldera Collapse, Dolomieu, Displacements, InSAR

Introduction

From 30 March to 1 May 2007, Piton de la Fournaise experienced one of its major eruptive crises of XXth and XXIth centuries. The large and complex ground displacements that occurred during this event and in the following months were recorded both by the radar ASAR on board of the European satellite ENVISAT and by the radar PALSAR on board of the Japanese satellite ALOS. In this paper we describe how the ASAR and PALSAR InSAR data provide new insights on the processes acting during the April 2007 events.

InSAR derived co-eruptive displacements

From three ASAR and two PALSAR interferograms spanning the March-April 2007 eruption we have inverted the EW and vertical co-eruptive displacements. On the resulting displacement maps, four main signals are visible (Figure 1) :

- The entire western part of Central Cone is affected both by eastward and downward displacement indicating a centripetal subsidence with a maximum of about 50 cm at the north western rim of Dolomieu crater.
- At the eastern flank of the central cone, the displacement maps reveal a large inflation axis that extends NS on about 4 km from the Faujas cone to the Langlois cone. The horizontal component indicates a total opening of about 20 cm to the North and up to 45 cm to the South while the vertical component map exhibits a maximum uplift of about 25 cm on the south-eastern flank of the Central Cone. At its southern end, the axis divides in two N150° branches. The easternmost branch coincides with the location of the March 30 eruptive fissure, suggesting that the whole NS uplift axis was produced by the March 30 intrusion.
- To the East of the Central Cone, the Grandes Pentes are marked by a large displacement pattern. On the horizontal component map, the pattern covers a roughly triangular area of about 4.5 × 4 km^2, indicating a global eastward displacement with a maximum up to 1.4 m. The vertical component map shows a more complicated pattern, with a global subsidence of the Grandes Pentes, up to 33 cm, intersected in its central part by an uplift reaching 37 cm. These observations suggest the superimposition of a large wavelength downslope sliding of the entire Grandes Pentes, except its southern part, and a shorter wavelength uplift of its central part.
- At the SE base of the Grandes Pentes, a N125-130 subsiding axis is clearly visible on the vertical component map, with a maximum displacement of 28 cm downward. Its SE end points at the location of the 2 April eruptive fissure suggesting that the subsidence is directly related to the magma migration from the central cone area to the place of the 2 April eruption.

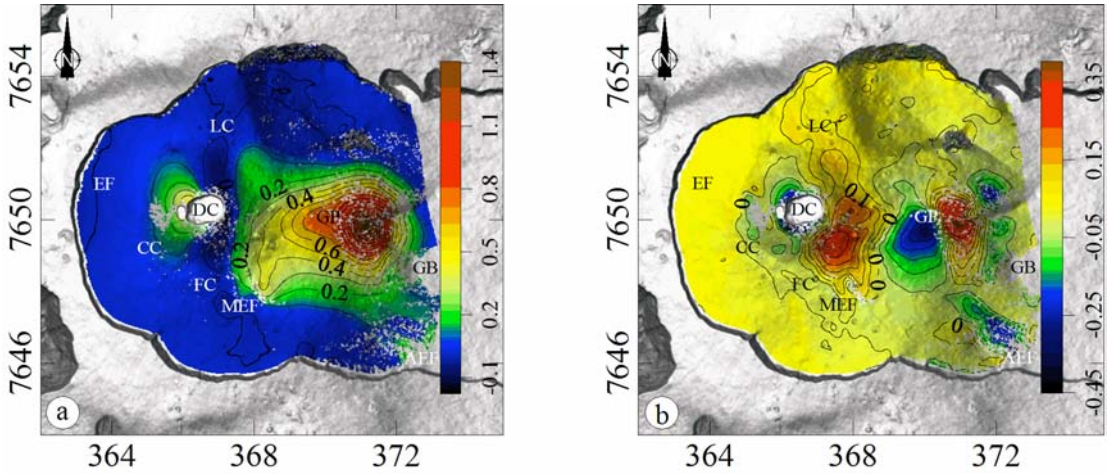

Fig. 1 - Co-eruptive displacements draped on the shaded DEM. a) EW component, contour level interval is 0.1 m; b) vertical component, contour level interval is 0.05 m; AEF : 2 April 2007 Eruptive Fissure; CC : Central Cone; EF : Enclos Fouqué; FC : Faujas Cone; GB : Grand Brûlé; GP : Grandes Pentes; LC : Langlois Cone; MEF : 30 March 2007 Eruptive Fissure. Coordinates are in km UTM (40 zone South).

InSAR derived post-eruptive displacements

We calculated EW and vertical post-eruptive displacements from 167 ASAR and 11 PALSAR interferograms spanning different time intervals between May 2007 and September 2008. The resulting displacement maps show that the ground displacements continued at least one year after the end of the eruption, with an exponentially decreasing intensity, both at the Central Cone and in the Grandes Pentes (Figure 2).

- The entire Central Cone is affected by a centripetal subsidence that gives a nice symmetrical displacement pattern on the horizontal component map with a maximum eastward displacement of the western flank of 19 cm. On the vertical component map, the displacements pattern is concentric with a maximum value of about 25 cm downward. The displacement wavelength suggests a relatively shallow source bellow or within the cone. Comparison of the co- and post-eruptive displacements on the western flank of the Central Cone shows a very slight decrease of the displacement wavelength. This observation suggests either the activity of a unique shallow deflating source, with a slight rising of the deflating centre or the coexistent activities of a deep and a shallow deflating source, the second one continuing deflating alone during the post-eruptive period.
- The Grandes Pentes are marked by a large trapezoidal displacement pattern indicating a general downslope sliding. It coincides partly with the large wavelength downslope sliding recorded on the co-eruptive interferograms. However, the co-eruptive and post-eruptive displacements patterns differ in some respects. First, the ratio between horizontal and vertical components is inverted with more than 30 cm of vertical displacement downward for a maximum of 12 cm of horizontal displacement to the East. Second, one does not observe the superimposition with the shorter wavelength uplift of the central Grandes Pentes that was evidenced during the co-eruptive period. This observation suggests that the inflation of the central Grandes Pentes is due to a transient process, active only during the co-eruptive period while the large wavelength downslope sliding continued a long time after the end of the eruption. A last difference arises from the evident structural control of the post-eruptive displacements that does not appear so manifest in the case of the co-eruptive displacements.

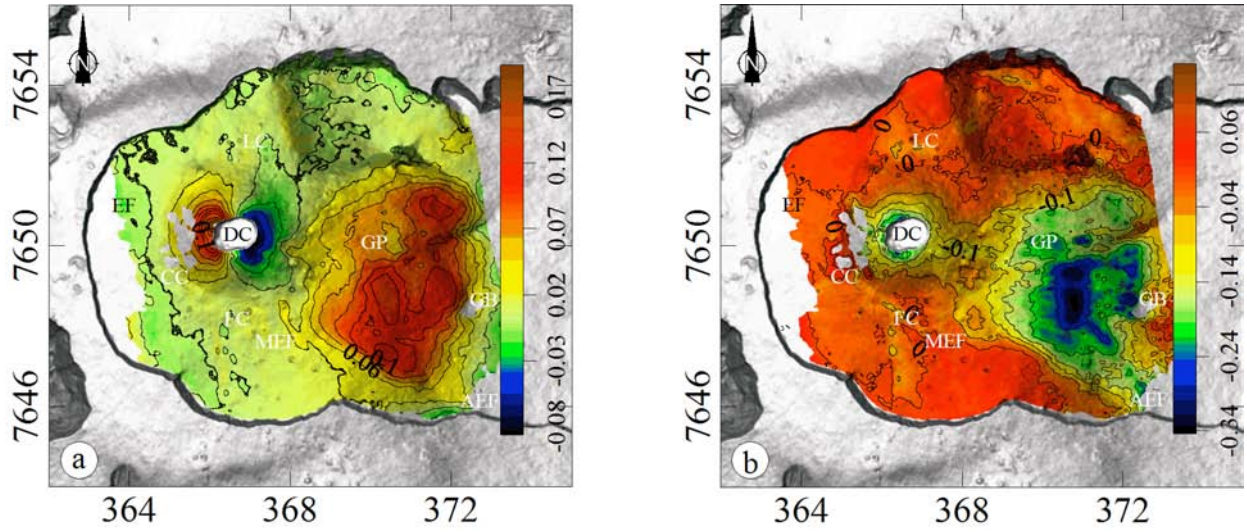

Fig. 2 - One year post-eruptive displacements draped on the shaded DEM. a) EW component, contour level interval is 0.02 m; b) vertical component, contour level interval is 0.05 m; AEF : 2 April 2007 Eruptive Fissure; CC : Central Cone; EF : Enclos Fouqué; FC : Faujas Cone; GB : Grand Brûlé; GP : Grandes Pentes; LC : Langlois Cone; MEF : 30 March 2007 Eruptive Fissure. Coordinates are in km UTM (40 zone South).

Discussion - interpretations

Central Cone

The persistence of the centripetal subsidence at Central Cone during at least one year after the end of the eruption suggests that the displacements do not result from purely elastic process.

At least three alternative processes can be put forward to explain this behavior:

- The magma reservoir that feed the April 2007 eruption undergoes continuous deflation during the months following the end of the eruption, either by compaction or draining of the magma remaining within it, or by thermal contraction of the surrounding wall rocks.
- The rock column located between the Dolomieu floor and the roof of the magma reservoir is an intensely altered and brecciated medium, that behaves as a visco-poro-elastic body, damping in time the relaxation of central cone that occurred in response to the instantaneous change in shape of the topography induced by the Dolomieu collapse.

- The Dolomieu collapse triggers the large opening of a previously pressurized hydrothermal system resulting in its draining, massive immediately after the collapse and decreasing gradually in intensity in the following weeks and months.

Grandes Pentes

The origin of Enclos Fouqué - Grandes Pentes - Grand Brûlé structure has been discussed for a long time. The proposed interpretations range from classical caldera collapse to recurrent seaward landslides. It should be noticed however, that before our study, all the interpretation proposed for this structure were derived from indirect observations. Here, for the first time, thanks to the InSAR data, we provide direct evidences of a large active seaward sliding affecting the eastern flank of Piton de la Fournaise. This large flank motion seems obviously related with the intense magmatic activity occurred during the March-April 2007 eruption. However the way the two processes are related is still unclear. Two main scenarios can be proposed:

- The March 30 intrusion in the eastern flank of Central Cone triggered the Grandes Pentes sliding. In this scenario, we suppose, on one hand, that the sliding occurs on some basal decollement level (e.g. altered and or brecciated level) and, on the other hand, that it favoured in some way the magma migration from the Central Cone area to the 2 April eruptive fissure area.
- The Grandes Pentes sliding is triggered by the magma migration from the Central Cone area to the 2 April eruptive fissure area. In this scenario, the short wavelength uplift in the central part of Grandes Pentes, visible on co-eruptive vertical displacements map, could mark an intrusion that failed propagating up to the surface. This intermediate intrusion could have play the rule of a discontinuity on which the sliding of Grandes Pentes initiated.

The influence of the Grandes Pentes sliding on the stress state of the whole edifice and particularly of the magmatic reservoir host rock is an interesting issue that still needs to be addressed. It could have significant consequences, in particular, on the location and style of injections from the magmatic reservoir (dyke propagating from the roof, sill propagating from the sidewall). The Dolomieu collapse could have also been influenced by significant change in the edifice stress state and could have contributed, in return to modify again this stress state.

Appendix 6

Smietana, M., Bachèlery, P. and Hémond, C., 2010. Heterogeneity in the mantle source of La Réunion Island, Goldschmidt conference abstract 2010, *Geochem. Cosmochem. Act*., 74, 12, suppl. 1, A972.

^{13}C–depleted diamonds in Jericho eclogites: Diamond formation from ancient subducted organic matter

K.A. SMART*, T. CHACKO, L.M. HEAMAN, T. STACHEL AND K. MUEHLENBACHS

Dept. of Earth and Atmospheric Sciences, Univ. of Alberta, Edmonton, AB, Canada
(*correspondence: kasmart@ualberta.ca)

The high-MgO, diamond-bearing eclogites from the Jericho kimberlite in the northern Slave craton are unique in their high Mg# (82-87), high incompatible element contents, radiogenic Sr isotope ratios, and abundant diamonds (up to 20 modal %) that contain lower-Mg garnet inclusions (Mg#~54). As first noted by [1], these diamonds have the lightest carbon isotope compositions ever reported for diamonds ($\delta^{13}C$ = -37 to –41‰). Although upcoming SIMS $\delta^{13}C$ analyses will help delineate the mechanism of diamond formation, we note that $\delta^{13}C$ values of ca. –40‰ cannot reasonably be explained by Rayleigh-style fractional crystallization of diamond at mantle temperatures (T>800°C) from a parental fluid isotopically heavier than –35‰. Thus, these Jericho diamonds require the existence of a strongly ^{13}C-depleted carbon reservoir beneath the northern Slave craton.

The δ13C of organic carbon in modern marine sediments is ~ –20‰ [2], and therefore not a viable carbon source for the Jericho diamonds. Consequently, [1] invoked a heretofore unidentified, highly localized and ^{13}C-depleted carbon source for the Jericho high MgO eclogitic diamonds. We suggest that this anomalous carbon source may have been organic carbon formed by methane fixation by methanogenic bacteria in the Neoarchean (ca. 2.7 Ga) or Paleoproterozoic (ca. 2.0 Ga) times, which are characterized by $\delta^{13}C$ values as low as –50‰ [2, 3]. Interestingly, these time periods broadly correspond to hypothesized subduction events beneath the Slave Craton.

We propose that the protoliths of the high-MgO Jericho diamond eclogites were similar to those of common ‘basaltic’ eclogites, but melt depletion coupled with peridotite chemical equilibration produced the high-MgO compositions. Diamond formation was coincident with a semi-cryptic metasomatic event, which trapped some of the original, low-Mg eclogitic garnet and produced the incompatible-element-rich and radiogenic nature of the eclogites. The ca. -40‰ organic carbon may have been intrinsic to slab eclogitization during Neoarchean and/or Paleoproterozoic subduction events. Alternatively, the eclogites may have been older and metasomatized by slab-derived fluids generated during Neoarchean or Paleoproterozoic subduction events.

[1] De Stefano *et al.* (2009) *CMP* **158**, 295–315 [2] Freeman (2001) *in* Stable Isotope Geochem. **43**, 579–97. [3] Eigenbrode & Freeman (2006) *PNAS* **103**, 15759–64.

Heterogeneity in the mantle source of La Réunion Island

M. SMIETANA[1]*, P. BACHÈLERY[1] AND C. HÉMOND[2]

[1]Laboratoire Géosciences Réunion, UMR 7154, CNRS-IPGP, Université de La Réunion, Ile de La Réunion (*correspondence: magali.smietana@gmail.com)
[2]Domaines Océaniques, UMR 6538, CNRS-UBO, IUEM, Place Copernic, 29280 Plouzané, France

Piton des Neiges (PdN) and Piton de la Fournaise (PdF) volcanoes (La Réunion Island, Indian Ocean) are famous to produce lavas considerably more homogeneous than other hotspots worldwide. Their products show narrow ranges of $^{87}Sr/^{86}Sr$ (0.70397 – 0.70436), ε_{Nd} (3.1 – 4.6) and ε_{Hf} (7.9 – 11.0) throughout the whole 2 Ma volcanic history of the island [1, 2, 3, 4, 5]. Modest variations in Pb isotopes were identified which do not disrupt much the homogeneous picture of the magmas [3, 4].

We report for the first time Sr-, Nd-, Hf- and Pb-isotope compositions for submarine basalts dredged along the NE rift zone of PdF. The composition of the samples is enriched in incompatible elements ($1.10<K_2O<1.44$, $0.35<P_2O_5<0.56$, $2.58<(La/Sm)_{C1\ norm.}<2.93$) and radiogenic Sr, Nd and Hf [$^{87}Sr/^{86}Sr$ = 0.70460–0.70476, ε_{Nd} = 2.9–3.6 and ε_{Hf} = 7.5–8.3] and isotopically the most radiogenic ever published (Fig. 1).

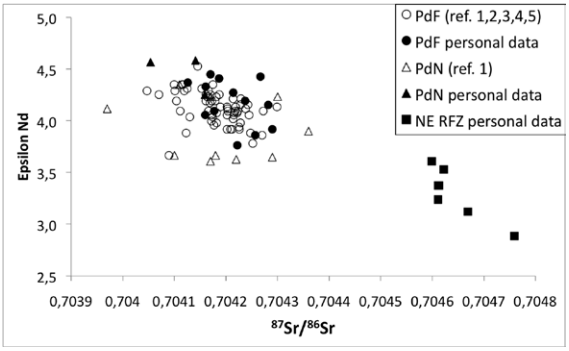

Figure 1: Plot of $^{87}Sr/^{86}Sr$ ratio vs ε_{Nd} values.

Pb isotope data ($^{206}Pb/^{204}Pb$ = 18.943 – 18.974; $^{207}Pb/^{204}Pb$ = 15.598 – 15.606; $^{208}Pb/^{204}Pb$ = 39.045 – 39.141), design a specific trend in $^{206}Pb/^{204}Pb$ – $^{208}Pb/^{204}Pb$ with respect to PdN and PdF’s trends. One of these samples is dated by K-Ar at 3.3 Ma corresponding to the oldest dated rock of all the edifices. Our new data shed lights on the existence of a third volcano at La Réunion Island.

[1] Fisk *et al.* (1988) *JGR* **93**, 4933–4950. [2] Albarède *et al.* (1997) *J. Petrol.* **38**, 171–201. [3] Bosch *et al.* (2008) *EPSL* **265**, 748–768. [4] Vlastélic *et al.* (2009) *JVGR* **184**, 63–78. [5] Pietruszka *et al.* (2009) *J. Petrol.* **50**, 661–684.

Appendix 7

Bachèlery, P., Saint-Ange, F., Villeneuve, N., Savoye, B., Normand, A., Le Drezen, E., Barrère, A., Quod, J.P., Deplus, Ch., 2010. Huge lava flows into the sea and caldera collapse, April 2007, Piton de la Fournaise volcano. IAVCEI Third Workshop on Collapse Calderas, La Réunion, abstract.

Huge lava flows into the sea and caldera collapse, April 2007, Piton de la Fournaise volcano.

Patrick Bachèlery[1,2], Francky Saint-Ange[1,3], Nicolas Villeneuve[4], Bruno Savoye[5], Alain Normand[5], Eliane Le Drezen[5], Alain Barrère[6,7], Jean-Pascal Quod[7], Christine Deplus[2]

[1] Université de La Réunion, Laboratoire GéoSciences Réunion, UMR CNRS 7154 IPGP, 15 Avenue René Cassin, 97715 Saint-Denis cedex 9, La Réunion, France.
[2] Institut de Physique du Globe de Paris, UMR CNRS 7154, Case 89, 4 Place Jussieu, 75252 Paris Cedex 05, France
[3] Geological Survey of Canada (Atlantic), Bedford Institute of Oceanography, P.O. Box 1006, Dartmouth, Nova Scotia, B2Y 4A2, Canada
[4] Université de La Réunion, CREGUR, 15 Avenue René Cassin, 97715 Saint-Denis cedex 9, La Réunion, France
[5] IFREMER, Géosciences Marines, Laboratoire Environnement Sédimentaire, BP70, 29280 Plouzané, France.
[6] Agence de Recherche et de Valorisation Marine, ARVAM, 3 rue Henri Cornu, Technopole de La Réunion, 97490 Sainte Clotilde, La Réunion, France
[7] Maison du Volcan, SEML Reunion Museo, RN3 Bourg Murat, 97418 Plaine des Cafres, La Réunion, France

Keywords: Piton de la Fournaise, submarine lava flow, collapse, caldera.

The eruption of April 2007 at Piton de la Fournaise volcano presents an exceptional character (Michon et al., 2007; Michon et al., 2009; Staudacher et al., 2009; Urai et al. 2007) by its rate and volume of discharged lava. More than 200.10^6 m^3 of oceanite (olivine enriched basalt) were emitted during a 30 days-long eruption. During this eruption the summit of Piton de la Fournaise collapse, which represent a fantastic example of caldeira formation on a basaltic volcano (Michon et al. 2007).

A close link between magma withdrawal during this lateral eruption and the collapse has been established (Michon et al., 2009 ; Staudacher et al. 2009). Collapse of the Dolomieu Crater was recognized on April 6 by a camera of the Piton de la Fournaise Volcanological Observatory, located at the summit of the volcano. Based on field observations (Michon et al., 2007; Staudacher et al., 2009) and analysis of thermal images and DEMs obtained by the ASTER satellite (Urai et al., 2007), the scale of the collapse was estimated to be 1,100 × 800 m in area, 330 ± 15 m in depth, and 0.9 to $1.2.10^8$ m^3 in volume. The volume of magma emitted is estimated to ~$100\text{-}140.10^6$ m^3, with an emission rate of 52 to 54 $m^3.s^{-1}$ - the largest values for the historical period (since 1640). The maximum emission rate during the paroxysmal phase has been estimated as high as 300 $m^3.s^{-1}$ (Staudacher et al., 2009).

The eruptive vent being located at low altitude, a large part of the emitted lavas reached the sea. 'A'a lava flow advances into the ocean building a 0.5 km^2 delta (1.5 km long and ~400 m wide). A minimum value of $4.6 .10^6$ m^3/day of lava was fed by channels, lava tubes and overflows. The building stage of the delta was linked to hydrovolcanic explosions. Due to high flow rates, large amounts of lava have flowed on the submarine slopes of the volcano, reaching depths of several hundreds of meters as testified by the unknown dead fishes collected during the climax of the eruption. The underwater extent of this type of flows is always difficult to evaluate. The characteristics of underwater flows are largely determined by various factors such as flow mode on land, output rates, nature of submarine slopes of the volcanic island and coastal hydrodynamic conditions.

In the case of the April 2007 eruption, we benefit of two exceptionally good data sets of high-resolution multibeam bathymetry and imagery obtained before (July 2006) and after (January 2008) the eruption and covering the distal parts of 2007 lava flow. In July 2006, a complete and detailed bathymetric survey was performed with the R.V. Beautemps-Beaupré around La Réunion Island including the Grand Brûlé area. The same area offshore Grand Brûlé was surveyed again in January 2008 with the R.V. Meteor by the same scientific team (ERODER 2 cruise). The two vessels were equipped with the same bathymetric system: a EM120 Simrad system. These data were supplemented with photographs carried out on the lava bench by scuba divers. The onshore – offshore transition studies were done from daily air photographs taken during the first days of the eruption, time during which emission rates was the strongest and certainly determined the longest submarine lava flow.

These data will be presented and discussed. They give a very good example of lava entering the sea. Data shows that emitted volume is largely under evaluated when considering only onshore products. The comparison of bathymetry obtained in 2006 and 2008 and interpretation of backscatter images enable us to clearly determine the submarine extension of the lava flow. Significant depth changes occurred offshore the Grand Brulé

area with high-relief tongues on each side of the "eastern plateau" (see Lénat et al, 1989). This is also clearly identifiable on the acoustic images where a high backscatter can be undoubtedly associated with the new lava flow that reaches more than 850 meters in depth. The volume of new materials brought between the two surveys is evaluated around 34.10^6 m^3. This does not correspond to the total volume of submarine lava flows but only to the accumulation of lava on the common zone of the two surveys. In particular, it does not take into account the large volume accumulated near to the coast that constitutes the bench for which an estimate of 50 to 60.10^6 m^3 is given. With at least 90.10^6 m^3 of lava under the sea, 120.10^6 m^3 on-land and 20.10^6 m^3 trapped in the intrusions (dyke and/or sill - Staudacher et al, 2009), the volume of lava extracted from the magma chamber during the April 2007 event (~230.10^6 m^3) largely exceed the volume of the related collapse.

References

Lénat, J-F., Vincent, P., Bachèlery, P., 1989. The off-shore continuation of an active basaltic volcano: Piton de la Fournaise (Reunion Island, Indian Ocean): structural and geo-morphological interpretation from Sea Beam mapping. J. Volcanol. Geotherm. Res. 36, 1–36.

Michon, L., Staudacher, T., Ferrazzini, V., Bachelery, P. and Marti, J., 2007. April 2007 collapse of Piton de la Fournaise: A new example of caldera formation. Geophys. Res. Lett., 34: L21301, doi:10.1029/2007GL031248.

Michon L., Villeneuve N., Catry Th, Merle O., How summit calderas collapse on basaltic volcanoes: new insights from the April 2007 caldera collapse of Piton de la Fournaise volcano. J. Volcanol. Geoth. Res. 184 (1–2), 138–151.

Staudacher Th., Ferrazzini V., Peltier A., Kowalski Ph., Boissier P, Catherine Ph., Lauret F., Massin F., The April 2007 eruption and the Dolomieu collapse, two major events on Piton de la Fournaise. J. Volcanol.Geoth. Res. 184 (1–2), 126–137.

Urai, M, Geshi, N, Staudacher, T, 2007. Size and volume evaluation of the caldera collapse on Piton de la Fournaise volcano during the April 2007 eruption using ASTER stereo imagery, Geophys. Res. Lett., 34, L22318, doi:10.1029/2007GL031551.

Appendix 8

Servadio Z., Villeneuve N., Gladys A., Staudacher T., Urai M., 2008. Preliminary results of lava flow mapping using remote sensing in Piton de la Fournaise, La Réunion island. *Workshop on the "Use of Remote Sensing Techniques for Monitoring Volcanoes and Seismogenic Areas*", abstract, IEEE Naples.

Preliminary results of lava flow mapping using remote sensing in Piton de la Fournaise, La Réunion island.

Servadio Zarah
Laboratoire Géosciences Réunion et ESPACE Unit, Institut de Recherche pour le Developpement
Université de La Réunion
Saint Denis de la Réunion France
zarah.servadio@univ-reunion.fr

Villeneuve Nicolas
ESPACE Unit, Institut de Recherche pour le Developpement, Campus universitaire du Moufia
Sainte-Clotilde, île de la Réunion , France

Urai Minoru
Geological Survey of Japan
National Institute of Advanced Industrial Science and Technology (AIST), Tsukuba, Japan

Staudacher Thomas
Observatoire Volcanologique du Piton de la Fournaise
Institut de Physique du Globe (IPGP), CNRS, UMR 7154
La Plaines des Cafres, France

Gladys Astrid
Ecole Nationale des Sciences Géographiques
Marne la Vallée, France

Abstract—**The use of remote sensing is more and more incontrovertible in volcanic monitoring, especially in INSAR and thermal studies. A comprehensive database of high-resolution multispectral and multitemporal optical satellite imagery exists for Piton de la Fournaise, the active volcano on La Réunion Island. This database, however, remains relatively underexploited in volcanological studies of Piton de la Fournaise.**

Using a large image data set including SPOT 5 and 4, ASTER and aerial photography, we performed cartography of recent lava flows.

Different methods were applied for each sensor in order to extract and map lava flow contours and surface morphology. These methods include photo interpretation as well as fusion of thermal band and optical images. In addition we performed several tests with specific software combining object and spectral based techniques. Subsequently, a simple statistical comparison between different perimeters and areas mapped allowed us to determine a precision ratio. Results show that difficulties in extracting contours arise when the study area is a complex lava flow field where the different lava flows overlap, or have a similar textural and radiometric characteristics.

Keywords- remote sensing ; Piton de la Fournaise; Automatic Mapping; Principal components analysis

I. INTRODUCTION

Piton de la Fournaise (PDF) (Fig.1), on La Réunion Island, is one of the world's most active basaltic volcanoes with an average of one event every 8 months [1]. Between 1980 and 2008, 38 lava flows have been observed. The cartography of lava flows has particularly important implications for the knowledge of the lava emitted by the volcano, and can be very useful to increase the understanding of the PDF.

Even though remote sensing techniques have been used for volcanological studies for many years, there does not currently exist a methodology for automatic cartography that can be applied to all volcanoes.

This fact can be attribute to the poor use of high resolution imagery, the difficulties of timage reatment as applied to complex lava flow fields and the poor use of spectral and object-based automation approaches.

II. LAVA FLOWS MAPPING USING OPTICAL DATA

A. Presentation of the study area

Most of PDF's recent activity is located in the Fouqué Caldera. Eruptive fissures are mainly situated near the Dolomieu Crater, in the Grandes Pentes (Eastern part) and in the Northem and Southem parts of the caldera. Lava flows furthest from the caldera are easiest to map owing to their isolation.

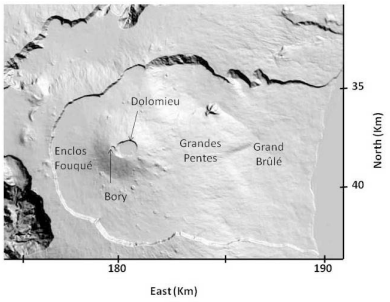

Figure 1: Piton de la Fournaise

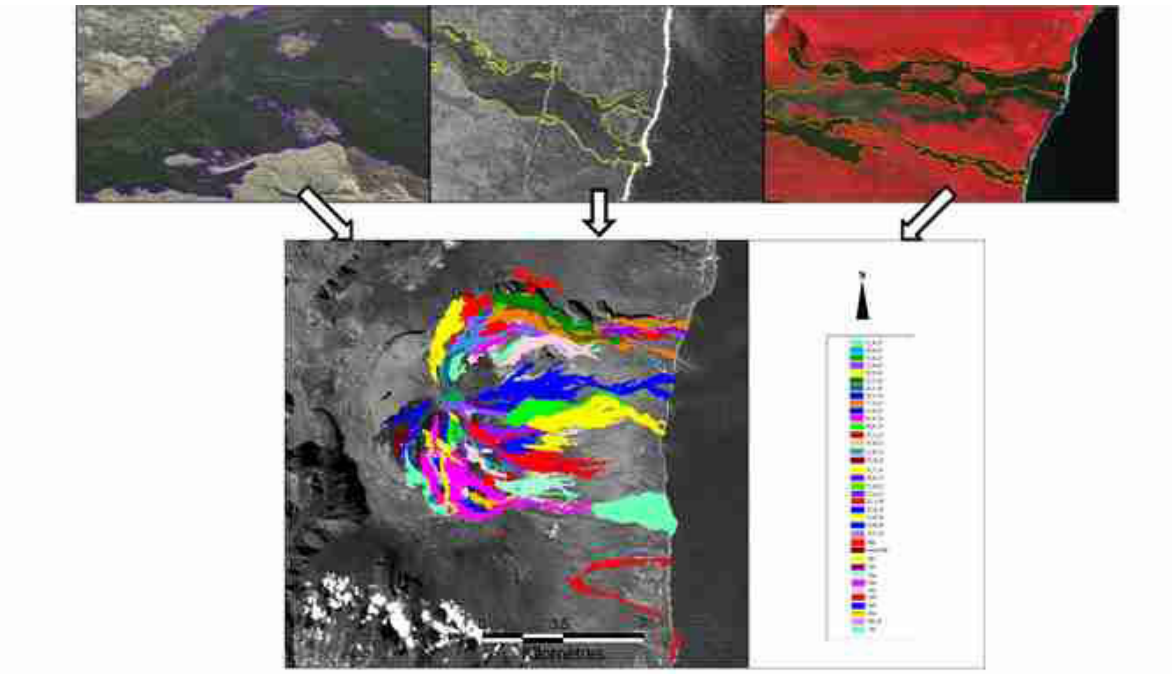

Figure 2 : Lava Flows Cartography between 1980 and 2007

B. Manual mapping

A large collection of high resolution multitemporal imagery was used for the manual mapping. This work has been done principally with aerial photography, SPOT 4 and 5 (Kalideos program, CNES, http://kalideos .cnes.fr) and ASTER (Advanced Spaceborne Thermal Emission and reflection Radiometer) data.

A total of 37 lava flows, between 1980 and 2007, have been digitized (Fig. 2). The accuracy with which each flow was digitized depends on the resolution of the imagery available. Is Lava flows mapped from aerial photography with resolution of 50cm do not have the same precision as those mapped from 20mSPOT 4 imagery.

C. Accuracy

Statistics have been gathered to compare the perimeters and areas of different digitized lava flows , depending on the data used to create the outline.

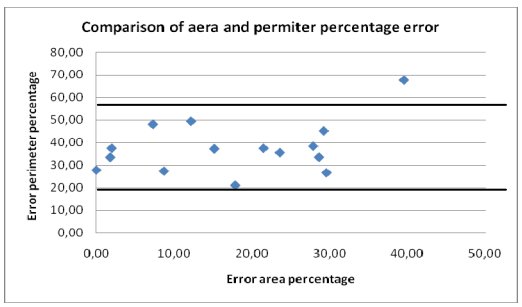

Figure 3: Comparison of area and perimeter percentage error

It was found that the perimeter of a lava flow digitized from SPOT 5 data can differ with up to 37.84% from the perimeter of that same lava flow when digitized from aerial photography. Similarly the area of lava flows can differ with up to 17.68%, depending on the data used as input. This would indicate that the perimeter obtained from the digitized lava flows cannot be used with certainty, but that the area can be used as a rough estimation.

Furthermore the relative perimeter and area errors are not correlated: the relative perimeter error does not influence the area error (Fig.3) The larger variation in perimeter than area, as well as the lack correlation between the errors in these variables is consistent with the behaviour of fractal shapes, which have fixed areas, but perimeters that increase with increasing detail (zoom) level.

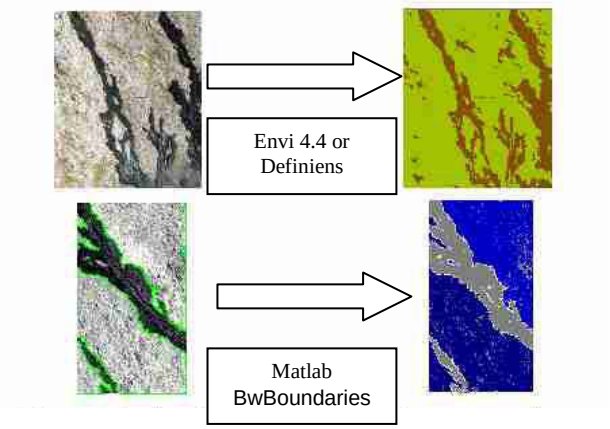

Figure 4: Isolated lava flows automatic cartography

III. AUTOMATIC CARTOGRAPHY

The aim is to produce an automatic cartography using a data treatment sequence not only for the visible surface information [2,3] but a complete one capable of obtaining the complete lava flow. During a first iteration a delimitation of the volcano influence area should be done. Different image processing methods can subsequently be used, depending on the lava flow type. The processing involved in extracting an isolated lava flow is significantly less complex than for overlapping flows. As a result, the processing of these two flow types are discussed separately.

A. Isolated lava flows

In the case of an isolated lava flow covering a vegetated area or a recent lava flow overlapping with older ones, the use of automatic classification or edge detection techniques allow us to obtain an automatic cartography using different software (Envi 4.4, Ecognition, Matlab…) as shown in Fig.4.

In these examples the spectral contrast of the lava flow with its surrounding material is sharp and the extraction of lava flows are relatively simple. When the spectral reflectance of the flow is similar to its surroundings, however, the treatment becomes more complicated.

B. Automatic cartography

To obtain an accurate automatic cartography, different image treatment processes have been used in Envi 4.4 (Fig. 5):

- a layer stacking of thermal and optical imagery;
- a principal component analysis;
- a decision tree classification;
- a classification to vector transformation.

Layer stacking was used to build a new multiband file from georeferenced data. During this process, thermal and optical imagery was resampled and reprojected to a common output image where all the data extents overlap. Using the thermal band allowed us to focus on one complete lava flow. This is an automatic discrimination by thermal wavelengths that correspond to an active area compared to its immediate environment.

Principal component analysis produce an image with spectrally uncorrelated output bands using a linear transformation to maximize the variance of the data. This transformation allows for an increase the optical reflectance variation in the area of high thermal activity.

The decision tree classification is a type of multilevel classifier. It is made up of a series of binary decisions that determine the classification of each pixel. For example, the use of a thermal threshold can delimit if a certain pixel falls inside the thermally active area or not. Inside the thermally active group a differentiation can be done between low and high thermal emission. The resulting classification yields the lava flow of interest as a specific class.

The classification to vector transform is executed to isolate and export the target class to a vector file.

C. Result accuracy

The total area obtained shows a variation of 11.5% of overestimation with the referenced one, and 13.1% for the perimeter. So the automatic mapping result obtain a good accuracy result. The aim of automatic cartography.

IV. OBJECT ORIENTED APPROACH

The use of object-oriented methods in classification automation is currently underexploited in volcanological studies [3, 4, 5, 6] .

A. Using image objects

In object-oriented segmentation, an image is divided into objects. An object is a group of similar, connected pixels that represent a region of relative homogeneity in an image. Regions in the image provide much more information than single pixels since the regions contain the spectral information of their constituent pixels, but can be analyzed further, based on color, shape, and texture.

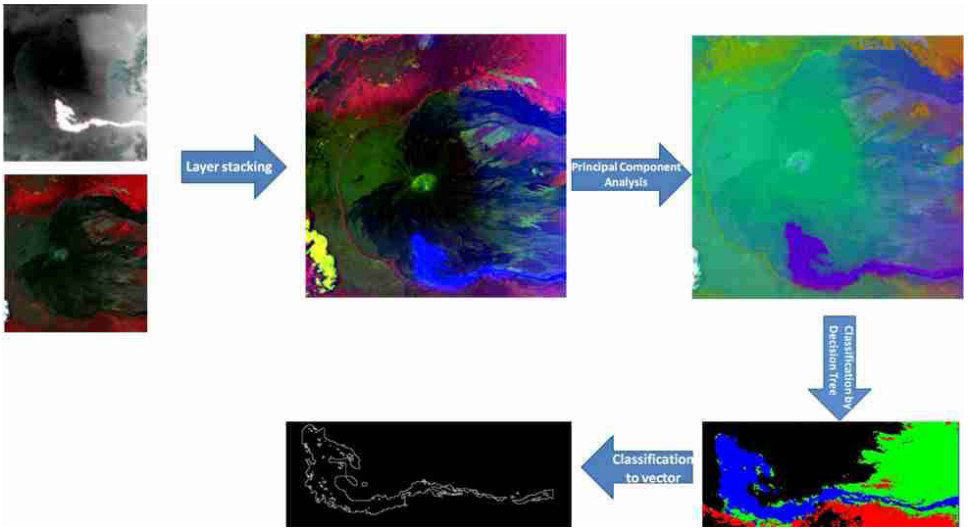

Figure 5: Automatic cartography treatment sequence

B. *Analysis*

The object-oriented classification automation was found to work only on isolated flows, the lava flow fields in Piton de la Fournaise being too complex for the segmentation when lava flows overlap. Newer flows overlying ancient ones can, however, be differentiated successfully (Fig.6).

Fissures on the volcano exhibit a strong contrast with characteristic reflectance, which makes it possible for them to be distinguished using object-oriented classification.. In this case the linearity of the fissures allow them to be identified using functions of shape and length of the image objects. Only some shadows can cause trouble in the automation. (Fig.6).

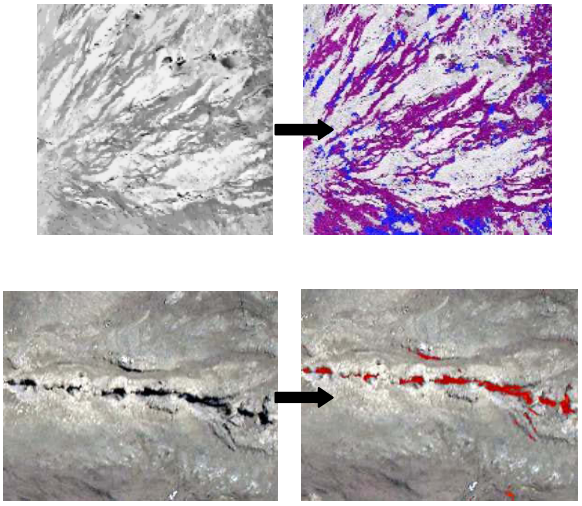

Figure 6: Recent lava flows and fissure cartography with Definiens

V. CONCLUSION

It is a cartographic objective that brings this automatic study. The aim to create an automated image processing chain is achieved. However the creation of a complete lava flow cartography using this technique is currently not feasible, because of the limited temporal frequency of available optical imagery, and the lack of sufficient thermal imagery.

ACKNOWLEDGMENT

Thanks to Kalideos program of Centre National d'Etude Spatial (CNES) for the SPOT data.

REFERENCES

[1] N. Villeneuve and P. Bachèlery, "Revue de la typologie des éruptions au Piton de La Fournaise, processus et risques volcaniques associés," Cybergeo : Revue européenne de géographie, vol. 336, 2006.

[2] A. Legeley-Padovani, C. Mering, R. Guillande, and D. Huaman, "Mapping lava flows through SPOT images - an example of the Sabancaya volcano (Peru)," Int. J. Remote Sensing, vol. 18, n°18, pp. 3111-3133, 1997.

[3] M. Abrams, E. Abbott, and A. Kahle, "Combined use of visible, reflected infrared, and thermal infrared images for mapping Hawaiian lava flows : J Geophys Res V96, NB1, Jan 1991, P475-484," International Journal of Rock Mechanics and Mining Science & Geomechanics Abstracts, vol. 28, pp. A359-A359, 1991.

[4] Z. Lu, R. Rykhus, T. Masterlark, and K. G. Dean, "Mapping recent lava flows at Westdahl Volcano, Alaska, using radar and optical satellite imagery," Remote Sensing of Environment, vol. 91, pp. 345-353, 2004.

[5] C. Corbane, J.-F. Faure, N. Baghdadi, N. Villeneuve, and M. Petit, "Rapid Urban Mapping Using SAR/Optical Imagery Synergy " Sensors, In Press.

Appendix 9

Michon L., Villeneuve N., Catry T. and Merle O., 2009b. How summit calderas collapse on basaltic volcanoes: New insights from the April 2007 caldera collapse of Piton de la Fournaise volcano. *J. Volcanol. Geotherm. Res.,* 184, 138–151.

Journal of Volcanology and Geothermal Research 184 (2009) 138–151

Contents lists available at ScienceDirect

Journal of Volcanology and Geothermal Research

journal homepage: www.elsevier.com/locate/jvolgeores

How summit calderas collapse on basaltic volcanoes: New insights from the April 2007 caldera collapse of Piton de la Fournaise volcano

Laurent Michon [a,*], Nicolas Villeneuve [b], Thibault Catry [a,c], Olivier Merle [a,d]

[a] Laboratoire GéoSciences Réunion, Université de la Réunion, Institut de Physique du Globe de Paris, CNRS, UMR 7154 — Géologie des Systèmes Volcaniques, 15 avenue René Cassin, 97715 Saint Denis, France
[b] Institut de Recherche pour le Développement, US 140, BP172, 97492 Sainte-Clotilde cedex, France
[c] Dipartimento di Scienze della Terra e Geologico Ambientali, University of Bologna, Piazza di Porta S. Donato 1, 40127, Bologna, Italy
[d] Laboratoire Magmas et Volcans, UMR 6524 CNRS-IRD-Université Blaise Pascal, 5 rue Kessler 63 038 Clermont-Ferrand, France

ARTICLE INFO

Available online 14 November 2008

Keywords:
caldera
collapse dynamics
Piton de la Fournaise

ABSTRACT

In April 2007, Piton de la Fournaise volcano experienced a caldera collapse during its largest historical eruption. We present here a structural analysis both of the caldera and the surrounding area, and precise GPS data recorded with a dense GPS network specifically dedicated to the analysis of deformation related to the summit collapse structures. Despite a collapse of more than 300 m in the central zone, the geometry of the new caldera is similar in map view to that of the pre-existing collapsed structure, which was formed from the coalescence of several pit craters. The caldera shows an asymmetric inner geometry with sub-vertical walls in the NW quadrant and steep scarps composed of inward tilted blocks in the southern half. The presence of preserved polished surfaces on the lower part of the sub-vertical scarp indicates that it corresponds to the caldera north-western ring fault. The April 2007 caldera collapse led to the development and the reactivation of concentric fractures on the caldera rim, mostly along the southern limit of the caldera. GPS data show that fractures result from radial extensional stresses that are restricted within the first tens of meters of the caldera edge. GPS data also reveal that the caldera collapse was coeval with a centripetal deflation, whose magnitude is largest along the southern half of the caldera. The displacements recorded by GPS result from both a general deflation, due to magma withdrawal from Piton de la Fournaise's summit magma chamber, and additional local effects related to the caldera collapse. Comparison of the caldera collapses at Piton de la Fournaise, Miyakejima and Fernandina reveals striking similarities, with cyclic seismic signals accompanying small-scale deflation–inflation cycles. This strongly suggests a common mode of collapse. Hence, we propose a unifying model of caldera collapse in basaltic setting, in which the inward deflation due to magma withdrawal from the magma chamber prevents the collapse of the caldera roof until the gravitational stress acting on the rock column above the magma chamber exceeds the shear strength along pre-existing ring faults. The downward displacement stops when the pressure increase into the magma chamber is able to again sustain the rock column. The succession of (1) inward deflation that prevents the collapse, (2) collapse due to gravitational stress and (3) stopping of the downward motion is repeated many times. The frequency of the cycles is influenced by the rate of magma withdrawal and by the amount of intrusion of magma along the ring faults.

1. Introduction

Basaltic volcanoes present summit calderas, whose formation is related in most cases to lateral magma migration from a shallow magma reservoir (e.g. MacDonald, 1965). Observations of basaltic calderas worldwide, and the few recorded collapse events, show common structural characteristics and collapse mechanisms, which can be summarised as follows. First, caldera collapses are contemporaneous with a periodic seismicity underlined by either a very-long-period seismic signal (Miyakejima in 2000, Kumagai et al., 2001) or large earthquakes, i.e. between M_s 4.4 and 5.5 (Fernandina in 1968, Simkin and Howard, 1970; Filson et al., 1973). Despite differences in the type of seismic signal, their periodicity has been interpreted in the same way, i.e. an intermittent collapse of the rock column into the magma chamber (Simkin and Howard, 1970; Filson et al., 1973; Kumagai et al., 2001). Questions remain on the source of the periodicity which is interpreted as being controlled either by the constant magma outflow (Kumagai et al., 2001), by an irregular geometry of the bottom of the collapsing rock column (Filson et al., 1973) or by regular stress built up along the caldera fault, which is sporadically relieved by movement along the ring fault (Simkin and

* Corresponding author. Tel.: +33 262 262 93 82 04; fax: +33 262 262 93 82 66.
E-mail address: laurent.michon@univ-reunion.fr (L. Michon).

0377-0273/$ – see front matter © 2008 Elsevier B.V. All rights reserved.
doi:10.1016/j.jvolgeores.2008.11.003

Howard, 1970). Second, analyses of the surface deformation have long-revealed that collapses are coeval with centripetal deflation of the edifice (Wilson, 1935; Ryan et al., 1983). Both deformations, i.e. the collapse and the inward subsidence, result from pressure decrease within the magma chamber and/or the plumbing system (Mogi, 1958; Walsh and Decker, 1971; Ito and Yoshioka, 2002). Third, collapse calderas often show peripheral concentric extensional fractures hundreds of metres from the edge of their caldera rim (Simkin and Howard, 1970; Lénat and Bachèlery, 1990; Troll et al., 2002; Acocella, 2006; Carter et al., 2007). The various authors describe an increase of extension and vertical displacements close to the caldera rim, but their interpretations differ. The changes in rim geometry are thought to result from superficial processes postdating the caldera formation (Acocella, 2006), from extensional stresses related to the centripetal subsidence (Branney, 1995), or from inflation–deflation cycles (Lénat and Bachèlery, 1990).

In April 2007, Piton de la Fournaise volcano experienced a caldera collapse during its largest historical eruption (Michon et al., 2007). We present here the summit deformation accompanying this event. We integrate a detailed analysis of both concentric fractures and intra-caldera structures and faults, with high precision GPS data from a dense network implemented surrounding the caldera. Our study benefited from an initial field and GPS campaign carried out in March 2007, a few days before the onset of the eruption and collapse. The GPS network has been reoccupied twice, in May and November 2007, in order to determine the syn-collapse and post-collapse displacements, respectively. This paper aims at determining the relationship between the concentric fractures and the collapse. It also attempts to better understand the collapse mechanism and its relation to eruption dynamics. Finally, it addresses the role of pre-existing structures in the development of a new caldera.

2. Geological setting

Piton de la Fournaise volcano is one of the world's most active volcanoes (Lénat and Bachèlery, 1987). At the edifice scale, it is characterised by two NE and SE rift zones and an E–W U-shaped caldera formed around 4.5 ka ago (Bachèlery, 1981; Fig. 1a and b). The volcanic activity is concentrated in the upper part of the U-shaped structure, the Enclos caldera, where the accumulation of volcanic products has built up a steep central cone (Michon et al., 2009-this issue). Prior to April 2007, the summit of the active cone was cut by two collapse structures: Bory in the west, which is currently inactive, and Dolomieu in the east, the location of the caldera collapse during the large April 2007 eruption (Fig. 1c). Before this collapse, the elongated shape of the pre-existing Dolomieu was the result of the coalescence of several pit craters (Lénat and Bachèlery, 1990; Carter et al., 2007). The largest of these events occurred between 1933 and 1936, during which the eastern half of Dolomieu experienced a 150 m-deep collapse (Fig. 1d; Lacroix, 1939; Bachèlery, 1981). Until 1953, the western part of Dolomieu also suffered recurrent collapses that were accompanied by progressive subsidence of the crater floor. From 1953 the lava accumulated during the frequent summit eruptions and progressively filled the collapse structure, whose outer contour remained unchanged until March 2007, despite the small pit crater collapse in 1986 (Hirn et al., 1991) and a brutal but minor subsidence in 2002 (Fig. 1d; Longpré et al., 2007). It is noteworthy that the August 2006–January 2007 summit eruption created a lava pile of 20–30 m on the Dolomieu floor, filling the crater and overtopping the eastern caldera wall (Michon et al., 2007).

In 1990, a detailed structural analysis of the summit of the active cone revealed a complex network of concentric extensional fractures concentrated around Dolomieu only (Fig. 1d; Lénat and Bachèlery, 1990). It also highlighted the asymmetric distribution of the concentric fractures around the east and west parts of Dolomieu. The eastern rim of Dolomieu was characterised by a few fractures restricted to a 50–80 m wide zone. In contrast, concentric fractures were scattered within a 200–300 m wide zone around the western half of Dolomieu. The northern limit of this fracture network coincides with a topographic break-in-slope that corresponds to the hidden boundary of a paleo-pit crater (Lénat and Bachèlery, 1990; Michon et al., 2009-this issue). South of Dolomieu, the Petit Plateau paleo-pit crater, formed around 1911 (Bachèlery, 1981), consists of an independent system of concentric fractures that delimitates the hidden collapsed structure. The age of the overall fracture system is hard to determine. However, the lack of any significant fractures south of the western fracture zones, where the lava emitted by the 1936 and 1956 eruptive fissures covers the surface (Fig. 1d), suggests that fractures in the west predate these eruptions. In the east, the similar distribution of both the limits of the 1933–1936 pit crater and the peripheral concentric fractures supports a temporal relationship between the main collapse event and the development of extension fractures close to the rim. Since 1990, the only significant change in the concentric fracture system was observed during the August 2006–January 2007 eruption, during which fractures close to the rim in the south-eastern part of Dolomieu opened of a few tens of centimetres to a few metres. These fractures accommodated the progressive inward tilting of rock panels torn apart from the rim of the collapse structure.

The April 2007 caldera collapse of Piton de la Fournaise occurred during the largest historical eruption, starting on 30th March and ended the 1st May 2007. Although the detailed evolution of the eruption has already been presented (Michon et al., 2007; Staudacher et al., 2009-this issue), we summarise below the main characteristics that allow us to interpret the origin and dynamics of the caldera collapse. On 30th March, a first eruptive fissure opened south-east of the central cone at about 1900 m above sea level (Fig. 1b). After less than 10 h, the magma emission ceased, whereas the summit seismicity remained at a very high level. The magma emission started anew on 2nd April when an eruptive fissure opened at about 600 m asl, 7 km away from the summit (Fig. 1b). The rate at which magma was discharged, which was already large, increased during 5th April contemporaneously with a summit centripetal deflation. The first summit collapse occurred on 5th April at 20:48, contemporary to a magnitude 3.2 volcano-tectonic event (Michon et al., 2007). It was immediately followed by a sudden centrifugal uplift of the caldera rim (Michon et al., 2007; Staudacher et al., 2009-this issue). The collapse also had a striking impact at the eruption site where the seismic signal increased by around 50%. Then, both the seismic signal and the summit displacements began to occur in cycles characterised by an inward deflation accompanied by an increase of the seismic signal, ending with a sharp outward uplift contemporaneous with sudden decrease of the seismicity. The cycle frequency gradually increased from 2 h to 30 min (Michon et al., 2007; Staudacher et al., 2009-this issue). A total of 38 collapse events were distinguished between 5th April, 20:48, and 7th April, 00:40. First observations of the new caldera, in the afternoon of 6th April, revealed that the 16 first collapses triggered the development of most of the summit collapse caldera (Michon et al., 2007). Disregarding continued spalling of material from the caldera wall, the final geometry of the caldera was attained on 10th April. The eruption continued at a low level until the 1st May 2007.

3. Summit deformation related to the April 2007 eruption

3.1. Structural analysis

On 6th April, the first observations indicated that the collapse was elongated along an E–W axis and concentrated in the northern part of Dolomieu (see Fig. 4b in Michon et al., 2007). It was bounded by 200–300 m-high subvertical scarps in the east, west and north, and by subsiding terraces in the south. Two annular plateaus corresponding to the pre-existing floor of Dolomieu remained in the E and SW (see Fig. 4 in Michon et al., 2007).

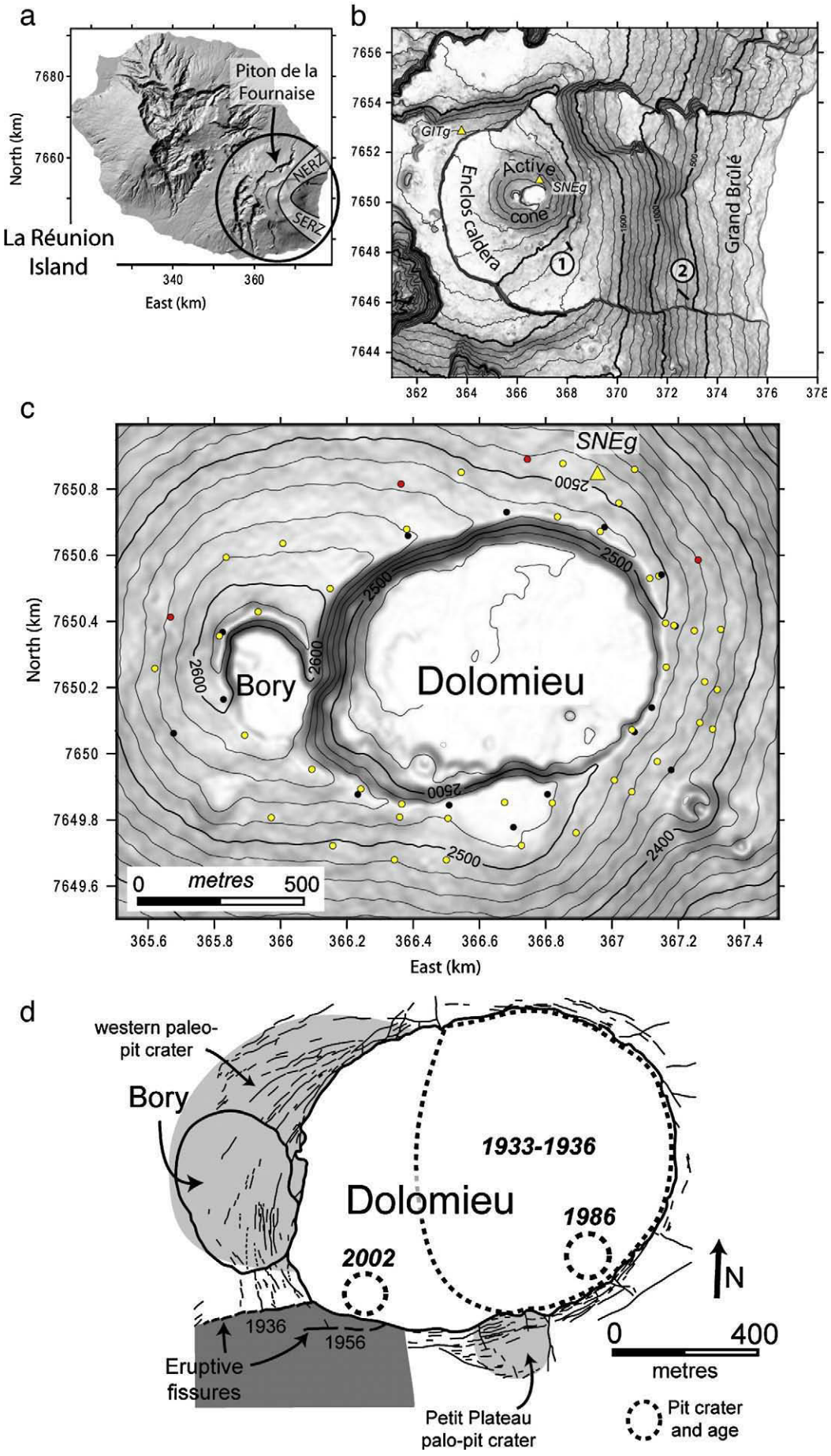
a
Piton de la Fournaise
NERZ
SERZ
La Réunion Island
North (km)
East (km)
b
GITg
Active cone
SNEg
Enclos caldera
Grand Brûlé
c
SNEg
Bory
Dolomieu
North (km)
East (km)
0 metres 500
d
western paleo-pit crater
Bory
1933-1936
Dolomieu
1986
2002
1936
1956
Eruptive fissures
Petit Plateau palo-pit crater
N
0 400
metres
Pit crater and age

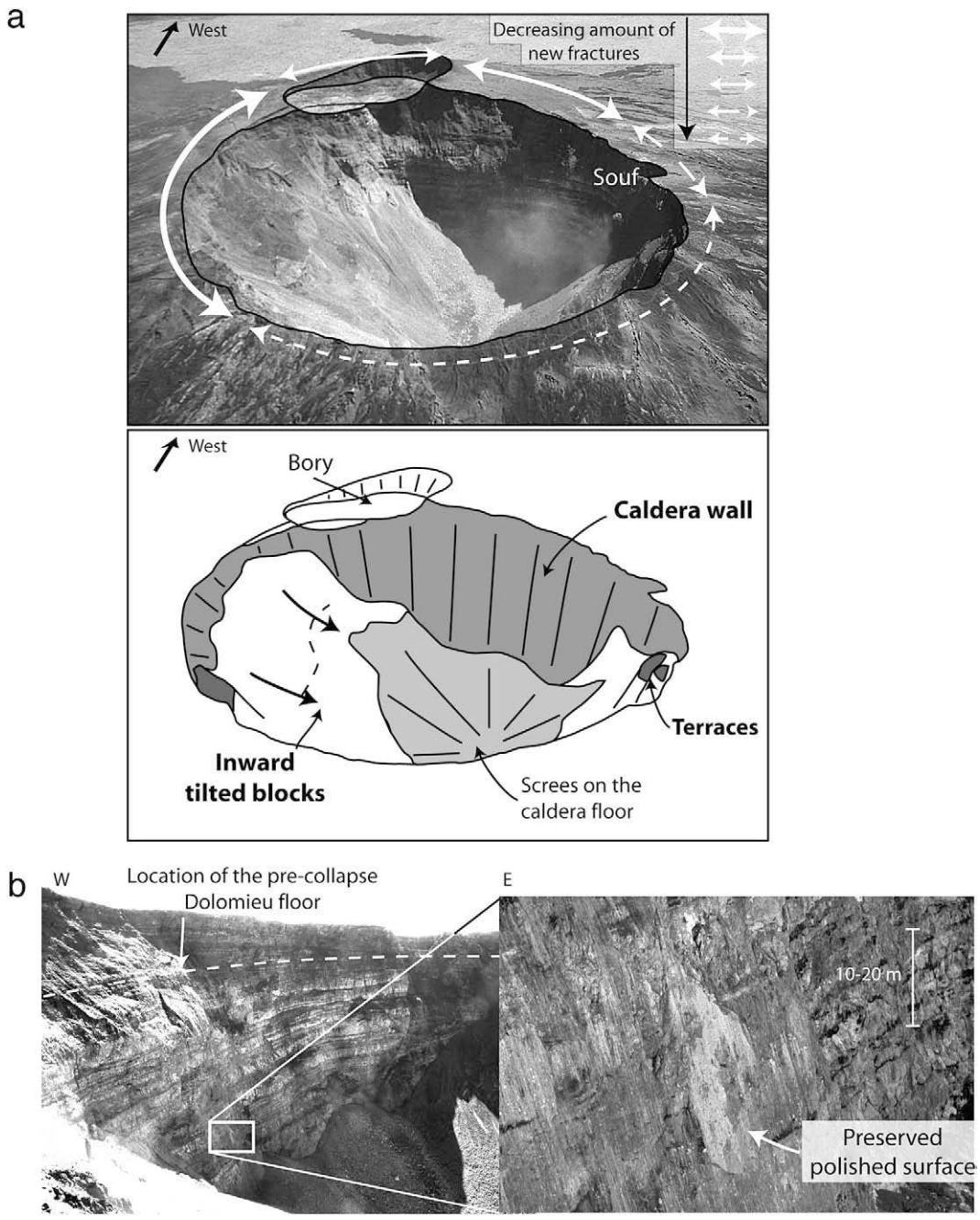

Fig. 2. a — The April 2007 caldera. The maximum depth is located in the northern half of the caldera. Note the differences between the northern and southern caldera flanks. New concentric fractures are represented by arrows. Fractures opened essentially south of the caldera. Souf: Soufrière pit crater. b — View of the north-western caldera wall. Several polished surfaces were preserved few days after the caldera collapse until destruction of this scarp by landslide in May 2007.

At the end of the collapse, on 10th April, the new caldera had a maximum depth of 320–340 m (Michon et al., 2007; Urai et al., 2007) at the location of the initial collapsed structure. The deepest part of the caldera is covered by scree resulting from the frequent rock slides from the caldera walls (Fig. 2a). Two different topographic expressions of the collapse are distinguished. The southern, eastern and north-eastern walls have average slopes of 40–50°, whereas the north-western wall is sub-vertical (70–80°). The distribution of these two distinct geometries coincides with the structure differences observed on 6th April. The north-western caldera flank already existed on 6th April, by which time it was bounding the northern collapse structure. The preservation of polished surfaces, found only on the lower half of this scarp (Fig. 2b), suggests that the north-western caldera wall corresponds to an inward-dipping ring fault. In contrast, the geometry

Fig. 1. a — Location of Piton de la Fournaise volcano on La Réunion Island. b — Location of the eruptive centre within the Enclos caldera. Eruptive fissures opened on March 30th and April 2nd are located by 1 and 2, respectively. SNEg and GITg correspond to the reference receivers of the summit GPS network. c — Distribution of the benchmarks around the summit collapsed structures of Dolomieu and Bory. Benchmarks measured in March and May 2007 (yellow), in May and November (black) and for both periods (red). d — Fracture network around the summit collapsed structures (after Lénat and Bachèlery, 1990).

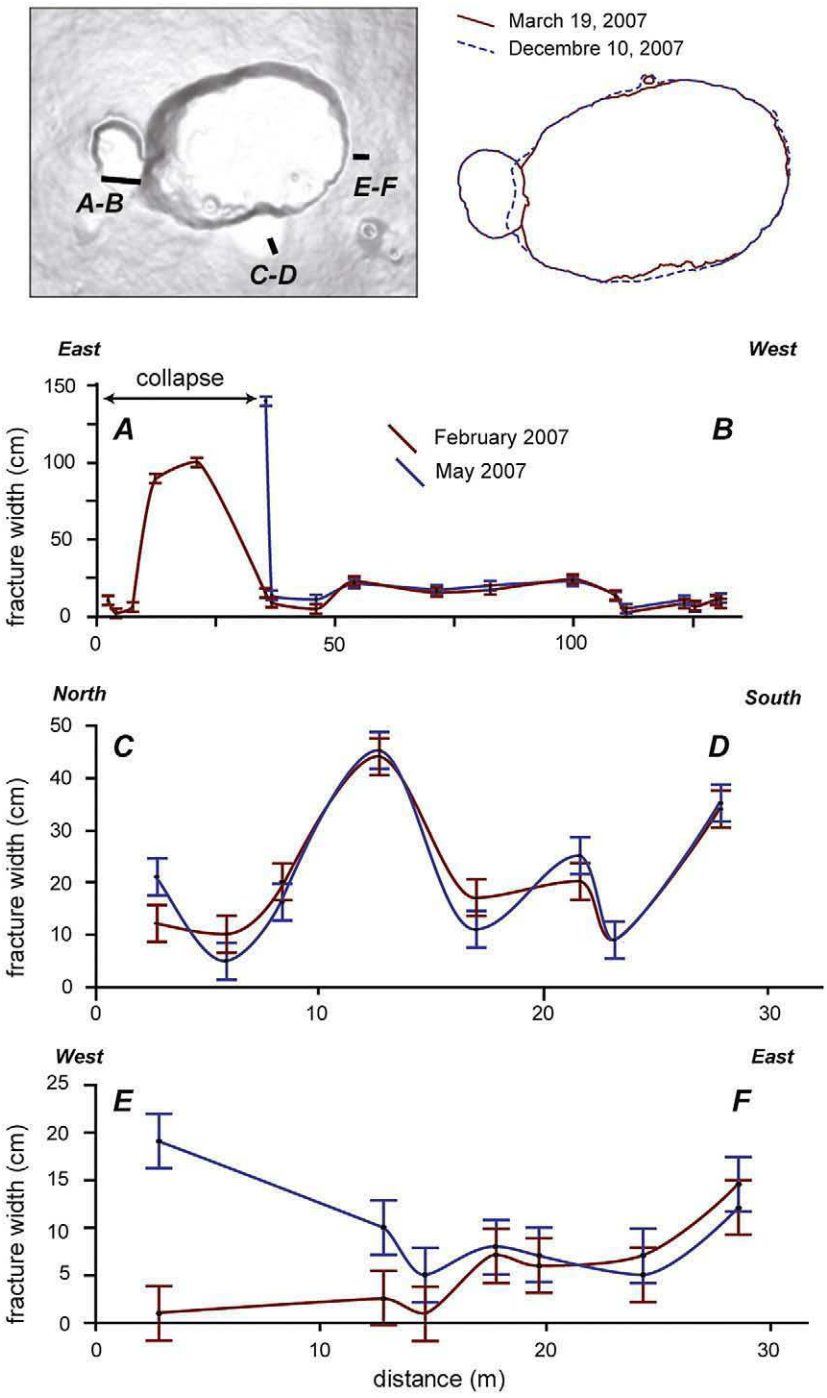

Fig. 3. Contours of the summit structures before and after the caldera collapse. Fracture width along three radial profiles measured in February and May 2007.

of the southern, eastern and north-eastern flanks post-dates 6th April. This likely results from the inward subsidence of the southern and eastern plateaus similar to that observed during the caldera formation at Miyakejima (Geshi et al., 2002).

In map view, Dolomieu was a 1–1.1 km-long and 0.76–0.80 km-wide elongated structure before the April 2007 eruption (Fig. 3). The April 2007 caldera collapse constitutes the largest collapse event ever observed at Piton de la Fournaise. However, despite a collapse of several hundreds of metres, the contour of the new caldera did not significantly change. The new caldera widened only a few tens of metres in the north, west and south parts, mostly a few days after the caldera collapse (Fig. 3). The similar geometry of the pre-existing collapse structure and the new caldera, and the lateral growth of the initial collapse up to the pre-existing Dolomieu boundary can be compared to the map view evolution of the caldera collapse at Miyakejima, where the initial caldera grew laterally up to approximately the limit of the pre-existing 2.5 ka-old Hatchodaira caldera (Geshi et al., 2002).

We also showed in Section 2 that, prior to 2007, the rim of Dolomieu was affected by asymmetrically distributed concentric fractures (Fig. 1). Three radial profiles were implemented in February 2007 around Dolomieu, at different distances from the caldera edge, in order to determine the potential reactivation of these fractures during collapse events (Fig. 3). The effect of the April 2007 caldera collapse has been evaluated by a reiteration of the profiles in May 2007. Fig. 3, which shows the fracture width before and after the collapse, illustrates the

influence of the April 2007 caldera collapse in the fracture system. It clearly shows that the collapse reactivated only the closest fractures to the caldera edge, and had no impact away from the edge. The concentration of the deformation is corroborated by the development of a narrow fracture system within the first tens of metres from the caldera edge, the density of which varies laterally. The new concentric fractures are densely distributed around the southern part of the caldera, whereas they are nearly non-existent in the east (Fig. 2a).

3.2. GPS data

Since 2001, the deformation of Piton de la Fournaise related to dyke intrusion has been regularly monitored by the GPS network of the Piton de la Fournaise Volcano Observatory (OVPF/IPGP; Peltier, 2007). This network, which is composed of about 80 stainless steel benchmarks cemented around the crater, on the flanks and at the base of the summit cone, accurately measures large scale deformation of the Piton de la Fournaise edifice, but is inadequate to evaluate in detail the summit deformation linked to collapse events. Hence, we implemented a new GPS network in November 2005, specifically dedicated to the structural analysis in a narrow zone around Bory and Dolomieu.

3.2.1. Methodology

The new GPS network is composed of 62 benchmarks (geodetic nails fixed into massive lava) installed along 24 radial profiles, and of two permanent receivers of the OVPF/IPGP located at the summit and outside the Enclos caldera (Fig. 1b and c). The position of each point of the network was measured before the eruption (in March 2007), and twice after the eruption (in May and November 2007). This allows the determination of the deformation related to the April 2007 caldera collapse and the residual subsidence following this event. Measurements were performed in differential mode with dual-frequencies receivers (2 Ashtech Zextrem and 2 Trimble NetRS). The SNEg summit receiver of the permanent GPS network of OVPF/IPGP (Fig. 1) was used as reference. Its position was systematically calculated with respect to a stable permanent receiver (GITg) located outside the Enclos caldera. The location of SNEg was precisely measured in static mode during 6 h with a 1 s sampling rate. In a way similar to measurements at Merapi volcano (Beauducel et al., 2006), measurements of the benchmarks were performed with a small base line (<1.5 km), a 1 s sampling rate and station on the benchmarks of 3 min. During each GPS campaign, several benchmarks were measured twice with a time interval of several hours in order to take into account not only the instrumental RMS values, but also the handling error. Thus,

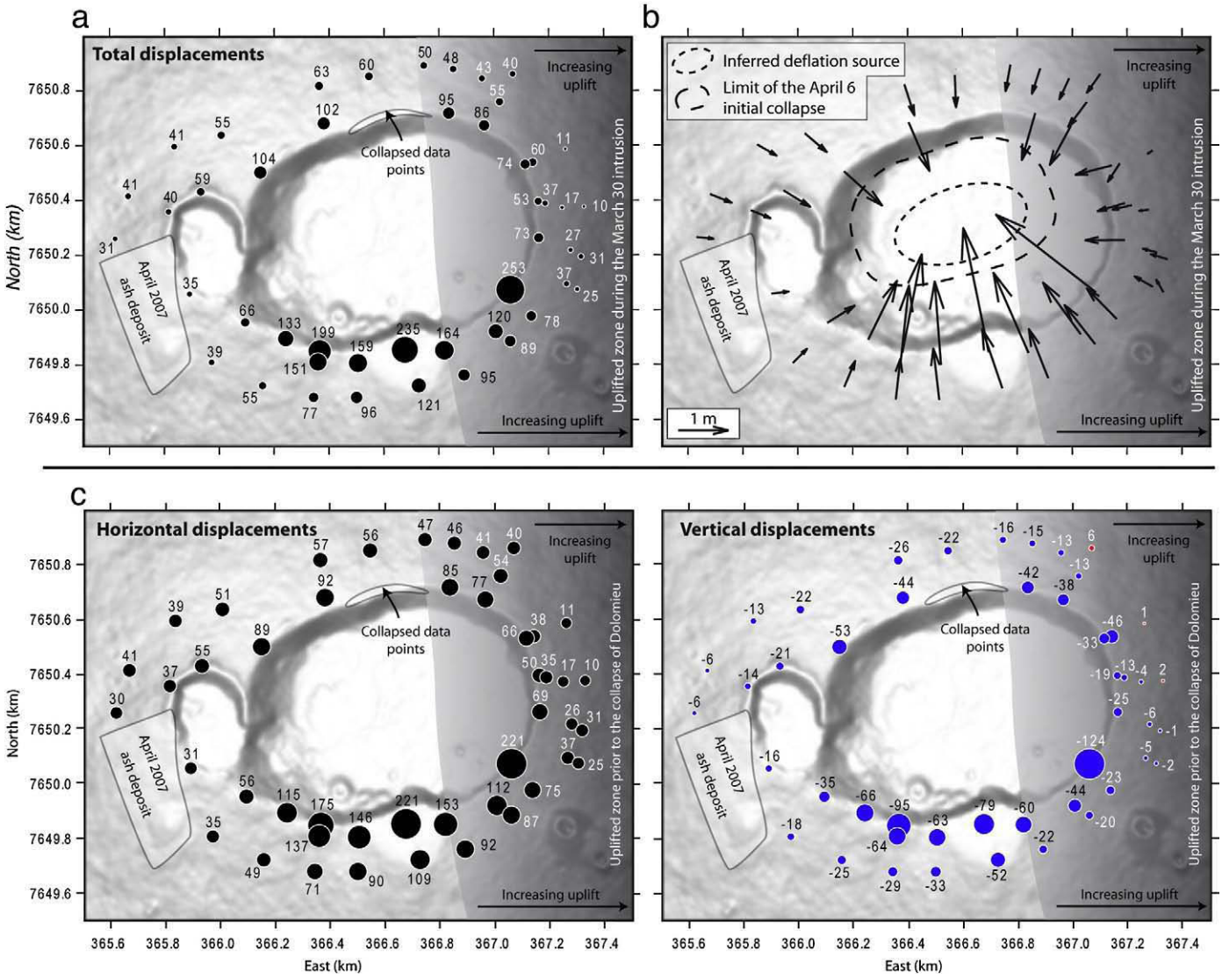

Fig. 4. Displacements between March and May 2007. a — Total displacements (in cm). b — Displacement vectors for horizontal components. c — Horizontal and vertical components (in cm).

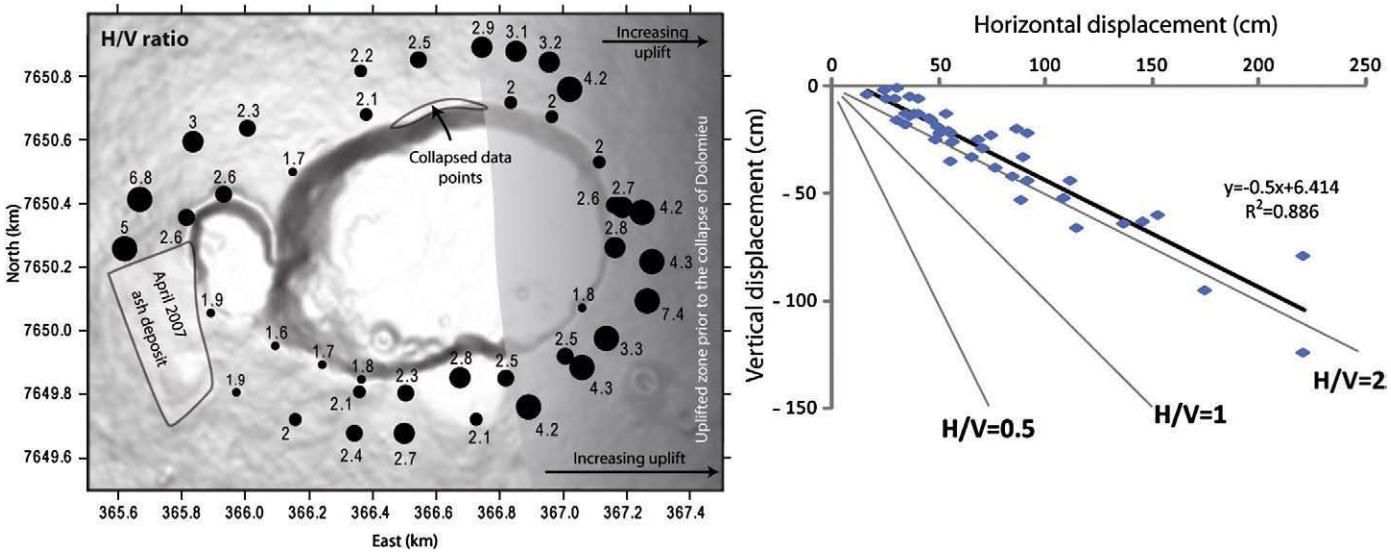

Fig. 5. Horizontal/vertical ratio for the period between March and May 2007. The *H*/*V* ratios are linearly organised suggesting a predominant common source of deformation.

the average horizontal precision calculated for each benchmark is of 1.1 cm and the vertical average precision is of 0.8 cm.

3.2.2. Displacements between March and May 2007

Between March and May 2007, the summit of Piton de la Fournaise experienced a progressive pre-eruptive outward inflation, additional uplift related to a dyke intrusion, and the caldera collapse. The permanent GPS network of the OVPF/IPGP clearly shows that the initial outward deformation was of minor importance with respect to the eastward dyke intrusion and much less than that measured during the caldera collapse (Peltier et al., 2009-this issue). Hence, most of the displacements inferred from our GPS campaigns in March and May 2007 result from the collapse event. Only the easternmost benchmarks are significantly influenced by the 30th March intrusion.

Our GPS data clearly show the large centripetal deformation related both to magma chamber deflation and the collapse event (Fig. 4b). When excluding the easternmost data points, which were also affected by the 30th March dyke intrusion that led to the opening of eruptive fissures SE of the cone (Fig. 1b), the displacement values range between 31 and 253 cm (Fig. 4a). It is likely that the latter value, which strongly differs from the surrounding ones, results from the displacement of an isolated block. The largest surface displacements are located on the southern caldera rim, where values higher than 130 cm are reached close to the caldera wall. Our data also exhibit a sharp decrease of the displacements (−38 to −61%) in the first two hundred metres from the northern and southern caldera edge. Such differences, which suggest the occurrence of extensional stresses on the proximal caldera rim, can be correlated with the location of the new concentric fractures, i.e. in a narrow zone around the western half of the caldera (Fig. 2a). Additional information can be found in the direction of the displacement vectors, which indicate the approximate location of the deflation source (Walsh and Decker, 1971). Here, the overall displacements suggest a deflation source elongated along a N75 axis that corresponds to the direction of elongation of the pre-existing Dolomieu and of the 6th April initial collapse (Fig. 2a).

The comparison of the horizontal and vertical components of displacement provides further information that can be used to better constrain the geometry of the deflation source (Dieterich and Decker, 1975). GPS data show that the summit deflation led mostly to horizontal displacements (Figs. 4c and 5). For every benchmark, the ratio between horizontal and vertical displacements, the *H*/*V* ratio, is always higher than 1 (Fig. 5). It shows a remarkably linear distribution with an average value around 2, confirming that most of the benchmark displacements measured between March and May result from a similar, and likely a single origin, i.e. the syn-collapse deflation. The GPS network of the OVPF/IPGP also recorded predominant horizontal displacements at the base of the cone (Peltier et al., 2009-this issue). Despite lateral variations between the western and eastern parts, along each transect, the closer to the caldera edge, the lower the *H*/*V* ratios (Fig. 5). Then, with the exception of the caldera walls, which suffered mostly vertical displacements, the central cone of Piton de la Fournaise experienced a predominant centripetal "horizontal collapse".

3.2.3. Displacements between May and November 2007

The GPS network has been reoccupied in November 2007 in order to identify post-collapse subsidence. Data show that during the 6 month-long period, the caldera rim continued to slightly subside (Fig. 6). According to Staudacher et al. (2009-this issue), 95% of the post-collapse deformation occurred during the first 3 months and the remaining 5% during July to November 2007. The distribution of the displacements for the period between May and November 2007 differs from that of the period between March and May 2007. The direction of the displacement vectors and the distribution of the largest displacements around the western half of the collapse caldera, could suggest a deflation source located below the western half of the caldera (Fig. 6). However, it cannot be excluded that the difference in the deformation pattern results from local deformation. It is noteworthy that the latest caldera wall destabilisations only occurred along the western scarps, where the inward displacements were still significant. Contrary to the *H*/*V* ratios for the period between March and May 2007, which show important lateral variations, the *H*/*V* ratios for the period between May and November 2007 present a homogeneous spatial distribution with values lower close to the caldera edge than at the distal extremity of the transects (Fig. 6c). This suggests an identical deformation style all around the caldera, which is independent of the amount of deformation. In consequence, our GPS data provides information both on the source and the mode of deformation.

Fig. 6. Displacements measured for the period between May and November 2007. a — Total displacements (in cm). b — Displacement vectors for horizontal components. c — Horizontal/vertical ratio.

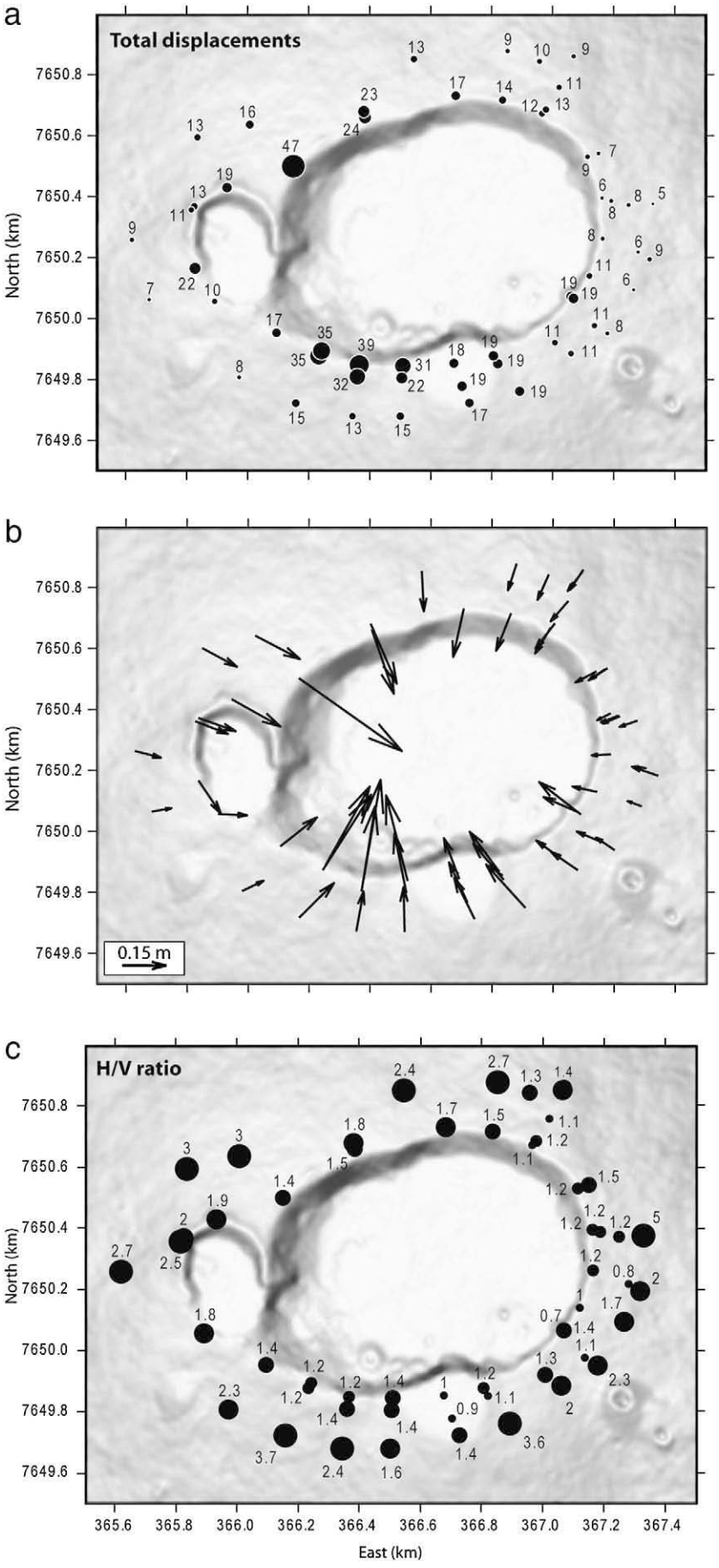
a
Total displacements
North (km)
7650.8
7650.6
7650.4
7650.2
7650.0
7649.8
7649.6
b
0.15 m
c
H/V ratio
365.6
365.8
366.0
366.2
366.4
366.6
366.8
367.0
367.2
367.4
East (km)

4. Discussion

4.1. Origin of the concentric fractures around basaltic calderas

Concentric fractures consist of extensional structures that are commonly observed around calderas. For example, at Erta 'Ale, (1) they are found within 20–60 m of the caldera rim, (2) their distance from the rim increases with the height of the caldera scarps, and (3) their opening width tends to increase when they are nearer to the rim (Acocella, 2006). Their development is consequently interpreted in terms of gravitational destabilisation of the caldera walls after the collapse (Acocella, 2006). At Fernandina, a similar fracture network has been observed around the caldera after the 1968 collapse (Simkin and Howard, 1970). Fractures are present on the rim 500 m from the edge and their density and size increase approaching the edge. Contrary to Erta 'Ale, the fracture network is interpreted as resulting from the collapse event (Simkin and Howard, 1971). These different interpretations of similar fracture networks raise the question of the multiple origins of the concentric fractures. Considering the concentric fracture network of Piton de la Fournaise, we propose several mechanisms that lead to the development or reactivation of concentric fractures.

1- The analysis of the fracture network before and after the April 2007 caldera collapse of Piton de la Fournaise reveals that concentric fractures do form on the caldera rim during collapse events. At Piton de la Fournaise, they are restricted to a few tens of metres of the caldera edge. A combination of GPS and structural data indicates that their formation is related to extensional stresses, which affected the proximal part of the caldera rim. They developed essentially south of the caldera where the sub-vertical part of the walls is of a few tens of metres (Fig. 2). The lack of correlation between the fracture density and the height of the caldera walls suggests that most of the extensional stresses do not result from local gravitational effects. This process can however not be entirely ruled out, specifically for the nearest fractures of the caldera edge. In consequence, we propose that most of the new concentric fractures result from extensional stresses that affect the proximal part of the caldera rim during the inward tilt of the caldera floor during successive collapses of the rock column. Such a mechanism is supported by the spatial correlation between the densest fracture zone and the tilted blocks around and into the southern half of the caldera. The development of the new fracture network was coeval with the reactivation of the pre-existing concentric fractures, which were the closer to the edge (Fig. 3).
2- Concentric fractures form at the limit of paleo-collapsed structures such as Petit Plateau and the western paleo-pit crater (Fig. 1d). The concentric fractures around these paleo-collapsed structures could result from a progressive subsidence due to compaction of the formations that filled the depression. However, 90–95% of the filling is composed of massive lava bodies that can hardly be compacted and the upper lava unit, which flowed outside the crater, is also affected by the concentric fractures. We propose that the whole paleo-collapsed structures may slightly subside during later collapses, triggering the development of circumferential extensional fractures above their hidden limits. Such a mechanism is suggested by our GPS data, which show for the period between March and May 2007 vertical displacements of the benchmarks located above the Petit Plateau paleo-pit crater between 20 and 40% greater than those outside the structure.
3- Finally, concentric fractures are reactivated during the progressive filling of the caldera. This process has been clearly observed during the August 2006–January 2007 summit eruption, during which concentric fractures progressively opened while lava accumulated within Dolomieu. It is likely that the extensional stresses that favour the fracture reactivation in a narrow zone around the caldera result from the increased weight of lava accumulated in the collapsed structure.

In summary, our observations of the concentric fractures between August 2006 and November 2007 allowed us to distinguish three mechanisms of fracture formation and reactivation. Contrary to Acocella (2006), we doubt that gravitational instabilities of the caldera wall explain the development of an entire concentric fracture network. The similarities between the fracture networks around the April 2007 caldera of Piton de la Fournaise and the caldera of Erta 'Ale rather suggest that the concentric fractures at Erta 'Ale may result from extension stresses related to the caldera collapse and maybe to the progressive filling of the caldera.

4.2. Origin and dynamics of caldera collapse

The geometry of caldera ring faults and the conditions required to promote a caldera collapse have been intensively studied during the last decades (e.g. Marti et al., 1994; Gudmundsson, 1998; Acocella et al., 2000; Roche et al., 2000, 2001; Roche and Druitt, 2001; Walter and Troll, 2001; Folch and Marti, 2004; Acocella, 2007). However, very few dealt with the dynamics of the collapse, i.e. continuous collapse or pulsating collapse, although the related magma deposits (Rosi et al., 1996; Reubi and Nicholls, 2004) and monitoring data (Filson et al., 1973; Kumagai et al., 2001) show contrasting behaviours. We compare, in what follows, the deformation and seismic data monitored during the caldera collapses of Fernandina, 1968, Miyakejima, 2000 and Piton de la Fournaise, 2007, in order to (1) stress the similarities between each event and consequently (2) determine a unifying mechanism that explains the different dynamics of caldera collapse.

Deformation data at Miyakejima and Piton de la Fournaise show that the caldera collapses have been preceded by an inward deflation of the edifice (Ukawa et al., 2000; Michon et al., 2007; Staudacher et al., 2009-this issue). The seismicity, which was characterised by frequent volcano-tectonic (VT) events before the onset of the subsidence, drastically changed once Miyakejima and Piton de la Fournaise started to deflate. The VT events disappeared and a low-frequency seismic signal progressively increased (Ukawa et al., 2000; Michon et al., 2007). The initial deflation phase ended by a sudden outward uplift of the edifice coeval with a magnitude 3.2 VT event at Piton de la Fournaise and a very-long-period event at Miyakejima (Kumagai et al., 2001; Michon et al., 2007). Afterwards, the edifices experienced identical deformation patterns with a succession of cycles characterised by a progressive deflation immediately followed by a sudden uplift (Fig. 7a). The deformation cycles were contemporaneous with a pulsating seismic signal (Kumagai et al., 2001; Michon et al., 2007). At Piton de la Fournaise, every cycle was characterised by a progressive amplification of the seismic signal, which then suddenly decreased to a low level (Fig. 7b). The periodicity of the cycles gradually increased from 2 h to 30 min. Among the 38 cycles, only the two earliest ones were ended by large volcano-tectonic events (Michon et al., 2007). At Miyakejima, the seismicity evolved during each deformation cycles from an increasing swarm-like activity of low-frequency earthquakes coeval with the progressive deflation, up to very-long-period seismic events during the outward uplift (Ukawa et al., 2000; Kumagai et al., 2001). The cyclic distribution of the seismicity at Piton de la Fournaise and Miyakejima shows striking similarities with the seismicity monitored by a regional seismic network mostly distributed in North and South America during the 1968 caldera collapse of Fernandina. Indeed, the caldera formation was coeval with the occurrence of 30 earthquakes, the magnitude of which exceeded 4.5 (Fig. 7b; Filson et al., 1973). Each main event was preceded by an increase of the seismicity and followed by an almost aseismic period. This distribution consequently suggests the existence of seismic cycles whose duration progressively decreased from 6 h to 2 h. Note that the largest earthquakes, M_s>5, appeared during the first seismic cycles

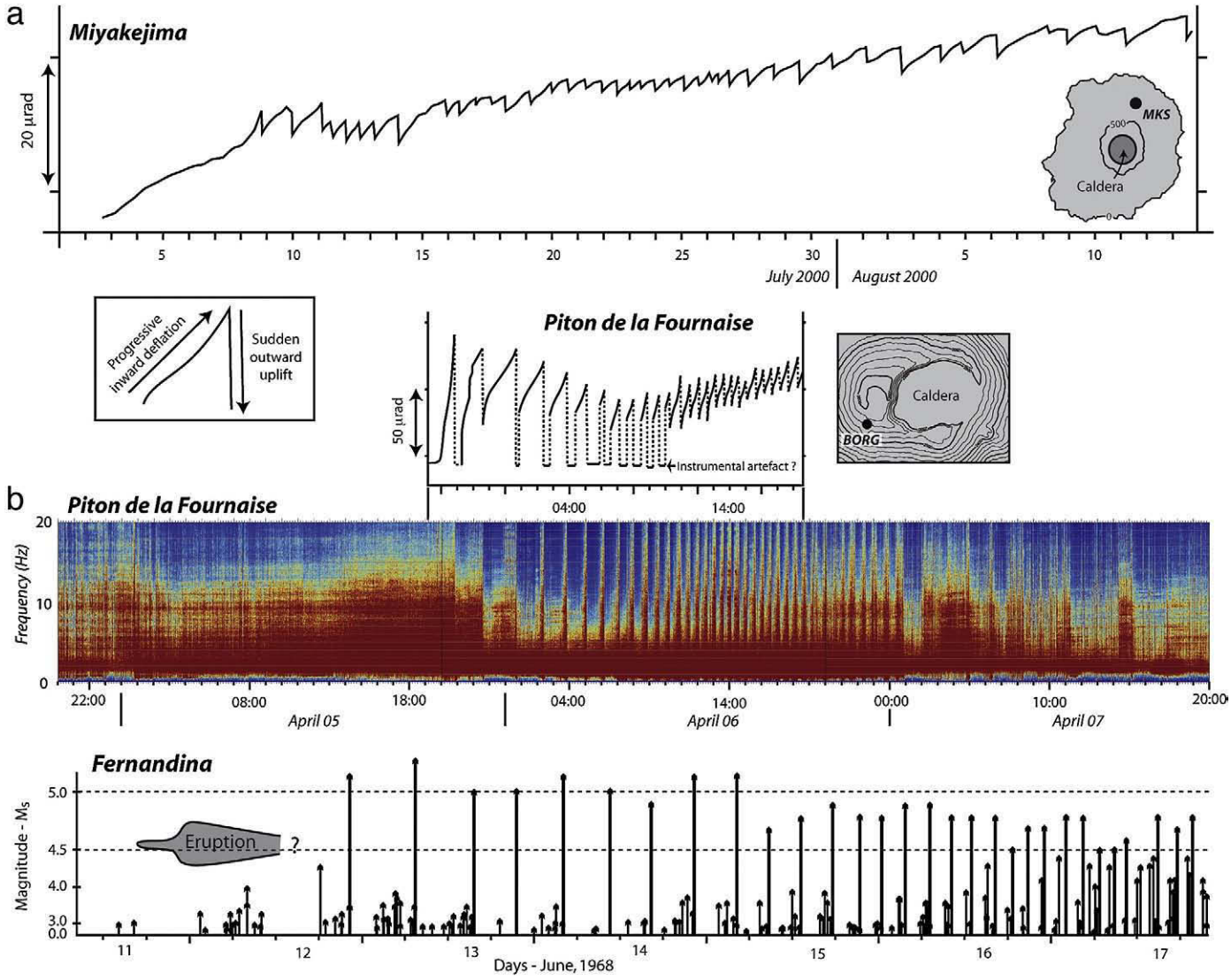

Fig. 7. a — Deformation recorded by radial tiltmeters at Miyakejima (Ukawa et al., 2000) and Piton de la Fournaise (Staudacher et al., 2009-this issue) during the caldera collapses. Here, the increase and decrease of angle (in microradian) indicate summit deflation and inflation, respectively. b — Seismicity during the collapse of Piton de la Fournaise (Michon et al., 2007) and Fernandina (Filson et al., 1973). See text for discussion.

(Fig. 7b). Despite differences in the type of seismic signal (VT or very-long-period events) that may originate from the geometry of the ring faults and the type of seismic networks, this overview of both the seismicity and the deformation recorded at Fernandina, Miyakejima and Piton de la Fournaise strongly suggests that each caldera collapse occurred in a similar way.

It has already been proposed that the main earthquakes at Fernandina, the very-long-period events at Miyakejima and the sharp decreases of the seismic signal at Piton de la Fournaise originate from the incremental collapse of the rock column into the magma chamber (Simkin and Howard, 1970; Filson et al., 1973; Kumagai et al., 2001; Michon et al., 2007). Although the periodicity is an obvious common feature, its origin has been interpreted in different ways for each volcano. The periodic very-long-period events and collapses at Miyakejima have been considered as to be caused by the constant magma outflow, which episodically sucked the rock column into the magma reservoir (Kumagai et al., 2001). At Fernandina, the irregular geometry of the bottom of the collapsing rock column (Filson et al., 1973) and the regular stress built up along the caldera fault, which is sporadically relieved by movement along the ring fault (Simkin and Howard, 1970), are two different mechanisms that have been proposed to explain the step by step collapse.

Combining the different characteristics of the caldera collapses at Fernandina, Miyakejima and Piton de la Fournaise, we put forward a unifying mechanism of basaltic caldera formation. We focus our discussion on calderas related to magma withdrawal from a magma chamber during eruptions or intrusions. Calderas formed by the deformation of the hydrothermal system (e.g. Merle and Lénat, 2003; Merle et al., 2006) are consequently not addressed in this paper.

First of all, the deformation of the summit of basaltic volcanoes is intimately linked to large lateral eruptions or magma intrusions (MacDonald, 1965). Natural examples of Piton de la Fournaise and Miyakejima reveal that calderas may develop over times of days to weeks during or after the magma withdrawal (Geshi et al., 2002; Wright and Sakai, 2004; Michon et al., 2007). The pressure decrease into the magma chamber caused by the magma withdrawal entails, above all, the centripetal subsidence of the edifice (Fig. 8b). The continuous inward deflation progressively changes the stress within the edifice. Despite the pressure decrease within the magma chamber, the centripetal deflation prevents the downward motion of the rock column due to gravitational stress by increasing both the shear stress τ opposite to the collapse and the shear strength along the pre-existing ring faults, which are common on long-lived volcanoes (Fig. 8b). The collapse of the rock column occurs when the difference between the

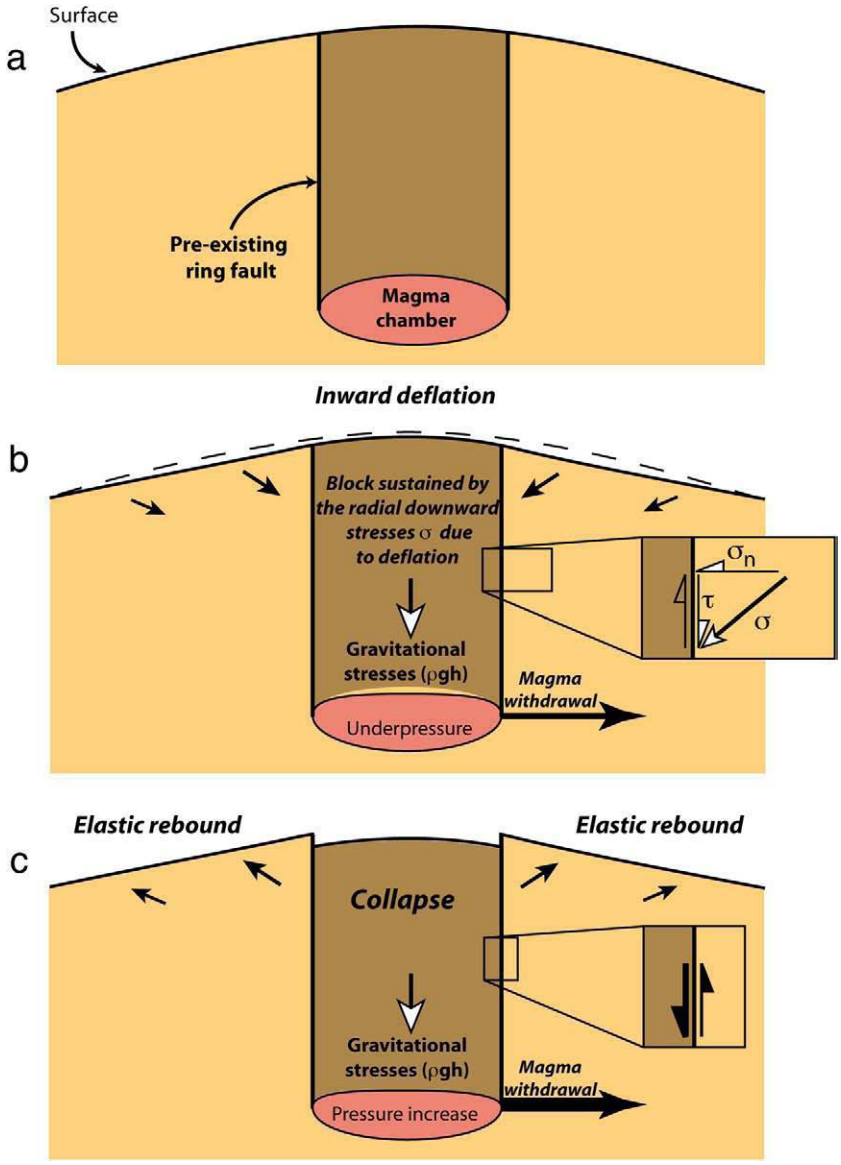

Fig. 8. Schematic representation of the mechanics of caldera collapse in basaltic setting. a — Initial stage. Long-lived volcanoes commonly present pre-existing ring faults resulting from previous caldera collapse. b — Inward deflation related to magma withdrawal from the magma chamber. Despite gravitational stresses acting on the rock column above the magma chamber, the column is sustained by additional normal and shear stresses applied on the ring fault and the remaining pressure within the magma chamber. The stress σ resulting from deflation acting on the fault is decomposed into a normal σ_n and a shear τ component. ρ, h and g correspond to the density and the height of the rock column, and gravitational acceleration, respectively. Black and white arrows represent displacement vectors and stresses, respectively. c — Collapse of the rock column when the gravitational stresses exceed the shear strength along the ring faults. The collapse of the column triggers an elastic rebound of the edifice by stress release. It may also induce an increase of the magma outflow as revealed by the step by step increase of the emission rate at the surface after the first collapses during the April 2007 eruption of Piton de la Fournaise (Michon et al., 2007). Each cycle is subsequently characterised by the succession of step b (inward deflation) and c (collapse and outward uplift).

gravitational stress and the pressure within the magma chamber is sufficient so that the shear strength of the ring faults is exceeded (Fig. 8c). Then, the downward displacement stops when the pressure increase into the magma chamber sustains the rock column anew.

We showed above that every collapse at Piton de la Fournaise and Miyakejima were coeval with outward uplift of the caldera rim. Such displacements were interpreted for Miyakejima as resulting from the expansion of the magma chamber when the rock column intrudes it (Kumagai et al., 2001). Although this hypothesis cannot be ruled out, we prefer the following alternative explanation. The immediate, short outward deformation of the caldera rim after the collapse corresponds to the elastic response of the edifice, when the downward stress is sporadically released during the motion of the rock column. The ongoing subsidence, which directly results from the magma withdrawal, promotes a new stress increase along the ring fault and prevents the collapse of the rock column. The collapse occurs anew when the shear strength is overcome by the gravitational stress exerted on the rock column. Each cycle is consequently characterised by the succession of (1) a deflation phase which inhibits the downward displacement of the rock column, and (2) a sudden collapse when the gravitational stress exceeds the shear strength along the faults. The duration between two collapses may be influenced by the injection of magmatic fluids along the ring faults. In such a case, their shear resistance declines (Anderson, 1951; Hubbert and Rubbey, 1959) and the time span between two collapses could therefore decrease like at Fernandina and Piton de la Fournaise for a constant or increasing magma withdrawal, and increase if the rate of magma outflow decreases. Recently Wright and Sakai (2004) proposed that calderas develop only following high rates of magma withdrawal. Following Druitt and Sparks (1984), Martí et al. (2000), Roche and Druitt (2001), Geyer et al. (2006), we think that the amount of magma withdrawal is the critical parameter that initiates

caldera formation. To this respect, one can note that the February and December 2005 lateral eruptions of Piton de la Fournaise, which shows similarities with the April 2007 eruption in terms of location of the eruption site and nature of magma, but a volume of magma one order of magnitude less important ($15–20 \cdot 10^6$ m^3 in 2005 and about $130 \cdot 10^6$ m^3 in April 2007; Staudacher et al., 2009-this issue), triggered a slight summit subsidence only (Peltier, 2007). Besides the volume of withdrawn magma, the occurrence of a caldera collapse is likely influenced by the strength of the edifice, the occurrence and geometry of pre-existing ring faults, the depth and size of the magma chamber (e.g. Acocella, 2007).

At Piton de la Fournaise, the step by step increase of both the tremor and the emission rate at the eruption site, after the first collapses, indicates that the rock column directly affected the magma chamber by increasing the pressure into the magma reservoir (Michon et al., 2007). Each collapse was accompanied by an ash plume composed of lithics solely above the summit (Staudacher et al., 2009-this issue). The simultaneity between deep and surface processes suggests a continuum of deformation from the roof of the magma chamber up to the surface. The collapse of such a piston-like rock column may explain the predominance of the horizontal component at both the base of the cone and the summit, where H/V values are around 2 for the period between March and April 2007. According to Dieterich and Decker (1975), such a displacement pattern is better explained by a vertically elongate axisymmetric source of deformation. This deflation source could correspond to the piston-like rock column that progressively moved downward. Hence, we propose that the predominantly horizontal centripetal deformation of the edifice results from the vertical motion of the piston-like column that allowed the "horizontal collapse" of the edifice.

This synthesis on the three best known basaltic calderas suggests that when the magma withdrawal-related inward subsidence is sufficiently advanced, the rock column between the magma chamber and the surface, intermittently collapses. We propose that the pulsating dynamics were resulting from a competition between deflation, which prevents the collapse, and gravity exerted on the block, which makes it possible despite deflation. It is noteworthy that pulsating eruption dynamics have also been proposed for several silicic calderas (Rosi et al., 1996, 1999; Troll et al., 2000; Reubi and Nicholls, 2004). This dynamic was mostly interpreted in terms of piecemeal caldera collapses. We assume that the collapse mechanism determined for basaltic calderas can be applied to silicic eruptions. The type of collapse, i.e., intermittent or continuous, would be then influenced by the emission rate. In summary, the volume and the rate of magma withdrawal would control the collapse initiation and dynamics, respectively.

4.3. Geometry of the collapse at Piton de la Fournaise

Carter et al. (2007) recently proposed that the magma chamber associated with the recurrent collapses of Dolomieu, before the April 2007 eruption, was located at around 1000 m below the surface, i.e. 1500 m asl. However, inversions of deformation data, GPS and interferometry, related to the eruptions of Piton de la Fournaise strongly suggest that dykes originate from a magma reservoir lying between 0 and 800 m asl (Fukushima et al., 2005; Peltier et al., 2007). Assuming that magma withdrawal from this magma chamber triggered the April 2007 caldera collapse, the aspect ratio of the caldera system, which corresponds to the depth versus width of the magma reservoir (Roche et al., 2000), is about 2. Analogue models indicate that for high aspect ratios multiple reverse faults break up the roof into large pieces and subsidence occurs as a series of nested cones (Roche et al., 2000, 2001). However, at Piton de la Fournaise, as at Miyakejima where the aspect ratio is also high (Geshi et al., 2002), the pulsating dynamics of the collapse rather suggests that the collapsed rock column behaved as a coherent block (Kumagai et al., 2001). We propose that the geometry differences between models and nature are mainly due to the presence of pre-existing ring faults in nature, whereas models are composed of isotropic materials.

On 6th April, 2007, the first observations of the caldera at Piton de la Fournaise indicated the occurrence of a first elongated collapse structure bounded by sub-vertical scarps (Michon et al., 2007). The presence of preserved polished surfaces on the scarps (Fig. 2b) suggests that the subsidence was controlled by inward steep normal faults in sub-surface (Fig. 9b). Considering the usual development of steep outward reverse faults in analogue models (e.g., Marti et al., 1994), we propose that the base of these inward faults is connected to outward dipping reverse faults, which are vertical at depth. The remaining southern and eastern plateaus subsequently collapsed on

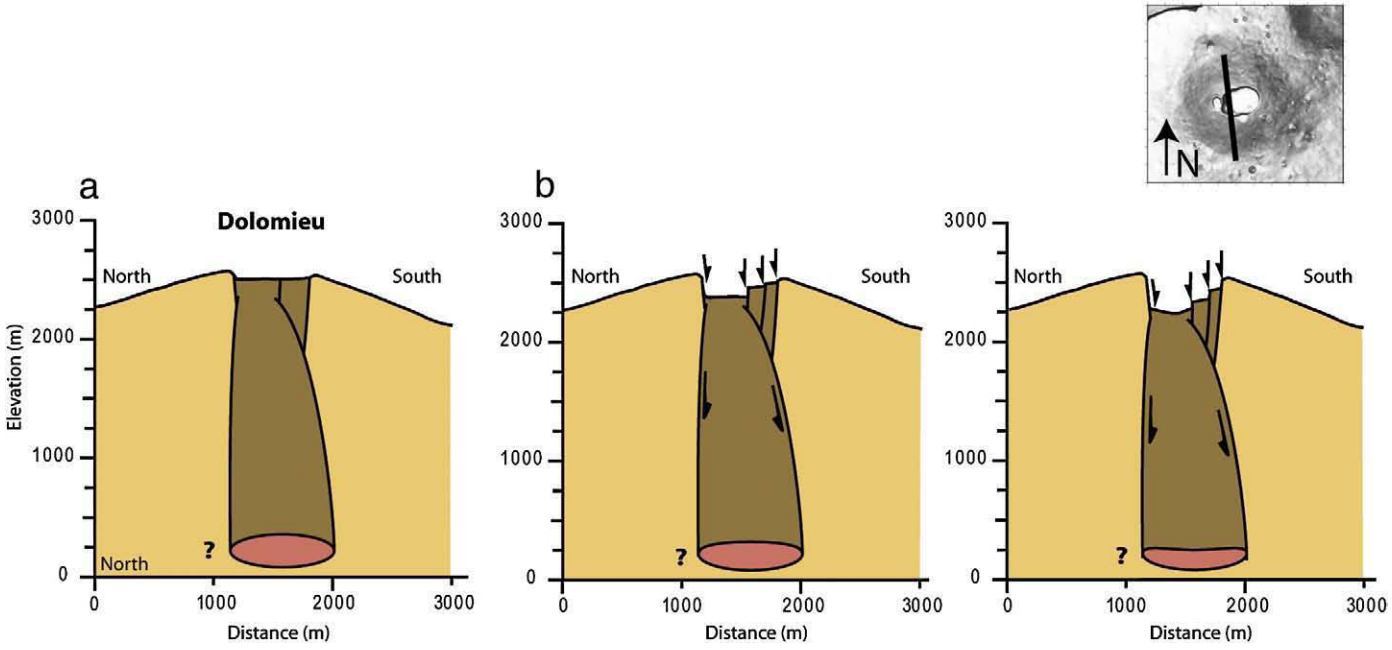

Fig. 9. Evolution of the caldera collapse during the April 2007 eruption inferred from the surface deformation. a — Initial stage. b — On April 6. c — After the collapse. The geometry and depth of the magma chamber is still poorly constrained.

7th April (see Fig. 4 in Michon et al., 2007). Their inward collapse can be usefully compared to the tilting blocks, which develop on analogue models between the central collapse and the outer normal ring faults (Roche et al., 2000, 2001; Acocella, 2007). Hence, the pre-existing southern and eastern boundaries of Dolomieu were probably reactivated in normal faulting mode (Fig. 9c). The inward deformation related to the tilt of the southern plateau probably affected the southern rim of the caldera as suggested by the occurrence of maximal inward displacements along its southern limit for the period between March and May 2007. Thus, the spatial correlation between the densest fracture zone, the maximal displacements of the caldera rim and the inward tilt of the southern plateau into the caldera suggests that the displacements recorded by GPS result from both a general deflation due to the magma withdrawal from the magma chamber and local effects due to the caldera collapse. Besides the clear control of pre-existing structures in the April 2007 collapse, the similar geometry of Dolomieu before and after the collapse suggests that the source of the collapse, i.e. the magma chamber, did not significantly change during the last hundred years.

5. Conclusion

We implemented in November 2005 a new GPS network around the summit collapsed structure of Piton de la Fournaise in order to determine the deformation related to collapse events. The present work clearly shows that the network allowed a precise determination of the summit deformation during and after the April 2007 caldera collapse. Moreover, combining GPS data and a structural analysis, we highlight the relationship between the inward displacements, the development of concentric fractures and the dynamics of collapse.

The paper also presents several sources leading to the formation of concentric fractures. Concentric fractures, which are restricted to the first tens of meters of the caldera edge result from extension stresses that are related to (1) the inward tilt of the caldera floor during the successive collapses of the rock column, (2) the reactivation of hidden limits of paleo-collapsed structures and (3) the progressive replenishment of the caldera by lava flows, the load causing a local downsag.

The seismicity and deformation data for the caldera collapses at Fernandina, 1968, Miyakejima, 2000, and Piton de la Fournaise, 2007, suggest a similar pulsating collapse mechanism. Taking into account the stress evolution into the edifice, we propose a unifying model of caldera collapse in basaltic setting that explains the cyclic deformation. The pulsating dynamics result from a competition between deflation, which prevents the collapse, and gravity exerted on the rock column above the magma chamber, which makes it possible despite deflation.

Finally, the structure of the new caldera of Piton de la Fournaise and its evolution during the collapse is explained by the collapse of a coherent block limited by vertical to outward dipping faults at depth and sub-surface normal faults. The similar contours of Dolomieu before the collapse and of the new caldera, remarkably shows the control of the pre-existing structures in the April 2007 caldera collapse.

Acknowledgments

The authors warmly thank Aline Peltier, Vincent Famin, Anthony Finizola and Isabelle Basile-Doelsh for participating to the network implementation and GPS campaigns. The paper benefited from the comments of Olivier Roche and Tom Wright. The Piton de la Fournaise Volcano Observatory kindly provided data of the permanent GPS receivers. The authors thank Ruth Andrew for improving an initial version of the manuscript. This is IPGP contribution #2414.

References

Acocella, V., 2006. Regional and local tectonics at Erta Ale caldera, Afar (Ethiopia). J. Struct. Geol. 28, 1808–1820.

Acocella, V., 2007. Understanding caldera structure and development: an overview of analogue models compared to natural calderas. Earth-Sci. Rev. 85, 125–160.

Acocella, V., Cifelli, F., Funiciello, R., 2000. Analogue models of collapse calderas and resurgent domes. J. Volcanol. Geotherm. Res. 104, 81–96.

Anderson, E.M., 1951. The dynamics of faulting. Trans. Edinb. Geol. Soc. 8, 387–402.

Bachèlery, P., 1981. Le Piton de la Fournaise (Ile de la Réunion). Etude volcanologique, structurale et pétrologique. PhD thesis, Univ. Clermont-Ferrand II, 215pp.

Beauducel, F., Agung Nandaka, M., Cornet, F.H., Diament, M., 2006. Mechanical discontinuities monitoring at Merapi volcano using kinematic GPS. J. Volcanol. Geotherm. Res. 150, 300–312.

Branney, J.M., 1995. Downsag and extension at calderas: new perspectives on collapse geometries from ice-melt, mining, and volcanic subsidence. Bull. Volcanol. 57, 303–318.

Carter, A., van Wyk de Vries, B., Kelfoun, K., Bachèlery, P., Briole, P., 2007. Pits, rifts and slumps: the summit structure of Piton de la Fournaise. Bull. Volcanol. 69, 741–756. doi:10.1007/s00445-006-0103-4.

Dieterich, J.H., Decker, R.W., 1975. Finite element modeling of surface deformation associated with volcanism. J. Geophys. Res. 80, 4094–4102.

Druitt, T.H., Sparks, R.S.J., 1984. On the formation of calderas during ignimbrite eruptions. Nature 310, 679–681.

Filson, J., Simkin, T., Leu, L.-K., 1973. Seimicity of a caldera collapse: Galapagos Islands 1968. J. Geophys. Res. 78, 8591–8622.

Folch, A., Marti, J., 2004. Geometrical and mechanical constraints on the formation of ring-fault calderas. Earth Planet. Sci. Lett. 221, 215–225.

Fukushima, Y., Cayol, V., Durand, P., 2005. Finding realistic dike models from interferometric synthetic aperture radar data: the February 2000 eruption at Piton de la Fournaise. J. Geophys. Res. 110, B03206. doi:10.1029/2004JB003268.

Geshi, N., Shimano, T., Chiba, T., Nakada, S., 2002. Caldera collapse during the 2000 eruption of Miyakejima Volcano, Japan. Bull. Volcanol. 64, 55–68.

Geyer, A., Folch, A., Marti, J., 2006. Relationship between caldera collapse and magma chamber withdrawal: an experimental approach. J. Volcanol. Geotherm. Res. 157, 375–386.

Gudmundsson, A., 1998. Formation and development of normal-fault calderas and the initiation of large explosive eruptions. Bull. Volcanol. 60, 160–170.

Hirn, A., Lépine, J.-C., Sapin, M., Delorme, H., 1991. Episodes of pit-crater collapse documented by seismology at Piton de la Fournaise. J. Volcanol. Geotherm. Res. 47, 89–104.

Hubbert, M.K., Rubbey, W.W., 1959. Role of fluid pressure in mechanics of overthrust faulting. Bull. Geol. Soc. Am. 70, 115–166.

Ito, T., Yoshioka, S., 2002. A dike intrusion model in and around Miyakejima, Niijima and Kozushima in 2000. Tectonophysics 359, 171–187.

Kumagai, H., Ohminato, T., Nakano, M., Ooi, M., Kubo, A., Inoue, H., Oikawa, J., 2001. Very-long-period seismic signals and the caldera formation at Miyake Island, Japan. Science 293, 687–690.

Lacroix, A., 1939. Les transformations récentes du sommet du volcan actif (Piton de la Fournaise) de l'Ile de la Réunion. Bull. Volcanologique, serie II tome V, pp. 3–18.

Lénat, J.-F., Bachèlery, P., 1987. Dynamics of magma transfer at Piton de la Fournaise volcano (Réunion Island, Indian Ocean). In: Chi-Yu, Scarpa (Eds.), Modeling of Volcanic Processes. Friedr. Vieweg and Sohn, Brauschweig/Wiesbaden, pp. 57–72.

Lénat, J.-F., Bachèlery, P., 1990. Structure and dynamics of the central zone of Piton de la Fournaise volcano. In: Lénat, J.-F. (Ed.), Le volcanisme de la Réunion, Monographie. Cent. De Rech. Volcanol., Clermont-Ferrand, pp. 257–296.

Longpré, M.-A., Staudacher, Th., Stix, J., 2007. The November 2002 eruption at Piton de la Fournaise volcano, La Réunion Island: ground deformation, seismicity, and pit crater collapse. Bull. Volcanol. 69, 511–525. doi:10.1007/s00445-006-0087-0.

MacDonald, G.A., 1965. Hawaiian calderas. Pac. Sci. 19, 320–334.

Marti, J., Ablay, G.J., Redshaw, L.T., Sparks, R.S.J., 1994. Experimental studies of collapse calderas. J. Geol. Soc. (Lond.) 151, 919–929. doi:10.1144/gsjgs.151.6.0919.

Martí, J., Folch, A., Macedonio, G., Neri, A., 2000. Pressure evolution during caldera-forming eruptions. Earth Planet. Sci. Lett. 175, 275–287.

Merle, O., Lénat, J.-F., 2003. Hybrid collapse mechanism at Piton de la Fournaise volcano, Reunion Island, Indian Ocean. J. Geophys. Res. 108, 2166. doi:10.1029/2002JB002014.

Merle, O., Barde-Cabusson, S., Maury, R.C., Legendre, C., Guille, G., Blais, S., 2006. Volcano core collapse triggered by regional faulting. J. Volcanol. Geotherm. Res. 158, 269–280.

Michon, L., Staudacher, Th., Ferrazzini, V., Bachèlery, P., Marti, J., 2007. April 2007 collapse of Piton de la Fournaise: a new example of caldera formation. Geophys. Res. Lett. 34, L21301. doi:10.1029/2007GL031248.

Michon, L., Cayol, V., Letourneur, L., Peltier, A., Villeneuve, N., Staudacher, T., 2009. Edifice growth, deformation and rift zone development in basaltic setting: Insights from Piton de la Fournaise shield volcano (Réunion Island). J. Volcanol. Geotherm. Res. 184, 14–30 (this issue). doi:10.1016/j.jvolgeores.2008.11.002.

Mogi, K., 1958. Relations of the eruptions of various volcanoes and the deformations of the ground surfaces around them. Bull. Earthq. Res. Inst. Univ. Tokyo 36, 99–134.

Peltier, A., 2007. Suivi, modélisation et évolution des processus d'injections magmatiques au Piton de La Fournaise (Réunion), à partir d'une analyse croisée des données de déformation, géochimiques et structurales. PhD Thesis, Univ. Réunion, 282p. http://tel.archivesouvertes.fr/index.php?halsid=gljus7suihg3og6qn3850l6jn5&-view_this_doc=tel-00167895&version=1.

Peltier, A., Staudacher, Th., Bachèlery, P., 2007. Constraints on magma transfers and structures involved in the 2003 activity at Piton de La Fournaise from displacement data. J. Geophys. Res. 112, B03207. doi:10.1029/2006JB004379.

Peltier, A., Staudacher, T., Bachèlery, P., Cayol, V., 2009. Formation of the April 2007 caldera collapse at Piton de La Fournaise volcano: Insights from GPS data. J. Volcanol. Geotherm. Res. 184, 152–163 (this issue). doi:10.1016/j.jvolgeores.2008.09.009.

Ryan, M.P., Blevins, J.Y.K., Okamura, A.T., Koyanagi, R.Y., 1983. Magma reservoir subsidence mechanics: theoretical summary and application to Kilauea Volcano, Hawaii. J. Geophys. Res. 88, 4147–4181.

Reubi, O., Nicholls, I.A., 2004. Variability in eruptive dynamics associated with caldera collapse: an example from two successive eruptions at Batur volcanic field, Bali, Indonesia. Bull. Volcanol. 66, 134–148. doi:10.1007/s00445-003-0298-6.
Roche, O., Druitt, T.H., 2001. Onset of caldera collapse during ignimbrite eruptions. Earth Planet. Sci. Lett. 191, 191–202.
Roche, O., Druitt, T.H., Merle, O., 2000. Experimental study of caldera formation. J. Geophys. Res. 105, 395–416.
Roche, O., Van Wyk de Vries, B., Druitt, T.H., 2001. Sub-surface structures and collapse mechanisms of summit pit craters. J. Volcanol. Geotherm. Res. 105, 1–18.
Rosi, M., Vezzoli, L., Aleotti, P., De Censi, M., 1996. Interaction between caldera collapse and eruptive dynamics during the Campanian Ignimbrite eruption, Phlegraean Fields, Italy. Bull. Volcanol. 57, 541–554.
Rosi, M., Vezzoli, L., Castelmenzano, A., Grieco, G., 1999. Plinian pumice fall deposit of the Campanian Ignimbrite eruption (Phlegraean Fields, Italy). J. Volcanol. Geotherm. Res. 91, 179–198.
Simkin, T., Howard, K.A., 1970. Caldera collapse in Galapagos Islands, 1968. Science 169, 429–437.
Staudacher, T., Ferrazzini, V., Peltier, A., Kowalski, P., Boissier, P., Catherine, P., Lauret, F., Massin, F., 2009. The April 2007 eruption and the Dolomieu crater collapse, two major events at Piton de la Fournaise (La Réunion Island, Indian Ocean). J. Volcanol. Geotherm. Res. 184, 126–137 (this issue). doi:10.1016/j.jvolgeores.2008.11.005.
Troll, V.R., Emeleus, C.H., Donaldson, C.H., 2000. Caldera formation in the Rum Central Igneous Complex, Scotland. Bull. Volcanol. 62, 301–317. doi:10.1007/s004450000099.
Troll, V.R., Walter, T.R., Schmincke, H.-U., 2002. Cyclic caldera collapse: piston or piecemeal subsidence? Field and experimental evidence. Geology 30, 135–138.
Ukawa, M., Fujita, E., Yamamoto, E., Okada, Y., Kikuchi, M., 2000. The 2000 Miyakejima eruption: crustal deformation and earthquakes observed by the NIED Miyakejima observation network. Earth Planets Space 52, xix–xxvi.
Urai, M., Geshi, N., Staudacher, Th., 2007. Size and volume evaluation of the caldera collapse on Piton de la Fournaise volcano during the April 2007 eruption using ASTER stereo imagery. Geophys. Res. Lett. L22318. doi:10.1029/2007GL031551.
Walsh, J.B., Decker, R.W., 1971. Surface deformation associated with volcanism. J. Geophys. Res. 76, 3291–3302.
Walter, T.R., Troll, V.R., 2001. Formation of caldera periphery faults: an experimental study. Bull. Volcanol. 63, 191–203.
Wilson, R.M., 1935. Ground surface movement at Kilauea Volcano, Hawaii. Univ. Hawaii Res. Publ. 10 (56p.).
Wright, T.L., Sakai, S., 2004. Interpretation of the Miyakejima 2000 eruption and dike emplacement using time animations of earthquakes. Bull. Earthq. Res. Inst., Univ. Tokyo 79, 1–16.